University of Technology Sydney
FACULTY OF ENGINEERING

DESIGN AND FABRICATION OF NOVEL NANOFIBER MEMBRANES VIA ELECTROSPINNING TECHNIQUE FOR MEMBRANE DISTILLATION

by

YUNCHUL WOO

A Thesis submitted in fulfilment for the degree of

Doctor of Philosophy

School of Civil and Environmental Engineering
Faculty of Engineering and Information Technology
University of Technology Sydney (UTS)
New South Wales, Australia

June 2017

CERTIFICATE OF ORIGINAL AUTHORSHIP

I certify that the work in this thesis has not previously been submitted for a degree nor has it been submitted as part of requirements for a degree except as part of the collaborative doctoral degree and/or fully acknowledged within the text.

I also certify that the thesis has been written by me. Any help that I have received in my research work and the preparation of the thesis itself has been acknowledged. In addition, I certify that all information sources and literature used are indicated in the thesis.

Signature of Student:

Date: 30/06/2017

ACKNOWLEDGEMENTS

First of all, I really appreciate my beloved wife, Hyelim Kim, for her sacrifice in support of my PhD study. Also, I would like to thank my parents (Mr. Kwanghee Woo and Mrs. Yookyung Kim) as they were continuously supporting and encouraging me. Without their support, I could not achieve a successful PhD study outcome.

I would like to express my heartfelt gratitude to my supervisor A/Prof. Ho Kyong Shon for giving me the opportunity to work with him at University of Technology Sydney (UTS). I will gratefully remember his unswerving encouragement, great mentorship, and strong support. Without his consistent guidance, this thesis would not have been possible. I would also like to thank my other supervisor, Dr. Leonard D. Tijing for his kind support and help during my study. He is a wonderful supervisor and I thank him for all his support and advices during my PhD. I appreciate their consistent support with inspiring optimism that guided me through this challenging journey. I also thank Dr. Sherub Phuntsho and A/Prof. Wang-Geun Shim for their support and encouragement during my study when I was facing very hard, stressful, and challenging moments. Their advices gave me the light and encouragement to keep up the momentum. I would also like to thank my MS supervisor Prof. Han-Seung Kim for his advices and encouragement in my PhD study.

I am very thankful to the external research collaboration groups that gave me chances to work with them. I would like to thank Dr. June-Seok Choi at Korea Institute of Civil Engineering and Building Technology for his support as well as the invitations to the seminars in his institution. Also, I want to acknowledge Prof. Tao He at Shanghai Advanced Research Institute, A/Prof. Alicia An at City University of Hong Kong, Prof. Seung-Hyun Kim at Kyungnam University, Prof. Long D. Nghiem at University of

Wollongong, A/Prof. Sangho Lee at Kookmin University, Prof. Seungkwan Hong at Korea University, and Prof. Enrico Drioli at Institute on Membrane Technology in the University of Calabria for giving me the chances to work with their groups. I also thank Dr. Dong-Han Seo at CSIRO, Dr. Ming Xie at Victoria University, Hung C. Duong at University of Wollongong, Dr. Eui-Jong Lee at Sungkyunkwan University, and Jeong Jun Lee at Myongji University for working with me.

Thanks to my friends and research group members at UTS who made this journey memorable. I want to thank Dr. Youngjin Kim, Dr. Laura Chekli, Dr. Soleyman Sahebi, Dr. Tahir Majeed, Dr. Mohammad Shahid, Dr. Jihye Kim, Minwei Yao, Jiawei Ren, Myoung Jun Park, Jung-Eun Kim, Sungil Lim, Youngkwon Choi, David Inhyuk Kim, Seungho Kook, Fezeh Lotfi, and Aaron Katz. I would like to acknowledge Mohammed Johir for his help in the laboratory. And the administrative support from Van, Trish and Viona are gratefully acknowledged as well.

My sincere thanks are passed to my examiners: Prof. Mikel Duke from Victoria University and Prof. Xiwang Zhang from Monash University for reviewing my PhD thesis and research findings. I also wish to thank the FEIT research administration officers for their help in facilitating my PhD studies.

Last but not least, I would like to thank the University of Technology Sydney (UTS) for offering me an IRS scholarship towards the completion of this thesis. My PhD research was also supported by a grant (17IFIP-B065893-05) from the Industrial Facilities & Infrastructure Research Program funded by the Ministry of Land, Infrastructure and Transport of the Korean government – my grateful thanks to them.

Book chapters and Journal Articles Published or Submitted**

1. L. D. Tijing, ***Y. C. Woo***, M. Yao, J. Ren and H. K. Shon, 'Electrospinning for membrane fabrication: Strategies and applications' in Reference Module in Chemistry, Molecular Sciences and Chemical Engineering, ***Elsevier***, 2017
2. ****Y. C. Woo***, C. Ying, L. D. Tijing, T. He, J. –S. Choi, S. –H. Kim and H. K. Shon, CF_4 Plasma-Modified Omniphobic Electrospun Nanofiber Membrane for Produced Water Brine Treatment by Membrane Distillation, ***Journal of Membrane Science***, 529 (2017) 234-242
3. E. –J. Lee, B. J. Deka, J. Guo, ***Y. C. Woo***, H. K. Shon and A. K. An, Engineering the re-entrant hierarchy and surface energy of PDMS-PVDF membrane for membrane distillation using a facile and benign microsphere coating, ***Environmental Science & Technology***, 51 (2017) 10117-10126
4. M. Yao, ***Y. C. Woo***, L. D. Tijing, C. Cesarini and H. K. Shon, Improving Nanofiber Membrane Characteristics and Membrane Distillation Performance of Heat-Pressed Membranes via Annealing Post-Treatment, ***Applied Sciences***, 7(1) (2017) 78-88
5. Y. Kim, S. Li, L. Chekli, ***Y. C. Woo***, C. –H Wei, S. Phuntsho, N. Ghaffour, T. Leiknes and H. K. Shon, Assessing the removal of organic micro-pollutants from anaerobic membrane bioreactor effluent by fertilizer-drawn forward osmosis, ***Journal of Membrane Science***, 533 (2017) 84-95
6. E. –J. Lee, A. K. An, P. Hadi, S. Lee, ***Y. C. Woo*** and H. K. Shon, Advanced multi-nozzle electrospun functionalized TiO_2/PVDF hybrid membranes for direct contact membrane distillation, ***Journal of Membrane Science***, 524 (2017) 712-720

7. *__***Y. C. Woo***__, L. D. Tijing, M. J. Park, M. Yao, J. -S. Choi, S. Lee, S. -H. Kim, K. –J. An, and H. K. Shon, Electrospun dual-layer nonwoven membrane for desalination by air gap membrane distillation, ***Desalination***, 403 (2017) 187-198
8. J. Ren, __***Y. C. Woo***__, M. Yao, L. D. Tijing and H. K. Shon, Enhancement of nanoscale zero-valent iron immobilization onto electrospun polymeric nanofiber mats for groundwater remediation, ***Process Safety and Environmental Protection***, (2017) In-press (DOI: http://dx.doi.org/10.1016/j.psep.2017.04.027)
9. Y. Kim, __***Y. C. Woo***__, S. Phuntsho, L. D. Nghiem, H. K. Shon and S. Hong, Evaluation of fertilizer-drawn forward osmosis for coal seam gas reverse osmosis brine treatment and sustainable agricultural reuse, ***Journal of Membrane Science***, 537 (2017) 22-31
10. *__***Y. C. Woo***__, L. D. Tijing, W. -G. Shim, J. –S. Choi, S. –H. Kim, E. Drioli, T. He and H. K. Shon, Water desalination using graphene-enhanced electrospun nanofiber membrane via air gap membrane distillation, ***Journal of Membrane Science***, 520 (2016) 99-110
11. __***Y. C. Woo***__, Y. Kim, W. -G. Shim, L. D. Tijing, M. Yao, L. D. Nghiem, J. -S. Choi, S. -H. Kim and H. K. Shon, Effects of graphene on the properties and performance of PVDF flat-sheet membrane for treatment of RO brine from CSG produced water by air gap membrane distillation, ***Journal of Membrane Science***, 513 (2016) 74-84
12. E. –J. Lee, A. K. –J. An, T. He, __***Y. C. Woo***__ and H. K. Shon, Electrospun nanofibrous membranes incorporated with fluorosilane coated TiO2

nanocomposite for direct contact membrane distillation, ***Journal of Membrane Science***, 520 (2016) 145-154

13. *L. D. Tijing, ***Y. C. Woo***, W. -G. Shim, J. -S. Choi, T. He, S. -H. Kim, and H. K. Shon, Superhydrophobic nanofiber membrane containing carbon nanotubes for high-performance direct contact membrane distillation, ***Journal of Membrane Science,*** 502 (2016) 158-170
14. M. Yao, ***Y. C. Woo***, L. D. Tijing, W. -G. Shim, J. -S. Choi, S. -H. Kim and H. K. Shon, Effect of heat-press conditions on electrospun membranes for desalination by direct contact membrane distillation, ***Desalination***, 378 (2016) 80-91
15. ***Y. C. Woo***, J. J. Lee, W. -G. Shim, H. K. Shon, L. D. Tijing, M. Yao and H. –S. Kim, Effects of powdered activated carbon on integrated submerged membrane bioreactor – nanofiltration process for wastewater reclamation, ***Bioresource Technology***, 210 (2016) 18-25
16. J. J. Lee, ***Y. C. Woo***, J. -S. Kang, C. Y. Kang and H. -S. Kim, Effect of various pretreatments on the performance of nanofiltration for wastewater reuse, ***Desalination and Water Treatment***, 57 (2016) 7522-7530
17. S. Sahebi, S. Phuntsho, ***Y. C. Woo***, M. J. Park, L. D. Tijing, S. Hong, H. K. Shon, Effect of sulphonated polyethersulfone substrate for thin film composite forward osmosis membrane, ***Desalination***, 389 (2016) 129-136
18. *L. D. Tijing, ***Y. C. Woo***, J. -S. Choi, S. Lee, S. -H. Kim and H. K. Shon, Fouling and its control in membrane distillation- A review, ***Journal of Membrane Science***, 475 (2015) 215-244
19. ***Y. C. Woo***, J. J. Lee, L. D. Tijing, H. K. Shon, M. Yao and H. -S. Kim, Characteristics of membrane fouling by consecutive chemical cleaning in

pressurized ultrafiltration as pre-treatment of seawater desalination, ***Desalination***, 369 (2015) 51-61

20. J. J. Lee, ***Y. C. Woo*** and H. -S. Kim, Effect of driving pressure and recovery rate on the performance of nanofiltration and reverse osmosis membranes for the treatment of the effluent from MBR, ***Desalination and Water Treatment***, 54 (2015) 3589-3595
21. L. D. Tijing, ***Y. C. Woo***, M. A. H. Johir, J. -S. Choi and H. K. Shon, A novel dual-layer bicomponent electrospun nanofibrous membrane for desalination by direct contact membrane distillation, ***Chemical Engineering Journal***, 256 (2014) 155-159

** Publications made during the PhD candidature including articles not entirely related to the Thesis. * Articles related to the Thesis.

Conference papers and presentation

1. ***Y. C. Woo***, M. Yao, L. D. Tijing, J. –S. Choi and H. K. Shon, Superhydrophobic co-axial electrospun nanofiber membranes for seawater desalination by direct contact membrane distillation, ***2017 International Congress on Membranes and Membrane Processes (ICOM 2017)***, 29 July ~ 04 August, 2017, San Francisco, USA
2. ***Y. C. Woo***, L. D. Tijing, M. Yao, J. –S. Choi and H. K. Shon, Surface-modified omniphobic membranes for treatment of challenging waters by membrane distillation, ***2017 International Congress on Membranes and Membrane Processes (ICOM 2017)***, 29 July ~ 04 August, 2017, San Francisco, USA

3. ***Y. C. Woo***, M. Yao, L. D. Tijing, J. –S. Choi and H. K. Shon, Superhydrophobic membranes via co-axial electrospinning for long-term membrane distillation operation, ***Engineering With Membranes (EWM2017)***, April 26 ~ 28, 2017, Singapore, Singapore
4. ***Y. C. Woo***, M. Yao, L. D. Tijing, J. –S. Choi and H. K. Shon, Co-axial nanofiber membranes for seawater desalination by membrane distillation, ***3rd International Conference on Desalination using Membrane Technology***, April 2 ~ 5, 2017, Gran Canaria, Spain
5. ***Y. C. Woo***, Y. Kim, M. Yao, L. D. Tijing, J. –S. Choi, S. –H. Kim and H. K. Shon, Omniphobic membrane to treat reverse osmosis brine from coal seam gas produced water by membrane distillation, ***The 9th International Membrane Science and Technology Conference (IMSTEC 2016)***, December 5 ~ 8, 2016, Adelaide, Australia
6. ***Y. C. Woo***, M. Yao, L. D. Tijing, J. –S. Choi, S. –H. Kim and H. K. Shon, Omniphobic membrane using layer-by-layer technique to treat RO brine from CSG produced water by AGMD, ***The 9th International Desalination Workshop (IDW 2016)***, November 13 ~ 15, 2016, Abu Dhabi, UAE
7. ***Y. C. Woo***, L. D. Tijing, M. Yao, J. –S. Choi and H. K. Shon, Treatment of RO brine from CSG-produced water using graphene/PVDF flat-sheet membrane distillation, ***IWA World Water Congress & Exhibition (IWA-WWC&E 2016)***, October 09 ~ 13, 2016, Brisbane, Australia
8. ***Y. C. Woo***, Omniphobic electrospun nanofiber membrane for the treatment of reverse osmosis brine from coal seam gas produced water via membrane distillation, ***The Faculty of Engineering and IT Research Showcase 2016,***

University of Technology Sydney (UTS), September 14, 2016, Sydney, Australia

9. ***Y. C. Woo***, L. D. Tijing, M. Yao and H. K. Shon, Graphene/PVDF membrane for the treatment of RO brine from coal seam gas produced water by membrane distillation, ***The 5th IWA Regional Conference on Membrane Technology (IWA-RMTC 2016)***, August 22 ~ 24, 2016, Kunming, China
10. ***Y. C. Woo***, M. Yao, L. D. Tijing and H. K. Shon, Fabrication of graphene enhanced membranes for brine treatment from coal seam gas (CSG) produced water by air gap membrane distillation, ***The 10th Aseanian Membrane Society (AMS7)***, July 26 ~ 29, 2016, Nara, Japan
11. ***Y. C. Woo***, L. D. Tijing, M. Yao, E. Drioli and H. K. Shon, Robust omniphobic electrospun nanofiber membrane for air gap membrane distillation, ***EDS Desalination for the Environment: Clean Water and Energy***, May 22 ~ 26, 2016, Rome, Italy
12. ***Y. C. Woo***, L. D. Tijing, J. –S. Choi, S. –H. Kim and H. K. Shon, Effects of new materials on the properties and performance of electrospun membranes for membrane distillation, ***EDS Desalination for the Environment: Clean Water and Energy***, May 22 ~ 26, 2016, Rome, Italy
13. L. D. Tijing, ***Y. C. Woo***, M. Yao and H. K. Shon, Evaluation of the potential and performance of superhydrophobic multicomponent nanofiber, ***2016 Membrane distillation and related technologies workshop***, January 15, 2016, Sydney, NSW, Australia.
14. ***Y. C. Woo***, Y. Kim, W. –G. Shim, L. D. Tijing, M. Yao, L. D. Nghiem, J. –S. Choi and H. K. Shon, Treatment of reverse osmosis brine produced from coal

seam gas (CSG) using membrane distillation, ***2nd International Conference on Desalination and Environment***, January 23 ~ 26, 2016, Doha, Qatar.

15. Y. Kim, W. –G. Shim, ***Y. C. Woo***, L. Chekli, S. Phuntsho and H. K. Shon, Selection of fertilizers as a draw solute for fertilizer-drawn forward osmosis – anaerobic membrane bioreactor hybrid system, ***2nd International Conference on Desalination and Environment***, January 23 ~ 26, 2016, Doha, Qatar.
16. L. D. Tijing, ***Y. C. Woo***, J. –S. Choi and H. K. Shon, Evaluation of the potential and performance of superhydrophobic multicomponent nanofiber, ***2015 AMTA/AWWA Membrane Technology Conference & Exposition***, March 2 ~ 5, Orlando, FL, United States (US).
17. H. K. Shon, L. D. T., ***Y. C. Woo***, M. Yao and K. –J. An, Dual-layer electrospun nanofibrous membrane for direct contact membrane distillation, ***12th IWA Leading Edge Conference on Water and Wastewater Technologies***, May 30 ~ June 3, 2015, Hong Kong, China.
18. ***Y. C. Woo***, L. D. Tijing, M. Yao and H. K. Shon, Nanofiber membranes for membrane distillation: Potential and performance, ***ICMAT 2015 & IUMRS-ICA 2015***, June 28 to July 03, 2015, Singapore, Singapore.
19. L. D. Tijing, ***Y. C. Woo***, J. –S. Choi and H. K. Shon, Electrospun nanocomposite membrane for membrane distillation, ***2IWMD 2015***, July 01 to 04, 2015, Ravello, Italy
20. ***Y. C. Woo***, L. D. Tijing, M. Yao, J. –S. Choi and H. K. Shon, Nanomaterial-incorporated nanofiber membranes for membrane distillation: Potential and Performance, ***2nd International Conference on Desalination on using Membrane Technology***, July 26 to 29, Singapore, Singapore

21. P. Hadi, K. -Jin An, E. J. Lee, ***Y. C. Woo*** and H. K. Shon, Functionalized CNT nanocomposite electrospun PVDF membrane for desalination by air gap membrane distillation, ***2nd International Conference on Desalination on using Membrane Technology***, July 26 to 29, Singapore, Singapore
22. ***Y. C. Woo***, Y. Kim, W. –G. Shim, L. D. Tijing, M. Yao, J. –S. Choi, L. D. Nghiem, S. –H. Kim and H. K. Shon, Preparation and fabrication of graphene-enabled cast membrane for the treatment of RO brine from CSG produced water by AGMD, ***The 8th International Conference on Challenges in Environmental Science & Engineering (The 8th CESE)***, Sep 28 ~ Oct 2, 2015, Sydney, Australia.
23. ***Y. C. Woo***, J. J. Lee, L. D. Tijing, W. –G. Shim, H. K. Shon, J. –S. Kang and H. –S. Kim, Effect of powdered activated carbon (PAC) on the performance of submerged membrane bioreactor (SMBR) – nanofiltration (NF) integrated process for wastewater reclamation, ***The 8th International Conference on Challenges in Environmental Science & Engineering (The 8th CESE)***, Sep 28 ~ Oct 2, 2015, Sydney, Australia.
24. ***Y. C. Woo***, L. D. Tijing, M. Yao, J. –S. Choi, and H. K. Shon, Nanofiber membranes for air gap membrane distillation desalination: Two-layer design and incorporation of graphene, ***The 8th International Conference on Challenges in Environmental Science & Engineering (The 8th CESE)***, Sep 28 ~ Oct 2, 2015, Sydney, Australia.
25. M. Yao, ***Y. C. Woo***, L. D. Tijing, W. –G. Shim, J. –S. Choi, and H. K. Shon, Effect of heat-press conditions on electrospun membranes for desalination by air gap membrane distillation, ***The 8th International Conference on***

Challenges in Environmental Science & Engineering (The 8th CESE), Sep 28 ~ Oct 2, 2015, Sydney, Australia.

26. ***Y. C. Woo***, M. Yao, Y. Kim, L. D. Tijing, W. –G. Shim J. –S. Choi, S. –H. Kim, L. D. Nghiem and H. K. Shon, RO brine treatment from coal seam gas (CSG) produced water by membrane distillation, ***International Desalination Workshop 2015 (IDW2015)***, Nov 18 to 21, 2015, Jeju island, Republic of Korea
27. L. D. Tijing, ***Y. C. Woo***, J. –S. Choi and H. K. Shon, High-flux membrane distillation using two-layer microporous nanofiber membranes via an electrospinning fabrication, ***The 10th International Congress on Membranes and Membrane processes (ICOM 2014)***, July 20 ~ 25, 2014, Suzhou, China.
28. L. D. Tijing, ***Y. C. Woo***, J. –S. Choi and H. K. Shon, Electrospun nanofibers with superhydrophobic properties for high flux and high rejection membrane distillation process, ***The 7th International Conference on Challenges in Environmental Science & Engineering (The 7th CESE)***, October 12 ~ 16, 2014, Johor Bahru, Malaysia.
29. L. D. Tijing, ***Y. C. Woo***, M. Yao, J. –S. Choi and H. K. Shon, Electrospun superhydrophobic nanofiber membranes for membrane distillation desalination, ***The 7th International Desalination Workshop (7th IDW 2014)***, November 5 ~ 8, 2014, Jeju, Republic of Korea.
30. M. Yao, ***Y. C. Woo***, L. D. Tijing, J. –S. Choi and H. K. Shon, Heat-press effect to electrospun nanofibrous membrane for seawater desalination by membrane distillation, ***The 7th International Desalination Workshop (7th IDW 2014)***, November 5 ~ 8, 2014, Jeju, Republic of Korea.

31. J. J. Lee, ***Y. C. Woo***, R. C. Eusebio, C. –Y. Kang, Y. –S. Kim and H. –S. Kim, Effect of various pretreatments on the performace of nanofiltration for wastewater reuse, ***The 7th International Desalination Workshop (7th IDW 2014)***, November 5 ~ 8, 2014, Jeju, Republic of Korea.
32. L. D. Tijing, ***Y. C. Woo***, J. –S. Choi and H. K. Shon, Potential of electrospun composite nanofibers as superhydrophobic membranes for enhanced membrane distillation performance, ***4th MSA ECR Membrane Symposium***, November 29 ~ 21, 2014, Melbourne, Australia.
33. L. D. Tijing, ***Y. C. Woo***, J. –S. Choi and H. K. Shon, Superhydrophobic PVDF-co-HFP nanofibrous membrane containing MWNTs for desalination by direct contact membrane distillation, ***4th IWA Regional Conference on Membrane Technology 2014***, December 3 ~ 6, Ho Chi Minh City, Vietnam.
34. ***Y. C. Woo***, L. D. Tijing, J. –S. Choi and H. K. Shon, Hydrophobic/hydrophilic dual-layer electrospun nanofibrous membranes for air gap membrane distillation, ***4th IWA Regional Conference on Membrane Technology 2014***, December 3 ~ 6, Ho Chi Minh City, Vietnam.

Presentation made during the PhD candidature including proceedings, oral and poster presentations.

LIST OF ABBREVIATIONS

2D	Two-dimensional
AD	Adsorption desalination
AED	Adsorption energy distribution
AFM	Atomic force microscopy
AGMD	Air gap membrane distillation
APS	Accelerated precipitation softening
ATR-FTIR	Attenuated total reflectance – Fourier transform infrared spectroscopy
$BaSO_4$	Barium sulfate
BET	The Brunauer-Emmett-Teller
BJH	The Barrett-Joyner-Halenda
BNNPs	Boron nitride nanoparticles
BTEAC	Benzyltriethylammonium chloride
CA	Contact angle
$Ca(OH)_2$	Calcium hydroxide
$CaCO_3$	Calcium carbonate
$CaSO_4$	Calcium sulfate
CBD	Coal bed methane
CDI	Capacitive deionization
CFP	Capillary flow porometry
CNTs	Carbon nanotubes
COD	Chemical oxygen demand
C-PVDF	Commercial PVDF membrane
CSG	Coal seam gas

CuO	Copper oxide
DC	Direct current
DCMD	Direct contact membrane distillation
DI	De-ionized
DMF	N, N-dimethylformamide
DS	Draw solution
EDX	Energy dispersive x-ray spectroscopy
ENM	Electrospun nanofiber membrane
ERD	Energy recovery device
$FeCl_3$	Ferric chloride
FO	Forward osmosis
FOHC	The FO-RO hybrid Desalination Research Center
FS	Feed solution
GMVP	The Global MVP project
G/PH	Graphene/Polyvinylidene fluoride-co-hexafluoropropylene
GO	Graphene oxide
GOR	Gain output ratio
HA	Humic acid
HCl	Hydrochloric acid
h-BN	The hexagonal boron nitride
iCVD	Initiated chemical vapor deposition
IP	Interfacial polymerization
IPA	Isopropanol
KORAE	The Korean Optimized RO desalination for Advanced Energy saving
LEP	Liquid entry pressure

LiCl	Lithium chloride
MBR	Membrane bioreactor
MCDI	Membrane capacitive deionization
MCr	Membrane crystallization
MDBR	Membrane distillation-membrane bioreactor
MED	Multi-effect distillation
MEMD	Multi-effect membrane distillation
MD	Membrane distillation
MF	Microfiltration
MGMD	Material gap membrane distillation
MSF	Multi-stage flash
MWNTs	Multi-walled nanotubes
N6	Nylon-6
NaCl	Sodium chloride
NaOH	Sodium hydroxide
NCC	Nanocrystalline cellulose
NIPS	Non-solvent induced phase separation
NOMs	Natural organic matters
NTIPS	Non-solvent with thermally induced phase separation
OCM	Orthogonal collocation method
ODEs	Ordinary differential equations
OMW	Olive mill wastewater
PA	Polyamide
PACl	Polyaluminum chloride
PAM	Polypropylene acid ammonium

PAN	Polyacrylonitrile
PDEs	Partial differential equations
PDMS	Polydimethylsiloxane
PEI	Polyetherimide
PES	Polyethersulfone
PET	Polyethylene terephthalate
PGMD	Permeate gap membrane distillation
PH	Polyvinylidene fluoride-co-hexafluoropropylene (PVDF-co-HFP)
PP	Polypropylene
PRO	Pressure retarded osmosis
PS	Polystyrene
PSD	Pore size distribution
PSf	Polysulfone
PTFE	Polytetrafluoroethylene
PVA	Polyvinyl alcohol
PVAc	Polyvinyl acetate
PVC	Polyvinyl chloride
PVDF	Polyvinylidene fluoride
PVDF-CTFE	Poly(vinylidene fluoride-co-chlorotrifluoroethylene)
RCW	Recirculating cooling water
RED	Reverse electrodialysis
RF	Radio frequency
RO	Reverse osmosis
SA	Sliding angle
SAED	Selected area electron diffraction

SCCM	Standard cubic centimetre per minute
SDS	Sodium dodecyl sulfate
SEC	Specific energy consumption
SEM	Scanning electron microscopy
SFE	Surface free energy
SGMD	Sweeping gas membrane distillation
SiO_2	Silicon dioxide
SMM	Surface modifying macromolecules
$SrSO_4$	Strontium sulfate
SUS	Stainless steel
SWRO	Seawater reverse osmosis
TB	Tri-bore
TCD	Tip-to-collector distance
TCM	Traditional Chinese medicine
TEM	Transmission electron microscopy
TIPS	Thermally induced phase separation
TiO_2	Titanium oxide
TFC	Thin film composite
TGA	Thermogravimetric analysis
TOC	Total organic carbon
TPC	Temperature polarization coefficient
TSS	Turbidity and fine particulates
UF	Ultrafiltration
UTM	Universal testing machine
VIPS	Vapor induced phase separation

VMD	Vacuum membrane distillation
VMEMD	Vacuum multi effect membrane distillation
VODE	Variable coefficient ordinary differential equation
XPS	X-ray photoelectron spectroscopy
XRD	X-ray diffraction

LIST OF SYMBOLS

A	Effective area of the membrane
C	Cold fluid
C_{AGMD}	Mass transfer coefficient
C_{AGMD-G}	Mass transfer coefficient related with the graphene effect
C_p	Permeate concentration
C_f	Feed concentration
C_m	Membrane mass transfer coefficient
C_p	Specific heat capacity
D_{AB}	Water vapor diffusion coefficient
d_h	Equivalent hydraulic diameter
$Flux_E$	Flux of each point
$Flux_I$	Flux of the initial point
g	Gravity
h	Heat transfer coefficient
H	Hot fluid
I_D	D band
I_G	G band
J	Water vapour flux
J_{AGMD}	Water vapour flux by AGMD
J_{AGMD-G}	Water vapour flux by AGMD with graphene effect
J/J_o	Normalized flux
k_x	Transversal thermal conductivity
k_z	Axial thermal conductivity

L	Channel length
LMH	L/m^2h
M_w	Molecular mass of water
P_{avgm}	Log mean air pressure based from both sides of the membrane
P_{avgma}	Log mean air pressure within the air gap
P_C	Water vapor pressure on the air gap layer
P_H	Water vapor pressure on the membrane surface
Pr	Prandtl number
P_T	Total pressure of water vapor and air
P_w	Vapor pressure of pure water
r	Membrane pore radius
R	Universal gas constant
R_a	Mean roughness
R_{AGMD}	Total mass transfer resistance in the AGMD
γ_m	Surface tension of the membrane in contact with air
γ_{ml}	Surface tension of the membrane in contact with liquid
γ_l	Surface tension of liquid in contact with air
γ_m^T	Total surface free energy
γ_m^{LW}	Lifshitz van der Walls interaction of the membrane
γ_m^{AB}	Lewis acid-base interaction of the membrane
γ_m^+	Electron acceptor parameter
γ_m^-	Electron donor parameter
Re	Reynolds number
R_G	Molecular diffusion resistance related with the graphene effect

R_K	Knudsen diffusion resistance
R_M	Molecular diffusion resistance
$R_{M\text{-}air}$	Molecular diffusion resistance in the air gap
RT	Room temperature
SR	Salt rejection ratio
$T_{avg,a}$	Average temperature based from both sides of the membrane
$T_{avg,m}$	Average temperature at the air gap
u	Flow velocity
W_1	Weight of the saturated membrane
W_2	Weight of the dry membrane
x_{NaCl}	Mole fraction of NaCl
x_w	Mole fraction of water
t	Operating duration
γ_w	Activity coefficient of water
δ	Thickness
δ_m	Membrane thickness
δ_a	Air gap thickness
Δg	Mass of permeate
ε	Membrane porosity
k	Thermal conductivity
λ	Latent heat of water
μ	Viscosity
ρ	Liquid density
ρ_e	Density of ethanol

ρ_d	Density of PVDF material
τ_m	Membrane pore tortuosity
Γ	Total flow rate of condensate at the bottom of the condensing surface
air	Air
cf	Condensate film
cp	Cooling plate
f	Feed
fl	Fluid
gap	Air gap
m	Porous membrane
si	Solid membrane

ABSTRACT

In recent decades, many regions of the world suffer from water scarcity, which is one of the most critical issues in the world. The main challenge is to supply fresh water to water shortage regions. In addition, waterborne illness has been caused through the consumption of the contaminated drinking water in these regions. Seawater desalination is one of the alternative ways to produce freshwater. However, current desalination technologies like reverse osmosis (RO), multi-stage flash (MSF), and multi-effect distillation (MED) have several issues such as high energy consumption, a low recovery rate of total water, and large footprint. Among the several techniques to replace conventional desalination techniques, membrane distillation (MD) is one of the promising technologies. Currently, microfiltration (MF) membranes are implemented for MD application due to their suitable pore size distribution. However, some properties of MD are still needed to be enhanced, especially the high hydrophobicity to avoid membrane pore wetting and high porosity to increase permeate flux. With the development of nanotechnology, electrospinning is becoming a promising technology to fabricate hydrophobic and highly porous membranes. Thus, the objectives of this dissertation are to fabricate a suitable membrane for MD technology by electrospinning technique.

Novel nanofiber membranes fabricated by electrospinning technique are herein proposed for MD application to treat seawater and RO brine from coal seam gas (CSG) produced water. The electrospun membrane could be tailored to have superhydrophobicity, high porosity, adequate pore sizes and narrow pore size distribution, and thin thickness, so it could be used in applications of high-performance MD process. To further improve the MD performance of the electrospun membranes,

three different methods were considered: (i) Janus-type hydrophobic/hydrophilic nonwoven membrane to reduce mass transfer resistance, (ii) nano-materials embedded membrane to improve liquid entry pressure (LEP), and (iii) surface modification of electrospun membranes to treat challenging wastewater sources.

Janus-type hydrophobic/hydrophilic dual-layer nanofiber nonwoven membranes were initially fabricated by a facile electrospinning technique and applied for desalination by air gap MD (AGMD). As-spun neat single and dual-layer nanofiber membranes composed of a hydrophobic polyvinylidene fluoride-co-hexafluoropropylene (PH) top layer with different supporting hydrophilic layer made of either polyvinyl alcohol (PVA), nylon-6 (N6), or polyacrylonitrile (PAN) nanofibers were fabricated with and without heat-press post-treatment. Surface characterization showed that the active layer (i.e., PH) of all electrospun nanofiber membranes (ENMs) exhibited a rough, highly porous (>80% porosity), and hydrophobic surface (CA > 140^{o}), while the other side was hydrophilic (CA<90^{o}) with varying porosity. Heat-pressing the membrane resulted to thinner thickness (from >129 μm to <100 μm) and smaller pore sizes (<0.27 μm). The AGMD experiments in a cross-flow set up were carried out with constant inlet temperatures at the feed and permeate streams of 60 ± 1.5 and 20 ± 1.5 ˚C, respectively. The AGMD module had a membrane area of 21 cm^2 and the thickness of the air gap was 3 mm. The neat single and dual-layer ENMs showed a water permeate flux of about 10.9 ~ 15.5 L/m^2 h (LMH) using 3.5 wt % NaCl solution as feed, which was much higher than that of a commercial PVDF membrane (~ 6 LMH). The provision of a hydrophilic layer at the bottom layer enhanced the AGMD performance depending on the wettability and characteristics of the support layer. The PH/N6 dual-layer nanofiber

membrane prepared under the optimum condition showed flux and salt rejection of 15.5 LMH and 99.2 %, respectively, which has good potential for AGMD application.

Three different nanomaterials were incorporated in polymeric solutions for the improvement of liquid entry pressure (LEP), which were carbon nanotubes (CNTs), graphene, and hexagonal boron nitride (h-BN). Firstly, superhydrophobic, robust, mixed PH nanofiber membranes were fabricated incorporating CNTs as nanofillers to impart additional mechanical and hydrophobic properties. The electrospun membrane has been designed to have two cohesive layers, a thin CNT/PH top layer and a thick neat PH bottom layer. Through different characterization techniques, CNTs were found to be widely distributed on/in the nanofibers, where more beads-on-string were formed at higher CNT content. However, the beads-on-string did not significantly affect the membrane porosity and pore size, as well as did not degrade the MD performance. Highly-porous structure was observed for all membranes and the nanofiber membrane showed comparable pore sizes with a commercial flat-sheet PVDF membrane but at a much higher porosity (>85%). The contact angle increased to higher superhydrophobicity at 158.5^{o} upon the incorporation of 5 wt% CNTs in the nanofiber due to increased roughness and added effect of hydrophobic CNTs. The liquid entry pressure also increased when 5 wt% CNT was added compared to the neat PH nanofiber membrane. The resulting flux of the 5 wt% CNT-incorporated nanofiber membrane (24-29.5 L/m^{2}h) was consistently higher than the commercial PVDF membrane (18-18.5 L/m^{2}h), with an average increase of 33-59% depending on the feed water type (35 or 70 g/L NaCl solution) without compromising the salt rejection (>99.99%). The present nanofiber membranes containing CNTs with one-step electrospinning fabrication show high potential for direct contact MD (DCMD) desalination application.

The following study demonstrated the development of a graphene-loaded electrospun nanofiber membrane and evaluation of their desalination performance in AGMD. Different concentrations of graphene (0-10 wt%) were incorporated in/on electrospun PH membrane to obtain a robust, and superhydrophobic nanocomposite membrane. The results showed that graphene incorporation has significantly enhanced the membrane structure and properties with an optimal concentration of 5 wt% (i.e., G5PH). Characterization of G5PH revealed membrane porosity of >88%, contact angle of >162^{o} (superhydrophobic), and high LEP of >186 kPa. These favorable properties led to a high and stable AGMD flux of 22.9 L/m^{2}h or LMH (compared with ~4.8 LMH for the commercial PVDF flat-sheet membrane) and excellent salt rejection (99.99%) for 60 h of operation using 3.5 wt% NaCl solution as feed (feed and coolant inlet temperatures of 60 and 20^{o}C, respectively). A two-dimensional dynamic model to investigate the flux profile of the graphene/PH membrane is also introduced. The present study suggests that exploiting the interesting properties of nanofibers and graphene nanofillers through a facile electrospinning technique provides high potential towards the fabrication of a robust and high-performance MD membrane.

Another study focused on h-BN embedded nanofiber membrane to maintain flux stability in a long-term AGMD process. The hexagonal lattices of the BN nanoparticles (BNNPs) were modified by hydroxide-assisted ball milling without damage occurred during the exfoliation processes, and they were encapsulated in PH electrospun nanofiber membrane. Characteristics of the BN-PH membrane indicated almost similar regarding membrane thickness, fiber size, porosity and pore size. However, contact angle (153.2^{o}) and LEP (214 kPa) of the BN-PH membrane were higher than that of the neat PH membrane, which showed that the BN-PH membrane could have less wetting

issues compared with the neat PH membrane. Besides, thermal conductivity of the neat PH and BN-PH was 0.025 W/mK and 0.009 W/mK, respectively, as expected that the BN-PH membranes could lead to a high MD water vapor flux performance due to reduced mass transfer resistance and also reduction in conductive heat loss via the membrane. The initial water vapor flux of the neat PH membrane was 11.42 LMH, however, it suffered wetting problem in less than 4 h operation. On the other hand, the BN-PH membrane showed a stable water vapor flux (18 LMH) and salt rejection (99.99%) performances even after 280 h of MD operation. This membrane has a good potential for long-term application of MD for seawater. Future interest in this study may be to find a mechanism for the improved water vapor flux performance of the BNNPs enabled electrospun nanofiber MD membrane.

MD process is also considered to treat wastewater or other challenging wastewater such as the one from textile, dye, and oil industries. However, MD membranes should be improved for preventing membrane wetting issues commonly caused by low surface tension liquids such as surfactants, benzene, methanol, and hexane. Thus, this study described the development and performance of an omniphobic poly(vinylidene fluoride) (PVDF) membrane fabricated by electrospinning and surface-modified by CF_4 plasma, for AGMD. The effect of different duration of plasma treatment on the nanofiber membrane characteristics was investigated. The AGMD performance of the membranes was evaluated using real RO brine produced from CSG produced water that was added with low surface tension liquid (surfactant) as feed solution. Results indicated the formation of new CF_2-CF_2 and CF_3 bonds after plasma treatment, which lowered the surface energy of the membrane, providing omniphobic property, as indicated by its wetting resistance to different low surface tension liquids such as methanol, mineral oil

and ethylene glycol. Though no appreciative changes in morphology of the membrane were observed after plasma treatment, optimal treatment condition of 15 min (i.e., P/CF-15 membrane) exhibited lotus effect membrane surface with increased LEP of 187 kPa compared to 142 kPa for neat membrane. AGMD performance showed stable normalized flux (initial flux of 15.3 L/m^2h) and rejection ratio (99.99%) for P/CF-15 even with the addition of up to 0.7 mM sodium dodecyl sulfate surfactant to the RO brine from CSG produced water feed, while commercial PVDF membrane suffered membrane wetting after 0.3 mM of surfactant addition. Based on the results, the present omniphobic membrane has good potential for producing clean water from challenging waters containing high salinity and organic contaminants.

The aim of this study is the development of suitable electrospun nanofiber membranes for MD. This study mainly focuses on the newly-developed one-dimensional and two-dimensional nano-materials embedded nanofiber membranes, which suffer less wetting issue and have improved water vapor flux performance in MD. It also investigates a simple surface modification technique to generate anti-wetting property on the membrane surface. Overall, this author successfully fabricated several electrospun nanofiber membranes with enhanced water vapor flux and stable salt rejection performances for the treatment of seawater, seawater RO brine and CSG RO brine by MD applications. The fabricated electrospun nanofiber membranes exhibited better performances than the commercial PVDF membranes due to their suitable morphologies and characteristics for MD application. Thus, proper membranes were fabricated which led to enhanced membrane properties such as superhydrophobicity and anti-wetting property. And their MD performances have been compared with the ones in the previous reports. This study may therefore contribute to future MD researches regarding

using electrospinning for the developments of a commercial electrospun nanofiber MD membrane.

TABLE OF CONTENTS

LIST OF FIGURES

LIST OF TABLES

CHAPTER 1

University of Technology Sydney
FACULTY OF ENGINEERING

INTRODUCTION

1.1 Introduction

Water scarcity is one of the most critical issues in the world at present. Nowadays, billions of people lack access to drinking water (Shannon et al. 2008). Most of the water resources on the earth are seawater (approximately 97%) while only 3% are freshwater. Even though human society has realized that water scarcity is a critical problem, it cannot be easily solved at present. To solve the issue, seawater desalination is considered as one of the practical technologies to increase the freshwater supply. Total capacity of seawater desalination plants is growing continuously to around 95.6 million ton/d in more than 120 countries (**Fig. 1.1**). Currently, seawater reverse osmosis (SWRO) desalination is considered as the first-priority system to be implemented into seawater desalination plants due to its lower cost and smaller foot-print compared with conventional thermal-desalination technologies even though it has several disadvantages such as membrane fouling and high management costs.

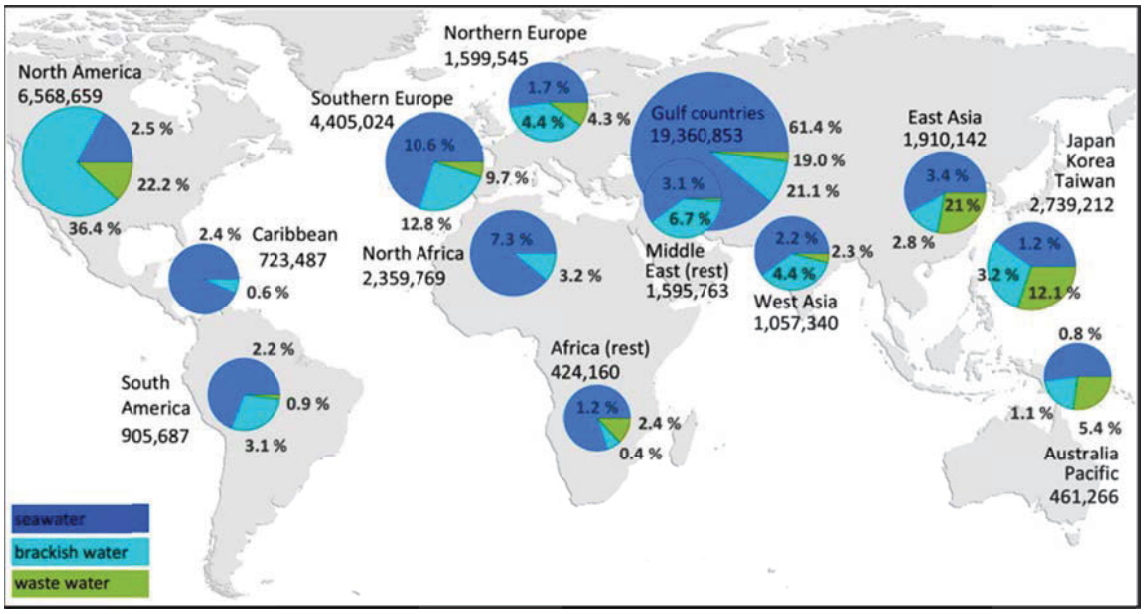

Figure 1.1. Desalination capacities installed in the World and percentages of feed water type (Shahzad et al. 2017).

Recently, several alternative processes such as membrane distillation (MD), forward osmosis (FO), capacitive deionization (CDI), and reverse electrodialysis (RED) have been developed desalination technologies (Chekli et al. 2016). Among all process, MD is becoming popular for its potentials to replace reverse osmosis (RO) in desalination process in terms of reducing the total volume of brine and total cost (Zhao et al. 2017). MD is a thermally-driven membrane separation process which can be applied in various applications such as seawater and brackish desalination, RO/multi effect distillation (MED)/multi-stage flash (MSF) brine treatment, resource recovery, treatment of mine and gas produced water, and wastewater reclamation. The number of studies about MD has been increasing through the years (Ge et al. 2012; Huang et al. 2016; Suárez et al. 2015; Tijing, Choi, et al. 2014; Zodrow et al. 2014). Fundamentally, MD has some advantages including high rejection of non-volatile components, lower operation pressure than RO, and lower operating temperature and smaller foot print than conventional distillation processes (Lawson & Lloyd 1997).

Figure 1.2 describes the schematic diagram of the four different MD configurations. MD has four different configurations, which are direct contact membrane distillation (DCMD), vacuum membrane distillation (VMD), sweeping gas membrane distillation (SGMD) and air gap membrane distillation (AGMD) (Wang & Chung 2015). A large number of researches have massively studied and compared the different MD configurations in terms of energy efficiency, heat loss, flux performance, etc (Alkhudhiri, Darwish & Hilal 2012; Essalhi & Khayet 2012, 2014; Fan & Peng 2012).

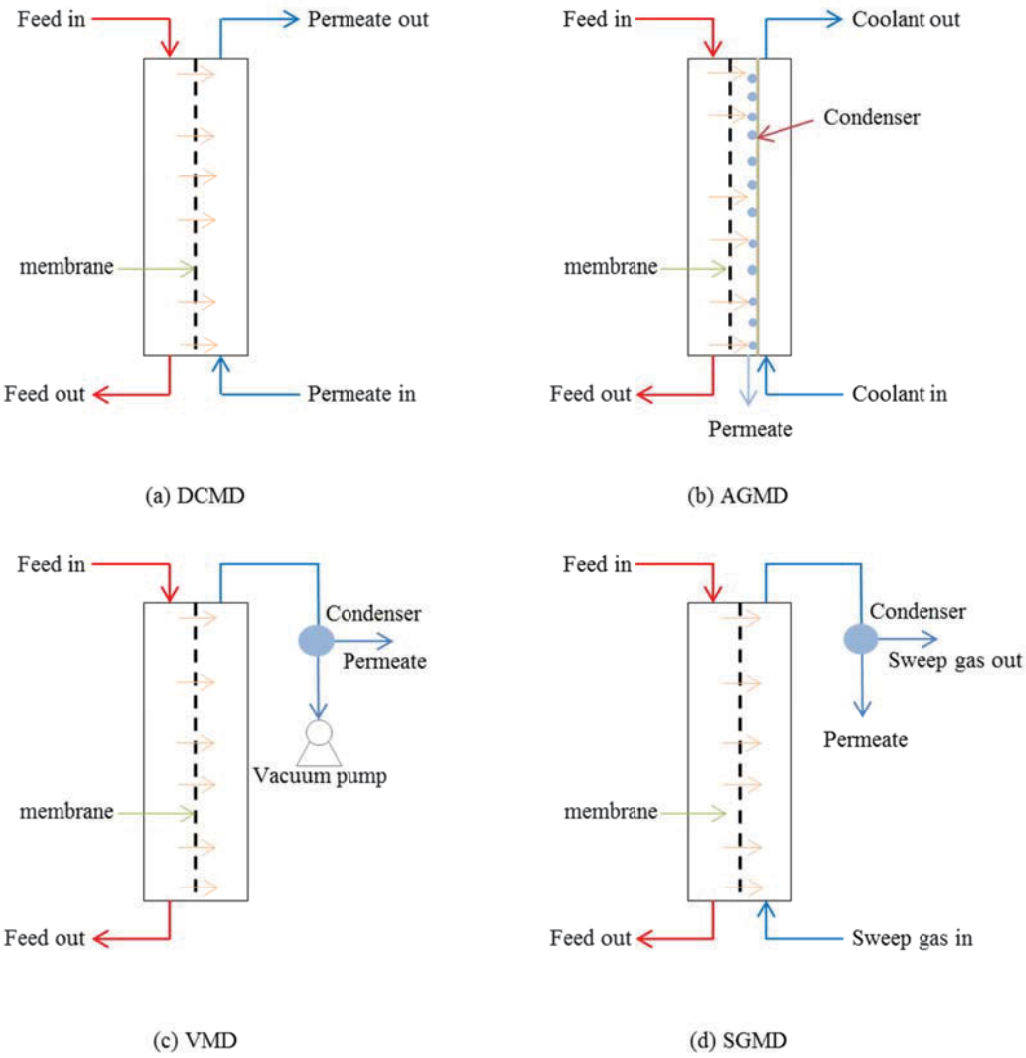

Figure 1.1. Different configurations of membrane distillation (MD) application: (a) Direct contact MD (DCMD), (b) Air gap MD (AGMD), (c) Vacuum MD (VMD) and (d) Sweep gas MD (SGMD).

In general, MD has two main challenges, which are high energy requirement for heating feed and inadequate membranes designed specifically for MD. The first one could be possibly addressed by utilizing renewable energy such as solar heat, or by employing waste or low-grade heat, due to the fact that MD can be operated at low temperatures. The lack of appropriate membranes especially designed for MD is another challenge (Drioli, Ali & Macedonio 2015; Geng et al. 2014; Khayet 2011).

In MD application, pure water vapor can penetrate via a high porous hydrophobic membrane from a hot feed side to cool permeate side (Li, Wang, et al. 2014). Currently, microfiltration (MF) membranes are used for MD even though it is the hydrophilic membrane. However, the MF membrane has limitations in terms of water permeability and membrane for a long-term MD operation due to its hydrophilicity (Su et al. 2017). Thus, there is a strong need to improve the design and structure of current MD membranes.

The main scopes of the membrane fabrication for MD application are improving water vapor permeability, mitigating fouling and scaling, preventing wetting issues. To accomplish these aims, several characteristics should be considered for MD. The characteristics of the MD membrane are high hydrophobicity (contact angle > 130°) and porosity (> 75%), narrow pore size (mean pore size < 0.6 μm), low thermal conductivity, thin membrane thickness, etc (Tijing, Choi, et al. 2014).

To fabricate a membrane, a large number of typical techniques such as sol-gel, spin-coating, track-etching, stretching, non-solvent induced phase separation (NIPS), thermally induced phase separation (TIPS), hollow fiber spinning, etc. have been applied (Lalia, Kochkodan, et al. 2013). The conventional techniques for MD have several drawbacks such as low hydrophobicity and low porosity, which consequently affect the membrane permeability and salt rejection (Lalia, Kochkodan, et al. 2013; Nejati et al. 2015). In recent years, electrospinning and 3D printing techniques have also been introduced to fabricate membranes for water purification (Low et al. 2017; Yao et al. 2017). However, the 3D printing technology is still at its infancy and its limitation,

especially on control of membrane pore sizes, and vast improvements in the future (Lee, Tan, et al. 2016).

Electrospinning is a well-developed technique to fabricate membranes by applying high electric fields on a polymer solution (Ahmed, Lalia & Hashaikeh 2015). Electrospun membranes have many advantages such as high surface area and porosity and adjustable membrane thickness and pore sizes, making them one of the most attractive candidates in membrane fabrication techniques (Yao et al. 2016).

Electrospinning can be utilized to fabricate support layer for ultrafiltration (UF), nanofiltration (NF), RO, FO, and pressure retarded osmosis (PRO) applications as well as active layer for MF and MD processes. It is a very versatile technique to produce suitable membranes for various processes (Feng et al. 2008). Thus, the technique to fabricate membrane for water treatment including desalination has been investigated.

Electrospun nanofiber membranes have garnered wide interest in the recent years as potential membranes for MD due to their unique characteristics (Liao et al. 2014). These membranes are fabricated through an electrospinning process, wherein a high voltage is applied to a polymer solution, which is emitted into jets and form into submicron-sized fibers and collected as a non-woven flat-sheet membrane. The overlapping structure of the nanofiber provides rough nano-scale surface which leads to increased hydrophobicity that is ideal for the MD process (Tijing, Choi, et al. 2014).

In the present study, the electrospinning is used to fabricate an ideally designed MD membrane. Developing a specially designed MD membrane is the most important factor to enhance both water vapor flux and salt rejection performances. For a high water permeate performance in MD, a narrow pore size distribution, high porosity, thin

thickness, high hydrophobicity and liquid entry pressure, and high thermal stability can be achieved on the MD membranes by the electrospinning technique.

1.2 Objectives and scope of the research

In recent years, the electrospinning technique has been studying for MD (Essalhi & Khayet 2013b; Lee, An, et al. 2016). However, it still needs to improve more to fabricate a proper MD membrane. The main objective of this study is therefore to fabricate appropriate membranes for MD application by electrospinning and evaluates its water vapor permeability and salt rejection performances. To improve water vapor permeability and prevent membrane wetting issues in MD, dual-layer electrospinning and nanoparticles embedded electrospinning techniques and a surface modification technique are proposed in the present study. The following are some of the specific objectives of the present study:

- To fabricate hydrophobic/hydrophilic dual-layer electrospun nanofiber membra ne to reduce mass transfer resistance for improvement of water permeability in MD
- To incorporate new nano-materials such as carbon nanotubes (CNTs), graphene and boron nitride (BN) due to their nature of hydrophobic property, which can be embedded in/on the electrospun nanofiber membrane to enhance their hydro phobic property and to improve water vapor permeability while maintaining a h igh salt rejection during MD application
- To apply CF_4 plasma modification methods on the membrane surface to acquire omniphobic property for the treatment of RO brine from CSG produced water

containing low surface tension liquids. CF_4 plasma modification can enhance anti-wetting properties of the membrane.

1.3 Structure of the study

The thesis consists of eleven chapters. Research backgrounds, objectives and scope of the study are presented in Chapter 1 (Introduction).

Chapter 2 covers literatures about membrane based desalination techniques, challenges of MD, techniques for membrane fabrication, and MD fouling and cleaning.

Chapter 3 provides information regarding materials and methods used in the present study.

Chapter 4 introduces the fabrication of hydrophobic/hydrophilic dual-layer composite membrane to reduce mass transfer resistance by a new versatile electrospinning technique.

Carbon nanotubes (CNTs) incorporated on/in electrospun nanofiber membrane to enhance water vapor permeability is developed in Chapter 5.

Chapter 6 suggests graphene nanofiber composite membrane to improve stability of permeability. Also, it investigates new coefficients for graphene nanofiber membrane using two-dimensional modeling.

Chapter 7 focuses on the fabrication of a boron nitride (BN) material and embedded on/in electrospun nanofiber membranes for seawater desalination in long-term MD application.

In order to improve a hydrophobic property and generate an omniphobic property, CF_4 plasma modified electrospun nanofiber membrane is described in Chapter 8.

Chapter 9 summarizes the specific findings at the end of each of these chapters. In addition, it presents the outcomes, concluding remarks, and recommendations for future researches.

CHAPTER 2

University of Technology Sydney
FACULTY OF ENGINEERING

LITERATURE REVIEW

2.1 Introduction

The present chapter describes a brief review associated with membrane distillation (MD) process to treat seawater and various wastewater sources. It begins with a general review of global water problems. This study also exhibits the important roles of the desalination which is one of the solutions to water scarcities, and several challenges in desalination technologies are covered. The review mainly presents the overall membrane distillation (MD) application. Especially, this study reports the membrane fabrication and modification techniques such as phase inversion, electrospinning, and surface modification for MD. Regarding the fouling and scaling, and chemical and other cleaning methods of MD membrane is studied. Various potential applications of MD are also discussed.

2.2 Global water scenario

Billions of people are suffering from many life-threatening issues such as epidemics, abnormal climate, and desertification around the world. Among these issues, water scarcity is one of the most critical global threats (Elimelech & Phillip 2011; Shannon et al. 2008). The majority of the water (approximately 97%) on Earth exists in oceans, which are saline, while the rest is freshwater. Freshwater is present in glaciers in the Arctic and Antarctic (68.7% of the freshwater), groundwater (30.1%), and stream/surface water (0.3%) (Gleick & Palaniappan 2010; Shiklomanov 1993). For the stream water, around 87% consists of lakes and swamps, which indicates that, at most, only 1% of the total water found on Earth is directly accessible for consumption. Water scarcity is affecting approximately 1.5 billion people, with another two billion is lacking the necessary technologies to obtain freshwater from rivers and ponds. Water scarcity

also leads to the hampered development in industrial and agricultural areas (Jackson et al. 2001; Shirazi, Kargari & Shirazi 2012).

Even though human society has realized that water scarcity is a critical problem, it cannot be easily solved at present because of the lack of new freshwater sources (Gagliardo et al. 1998). Therefore, two potential new water resources which are seawater and wastewater have been identified. Wastewater reclamation and seawater desalination have been deemed as major alternative water resources to release the water-stress in the world (Fragkou & McEvoy 2016).

Wastewater reclamation is suitable for producing non-potable water, but not for drinking purposes. Wastewater is still not enough to overcome water scarcity due to its low total volume (Garcia & Pargament 2015). Approximately 97% water in the world is seawater and therefore, seawater desalination is the most suitable technology to meet the increasing fresh water demands (Sahin, Stewart & Porter 2015). Moreover, natural organic matters (NOMs), bacteria and oil in seawater are much lower compared with the ones in wastewater and groundwater. Thus, seawater is more proper water resources to produce freshwater for drinking.

At present, seawater desalination plants have been operated in more than 120 countries around the world. Desalination plants have become the largest fresh water suppliers in the world (Shalaby 2017). Three decades ago, conventional thermal desalination plants needed large foot prints for a big capacity of water production. However, after that, reverse osmosis (RO) desalination plants appeared and are gradually replacing the conventional processes, as they require much less foot prints with higher capacity of water production. Since two decades ago, the introduction of energy recovery device

(ERD) for the RO desalination process has led to saving of up to 60% energy during operation (Harris 1999). Thus, RO desalination plants have been considered as the first-priority system to be implemented into seawater desalination plants at present (Shahzad et al. 2017; Shalaby 2017).

In order to reduce the energy consumption for desalination, several alternative processes such as membrane distillation (MD), forward osmosis (FO), pressure retarded osmosis (PRO), capacitive deionization (CDI) and reverse electrodialysis (RED) have been emerging for their potentials to replace or in conjunction with RO desalination process (Drioli & Macedonio 2010). Many studies are investigating these processes to develop a commercial desalination plant for reducing energy consumption and increasing the capacity of fresh water production (Chekli et al. 2016; Elimelech & Phillip 2011; Lin, Yip & Elimelech 2014; Xie et al. 2013; Yip & Elimelech 2014). It is believed that these new technologies will eventually be fully commercialized. This chapter is an extension of the research article published by the author in Journal of Membrane Science.

2.3 History of seawater desalination technologies

Seawater desalination process has a long history. Seawater is highly saline (salt concentration of approximately 35 g/L), which is not suitable for humans to directly drink and use for a wide range of purposes even though it composes 97% of the Earth's water. However, increasing potable water demands and the deficiency of surface water lead to the development of desalination technologies to obtain freshwater from seawater. In the mid-1600s, the first desalination process was used, which was a distillation system on the ship for the British Navy (**Fig. 2.1**). Afterward, the first patent regarding the desalination was presented as a distillation method in 1675. Also, a steam

distillation plant was constructed in 1869 in Britain, which was the first desalination plant on the land to recharge the freshwater supplies to ships at anchor in the harbor (Technology 2008). Since 1928, a desalination plant was established applying the distillation method on the island of Curacao in the Netherlands, which was the first plant to supply water for people living on land. Regarding the regions, desalination processes are very essential for the Middle East, Persian Gulf and North Africa as they are suffering from water scarcity due to their arid climates. During the World War II, many researchers conducted studies on desalination processes when the military needed access to fresh water in water scarcity regions. Many countries continued the researches to gain freshwater via desalination for human being despite the end of the war.

In the 1960s, an initial version of a modern distillation plant in Kuwait was established applying multi-stage flash (MSF) with a capacity of 4545.5 m^3/d. MSF involved flashing some of seawater into steam and repeating the process at a lower temperature (pressure), so the seawater became steam that is condensed to produce fresh water.

In 1977, UAE made the first attempt to build a multi effect distillation (MED) process with a capacity of 91 m^3/d. MED can produce freshwater in the following procedure: Seawater enters the first effect vessel and is raised up to 100°C by pre-heated tubes (Choi 2016; Nghiem et al. 2015). Then it is sprayed onto the surface of tubes in a thin film to advance boiling and evaporation. The tubes are then heated by the steam from a boiler, which is condensed on the opposite sides of the tubes.

Both MSF and MED processes consist of multiple stages or chambers to reduce the vacuum in different stages or chambers, which lead to a decrease in heat loss except additional heat. Nghiem et al. (Nghiem et al. 2015) reported that in terms of the specific

energy consumption (SEC), the MED is almost half that of the MSF. Many desalination plants (approximately 35.5%) have utilized both MSF and MED processes to produce freshwater (Choi 2016).

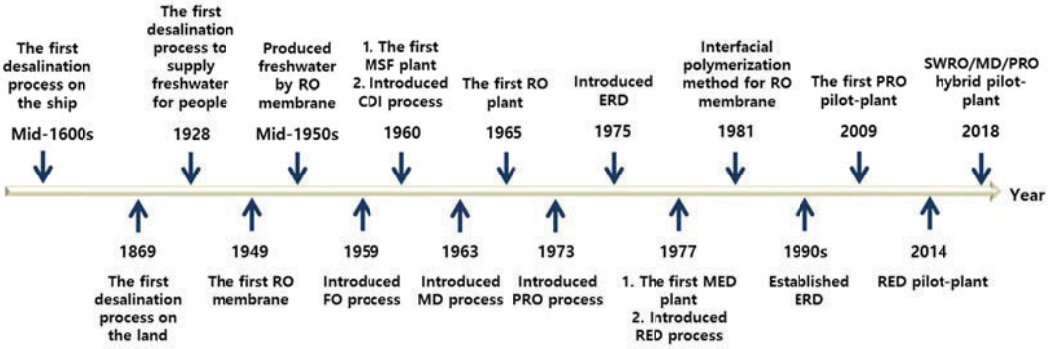

Figure 2.1. Timeline of the development of desalination technologies

Nevertheless, both systems showed a high SEC, suggesting that it should cost a lot to produce freshwater (**Table 2.1**). To reduce total cost of the desalination plant, membrane technology has risen rapidly as one of the alternative technologies in addition to both MSF and MED processes for seawater desalination since 1950s. Especially, reverse osmosis (RO) process has become the most popular membrane technology to treat seawater since 1980s. The first attempt of the RO desalination plant was in the United States in 1965. RO utilizes a semi-permeable membrane (Gagliardo et al. 1998) and therefore the seawater RO (SWRO) process needs to accommodate many pre-treatments to reduce fouling issues at the RO stage.

As shown in **Fig. 2.2**, driving force of the feed in RO is a high pressure (over 40 bar). High saline water as the feed is flowing into a RO module under high pressure. After that, fresh water is obtained as basically only water penetrates the semi-permeable RO membrane. Many studies have been conducted investigating for RO process as RO could be more efficient than thermal technologies due to its relatively lower energy

consumption (Ebrahim, Jawad, et al. 2001; Greenberg, Hasson & Semiat 2005; Qi et al. 2016). The RO process has also been used to produce freshwater from seawater. Currently, there are more than 18,000 desalination plants including MSF, MED and RO worldwide with a maximum production capacity of approximately 95.6 million m^3/d in more than 120 countries (Virgili & Pankratz 2017).

Table 2.1. Classification and overview of desalination technologies

Classification by	Thermal	Membrane
Desalination technologies	MSF and MED	NF, FO, PRO and RO
Separation mechanism	Phase change	Diffusion
Main type of energy requirements	Thermal	Electricity
Driving force	Heat	Pressure
Specific energy consumption	High	Low

2.4 Improvements of desalination technologies

2.4.1 RO technologies

Currently, the RO process is replacing MSF and MED in desalination plants due to its lower energy consumption and less operating cost (**Fig. 2.2**). **Fig. 2.2(a)** shows the SEC of each process compared to energy consumption in desalination plants. In 1970s, SWRO processes had a high SEC, which was similar to MSF and MED processes. However, in 2010s, two major achievements are responsible for the reduction of SEC in RO process, which are: (a) significant improvement of RO membrane and (b) development of energy recovery device (ERD). RO uses electrical energy as the highly

dominant portion of the total energy cost for desalination (**Fig. 2.2(c)**). Therefore, the RO processes minimize the use of total energy in desalination plants compared with other processes, which results in increasing popularity of RO desalination plants to date.

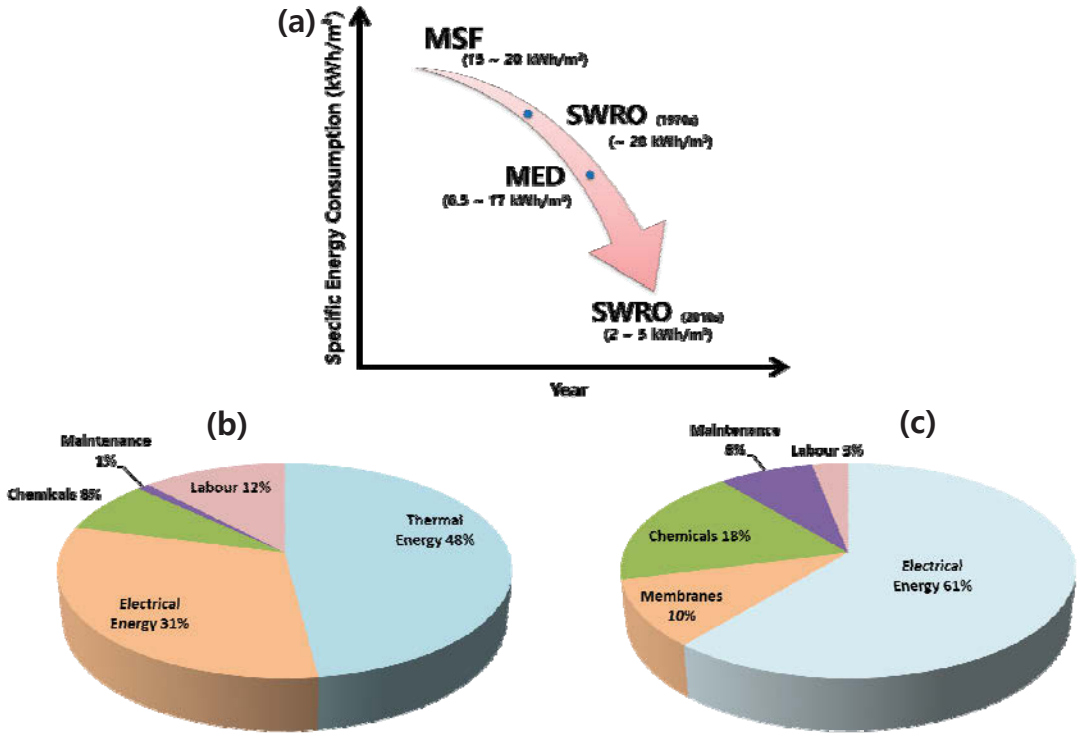

Figure 2.2. (a) Total specific energy consumption (SEC) of each process for seawater desalination. (b, c) Comparison of the operating cost components for MSF and RO technologies (adapted from (Ghaffour, Missimer & Amy 2013; Shahzad et al. 2017)).

2.4.1.1 Development of energy recovery device (ERD)

Generally, RO exhibits high electric energy consumption because of the need of a high hydraulic pressure as a driving force. Thus, a large amount of energy is consumed during SWRO operation without further recovery of energy in the brine, which is wasted eventually.

The ERD is one type of hydraulic devices. It transfers the hydraulic energy of the high pressure brine into mechanical energy and is later converted into hydraulic energy of the low pressure feed (Harris 1999). After the SWRO-ERD integrated process was applied in the 1990s, SEC of the process has significantly been reduced from 20 kWh/m^3 to 2 ~ 5 kWh/m^3. Due to the introduction of ERD, the SWRO process has become the most energy-efficient system compared with the conventional thermal desalination technologies (Ghaffour, Missimer & Amy 2013). Even though energy consumption of SWRO can be reduced by ERD, several issues such as leakage and large amounts of pressure loss during operation still remain to be improved.

2.4.1.2 Evolution of reverse osmosis membrane

A suitable semi-permeable membrane of RO should have high water permeability, good mechanical strength and thermal stability as well as high chemical resistance (Shenvi, Isloor & Ismail 2015). Cellulose acetate is one of the well-acceptable polymers to fabricate RO membrane because of its low protein adsorption, good water affinity, high mechanical strength and low cost. However, cellulose acetate has a low fouling resistance and poor thermal stability. Besides, cellulose acetate RO membranes show a very low flux (Hao et al. 1996).

On the other hand, polyamide (PA) thin film composite (TFC) membrane was developed in the early 1970s, which improved the RO performance drastically. TFC membrane consists of a dense top layer and a highly porous support layer. It has become the most popular membrane fabrication technique for SWRO membranes at present due to its merits such as a high water permeability, low operating pressure, and separation of organic foulants (Choi et al. 2017).

Among many methods to fabricate TFC RO membranes, interfacial polymerization (IP) is one of the most widely used techniques. The PA TFC RO membrane shows salt rejection of 99% with a high water flux as well as a high thermal efficiency although it can be damaged by chlorine and ozone during chemical cleaning (Choi et al. 2013). Many studies are still focusing on the PA TFC membrane for the RO process as well as for FO, nanofiltration (NF), and PRO processes due to its advantages at present (Choi et al. 2013; Choi et al. 2017; Rangarajan et al. 2011).

In general, many SWRO plants are using spiral wound module of RO membrane. Spiral wound module is preferred for SWRO due to easy operation, fouling control, permeation rate, and high packing density even though hollow fiber RO membrane is also available for limited applications.

2.4.2 Hybrid thermal desalination processes

MSF and MED are showing low water production because of the process limitations such as scaling and high energy consumption. An integrated MSF with the MED process has been designed to overcome the limitations of the single process (Dahdah & Mitsos 2014). The hybrid MSF-MED process has several merits like reducing the specific water unit price (32% lower than MSF and 20% lower than MED), decreasing heat transfer area, increasing the water production, and 57% lower SEC than MSF (Dahdah & Mitsos 2014). In addition, by dosing anti-scalants into a pre-treatment process, both processes can increase the temperature up to 130°C, which leads to further improvement of water productivity and reduction in SEC (Shahzad et al. 2017).

Adsorption desalination (AD) is one of the possible processes to operate below ambient conditions for MED process. AD relies on employing adsorbent materials like silica

aerogel (Kim et al. 2016). It mimics the evaporation by a low temperature solar collectors and condensing vapor at a high height to produce pure water. An integrated MED with AD has been studied for improved performance of thermal desalination plants in terms of the water production rate (Thu et al. 2015). The integrated process also showed around 40% improved gain output ratio (GOR) and around 61% reduced SEC compared with a conventional MED process. As well, the MED-AD hybrid process mitigates fouling and scaling because of the low temperature operation of AD (Thu et al. 2015).

2.5 Alternative membrane based-technologies for desalination

In order to decrease the total cost of a desalination plant including the management expenses and initial facility cost, new alternative membrane technologies such as forward osmosis (FO), pressure retarded osmosis (PRO), membrane distillation (MD), capacitive deionization (CDI), reverse electrodialysis (RED), and etc. have been explored (Drioli, Stankiewicz & Macedonio 2011). Their hybrid processes or stand-alone system can save energy consumption.

2.5.1 Forward osmosis

FO utilizes a spontaneous water transport by osmotic pressure from the feed saline water to the draw solution (DS) across a semi-permeable membrane (Phuntsho et al. 2014). The FO process is considered as a suitable pre-treatment for desalination. When FO is used as a pre-treatment for the RO process, it can mitigate membrane fouling and scaling problems at RO stage and reduce energy consumption (Xie et al. 2014). It has a strong potential to establish a seawater desalination plant using FO-RO hybrid system.

The FO-RO hybrid Desalination Research Center (FOHC) has investigated with the aims of this research that are the construction of the FO-RO hybrid pilot plant (capacity of 1,000 m^3/d) and reducing energy consumption approximately 35% compared with the conventional SWRO plant.

Figure 2.3 shows schematic illustration of the FOHC pilot plant. Pre-treated wastewater effluent and pre-treated seawater are used as the feed solution and draw solution, respectively, in the first stage of FO. The diluted seawater from the first stage of FO process is treated by RO process to produce freshwater. Afterward, concentrated wastewater effluent from the first stage of FO and the RO brine are applied as the feed and draw solutions, respectively, for the second stage of FO process. The diluted RO brine from the second stage of FO process can be discharged to sea. Also, a highly concentrated wastewater effluent is used as fertilizers.

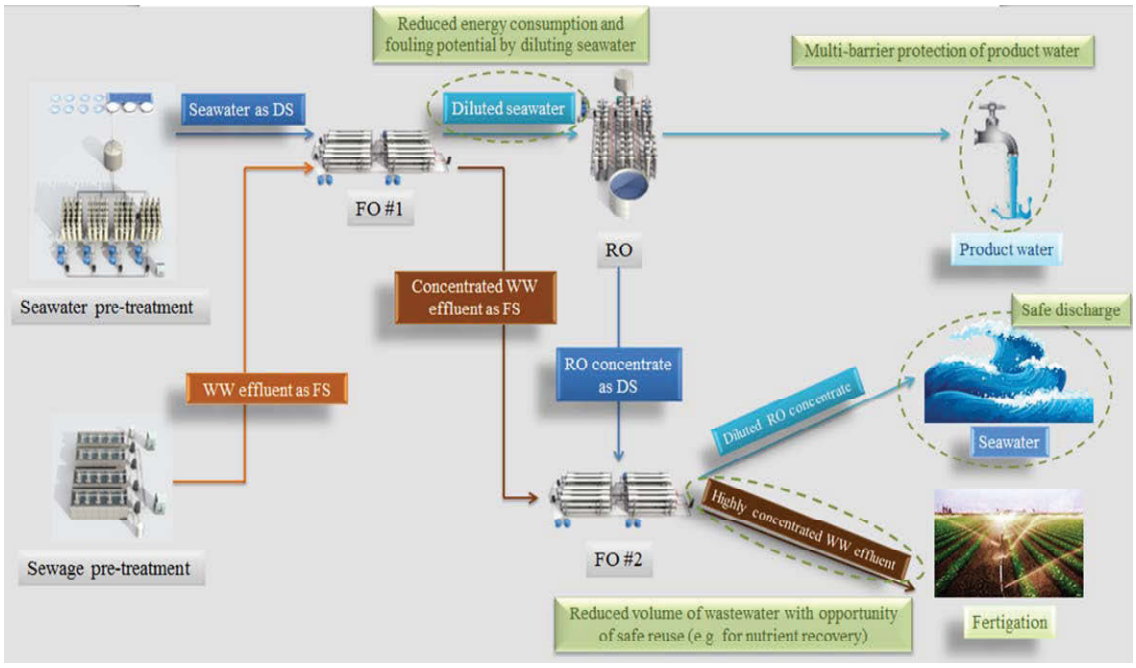

Figure 2.3. Schematic diagram of the FOHC hybrid desalination demonstration plant (adapted from (Chekli et al. 2016))

2.5.2 Pressure retarded osmosis

The other alternative process utilizing spontaneous transport of water is PRO where the driving force is generated from the difference in osmotic pressures between a low salinity feed stream and a pressurized high salinity DS stream. During PRO operation, the osmotic power can be produced by the transmembrane pressure while water penetrating the membrane, which can be harvested as renewable energy (Choi, Vigneswaran & Lee 2016). Despite the benefits of PRO, it still suffers from membrane fouling due to its pressurized operation (Kim, Kim, et al. 2015). Moreover, membrane performance needs to be improved regarding mitigation of fouling and water permeability for the PRO process while numerous studies are expected to improve the flux performance (Han et al. 2013).

In Japan, the Mega-ton Water System was established in early 2010. The scope of the project was to reduce 50% water production cost and 30% energy consumption by incorporation of new ERD with low pressure RO membrane and the PRO process (Kurihara & Hanakawa 2013). PRO is the main target of the Mega-ton Water System for reduction of energy consumption and water production cost. The project also introduced newly developed PRO hollow fiber membrane (Toyobo CTA membrane) module and achieved the power density of 13.3 W/m^2 by prototype plant using a 10-inch module (Kurihara & Hanakawa 2013).

2.5.3 Membrane distillation (MD)

Prolonged research activities to replace the conventional desalination process recently highlight remarkable membrane distillation (MD) technology. MD is one of the

emerging desalination technologies for the production of fresh water. MD is a thermally-driven transport of water molecules (in vapor phase) through porous and hydrophobic membranes. One side of the porous membrane is a hot feed with high salinity and the other side is a cold permeate. The temperature gradient between the two sides creates a pressure vapor difference that drives the vapor to pass through the membrane and collected or condensed to pure water in the other side. MD has reduced sensitivity to concentration polarization, allowing it to operate even at high NaCl concentrations at the feed side (Curcio et al. 2010). MD has several advantages such as: (a) theoretically 100% salt rejection, (b) lower operating temperature than conventional distillation processes, (c) low energy consumption when waste heat or alternative energy source is used, (d) less requirements of membrane mechanical properties, (e) and lower operating pressure compared to conventional pressure-driven membrane processes such as RO (Al-Obaidani et al. 2008; Khayet & Matsuura 2001; Razmjou et al. 2012; Wang, Teoh & Chung 2011; Yang et al. 2011). MD can be employed for water desalination, removal of organic matters in drinking water production, treatment of water and wastewater, recovery of valuable components, and treatment of radioactive wastes (Alkhudhiri, Darwish & Hilal 2013; Banat, Al-Asheh & Qtaishat 2005; Criscuoli et al. 2008; Gryta & Karakulski 1999; Liu & Wang 2013; Zolotarev et al. 1994). However to date, MD has not found large-scale industrial application yet although a number of pilot systems have been carried out in recent years (Banat et al. 2007; Ben Abdallah, Frikha & Gabsi 2013; Guillén-Burrieza et al. 2011; Guillen-Burrieza et al. 2014; Guillén-Burrieza et al. 2012; Koschikowski, Wieghaus & Rommel 2003; Meindersma, Guijt & de Haan 2006; Raluy et al. 2012; Song et al. 2008; Xu, Zhu & Xu 2006). This is due to the fact that there is no commercially-available membrane for MD application because it doesn't find a proper market. Thus, several membrane fabrication

techniques have been applied like phase separation, dip-coating, sol-gel, and etc. (Baghbanzadeh et al. 2015; Efome et al. 2015; Khayet, Matsuura & Mengual 2005; Zhao et al. 2017). However, these membranes still suffer from low water permeability and membrane pore wetting problem. Hence, a new attractive membrane fabrication technique needs to be developed.

2.5.4 Capacitive deionization

CDI, including membrane CDI (MCDI), is an emerging technology for seawater and brackish desalinations (Choi, Lee & Hong 2016). CDI is a different type of desalination processes that remove ions from the saline water stream at atmospheric pressure using direct current (DC) power. Electrodes become positively and negatively charged when DC power applies to CDI electrodes. During CDI operation, ions in saline water are adsorbed on the cathode and anode. After that, ions are desorbed from the electrodes by discharging of CDI. CDI is operated by the charging and discharging processes to produce freshwater (Choi, Lee & Hong 2016).

Even though CDI has some benefits such as energy efficient, cost effective, and high rejection ratio, the commercialization of CDI is limited due to lack of suitable materials for electrodes. Mossad and Zou., (Mossad & Zou 2013) and Li et al., (Li et al. 2010) have explained potential materials like silica nanoparticle, activated carbon, and carbon aerogel to fabricate electrodes.

Mossad and Zou., (Mossad & Zou 2013) used porous activated carbon electrodes with a specific area of 800 m^2/g to apply for a small CDI prototype. Using low salinity feed (< 2,000 ppm), CDI shows the total cost of 0.11 $\$/m^3$, which is lower than RO (0.35 $\$/m^3$). The SEC of CDI is also possible to be reduced at 0.59 kWh/m^3. For high saline water

like seawater, further improvement of CDI is needed to reduce the total cost. When a cheaper and suitable material is found for electrode, CDI can be very competitive with the RO process for seawater desalination. The Korean Optimized RO desalination for Advanced Energy saving (KORAE) has started with the CDI process funded by South Korea. The project aims at reducing SEC at 3.3 kWh/m^3 by the RO-CDI hybrid system.

2.5.5 Reverse electrodialysis

Like the PRO process, extraction of electricity by RED is sustainable since salinity gradient energy is a renewable and environmentally friendly process (Farrell et al. 2017). RED is mainly the combination of high concentration solution like seawater and low concentration solution like tap water and river water. During RED operation, an ionic current is generated by alternately arranged anion and cation exchange membranes, which is converted to an electric current at the electrode by redox reactions (Scialdone et al. 2014). Recently, a number of studies have been focused on ion-exchange membrane based technologies and their pilot-scale experiments (Farrell et al. 2017; Post et al. 2010; Tedesco et al. 2016).

Small and large prototype RED plants have been operated in the South of Italy. It is related to the REAPower project funded by EU. The project uses brine as the high concentration solution and seawater as the low concentration solution. The harvesting energy in the RED plant shows total power and power density of approximately 62 W and 2.6 W/m^2, respectively. Even though it has lower harvesting energy than the Mega-ton Water System in terms of the power density, the project will expand the current plant into bigger size and plan to achieve a power capacity of 1 kW (Tedesco et al. 2016).

2.6 Membrane Distillation (MD)

2.6.1 Overview of MD

MD is mainly used to remove salts from a saline solution through the use of a hydrophobic porous membrane and thermal energy. It is also used to separate heavy metals from contaminated water or to remove trace volatile organic compounds (Banat & Simandl 1996; Chiam & Sarbatly 2013), and to concentrate different kinds of aqueous solutions such as orange juice, whey protein solution and acid solution (Alves & Coelhoso 2006; Christensen et al. 2006; Galaverna et al. 2008; Gunko et al. 2006; Nene et al. 2002; Tomaszewska, Gryta & Morawski 1998). The MD membrane acts as a barrier layer for the separation of vapor and water. Water evaporates at the feed-pore interface, then the water vapor diffuses through the membrane pores, where it is then collected or condensed at the permeate side by different methods (Alkhudhiri, Darwish & Hilal 2012). There are four main MD configurations depending on how the permeate is processed: DCMD, AGMD, VMD, and SGMD (El-Bourawi et al. 2006; Lawson & Lloyd 1997). In recent years, new MD configurations have been employed such as MEMD, MGMD, PGMD, and VMEMD (Dotremont et al. 2010; Essalhi & Khayet 2014; Francis, Ghaffour, et al. 2013; Jansen et al. 2013; Khayet & Matsuura 2011; Winter, Koschikowski & Wieghaus 2011; Zhao, Heinzl, et al. 2013). Heat and mass transfer simultaneously occur during the MD process, wherein the heat transfer resistances across the boundary layers of the membrane surface are often the rate-limiting step (Khayet 2011). The design and structure of the membrane are very important factors to consider for an effective MD process. In fact, the membrane unit is reported to entail 20-25% of the total capital cost of a desalination plant (Dydo et al.

2004). It is essential to understand the factors affecting the membrane performance and lifetime, especially on the issue of fouling, which affects much of the MD efficiency.

The important characteristics of a good MD membrane include high hydrophobicity, high porosity, uniform pore size and narrow pore size distribution, low tortuosity, and thin thickness. Though MD holds a good promise as an alternative to the present pressure-driven processes, it is still not fully commercialized in industrial setting due to the following issues associated with MD: (a) compared to RO, MD has relatively lower permeate flux (Chew, Krantz & Fane 2014; El-Bourawi et al. 2006); (b) temperature and concentration polarization effects and membrane fouling leading to permeate flux decay; (c) membrane and module design for MD; and (d) it is a highly thermal energy-intensive process (El-Bourawi et al. 2006). However, recent progress of the possibility of utilizing low-grade waste heat and solar or geothermal energy sources to save in electrical energy cost has made MD more attractive as an alternative to or in conjunction to RO. Additionally, a lot of efforts have been made in recent years in the fabrication of new and improved MD membrane design and structure including flat-sheet, hollow fiber and nanofiber membranes with high MD flux and salt rejection performance that makes MD more viable for many applications (Alkhudhiri, Darwish & Hilal 2012; Khayet 2011; Tijing, Choi, et al. 2014; Tijing, Woo, et al. 2014).

Long-term stable flux performance and salt rejection are important aspects to consider for the industrial implementation of MD. However, flux decline is usually encountered in MD operation, which is largely caused by temperature polarization effect (El-Bourawi et al. 2006; Martínez-Díez & Vázquez-González 1999), wetting, and membrane fouling. Fouling is a serious problem that when left unaddressed, the MD performance especially for long term will suffer and can cause major damages and costs

in the MD process. It is worth noting that different opinions and results have been reported in literature about the role of fouling in MD. Some studies reported no significant effect of fouling to the MD permeate flux, while other studies showed major drop in flux performance due to fouling. With the rapid expansion of the applications of MD, including treating wastewaters, complex solution make-up and characteristics can be encountered in real-world processes, leading to not only a single component fouling mechanism, but a combination of different fouling mechanisms that would be difficult to control or clean. For example, an investigation of a fouling layer after seawater pretreatment found a combination of organic, inorganic and biological fouling matters (Al-Amoudi & Farooque 2005).

2.6.2 Theoretical background

2.6.2.1 Mass transfer

In MD, the driving force is the gradient of partial pressure of vapor at the interface between the liquid and the hydrophobic membrane, and the trans-membrane flux for mass transfer can be expressed as (Martínez & Rodríguez-Maroto 2007; Schofield, Fane & Fell 1987):

$$J = C_m (p_{fm}-p_{pm}) \quad \text{(eq. 2.1)}$$

where J is the mass transfer flux, C_m is the overall mass transfer coefficient, and p_{fm} and p_{pm} refer to the partial vapor pressures at the feed and permeate vapor-liquid interfaces (Martínez & Rodríguez-Maroto 2007). The vapor pressure is related exponentially to the temperature of the solution (Antoine equation, $p=e^{(A-(B/(C+T)))}$) (Lawson & Lloyd 1997), thus at higher temperature difference, a higher driving force is expected leading to increased permeate flux. Expounding **eq. (2.1)** based on the Knudsen-molecular

diffusion model would lead to the following equation (Phattaranawik, Jiraratananon & Fane 2003):

$$J = \frac{\varepsilon}{\tau\delta}\frac{pD_{AB}}{RT_m} ln \frac{(p-p_{pm})/pD_{AB} + (3/4d)\sqrt{2\pi M_A/RT_m}}{(p-p_{fm})/pD_{AB} + (3/4d)\sqrt{2\pi M_A/RT_m}} \quad \text{(eq. 2.2)}$$

In this equation, all factors affecting the DCMD flux are included such as membrane characteristics (d, ε, δ, τ), temperatures of the feed and permeate fluids (p_{fm}, p_{pm}), diffusivity (D_{AB}) and molecular weight (M_A) of transported component, fluid properties, and dynamics of the fluid in the membrane module (Ding et al. 2010).

Vapor pressure at the feed and permeate sides is affected by temperature at both surfaces of the membrane, which is determined by the resistances offered by polarization effects at both sides of the membrane, and the microporous membrane. However, when the feed solution contains foulants, a fouling layer can be formed on the membrane surface, which could provide additional flux resistance. Several theoretical models have been presented to describe heat and mass transfer in MD (Adnan et al. 2012; Alkhudhiri, Darwish & Hilal 2012; Alklaibi & Lior 2006; Ding et al. 2010; Gilron, Song & Sirkar 2007; Martínez & Rodríguez-Maroto 2007; Schofield, Fane & Fell 1987; Song et al. 2007; Srisurichan, Jiraratananon & Fane 2006; Wang, Li, et al. 2014) including the effect of the fouling layer. The additional layer due to fouling is known to add heat transfer resistance in the MD process. This is particularly true for fouling layers that are porous such as those formed from inorganic salts and cake-forming humic materials. However, there are fouling layers that have very small pores (<50 nm) or free volume, typically due to NOM in the form of proteins, amino sugars, polysaccharides and polyhydroxyaromatics, which usually have thin thickness (<100 μm) (Chew, Krantz & Fane 2014; Goh, Zhang, Liu, et al. 2013; Gryta 2008).

Recent studies (Goh, Zhang, Liu, et al. 2013; Goh, Zhang, Zhang, et al. 2013; Gryta 2008; Phattaranawik et al. 2009) speculated that aside from heat transfer resistance, the gel-like fouling layer with small pores or free volume can add hydraulic resistance to water permeation. However, these studies did not attempt to incorporate the hydraulic resistance due to fouling into an MD model. It was reported that the fouling layer with small pore (typically less than 50 nm) or free volume causes vapor-pressure depression owing to the Kelvin effect leading to the reduction of driving force, and consequently reduced flux (Goh, Zhang, Zhang, et al. 2013). The study explained that liquid water is drawn inside the gel-like hydrophilic biofouling layer via a capillary action, forming a concave liquid/vapor interface within the biofouling layer that results to vapor depression (Goh, Zhang, Zhang, et al. 2013). However, the Kelvin effect was not attempted to incorporate in a model.

In a new study, Chew et al. (Chew, Krantz & Fane 2014) incorporated the effect of hydraulic resistance due to fouling in their DCMD model for MD-membrane bioreactor (MDBR) application. In their study, taking into account the vapor depression at the feed side due to the presence of gel-like biofouling layer with small pores (d < 50 nm), **eq. 2.1** becomes (Chew, Krantz & Fane 2014):

$$J_{vd} = C_m (p'_{fm} - p_{pm}) \quad \text{(eq. 2.3)}$$

where p'_{fm} is the reduced vapor pressure due to vapor pressure depression. The Kelvin equations (Fisher & Israelachvili 1981; Mitropoulos 2008) give the relationship between the reduced vapor pressure and the normal vapour pressure at the feed side expressed as (Chew, Krantz & Fane 2014):

$$ln \frac{p'_{fm}}{p_{fm}} = -\frac{4\gamma V_w}{RT_{fm}d} \equiv -\beta \quad \text{(eq. 2.4)}$$

According to Chew et al. (Chew, Krantz & Fane 2014), depression of p'_{fm}/p_{fm} becomes significant at d < 50 nm, reaching to 46% depression at d = 4 nm. Increasing value of dimensionless β indicates decreasing pore diameter. Incorporating the Kelvin equations (**eq. 2.4)**) into **eq. 2.3** yields the following:

$$J_{vd} = C_m (p_{fm}e^{-\beta} - p_{pm}) \quad \text{(eq. 2.5)}$$

By perturbation expansion in the small parameter β, which characterizes the pore diameter, and further solution truncating after the first order, the mass flux considering the effect of vapour pressure depression owing to Kelvin effect is expressed as (Chew, Krantz & Fane 2014):

$$J_{vd} = J - C_m p_{fm} \beta \quad \text{(eq. 2.6)}$$

Eq. (6) indicates that the Kelvin effect reduces the flux by a factor of $C_m p_{fm} \beta$. Converting **eq. (6)** into a normalized equation results to:

$$\frac{J_{vd}}{J} = 1 - \frac{1}{1-\left(\frac{p_{pm}}{p_{fm}}\right)}\beta = 1 - \left[\frac{1}{1-\left(\frac{p_{pm}}{p_{fm}}\right)}\left(\frac{4\gamma V_w}{RT_{fm}d}\right)\right] \quad \text{(eq. 2.7)}$$

2.6.2.2 Heat transfer

Heat transfer in the MD process can be analyzed from the resistance of transport process. The resistances to heat transfer without fouling involves three main sections: the resistances due to the hydrodynamic boundary layers at the feed and permeate sides, and the membrane resistance. When a fouling layer is present, the layer provides an additional thermal resistance to heat transfer. The four heat transfer steps have their own driving force and thermal resistances, and in a steady state condition, the heat transfer is equal to each other and is expressed as follows (Chew, Krantz & Fane 2014; Ding et al. 2010):

$$q = \frac{t_f - t_{fl}}{R_1} = \frac{t_{fl} - t_{fm}}{R_2} = \frac{t_{fm} - t_{pm}}{R_3} = \frac{t_{pm} - t_p}{R_4} = \frac{1}{R_t}\left(t_f - t_p\right) \quad \text{(eq. 2.8)}$$

where $R_1 = 1/h_1$ and $R_4 = 1/h_4$ are convective heat transfer resistances associated with the hydrodynamic boundary layers at the feed and permeate sides, respectively; $R_2 = \delta_2/k_2$ is associated with the heat conduction at the fouling layer, and $R_3 = \frac{1}{\frac{1}{R_m} + \frac{1}{R_v}} = \frac{1}{(k_m/\delta_m) + \lambda C_m\left(\frac{dp}{dT}\big|_{T_m}\right)}$ is associated with the heat conduction at the membrane (considering the solid part and the pores) and the heat flux required to vaporize the water through the membrane (Chew, Krantz & Fane 2014); and R_t is the total heat transfer resistance from the hot feed to the cold permeate. A solution of **eq. 2.8** allows the determination of the individual temperatures at both sides of the membrane surfaces (t_{fm} and t_{pm}) (Chew, Krantz & Fane 2014):

$$t_{fm} = t_f - \frac{R_{12}(t_f - t_p)}{R_3 + (R_1 + R_2 + R_4)} = t_f - \frac{R_{12}(t_f - t_p)}{R_3 + R_{124}} \quad \text{(eq. 2.9)}$$

$$t_{pm} = t_p - \frac{R_4(t_f - t_p)}{R_3 + (R_{124})} \quad \text{(eq. 2.10)}$$

The unknown temperature difference, $t_{fm} - t_{pm}$ in relation to the known temperature difference, $t_f - t_p$ can then be expressed as (Chew, Krantz & Fane 2014):

$$t_{fm} - t_{pm} = \frac{R_3(t_f - t_p)}{R_3 + (R_1 + R_2 + R_4)} = \frac{R_3(t_f - t_p)}{R_3 + (R_{124})} \quad \text{(eq. 2.11)}$$

2.6.2.3 Temperature polarization coefficient (TPC)

Heat and mass transfer occur simultaneously in MD. The temperatures at the boundary layers of both the feed and permeate sides are different from those at the bulk temperatures due to temperature polarization. Changes in the driving force (i.e., difference in partial water vapor pressure brought about by temperature difference) are

usually evaluated through TPC presented as follows (Alklaibi & Lior 2005; Gryta 2005b; Schofield, Fane & Fell 1987):

$TPC = (t_{fm}\text{-}t_{pm})/(t_f\text{-}t_P)$ (eq. 2.12)

TPC indicates the thermal efficiency of the MD system, wherein a value nearing unity suggests good thermal efficiency, and values nearing zero means otherwise. It must be noted though that TPC is not a direct coefficient of the reduction in MD driving force, which means that the same TPC values do not necessarily mean having the same driving force values (Martínez-Díez & Vázquez-González 1999).

Considering the effect of a fouling gel-like layer (such as biofouling) with very small pores or free volume formed on the membrane surface, TPC becomes (Chew, Krantz & Fane 2014):

$$TPC = \frac{\Delta T_K}{t_f - t_p} = \left(1 - \frac{1}{1-\left(\frac{p_{pm}}{p_{fm}}\right)}\beta\right)\left(\frac{t_{fm}-t_{pm}}{t_f-t_p}\right) = \left(1 - \frac{1}{1-\left(\frac{p_{pm}}{p_{fm}}\right)}\beta\right)\left(\frac{R_3}{R_3-R_{124}}\right) \quad \text{(eq. 2.13)}$$

TPC was found to decrease with the decrease of the pore diameter of the biofouling gel-like layer and also with the decrease of the membrane resistance R_3 with respect to the external resistance R_4. In the analysis of Chew et al. (Chew, Krantz & Fane 2014), they suggested that one possible way of mitigating the effect of vapor pressure depression due to the gel-like biofouling layer with small pores is through increasing the heat transfer resistance of the membrane. This mitigating strategy is especially effective for fouling layer with larger characteristic pore diameters. Thus, a low thermal conductivity membrane would possibly help in lessening the effect of vapor pressure depression, and at the same time, it can reduce the conductive heat losses during the MD process. Further suggestion was to utilize a dual-layer membrane wherein a hydrophilic layer

with reasonably larger pores (d > 50 nm) is facing the side with biofouling gel layer (Chew, Krantz & Fane 2014).

2.6.3 MD membrane characteristics

2.6.3.1 Liquid entry pressure (LEP)

In MD application, membrane fouling and wetting are one of the important challenges. Especially for long-term operations, progressive membrane wetting has been observed (Gryta 2005a). To lessen the possibility of wetting and water penetration, hydrophobic materials (i.e., with high contact angles) such as polypropylene (PP), polytetrafluoroethylene (PTFE), and polyvinylidene fluoride (PVDF) with small maximum pore size and good pore size distribution (PSD) are used for membranes in MD. **Figure 2.4** shows the different degrees of membrane wetting (Gryta 2007), namely: (a) non-wetted, (b) surface wetted, (c) partial-wetted, and (d) fully-wetted membrane. Surface wetting (**Fig. 2.4B**) usually happens due to the phenomena in the surface and also associated with long term use, but the membrane still maintains a gap for the vapor to pass through, and proceeds with the vaporization-distillation process. Partial wetting (**Fig. 2.4C**) has some portions of the membrane open for water to pass through while other pores have decreased gap between the feed and permeate. And fully-wetted membrane (**Fig. 2.4D**) leads to inefficient MD performance, as the feed just flow through the membrane leading to low-quality permeate.

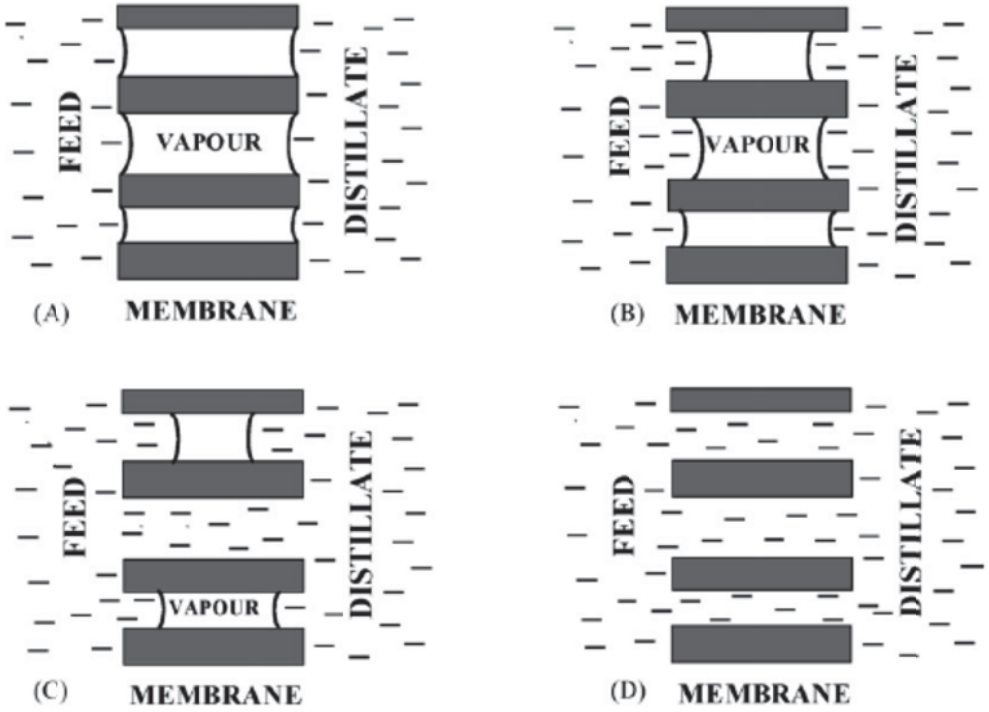

Figure 2.4. Different forms of wettability of a membrane: (A) non-wetted, (B) surface-wetted, (C) partial-wetted, and (**D**) fully-wetted (adapted from (Gryta 2007)).

The surface energy of the material, surface tension of solution, and membrane pore size and geometry are factors affecting the LEP of the membranes. **L**EP is the pressure at which the liquid starts to penetrate the pores of the membrane, until the liquid passes through the membrane. LEP is calculated by the following Laplace-Young equation (Alkhudhiri, Darwish & Hilal 2012):

$$LEP = (-4B\sigma \cos \theta)/d_{max} \quad \text{(eq. 2.14)}$$

where B is a pore geometric factor (B =1 for cylindrical pores), σ is the surface tension of the solution, θ is the contact angle between the solution and membrane surface, and d_{max} is the diameter of the largest pore size in the membrane. High LEP is needed for better MD efficiency. From eq. 2.14, LEP can be increased by increasing the contact angle of the material, or using hydrophobic or superhydrophobic materials or by having

smaller pore sizes. However, other factors such as the presence of surfactants in the solution can make the membrane wet, but the major contributor to membrane wetting is fouling (Gryta et al. 2009).

2.6.3.2 Pore size distribution (PSD)

The mean and maximum pore sizes and PSD are significant factors to determine water vapor flux performance of MD. High water vapor flux in MD and LEP of the membrane could be optimized by modifying pore size. Although a bigger pore size of membrane can lead to higher water flux, occurrence of pore wetting problem will be more likely (Lalia, Guillen-Burrieza, et al. 2013). On the contrary, reducing pore size of membrane can prevent pore wetting, however, membrane with smaller pore sizes has low water flux in MD. To achieve both improved water flux and no pore wetting, Liao et al. (Liao et al. 2013) suggested that maximum pore size below 0.6 μm of a membrane is suitable range for MD. Thus, high water flux and mitigation of pore wetting can be obtained by the optimum maximum pore size of the membrane at 0.6 μm. A number of other studies reported that MD flux increased when increasing pore sizes from 0.1 μm up to 0.6 μm of commercial or lab-fabricated membranes (Lalia, Guillen-Burrieza, et al. 2013; Liao et al. 2014; Liao et al. 2013; Prince et al. 2012).

Generally, there are three parameters regarding pore size, which are mean pore size, maximum pore size, and minimum pore size. To fabricate highly water vapor permeable membrane, range of pore sizes should be narrow for a uniform pore structure of the membrane (Lee et al. 2017). Thus, PSD plays a primary role in the MD application even though only very few studies have investigated effect of PSD on MD performance. If a PSD is broad, solutes or feed solutions can easily penetrate through the membrane.

2.6.3.3 Porosity

Porosity is relevant to the void volume fraction in the membrane, which greatly affects the MD water vapor flux performance. To achieve more evaporation surface area and/or pore channels for molecular diffusion, porosity should be as high as possible. So, high porosity leads to high water vapor permeate flux performance in MD application. Besides, air, which exists in the pores, has a much lower thermal conductivity than the polymeric material of the membrane, so the thermal resistance can be increased due to the presence of more voids in the membrane. Thus, both water vapor permeability and heat efficiency are improved by increased porosity of the membrane.

Porosity of MD membrane ranges from 35% up to 93% reported in previous studies (Essalhi & Khayet 2014; Khayet, Godino & Mengual 2004; Khayet, Matsuura & Mengual 2005; Qtaishat, Khayet & Matsuura 2009b; Tijing, Choi, et al. 2014; Tijing, Woo, et al. 2014; Wang, Hou & Lin 2016; Wei et al. 2012). Tijing, Woo et al. (Tijing, Woo, et al. 2014) also reported that porosity is one of the most influencing characteristics on the performance of DCMD.

2.6.3.4 Thickness

The membrane thickness has a significant effect on water flux performance, which is determining the mass transfer resistance (Cui, Drioli & Lee 2014). Generally, a low water permeate flux is caused by an increased mass transfer resistance due to the increased thickness of a membrane. On the other hands, a thin membrane can have a high water permeate flux due to its low mass transfer resistance as well as short vapor transport paths. However, although thin membrane has lower mass transfer resistance,

the thermal resistance is also reduced which results in a low interface temperature difference. Thus, for MD membrane, a suitable thickness should be determined to balance between water flux performance and thermal resistance.

2.6.3.5 Hydrophobicity of the MD membrane

MD membrane should be fabricated with highly hydrophobic materials to prevent a penetration of liquids through it (Lin et al. 2014). Thus, only vapor can penetrate highly hydrophobic MD membrane. Chemical and physical compositions of the materials and geometrical structure of the membrane surface determine the wettability of the membrane surface. As earlier mentioned at **Sec. 2.5.1**, the MF membrane which is fabricated by conventional membrane fabrication techniques is currently used for MD application although it is not ideally designed MD membrane. As a result, the MD membrane cannot prevent wetting issue in MD for long-term operation. In general, PP, PVDF and PTFE have been usually used to fabricate hydrophobic porous MD membranes in recent decades due to their good thermal and chemical resistance, which is required for MD application. Among these materials, PTFE MD membrane shows the highest hydrophobic property on the membrane surface, which means that it has the lowest surface free energy (Shim et al. 2015). Albeit PTFE has the merit for MD membrane fabrication, PVDF material has been more widely used for MD membrane fabrication because it is easy to be processed. To enhance the hydrophobicity of the membrane surface, low surface free energy materials should be used. Another method to improve hydrophobicity of the membrane is to apply surface modification techniques to increase surface roughness with hierarchical nanostructure (Razmjou et al. 2012).

2.6.4 Membrane fabrication and modification for MD

MD is an alternative desalination and water treatment process. However, so far, it is suffering from lack of appropriate membrane. Currently, most of MD studies usually use MF membranes. However, they are not ideally-designed MD membrane. So, MD process with these membranes suffers from low permeability and wetting problem in long term operation (Meng et al. 2014; Yang et al. 2011). Hence, there is a need to design new membranes for MD.

To fabricate a suitable MD membrane, numbers of research studies are reported using phase separation, dip-coating, hollow fiber spinning, and electrospinning techniques for MD application. These techniques are showing several advantages and disadvantages. Thus, they will be discussed individually in this chapter.

2.6.4.1 Phase separation techniques

Phase inversion technique is commonly used to fabricate flat-sheet and hollow fiber MD membranes (Bonyadi & Chung 2007). Among all phase inversion techniques, non-solvent induced phase separation (NIPS) and thermally induced phase separation (TIPS) techniques are most popular in the recent decade (Teoh, Bonyadi & Chung 2008). The NIPS technique has three major components which is polymer, non-solvent, and solvent. Polymeric membranes are fabricated by an interaction between the polymer and solvent. The fabricated membrane by NIPS technique typically shows a dense surface active layer with an asymmetric structure (Su et al. 2010). On the contrary, the TIPS technique is used with a semi-crystalline polymer. The driving force of the technique involves removing the thermal energy from the dope polymeric solution. The fabricated membrane via the TIPS technique indicates a highly porous and symmetric morphology,

which leads to increased water flux performance for MF, UF, and MD membrane (Tang et al. 2016). Especially, the TIPS technique has only two components, which are polymer and solvent. The fabricated membranes by the TIPS technique are easy to be reproduced due to the simplicity of its characteristics (Song et al. 2012). Even though the technique needs high energy consumption, it allows a diverse selection of polymers and solvents due to a high operating temperature. Despite high energy consumption, TIPS technique is capable of fabricating PVDF membranes with higher porosity and narrower pore size distribution, which are desired properties for MD application compared with NIPS technique.

Nowadays, numbers of reports focused on phase separated flat-sheet and hollow fiber MD membranes (Bonyadi & Chung 2007; Nejati et al. 2015; Song et al. 2012; Yang et al. 2011). A general summary for polymeric flat-sheet and hollow fiber fabricated membranes using various phase separation techniques in literature for MD application is given in **Table 2.2** below. Zhang et al. (Zhang et al. 2013) fabricated flat-sheet membrane using PVDF polymer by NIPS method. The fabricated PVDF NIPS flat-sheet membrane had flux of 13 LMH and salt rejection of 99.27% for DCMD application, which had lower flux and salt rejection performances compared with the commercial PVDF (GVHP, Millipore) membrane (flux of 22 LMH and salt rejection of 99.98% (Yao et al. 2016)). Li, Peng, et al. (Li, Peng, et al. 2014) made a silica nanoparticle embedded polysulfone (Psf) flat-sheet membrane by vapor induced phase separation (VIPS) technique, which is a process to cast the solution at an atmosphere (Meng, Lin & Xiong 2017). A porous structure of a VIPS membrane will be formed from the separated phases after the solvent completely evaporated (Li, Peng, et al. 2014). However, flux and salt rejection performances of the Psf VIPS flat-sheet membrane was

also lower than GVHP membrane. Nejati et al. (Nejati et al. 2015) used solvent phase separation with NIPS technique to fabricate a flat-sheet MD membrane. PVDF polymer was firstly dissolved in triethyl phosphate (TEP), which was one of the green solvent, and then casted onto a glass plate. After that, the casted film was immersed into 2-propanol coagulation bath and then was transferred and immersed again into DI water coagulation bath. The fabricated membrane showed a high water vapor flux performance (approximately 26 LMH) and stable salt rejection performance (99.99%) for 1 h DCMD test (feed solution is 1 M NaCl). Even though it indicated high water flux performance compared with GVHP membrane, a long-term performance test is still needed for assessment. Xiao et al. (Xiao et al. 2015) employed an NTIPS technique which combined NIPS and TIPS technique. Various PVDF concentrations from 12 wt% to 25 wt% were prepared at high temperature (130 – 150°C), and casted onto the glass plate by an automated high-temperature casting machine. After that, the casted film was immersed into a DI water coagulation bath at room temperature, which completed the NTIPS process. The NTIPS flat-sheet membrane showed flux of approximately 40 LMH and salt rejection of 99.99%. As shown in **Table 2.2**, it had the highest water vapor flux performance compared with other phase separated flat-sheet MD membranes. Nevertheless, a long-term MD test should be conducted with the membrane in terms of membrane stability.

To fabricate an appropriate hollow fiber MD membrane, numbers of studied focused on manipulation of structure like single-layer and dual-layer formations and the fabrication technique. A TIPS hollow fiber membrane showed high water vapor flux and stable salt rejection performances (Wang, Sun, et al. 2014). Generally, a TIPS membrane indicated a high water vapor flux performance compared with a NIPS membrane due to its highly

porous structure and narrow pore size distribution. Since 2016, NIPS hollow fiber membranes have achieved high water vapor flux performance compared to TIPS membranes. Lu, Zuo and Chung et al. (Lu, Zuo & Chung 2016) employed a specific technique using tri-bore (TB) spinneret with a blossom geometry (**Fig. 2.5**) to fabricate NIPS hollow fiber membrane for MD. The flux and salt rejection of the TB NIPS hollow fiber membrane showed 25 – 30 LMH and 99.99%, respectively. However, when it was operated over 200 hours by DCMD, it suffered wetting problems. So, the TB NIPS hollow fiber membrane needs to be improved by surface modification. They also studied functionalized graphene oxide (GO) embedded hollow fiber MD membrane (Lu, Zuo & Chung 2017). GO was modified by n-butylamine for functionalization. The functionalized GO was added in the PVDF solution, and the membranes were fabricated via single-bore NIPS technique. They observed effect of the functionalized GO loading on/in the membrane. The functionalized GO-PVDF hollow fiber membrane showed flux of approximately 28 LMH and salt rejection of 99.99%, respectively.

Table 2.2. Reports in literature on flat-sheet and hollow fiber membranes using phase separation techniques for MD application (Inlet temperatures: feed = 60°C, permeate = 20°C and feed water: 3.5 wt% NaCl).

Fabrication technique	Membrane type	Polymer type	MD application	Flux ($L/m^2 h$)	Salt rejection (%)	Reference
NIPS or solvent phase separation	Flat-sheet	PVDF	DCMD	16 - 39	99.99	(Munirasu et al. 2017)
NIPS	Flat-sheet	PVDF with CuO nanoparticle	VMD	4.5[a]	99.99	(Baghbanzadeh et al. 2015)
VIPS	Flat-sheet	Polysulfone (PSf) with silica nanoparticle	DCMD	12.5 - 14[b]	99.9	(Li, Peng, et al. 2014)

Solvent phase separation	Flat-sheet	PVDF	DCMD	26	99.99	(Nejati et al. 2015)
Phase separation	Flat-sheet	PVDF with MWNTs	DCMD	36.8[e]	99.99	(Roy, Bhadra & Mitra 2014)
NTIPS	Flat-sheet	PVDF	DCMD	40.9	99.99	(Xiao et al. 2015)
NIPS	Flat-sheet	PVDF	DCMD	13[d]	99.27	(Zhang et al. 2013)
NIPS (Dry-wet phase inversion and spinning techniques)	Flat-sheet and hollow fiber	PVDF-CTFE	DCMD	Flat-sheet: 26.5 Hollow fiber: 22.5	99.99	(Wang et al. 2016)
VIPS/NIPS	Flat-sheet	PVDF	DCMD	10.8 – 18.0	99.99	(Kharraz, Bilad & Arafat 2015)
NIPS	Flat-sheet	Polyvinyl chloride (PVC)	VMD	37.5[e]	-	(Tooma et al. 2015)
NIPS or solvent phase separation	Flat-sheet	PVDF with MWNTs	DCMD	32.4	-	(Silva et al. 2015)
NIPS	Flat-sheet	Polyethersulfone (PES) with titanium oxide nanotubes	VMD	5.5[f]	96.7	(Abdallah et al. 2014)
NIPS	Flat-sheet	PVDF	DCMD VMD	3.8 - 4.8	-	(Thomas, Guillen-Burrieza & Arafat 2014)
TIPS	Flat-sheet	PP with ethylene vinyl acetate co-blending polymer	VMD	27.6[g]	-	(Tang et al. 2016)
NIPS	Flat-sheet	PVDF	VMD	2 – 12	99.0	(Devi et al. 2014)
NIPS	Flat-sheet	PVDF	DCMD	5.0	99.22	(Lai & Cheng 2014)
NIPS	Flat-sheet	PVDF with fluorinated silica nanoparticles	VMD	15.23[h]	-	(Sun et al. 2015)
NIPS	Flat-sheet	PVDF	DCMD	12.45	-	(Hou et al. 2014)
NIPS	Flat-sheet	PVDF on hydrophilic support layer	DCMD	20	-	(Hou, Dai, et al. 2012)
VIPS	Flat-sheet	PSf	DCMD	10.9[i]	99.99	(Peng et al. 2013)
NIPS with solvent phase separation	Flat-sheet	PVDF	DCMD	17[j]	99.9	(Hamzah & Leo 2017)

NIPS	Flat-sheet	PVDF with graphene nanoparticle	AGMD	20.5	99.99	(Woo et al. 2016)
TIPS	Hollow fiber	PVDF	DCMD	27 - 29[k]	99.9	(Wang, Sun, et al. 2014)
NIPS (Dry-jet wet phase inversion)	Hollow fiber	PVDF	DCMD	16[l]	99.99	(Wang & Chung 2012)
TIPS	Hollow fiber	PVDF	DCMD	8 – 10	99.99	(Song et al. 2012)
NIPS (Dry-jet wet phase inversion)	Hollow fiber	PVDF/PTFE composite	DCMD	18 – 20	99.99	(Teoh, Chung & Yeo 2011)
NIPS (Dry-jet wet phase inversion)	Hollow fiber	PVDF/PAN dual-layer (hydrophobic/hydrophilic)	DCMD	38	99.99	(Su et al. 2010)
NIPS (Dry-jet wet phase inversion)	Hollow fiber	PVDF	VMD	14.5	99.99	(Simone et al. 2014)
NIPS (Dry-jet wet phase inversion)	Hollow fiber	PVDF	DCMD VMD	8 ~ 18	-	(Tang et al. 2012)
NIPS	Hollow fiber	PVDF	DCMD	19.8	-	(Hou et al. 2009)
NIPS	Hollow fiber	PVDF/PVA (hydrophobic/hydrophilic dual-layer)	DCMD	8.2	99.99	(Feng et al. 2017)
NIPS (Dry-jet wet phase inversion)	Hollow fiber	PVDF	DCMD	32	-	(Zhao et al. 2017)
NIPS (Dry-jet wet phase inversion)	Hollow fiber	PVDF with modified graphene oxide	DCMD	28.2	99.99	(Lu, Zuo & Chung 2017)
NIPS (Co-extrusion spinning process)	Hollow fiber	PVDF	VMD	36.0	-	(Zhao et al. 2016)
Immersion-induced phase inversion with sintering	Hollow fiber	PVDF with alumina nanoparticle	VMD	42.5[m]	-	(Fang et al. 2012)
NIPS (Dry-jet wet phase inversion)	Hollow fiber	PVDF/PVA (hydrophobic/hydrophilic dual-layer)	DCMD	7.5	99.99	(Zhu, Jiang & Matsuura 2015)
NIPS (Dry-jet wet phase inversion)	Hollow fiber	PVDF	DCMD VMD	8.2[n] 41.8	-	(Drioli et al. 2013)
NIPS (Dry-jet wet phase inversion)	Hollow fiber	PVDF with $CaCO_3$ particles	DCMD	20	-	(Hou, Wang, et al. 2012)
NIPS (Dry-jet wet phase inversion)	Tri-bore hollow fiber	PVDF	DCMD	25 – 30	-	(Lu, Zuo & Chung 2016)

[a] Feed solution is pure water, feed temperature is 60°C and vacuum pressure is 1.2 kPa.

[b] Feed and permeate temperatures are 73°C and 25°C, respectively.

[c] Feed solution is 1.0 wt% NaCl and feed temperature is 70°C.

[d] Feed temperature is 69.85°C.

[e] Vacuum pressure is 2 mbar and feed solution is distilled water.

[f] Vacuum pressure is 300 mbar.

[g] Vacuum pressure is3 kPa and feed temperature is 70°C.

[h] Vacuum pressure is 80 kPa, feed temperature is 50°C and feed is 2.0 wt% NaCl

[i] Feed and permeate temperatures are 73°C and 25°C.

[j] Feed temperature is 70°C and feed water is 5.0 wt% NaCl.

[k] Feed and permeate temperatures are 60°C and 25°C, respectively.

[l] Feed temperature is 70°C

[m] Feed temperature is 80°C

[n] Feed temperature is 50°C

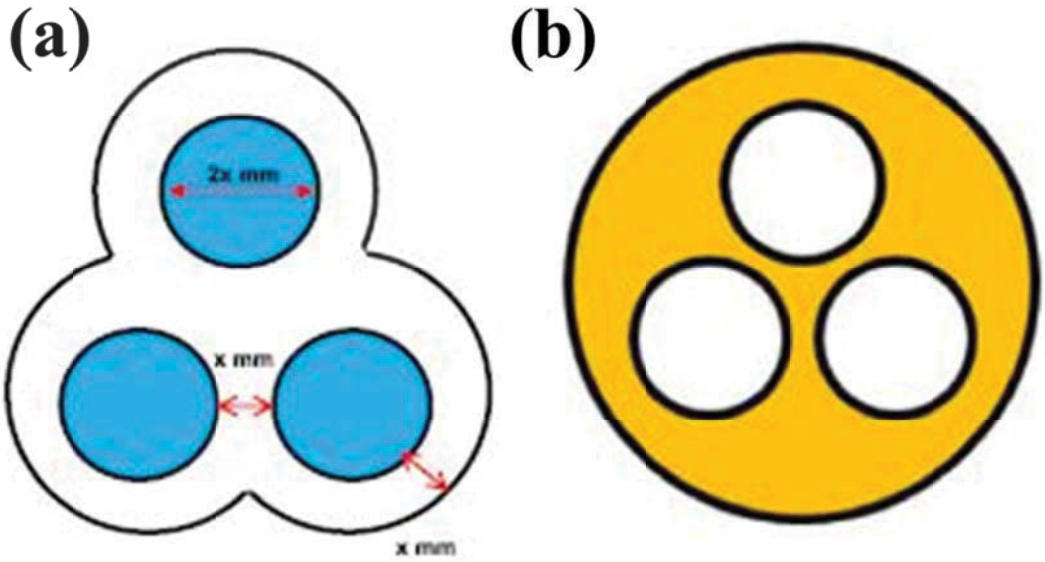

Figure 2.5. (a) Bottom view of tri-bore spinneret and (b) cross sections of tri-bore hollow fiber membrane (adapted from (Luo et al. 2014)).

2.6.4.2 Electrospinning technique

Electrospinning is a simple and versatile technology to produce nanofibers and has high potential for commercialization. A high electric field applied on a polymeric solution

during electrospinning will generate nanofibers, which can be attached on a collector (Liao et al. 2013). Formhals registered several US patents regarding the elctrospinning device from 1934 to 1944. Since 2000, there was a sharp increase in the numbers of reports involving electrospinning (**Fig. 2.6**). Lots of universities and research institutions focused on the development of electrospinning to enhance nanofiber properties. Due to increased numbers of studies, electrospinning can produce nanofibers using more than 200 polymers. Moreover, many different nanofiber morphologies can be designed and fabricated using differently configured collectors.

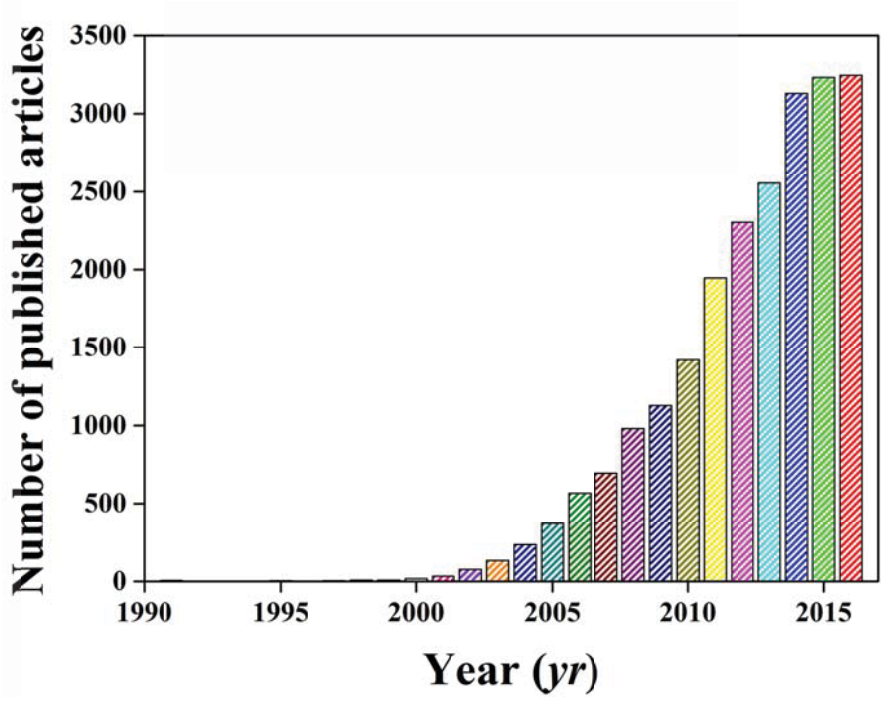

Figure 2.6. Since 1990, annual publication on the electrospinning as searched via Scopus.

The electrospinning device consists of three parts (**Fig. 2.7(a)**): (i) the high voltage supply (0 – 30 kV); (ii) the syringe containing polymeric solution on a pressure syringe pump with a metallic tip, and; (iii)rotating drum collector collecting fibers (Baji et al.

2010). A syringe containing polymeric solution is pressurized by a syringe pressure pump and the high voltage supply is applied onto the metallic tip. When the applied electric field is high enough to overcome the surface tension of the solution in the metallic tip, Taylor cone shape droplet of the solution will form on the metallic tip and fine nanofibers will be produced (Peining et al. 2012). The produced nanofibers are ejected from the tip and deposited on the rotating drum collector (**Fig. 2.7(b)**). The produced fibers can be greatly elongated by electrostatic repulsion and Coulombic forces and the solvent evaporate during the process.

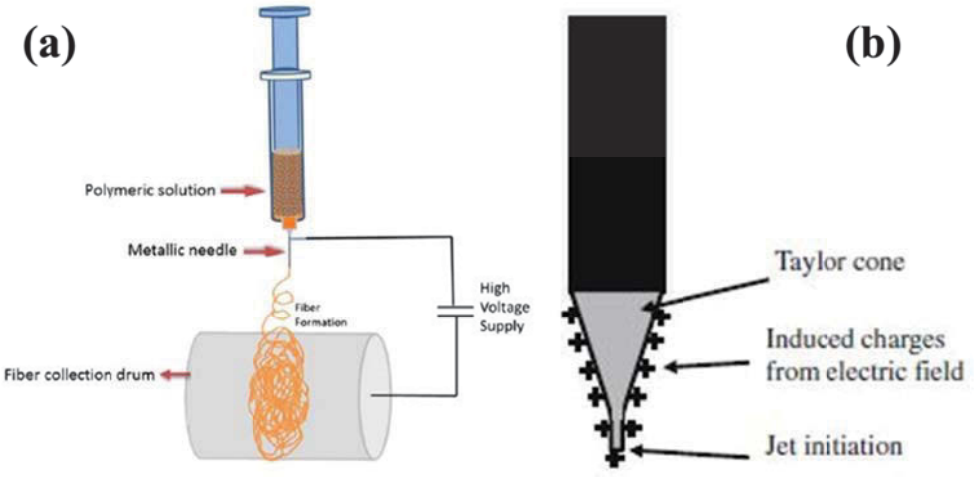

Figure 2.7. Schematic illustration of (a) electrospinning device and the Taylor cone formation (adapted from (Ahmed, Lalia & Hashaikeh 2015; Baji et al. 2010)).

2.6.4.2.1 Electrospinning parameters

The electrospinning technique can fabricate membranes with desired functionalities, morphologies, and structures by manipulating various operational and environmental parameters (Baji et al. 2010). During electrospinning, several operation parameters can be controllable such as voltage, tip-to-collector distance (TCD), solution flow rate, and drum rotating speed. Besides, several tools such as different needle (tip) size, nozzle

type (e.g. single nozzle, multi-nozzle, co and triple axial nozzles), and collector design can be changed in electrospinning device. In terms of solution parameters in electrospinning, the nanofiber membrane could be affected by the type of polymer, polymer concentration and viscosity, polymer solution conductivity, and surface tension (Kim, Kim & Yang 2012). Apart from the adjustable elements in electrospinning, humidity and temperature of the ambient surrounding environment can also be controlled for nanofiber fabrication. All above-mentioned parameters should be considered to fabricate a suitable nanofiber membrane by electrospinning.

2.6.4.2.2 Electrospinning for membrane separation technology

Electrospinning is currently one of the most versatile technologies to fabricate a water filtration membrane (Tijing, Choi, et al. 2014). It has several advantages such as high surface volume ratio, high porosity, controllable pore size, etc., which shows why it is better than conventional membrane fabrication techniques (Essalhi & Khayet 2013a). Recently, most membrane-based water and wastewater treatment processes such as MF, UF and membrane bioreactor (MBR), desalination processes like NF and RO and emerging technologies such as MD, RED, CDI, FO and PRO have gradually become interested at electrospun membranes (Ahmed, Lalia & Hashaikeh 2015). The membranes used in water treatment and desalination processes differ principally in their pore sizes (**Fig. 2.8**). Hence, numbers of studies have been carried out focusing on the use of electrospun layer as active top layers and/or support bottom layers for different processes (Bai et al. 2014; Daels et al. 2010; Islam, McCutcheon & Rahaman 2017; Tian, Wang, et al. 2015; Tian et al. 2017). A summary of several applications using electrospun membranes is given in **Table 2.3**.

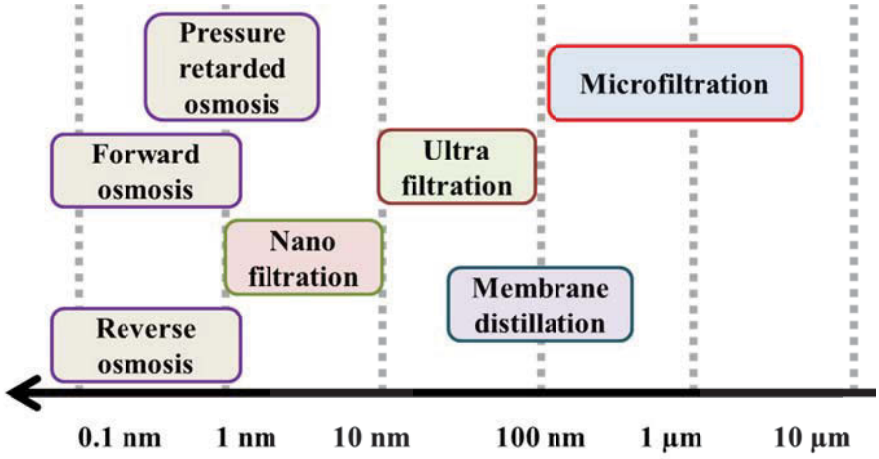

Figure 2.8. Average pore size of the membranes used in different membrane processes (Lalia, Kochkodan, et al. 2013).

Table 2.3. Reports in literature on electrospun membrane for various membrane-based water filtration treatment applications

Application	Layer format	Polymer type	Notes	References
CDI	Electrode	Graphene oxide in PAN	Graphene oxide embedded porous carbon nanofiber electrode	(Bai et al. 2014)
MBR	Active top layer	Polyamide (PA)	Synthetic wastewater with tap water as feed water was used	(Daels et al. 2010)
MF	Active top layer	Polyvinyl acetate (PVAc)-coated nylon 6/silica	Separation of oil from oil-water emulsions	(Islam, McCutcheon & Rahaman 2017)
FO	Active top layer and support layer	PVDF	A dense PA active layer was formed on a smaller pore size support layer	(Tian et al. 2013)
FO	Support layer	Polyetherimide (PEI) with silica	Silica can reinforce the nanofiber support to resist the thermal compaction	(Tian et al. 2017)
PRO	Support layer	PEI with MWNTs	An electrospun support was post-treated by a heat-press to attach the nanofiber layer	(Tian, Wang, et al. 2015)
MF	Active top layer	Polyacylonitrile (PAN)	To observe effects of fiber diameters, porosity and thickness	(Wang et al. 2017)
NF	Active top layer	Carboxyl methylcellulose with PVA	It showed decreased fouling	(Wasim et al. 2017)
UF	Active top layer or support layer	PVDF with zeolite	Surface modification by thin chitosan coating	(He et al. 2014)
UF	Active top layer and support layer	PAN with MWNTs active layer/PAN supporting layer	Crosslinking of PAN with MWNT active layer	(You et al. 2013)

2.6.4.2.3 Electrospinning for MD membrane

Recently, flat-sheet and hollow fiber membranes by NIPS and TIPS have been studied a lot. However, both methods still have a limitation in MD application to obtain high enough water permeate due to low porosity and sponge-like structure of membrane fabricated via both methods (Nejati et al. 2015). To solve the issue, electrospinning technique is applied to fabricate membranes for MD application.

Electrospun nanofiber membranes are suitable for MD process due to their high hydrophobicity, high porosity, and proper pore sizes. Generally, reports in literature detailed improved permeation flux and salt rejection performance for nanofiber membranes compared with other conventional membranes (Lee, Boo, et al. 2016). However, issues of long-term stability and fouling formation are still not clearly examined.

Similar with other methods, the electrospun membrane also have different layer formations such as single, dual and triple layers (**Table 2.4** and **Fig. 2.9**). Generally, many studies focused on single-layer electrospun membranes. PVDF or PVDF-co-HFP (PH) is usually used for electrospun membranes due to its hydrophobicity and easy to fabricate (Yao et al. 2017). Lee, An et al. (Lee, An, et al. 2016) used PVDF-co-HFP polymer to fabricate electrospun membrane for MD. Based on the results, a 20 wt% PVDF-co-HFP electrospun membrane showed flux ranging from 30 to 40 LMH for 50 h DCMD test. During the DCMD operation, salt rejection sharply decreased after 30 h operation. It is believed that a single-layer neat PVDF or PVDF-co-HFP membrane is not adoptable for MD application. To solve the problem, dual-layer or triple-layer electrospun membrane has been employed.

Tijing, Woo et al. (Tijing, Woo, et al. 2014) noted that a hydrophobic/hydrophilic dual-layer electrospun membrane was attributed to increased hydrophobicity of the active layer, thereby preventing wetting issue. Besides, thinner hydrophobic active layer with thicker hydrophilic layer led to decreased mass transfer resistance. Thus, the hydrophobic/hydrophilic dual-layer electrospun membrane could achieve a higher water vapor flux performance by preventing wetting problems compared with single-layer electrospun membrane.

As I mentioned before, single-layer electrospun membranes suffer wetting problem during MD operation. To address the issue, several hydrophobic nanoparticles such as functionalized SiO_2 and TiO_2, clay particles, surface modifying macromolecules (SMMs), etc. have been incorporated in a single-layer membrane, individually. Greatly improved wetting resistance was achieved (Lee et al. 2017; Lee, An, et al. 2016; Prince et al. 2014; Prince et al. 2012). These studies indicated that hydrophobic nanoparticles incorporated electrospun membrane showed superhydrophobic property on the membrane surface (**Fig. 2.9**). Dumée et al. (Dumée et al. 2011) claimed that increased hydrophobic property on the membrane led to not only prevention of wetting problems but also improved water vapor permeability in MD operation. Thus, hydrophobic nanoparticles incorporated electrospun membrane has a potential for a commercialized MD fabrication process.

Table 2.4. Reports in literature on electrospun nanofiber membrane for MD application (Inlet temperatures: feed = 60°C, permeate = 20°C).

MD application	Layer format	Active layer	Pore size (μm)	Porosity (%)	Contact angle (deg)	Flux ($L/m^2 h$)	Salt rejection (%)	Reference
DCMD	Dual-layer	PVDF/silica	0.36	64	150.0	16 ~ 27	99.99	(Liao et al. 2014)
AGMD	Single-layer	PVDF	-	-	-	4.2	-	(Feng et al. 2008)
DCMD	Single-layer	PVDF-co-HFP with benzyltriethylammonium chloride (BTEAC)	0.42	-	~ 130	36	99.99	(Lee, Boo, et al. 2016)
DCMD	Dual-layer	Polystyrene (PS) on PET support layer	0.76	69	150.2	~ 58	-	(Li, Wang, et al. 2014)
AGMD	Triple-layer (Casting with electrospinning)	PVDF	0.10	-	145.0	15.2	-	(Prince et al. 2013)
DCMD	Dual-layer	PVDF with SiO_2 on nonwoven support (hydrophobic/hydrophilic dual-layer)	0.36	62	~ 150	21	99.99	(Liao et al. 2014)
DCMD	Dual-layer	PVDF with surface modifying macromolecules (SMMs) / PVDF phase-inversion support layer	0.06	-	148.4	10	99.98	(Prince et al. 2014)
DCMD	Single-layer	PVDF	0.31	79	138	36	-	(Liao, Wang & Fane 2013)
DCMD	Single-layer	PVDF-co-HFP	0.73	~ 91	134	-	-	(Lalia, Guillen-Burrieza, et al. 2013)
DCMD	Single-layer Dual-layer	PVDF PVDF/SiO_2	0.68 0.69	85 82	142.8 156.3	~ 12 ~ 19	- 99.99	(Liao, Wang & Fane 2014)
DCMD	Single-layer	Matrimid 5218	2.15	-	130.0	~ 24	99.99	(Francis, Maab, et al. 2013)
DCMD	Single-layer	PVDF	0.18	71.4	138	~ 10	-	(Liao et al. 2013)
VMD	Single-layer	PTFE/PVA composite membrane	-	81.5	156.7	~ 10[a]	99.11	(Zhou et al. 2014)
DCMD	Single-layer	PVDF-co-HFP with nanocrystalline cellulose (NCC)	~ 0.2	70	~ 127	10.2 ~ 11.5	99	(Lalia et al. 2014)
DCMD	Single-layer	PVDF/SiO_2	0.23	79	152	25	99.99	(Su et al. 2017)

DCMD	Single-layer	PVDF with clay particles	0.64	81	154.2	~ 2	99.97	(Prince et al. 2012)
AGMD	Triple-layer	PVDF nanofiber (top)/ PVDF phase separation (middle)/ PET support (bottom)	0.1	-	145.02	~ 10	99.99	(Prince et al. 2013)
DCMD	Single-layer	PTFE/PVA with PAN	0.79	81.1	143.6	14.59	99.8	(Huang et al. 2017)
DCMD	Dual-layer	PVDF-co-HFP/PAN (hydrophobic/hydrophilic)	1.0	90	150	30	98.5	(Tijing, Woo, et al. 2014)
DCMD	Single-layer	PVDF-co-HFP	1.4	91	153	18	-	(Yao et al. 2017)
VMD	Single-layer	PVDF-SiO_2	0.22	55	121.5	15[b]	-	(Dong, Ma, et al. 2015)
DCMD	Single-layer by dual-nozzle	PVDF-co-HFP with functionalized TiO_2 nanoparticles	0.76	89.8	153.4	40[c]	99.99	(Lee et al. 2017)
DCMD	Single-layer	PVDF-co-HFP with fluorosilane coated TiO_2	0.75	91.6	149.0	37.8[c]	99.99	(Lee, An, et al. 2016)

[a] Vacuum pressure is 30 kPa

[b] Vacuum pressure is 9 kPa

[c] Feed solution is 7.0 wt% NaCl

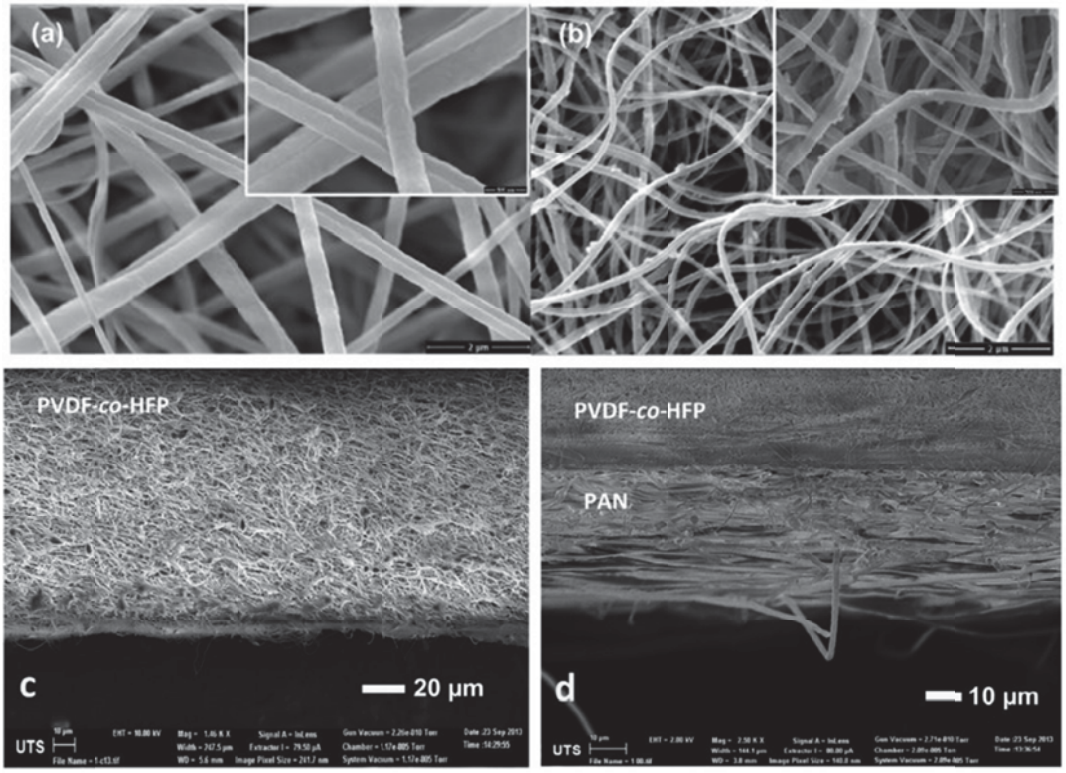

Figure 2.9. (a, b) Surface SEM images of (a) 20 wt% PVDF-co-HFP and (b) 10 wt% PVDF-co-HFP with 10 wt% TiO_2 electrospun membranes and (c, d) cross-sectional SEM images of (c) PVDF-co-HFP single-layer and (d) PVDF-co-HFP/PAN dual-layer electrospun membranes (adapted from (Lee, An, et al. 2016; Tijing, Woo, et al. 2014)).

2.6.4.3 Surface modification

In recent years, a number of research studies have been geared on membrane surface modification to enhance hydrophobicity and anti-fouling properties of MD membranes. Different superhydrophobic coatings were applied on various substrates, and results showed less biofouling formation on these coated substrates than the uncoated ones (Privett et al. 2011; Zhang, Lamb & Lewis 2005). A previous study has reported the control of organic fouling by hydrophilization of the membrane surface. By coating a PTFE membrane with sodium alginate hydrogel, the adsorption of citrus oil on the membrane surface was significantly lessened (Xu et al. 2004).

Increasing the hydrophobicity of a membrane usually leads to higher LEP and consequently more resistance to pore wetting. Razmjou et al. (Razmjou et al. 2012) fabricated a superhydrophobic PVDF membrane by incorporating TiO_2 nanoparticles via a low temperature hydrothermal process. DCMD tests were carried out including the effect of fouling formation using humic acid (HA) and calcium chloride as foulants. The deposition of TiO_2 forming hierarchical structure with multilevel roughness on the surface has increased the hydrophobicity up to 166^o, and consequently increasing the LEP to 195 kPa. Fouling tests revealed similar fouling behavior for both virgin and modified membranes, but the modified membrane showed much higher flux recovery, indicating a better anti-fouling property.

In addition, Liao, Wang & Fane (Liao, Wang & Fane 2013) fabricated electrospun nanofiber membrane using PVDF polymer. The electrospun nanofiber membrane showed flux of 36 LMH although it suffered wetting problems during DCMD test. That is the reason why they employed surface modification to improve its wetting resistance with enhanced hydrophobic property on the active layer of the electrospun nanofiber membrane. In addition, they also studied to prevent wetting issue by post-treatment like heat-press (Liao et al. 2013). Heat-press can enhance LEP, characteristics, tensile strength and morphology of the membrane. Thus, heat-press technique is strongly suggested for electrospun membrane to improve their characteristics and water vapor flux performance in MD operation (Yao et al. 2016).

In another study, Zhang et al. (Zhang et al. 2013) fabricated a superhydrophobic PVDF flat-sheet membrane by casting and spraying a mixture of polydimethylsiloxane (PDMS) and hydrophobic SiO_2 nanoparticles onto the membrane surface. The modified membrane showed a contact angle (CA) of 156^o, which was much higher than that of

the original membrane (CA = 107°). The DCMD flux performance of the modified membrane however showed lower than that of the original membrane, but is compensated with high salt rejection efficiency. Fouling tests were carried out at very high concentration of 25wt% NaCl solution. The results showed in the first 40 h, the flux profile was similar for both membranes, however after 40 h, there was a steep flux decline for the original membrane, indicating membrane wetting and fouling. The modified membrane showed more stable flux. By examining the membranes after the test, NaCl deposits were found on the original membrane surface, with some are blocking the pores, while on the modified membrane surface, almost no deposits were found. This study indicated the potential of surface modification by SiO_2 nanoparticles as a good method in fabricating anti-fouling MD membranes. Membranes was modified using various techniques for MD application which were reported in literature are outlined in **Table 2.5**.

Table 2.5. Reports in literature on modified membranes using various modification techniques for MD application (Inlet temperatures: feed = 60°C, permeate = 20°C).

Modification technique	Membrane type	MD application	Flux ($L/m^2 h$)	Salt rejection (%)	Reference
Spraying using an airbrush	Flat-sheet	DCMD	8[a]	99.99	(Zhang et al. 2013)
Filtration coating	Hollow fiber	DCMD	28	99.99	(Zhao et al. 2017)
Grafting	Hollow fiber	VMD	18	-	(Fang et al. 2012)
Cross-linking	Hollow fiber	DCMD	10.5	99.99	(Yang et al. 2011)
Dip-coating	Hollow fiber	DCMD	21	99.99	(Lu, Zuo & Chung 2016)

Filtration coating	Hollow fiber	DCMD	29.9[b]	-	(Yan et al. 2017)
Initiated chemical vapor deposition (iCVD)	Flat-sheet	AGMD	8	-	(Guo et al. 2015)
Dip-coating	Flat-sheet	DCMD	~ 12	99.99	(Lee, Boo, et al. 2016)
Grafting	Flat-sheet	DCMD	25.2	99.99	(Dong, Wang, et al. 2015)
Dip-coating	Flat-sheet	DCMD	31.8	99.99	(Liao, Wang & Fane 2013)
Heat-press	Flat-sheet	DCMD	20 – 22	99.99	(Lalia, Guillen-Burrieza, et al. 2013)
Heat-press	Flat-sheet	DCMD	20.6	99.99	(Liao et al. 2013)
Heat-press	Flat-sheet	DCMD	29	99.99	(Yao et al. 2016)
Annealing	Flat-sheet	DCMD	~ 35	99.99	(Yao et al. 2017)
Grafting	Flat-sheet	VMD	31.5[c]	99.99	(Dong, Ma, et al. 2015)

[a] Feed temperature is 69.85°C.

[b] Feed temperature is 70 °C

[c] Vacuum pressure is 9 kPa

2.6.5 MD fouling

Fouling in general is the accumulation of unwanted deposits on the surface of the membrane or inside the pores of the membrane that degrade its permeation flux performance (Gryta 2007; He et al. 2008). This is one of the major problems in membrane-based processes. Particularly in pressure-driven processes (i.e., RO, NF, UF), fouling could pose a very detrimental effect to the desalination and purification process. Generally, the foulants are colloidal in nature that interact with each other, and/or interact with the membrane surface to form deposits. Fouling formation mechanism can

be understood by examining the forces of interaction between the particles (foulants) and the membrane surface, and is best described by the classical DLVO theory (Derjaguin & Landau 1941; Verwey & Overbeek 1948). The DLVO theory states that the net particle-surface interaction (or particle-particle) is a summation of the van der Waals and the electrical double layer forces. If the particle and surface have different charges, they will have attractive interaction, while if the particle and surface have similar charges, they will be repulsive of each other. In order to minimize fouling, the surface and the particle should be kept repulsive of each other or reduce the interaction between them. Moreover, particles in a solution can agglomerate and form particulates and deposit on the membrane surface. The agglomeration rate is a function of particle collision and attachment coefficient, wherein higher frequency of collision and large attachment coefficient could lead to more aggregation (Filella 2007). The electric double layer interaction is weak at high ionic strength such as in seawater and the particle-particle interaction is dominated by acid-base interaction (Jin, Huang & Hoek 2009; Kühnl et al. 2010), while the van der Waals interaction has low sensitivity to changes in pH and concentration of electrolytes.

All known kinds of fouling found in other membrane-separation processes also exist in MD. A fouling layer gives additional thermal and hydraulic resistances, which depend on the characteristics of the fouling layer such as porosity and thickness (Curcio et al. 2010; Srisurichan, Jiraratananon & Fane 2005). As can be seen in **Fig. 2.10a**, the formation of fouling layer reduces the temperature difference across the membrane or an increase in temperature polarization (Hsu, Cheng & Chiou 2002), which translates to lesser driving force. If the fouling layer is non-porous, it is likely to contribute to both thermal and hydraulic resistances, while a porous fouling layer may only result to

thermal resistance (Gryta 2008). Gryta (Gryta 2008) investigated the fouling mechanisms of different foulants from wastewater with proteins, bilge water, brines and from the production of demineralized water in a DCMD set-up using polypropylene capillary membranes. Varying fouling tendencies and intensities were observed for the different feed waters. Two types of fouling layers were observed both of which decreased the permeate flux: the porous (**Fig. 2.10b**) and non-porous **(Fig. 2.10c**) deposit layers. The porous deposit layer provides additional heat resistance, thus decreasing the permeate flux. On the other hand, the non-porous deposit lessens the transport of water vapor across the membrane or more mass transfer resistance. Due to membrane pore size, properties, and operational parameter differences, the role of fouling in MD may be different compared to pressure-driven membrane processes, and much more different compared to that encountered in heat exchangers (Bott 1995; El-Bourawi et al. 2006). Previous studies (Gryta 2008; Gryta, Tomaszewska & Karakulski 2006; He et al. 2008) have reported a more severe fouling due to deposition of protein and $CaCO_3$ scaling as the feed water temperature increased. **Figures 2.10b-d** show the microscopic images of virgin (un-fouled) (**Fig. 2.10d**) and fouled membranes covered with $CaCO_3$ (**Fig. 2.10b**) and protein (**Fig. 2.10c**) deposits. The flow velocity was observed to affect the growth rate of the fouling layer as well as the morphology and size of the deposits. Higher velocity led to smaller crystal formation and porous deposit layer, while lower velocity produced thicker deposits in the form of “mountain-like” structures (Gryta 2008).

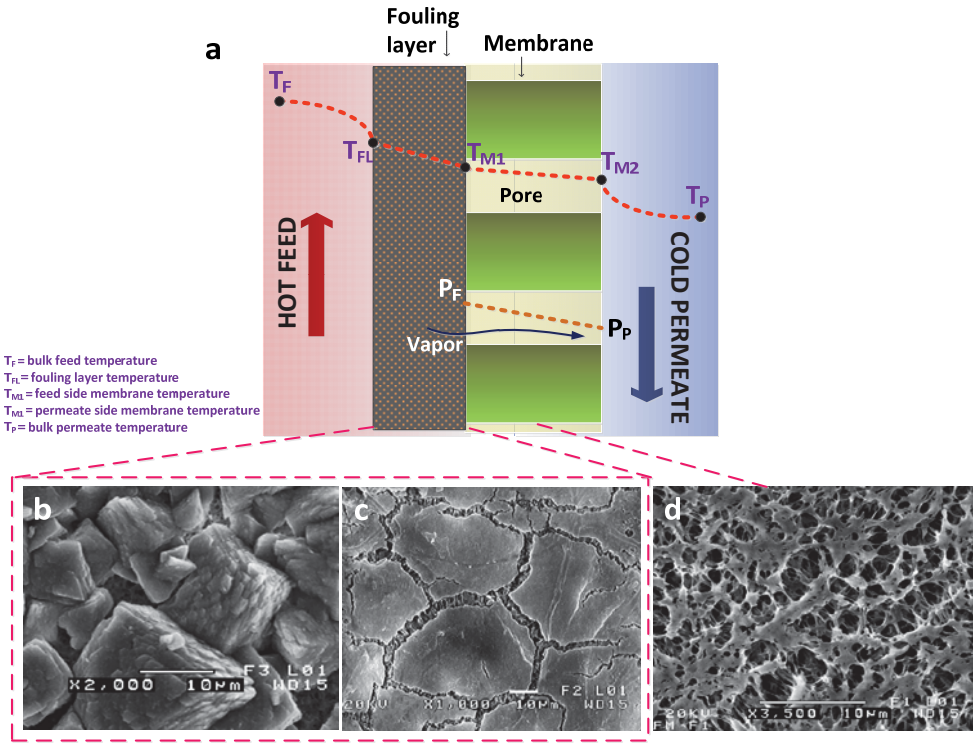

Figure 2.10. (a) The effect of fouling on the temperature distribution of DCMD membrane, and; microscopic images of membranes fouled by (b) $CaCO_3$ and (c) protein, and (c) a virgin (un-fouled) membrane (Figures b-d are adapted from (Gryta 2008)).

Fouling is a complex phenomenon, which is affected by different factors in its formation on/in the MD membrane surface. Understanding the fouling phenomena is a requisite to have a better approach in minimizing, mitigating, and cleaning the fouling formation. Generally, the following factors affect the fouling formation process: (a) foulant characteristics, (b) feed water characteristics, (c) membrane properties, and (d) operational conditions (Tang, Chong & Fane 2011). **Figure 2.11** shows the different factors affecting fouling grouped into four: (a) foulant characteristics (concentration, molecular size, solubility, diffusivity, hydrophobicity, charge, etc.); (b) membrane properties (hydrophobicity, surface roughness, pore size and PSD, surface charge,

surface functional groups); (c) operational conditions (flux, solution temperature, flow velocity), and; (d) feed water characteristics (solution chemistry, pH, ionic strength, presence of organic/inorganic matters). The type of fouling that will occur on the membrane surface is mainly affected by the kind, concentration and properties of foulants present in the feed water, and the solution chemistry of the feed water. On the other hand, interaction between the foulants and the membrane surface could enhance the fouling propensity, thus membrane properties can significantly affect fouling. The operational conditions such as feed temperature and flow velocity can also affect the extent of fouling.

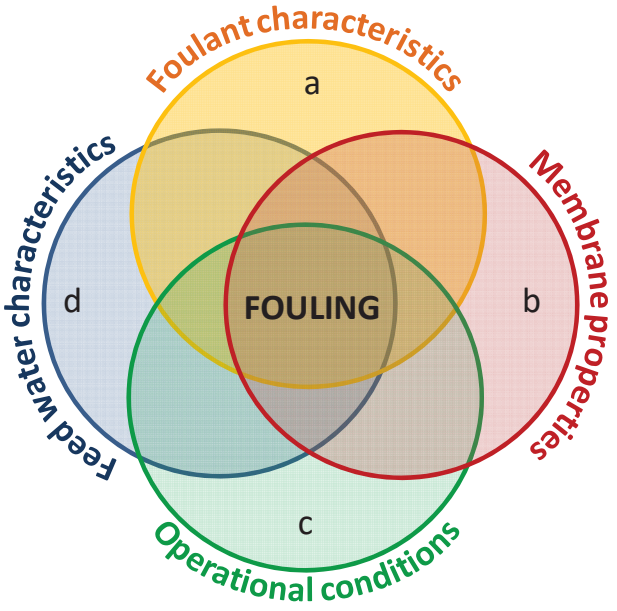

Figure 2.11. Factors affecting membrane fouling: (a) foulant characteristics (concentration, molecular size, solubility, diffusivity, hydrophobicity, charge, etc.); (b) membrane properties (hydrophobicity, surface roughness, pore size and PSD, surface charge, surface functional groups); (c) operational conditions (flux, solution temperature, flow velocity), and; (d) feed water characteristics (solution chemistry, pH, ionic strength, presence of organic/inorganic matters).

The sites where fouling occurs can be divided into external surface fouling or pore blocking fouling (see **Fig. 2.12**) (Knyazkova & Maynarovich 1999). As the name implies, external surface fouling refers to the build-up or formation of deposits or cake/gel-like layers on the outer surface of the feed-side of the membrane. Pore blocking happens when scales or foulants are formed inside the pores of the membrane by partial blocking or gradual narrowing of the pore, or by complete pore blocking, wherein the full diameter and depth of the pores are covered with deposits (Zhu & Nyström 1998). External surface fouling is usually reversible and can be cleaned by chemical cleaning, while internal fouling or pore blocking is in most cases, irreversible, due to compaction of foulants, and membrane degradation (Hoek et al. 2008). In a previous study (Gryta 2008), closer inspection of the fouled membrane showed that scales were not only observed on the membrane surface, but also inside the pores of the membranes. The study observed that scale formation inside the pores could lead to damage of the membrane.

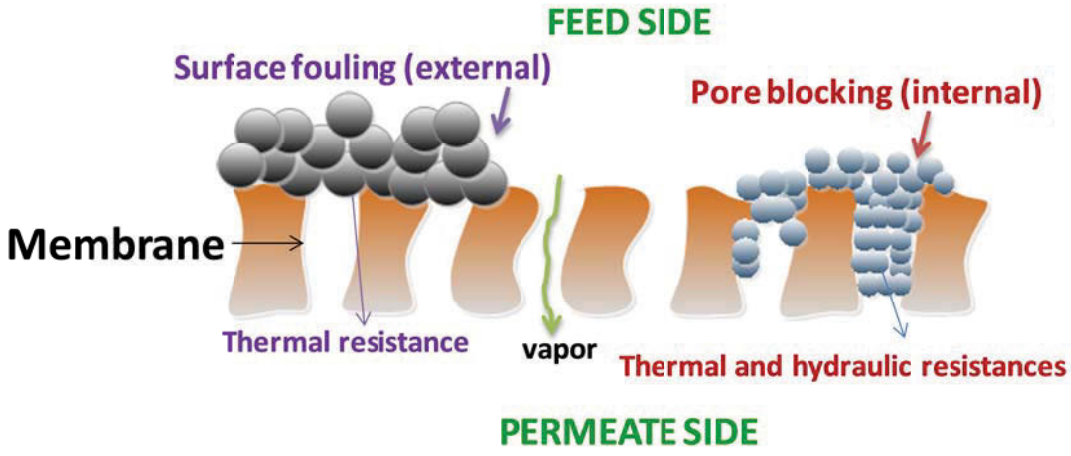

Figure 2.12. The fouling sites on a membrane can be divided into surface fouling (external) or pore blocking (internal).

The foulants found in membrane technology including MD can be divided into three broad groups according to the fouling material (Meng et al. 2009): (a) inorganic fouling, (b) organic fouling and (c) biological fouling (see **Fig. 2.13**). Inorganic fouling is caused by crystallization or precipitation of hard mineral salts from the feed such as calcium carbonate, calcium sulphate, silicate, NaCl, calcium phosphate, $BaSO_4$, $SrSO_4$, ferric oxide, iron oxide, aluminum oxide, etc., and/or the deposition of inorganic colloidal particles and particulates. Organic fouling is due to the deposition of organic matters such as HA, fulvic acid, protein, polysaccharides, and polyacrylic polymers. And biological fouling is caused mainly by microorganisms such as bacteria and fungi, sludge, algae, yeast, etc. However, in most cases, a single fouling mechanism does not occur in real MD processes, but a combination of different fouling mechanisms that make it more complicated to deal with as depicted in **Fig. 2.13**.

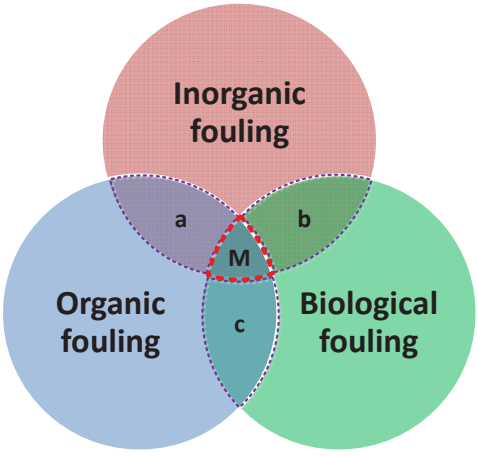

Figure 2.13. Schematic representation of the different fouling mechanisms according to fouling material found in MD. In the real world processes, fouling usually occurs as mixed fouling, i.e., the combination of different of fouling mechanisms happening simultaneously. The dotted lines in the diagram with areas a, b, c and M show the different instances of mixed fouling between two or more fouling mechanisms.

2.6.6 MD fouling control and cleaning

Several efforts have been undertaken to address the issue of fouling, especially on cleaning. However, effective fouling control techniques for MD are still lacking. The current techniques for the control of fouling are feed pretreatment and membrane cleaning (Alkhudhiri, Darwish & Hilal 2012). Some other approaches include making of new membrane with new design and materials, changing the flow regimes, development of anti-fouling membranes including membrane surface modification, design of new membrane modules, and use of physical and chemical techniques (Al-Shammiri, Safar & Al-Dawas 2000; Gryta 2008).

2.6.7 Pre-treatment for MD

Pretreatment of feed is an effective way of minimizing the extent of fouling on membrane-separation processes, thus resulting to increased quality of the permeate (Huang, Schwab & Jacangelo 2009). In fact, pretreatment is a requirement for seawater RO desalination to combat fouling (Shon et al. 2009). Ineffective or unreliable pretreatment can lead high rates of membrane fouling, high frequency of membrane cleanings, lower recovery rates, high operating pressure, poor product quality and reduced membrane life (Wolf, Siverns & Monti 2005). Pretreatment can alter the physico-chemical and/or biological properties of the feed water resulting to lesser fouling formation and improved desalination performance. Pretreating seawater in a biofilter was found to reduce the nutrient concentration, thus significantly declining the biofilm formation in RO systems (Griebe & Flemming 1998). Several methods such as coagulation/precipitation, media filtration, sonication, boiling (thermal water softening),

membrane filtration, etc. are used as pretreatment methods for desalination and water purification processes (Ebrahim, Abdel-Jawad, et al. 2001). The efficiency of pretreatment depends on many parameters such as the agents used, temperature, dosing point, solution and foulant properties, and the characteristics of the membrane (Gao et al. 2011). MD is anticipated to require less intensive pretreatment compared to pressure-driven membrane processes due to the absence of high pressure that lead to the compaction of fouling layers. However, the importance of pretreatment in MD cannot be underestimated because it acts as the first line of defense for membrane fouling especially in industrial desalination setting. Different real feed source waters contain mixed constituents (i.e., inorganic, organic, colloids and particulates, and microorganisms) and may be exposed to variable feed water qualities, hence pretreatment is a necessary first step for practical MD application, but is not as intensive compared to pretreatment in pressure-driven desalination technologies. In general, pretreatment in MD must be applied to the feed to initially remove macro particles and microorganisms. The removal of turbidity and fine particulates (TSS) is necessary for seawater RO but not required for MD (Hsu, Cheng & Chiou 2002). However, when real seawater is used as feed, pretreatment is an essential process for MD to reduce fouling formation (Hsu, Cheng & Chiou 2002). Many pilot scale MD plant studies employ different pretreatment methods in their experiments. For example, Jansen et al. (Jansen et al. 2013) operated an MD pilot plant based on liquid gap MD and employed filtration and degassing to pretreat the feed seawater. High quality permeate could be obtained with simple pretreatment (such as sieving at ~40 μm). One notable small DCMD pilot plant study was carried out by Song et al. (Song et al. 2008) and successfully operated on a daily basis for three months. The hot brine used was either city water at different salt concentrations (3.5, 6, and 10 %) or trucked-in seawater. The results indicated high

water recovery and relatively stable water vapor flux, with no salt contamination in the distillate side. Concentrating the seawater up to 19% did not result to fouling of the modules, even though scaling salt precipitates were floating around. This pilot study applied pre-filtration using 1 μm PP pre-filter as pretreatment to the DCMD pilot plant, which could explain its less fouling propensity as the pre-filter prevented macro particles, biological and other slimy materials in seawater from coming and fouling the membrane modules. In contrast, direct use of coastal seawater as feed without pretreatment from the Mediterranean Sea taken during the summer and autumn seasons (Krivorot et al. 2011) showed biofilm formation on the membrane surfaces after sufficient operating time.

Coagulation is recognized as one of the effective and low-cost pretreatment methods for membrane separation processes. The coagulants can change the stability of the particles present in the feed by neutralizing the charge and allows the small suspended particles to collide and agglomerate into bigger and heavier particles. Previous studies have indicated that MD has lower pretreatment requirements for water desalination compared to high-pressure membrane separation processes (El-Bourawi et al. 2006; Macedonio, Curcio & Drioli 2007). Wang et al. (Wang et al. 2008) investigated the effect of PACl coagulant as a pretreatment for the desalination by MD of Recirculating cooling water (RCW). Distorted rhombic magnesium-calcite scales were formed when coagulation pretreatment was used compared to loosely-packed deposits with small-size particles when no coagulation was employed. Coagulation was found to remove substantial parts of NOM including total organic carbon and total phosphorus, and also removed some antiscalant additives, which lead to the formation of large crystals on the membrane surface. The formation of bigger crystals due to coagulation reduces the tendency of

membrane partial wetting, because the bigger crystals find it difficult to enter the membrane pores, and just deposit on the surface. The results revealed that coagulation pretreatment has improved the MD flux by 23% compared to that without pretreatment (Hwang, Chan & Chen 2008). In another study, pretreatment by precipitation of foulants by $Ca(OH)_2$ was found to significantly limit the occurrence of membrane fouling during the MD treatment of generated effluents from the regeneration of ion exchangers (Gryta et al. 2005).

Membrane-based filtration pretreatments such as the use of MF, UF and even NF are gaining increasing attention due to their efficient removal of particulate materials and large macromolecules in the feed. El-Abbassi et al. (El-Abbassi et al. 2013) investigated the effect of two pretreatment methods (coagulation/flocculation and MF) in the treatment of olive mill wastewater (OMW) by DCMD. They found that between the two pretreatment methods, MF showed the better results when integrated with DCMD. A reduction of 30% in total solids was observed when using MF as pretreatment compared to a reduction of 23% total solids using coagulation/flocculation method. Pretreatment by MF prior to MD process was found to increase the permeate flux by 25%, thus rendering pretreatment as an effective technique to enhance the flux performance (Alklaibi & Lior 2005). Zhiqing et al. (Zhiqing et al. 2013) investigated the effect of UF with coagulation as pretreatment on membrane fouling and VMD performance of RO concentrated wastewater. PACl, $FeCl_3$, and PAM were selected as coagulants. After coagulation with optimized dosages, the feed solution was further treated with UF hydrophilic membrane by dead-end filtration process. The feed solution flowed through the hollow fiber membranes and the vacuum system was connected to the module. The results showed that the flux of VMD process was increased after pretreatment by

coagulation and UF, and when the concentration factor reached 8, the flux of VMD process using properly pretreated solution was 30 % higher than that using un-pretreated solution. The COD_{cr} removal also reached 40%. Among the coagulants used, PACl showed the best results compared with PAM and $FeCl_3$. Pretreated feed water by PACl and UF showed higher normalized flux and low fouling tendency than those of un-pretreated feed and the feed treated with PACl only. In another study, NF was used as pretreatment, which significantly improved the performance of a DCMD module using tap water as feed (Karakulski & Gryta 2005). However, some silica precipitation after NF pretreatment was found that blocked the DCMD module inlet. This blocking problem was resolved by just adding a filtration net after NF and prior to the module inlet, and the process was run without flux decline for 1100 h. The use of cartridge filters/screens is reported to be enough in effectively removing particulates from the feed water.

Thermal pretreatment or boiling of water to remove most bicarbonates from water was also reported to minimize the scaling of the membrane in MD (Gryta 2010b). This treatment would be more beneficial when utilizing groundwater that usually contains high hardness by intentionally breaking down bicarbonates at high temperature. In another study, boiling and filtration of saline wastewater was found to reduce the occurrence of protein fouling (Gryta 2008). The wastewater was boiled for 30 min and then after cooling to room temperature, was filtered out using a filter paper. As a result, the total organic carbon (TOC) and turbidity of the wastewater decreased by 60 and 79%, respectively after boiling. This lead to the prevention of rapid flux decline in DCMD, confirming that the thermal (boiling pretreatment) has removed protein foulants from the feed.

Conventional precipitation as water softening method is often used to induce $CaCO_3$ precipitation by chemical dosing using lime, caustic and soda ash (AWWA 1999). However, this method requires longer time for settling and has low solid production (2-30% solid content) (AWWA 1999). To aid in this deficiency, seeded precipitation process was developed. In a previous work, APS method was used as pretreatment for the high-recovery desalination of RO concentrate by DCMD. Qu et al. (Qu et al. 2009) employed APS method by pH adjustment with sodium hydroxide together with calcite seeding, and followed by MF. The APS pretreatment removed 92% of calcium, leading to the reduction of scaling potential from $CaCO_3$ and $CaSO_4$. The permeate flux was found to only decline by 20% after 300 h of operation. Controlling the pH of the feed solution is a good pretreatment strategy to alleviate the effect of scaling in MD. Many researchers add acid such as HCl to bring feed water to pH 4 or 5 and found effective mitigation of $CaCO_3$ scaling (He, Sirkar & Gilron 2009b; Hwang, Chan & Chen 2008), but not much success for silica (Karakulski & Gryta 2005). One issue of this is the cost associated with the use of acid, which could be costly depending on the usage volume and the desired pH.

Table 2.6 shows some MD studies reported in literature using pretreatment to control the effect of fouling. These studies show that pretreatment can positively affect the performance of MD through an improved permeate flux and lower occurrence of membrane fouling. The availability of renewable energy such as solar and geothermal, and the possibility of coupling MD with waste heat, can provide a more energy efficient MD process together with pretreatment. It is ought to be emphasized that pretreatment in MD is a necessary step toward practical industrial and pilot-scale desalination, water

treatment and purification processes, that would lead to lesser fouling formation, and more efficient MD operation.

Table 2.6. Some pretreatment strategies for MD application reported in literature

MD configuration	Feed type	Pretreatment	Observation/Remarks	Ref
DCMD (PVDF hollow fiber)	Recirculating cooling water	PACl coagulation, precision filtration, acidification and degasification	- MD flux improved by 23% after employing coagulation pretreatment in 30 days operation.	(Wang et al. 2008)
DCMD (PP hollow fiber)	Tap water	NF and filtration net	- NF pretreatment and filtration net prior to module inlet has improved the long-term DCMD performance up to 1100 h.	(Karakulski & Gryta 2005)
DCMD (PP hollow fiber)	Groundwater, tap water, lake water	Thermal softening or boiling and filtration by filter paper	- Bicarbonate ions were found to lower by 2–3 times after boiling water for 15 min. - Boiling only benefits underground waters with high hardness.	(Gryta 2010b)
DCMD (PVDF hollow fiber)	RO concentrate	Accelerated precipitation softening (i.e., pH adjustment + calcite seeding + MF)	- APS treatment resulted to high removal of calcium and total hardness. - Flux was improved dramatically after APS treatment, with only 20% flux decline in 300 h.	(Qu et al. 2009)
DCMD (PP hollow fiber)	Bilge water, saline wastewater	- (1) Sedimentation + UF - (2) thermal pretreatment + filtration	-Significant flux decline was observed for pretreatment (1) - Rapid flux decline was prevented for pretreatment (2) due to removal of protein from boiling	(Gryta 2008)
MD pilot plant (PVDF, PP, UHM-PE)	Seawater	Filtration + degassing	- Production of excellent product water quality with little need of pretreatment	(Jansen et al. 2013)
DCMD (PP hollow fiber)	$CaCO_3$ and $CaSO_4$ solutions, Mixed $CaCO_3$/$CaSO_4$ solution	Acidification with HCl to pH 4	- Induction period was extended for at least 7 h - Stable flux was obtained from beginning to end	(He, Sirkar & Gilron 2009b)

2.6.8 Membrane flushing

Nghiem and Cath (Nghiem & Cath 2011) investigated a scaling mitigation approach by regular membrane flushing during DCMD. Scaling tests were performed on a PTFE

membrane at different feed inlet temperatures (40-60^{o}C) using $CaSO_4$, $CaCO_3$ and silicate as foulants. The initial results found that $CaSO_4$ scaling has more severe occurrence than the other two foulants, thus additional tests were only carried out with $CaSO_4$. The induction period of $CaSO_4$ scaling was found to decrease with the increase in feed temperature (Nghiem & Cath 2011) as was also previously observed by another study (He et al. 2008). The precipitated $CaSO_4$ crystal sizes showed increasing sizes with the increase of feed temperature, which is consistent with the $CaSO_4$ precipitation kinetics and thermodynamics (He et al. 2008; He, Sirkar & Gilron 2009a). The effect of $CaSO_4$ feed concentration showed varying duration of induction period. The results suggest that membrane scaling is not only due to the attainment of supersaturation, but also it can occur after a sufficient induction time. As long induction period was observed, it provides an opportunity for mitigation strategies if one can reset the induction period. If the nucleation sites at the membrane surface are constantly removed before rapid crystallization, membrane scaling can be effectively controlled. **Figure 2.14** shows the flux results after regular flushing of Milli-Q water for every 20 h interval of DCMD test with 2000 mg/L $CaSO_4$ solution. The flux was held constant for the whole duration of DCMD test after regular flushing, showing the effectiveness of simple flushing of Milli-Q water in removing nucleation sites during the induction period even at a supersaturated condition (i.e., at 2000 mg/L $CaSO_4$).

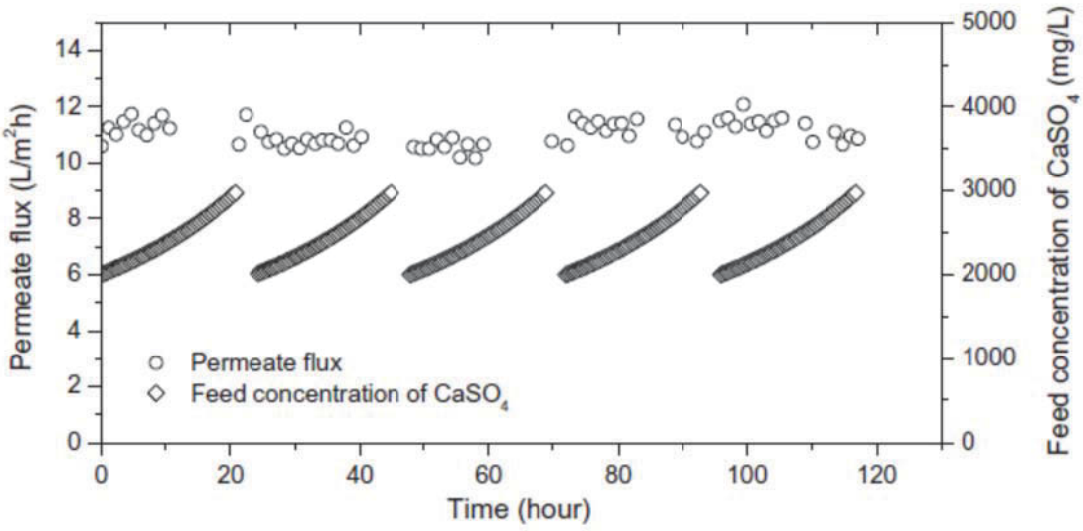

Figure 2.14. Permeate flux and feed concentration of $CaSO_4$ versus time during five repetitive DCMD tests with membrane flushing after each test. A fresh 2000 mg/L $CaSO_4$ was used after each test (adapted from (Nghiem & Cath 2011)).

2.6.9 Gas bubbling

The formation of mineral deposits on the membrane surface decreases the permeate flux and deters the life of a membrane. The formation of deposits on the membrane surface can be minimized by increasing the shear rate at the surface to constantly remove fouling layers (Teoh, Bonyadi & Chung 2008; Yang, Wang & Fane 2011). One way of doing this is through gas bubbling method, which forms a gas-liquid two phase flow that induces secondary flows increasing the maximum shear stress at the membrane surface (Ratkovich et al. 2009; Yeo, Law & Fane 2007). The following are identified as the mechanisms of gas bubbling in controlling fouling (Cui, Chang & Fane 2003): (a) bubble induced secondary flow, (b) physical displacement of the concentration polarization layer, (c) pressure pulsing caused by passing bubbles, and (d) increase in superficial cross-flow velocity. The effect of gas bubbling on the scaling of a PVDF hollow fiber membrane in a high salt concentration DCMD set-up was investigated by

Chen et al. (Chen et al. 2013). A nozzle connected to an air pump was placed at the inlet side of the feed (**Fig. 2.15**) to disperse air and bubbles inside the MD module. The utilization of gas bubbling was found to increase the permeate flux enhancement ratio by about 1.72 at an optimized gas flow rate. It was found that gas bubbling could reduce temperature polarization and could enhance the surface shear rate, leading to delay of crystallization of scales at the surface. This means that scaling of membrane was reduced due to the introduction of gas bubbling. It was suggested that together with gas bubbling, a higher enhancement in flux could be realized by operating at higher feed temperature, or at lower feed and permeate velocities, or by using an inclined module, shorter fiber length or lower fiber density. However, one must also take note that the effectiveness of gas bubbling is greatly affected by the size of induced bubbles, wherein uniformly distributed fine bubbles showed better result than coarse bubbles (Lu et al. 2008). Utilizing direct observation and statistical analysis, their succeeding study (Chen et al. 2014) confirmed that it is preferential to employ bubbles with narrow size distribution and small mean bubble size to create even flow distribution, intensity mixing, and enhance the shear rate.

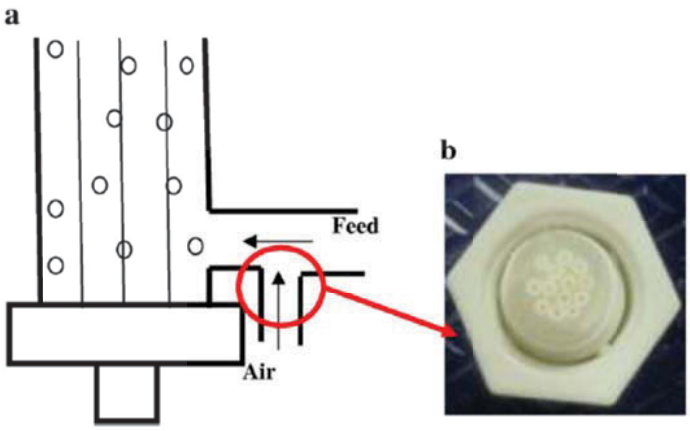

Figure 2.15. Schematic of the (a) air inlet position in the feed side of the MD module and the (b) photographic image of the air nozzle (adapted from (Chen et al. 2013)).

In another study, Ding et al. (Ding et al. 2011) used intermitted gas bubbling to mitigate fouling during the concentration of TCM extract via DCMD. Gas bubbling was introduced into the DCMD module with PTFE membrane by a fan connected at the entrance side of the feed. The influence of gas flow rate, bubbling duration and MD duration in each cycle on the fouling mitigation were investigated. In the initial test, it was observed that the permeate flux started to decline at the start of bubbling, and the flux remained at low level at continuous introduction of bubbles in the module. This could be due to the tendency of the bubbles to occupy part of the membrane surface, which reduces the contact area of the feed liquid to the membrane. Additionally, it could also be that some bubbles would stay inside the membrane pores, which affect the partial vapor pressure at the membrane pore leading to reduced flux. Thus, to address this tendency, intermittent gas bubbling was carried out for a duration of 1-3 min. Effective reduction of fouling was realized with the use of intermittent bubbling, wherein its mitigating or cleaning efficiency is improved with the increase of gas flow rate and gas bubbling duration, and the decrease of MD duration. Due to its mechanism

of increasing the shear rate at the membrane surface, gas bubbling is mainly effective in addressing external membrane fouling.

2.6.10 Chemical cleaning

Chemical cleaning agents are abundant commercially, which include acids, alkalis, metal chelating agents, surfactants, enzymes and oxidizing agents (Al-Amoudi & Lovitt 2007; Lee et al. 2001). In MD processes, strong or weak acids are usually used for cleaning especially those dealing with $CaCO_3$ fouling (Gryta 2007). Generally, rinsing with acid is particularly effective in removing inorganic scales, while rinsing with basic/alkali solution is relatively effective in the reduction of organic fouling. Depending on the location of the scales, rinsing can usually recover the initial flux if the scales are only deposited on the surface. However, formation of crystals inside the pores of the membrane could be harder to remove, and could lead to pore wetting if rinsed repeatedly, thus full recovery is impossible in this case. A study has shown that rinsing the module with 3 wt% HCl solution can effectively remove fouling and obtain permeate flux close to the initial flux. Microscopic images of acid-cleaned surface showed similar characteristics as those of a new membrane (Gryta 2010a). Wang et al. (Wang et al. 2008) utilized 2 wt% HCl or 2 wt% NaOH solutions to remove the $CaCO_3$ scales from fouled hollow fiber membranes. The rinsing using both acid and base solutions resulted to the removal of the majority of the deposits, recovering the hydrophobic property of the membrane. In a recent study, membrane fouling and cleaning were investigated on a pilot-scale MD plant in Spain (Guillen-Burrieza et al. 2014). The main prevention method for biofouling is continuous dosage of biocides.

2.6.11 Management of seawater brine by hybrid MD process

During RO, MSF, and MED operations, a huge amount of brine has to be discharged back to sea. However, the brine contains almost two times higher concentration of salts than raw seawater as feed, which could have negative impact on local ecological system. Therefore, to develop new technologies including hybrid process to treat brine as well as gain and recover minerals such as lithium chloride and sodium chloride from it has become important (Drioli, Ali & Macedonio 2015).

2.6.11.1 Membrane crystallization (MCr)

Membrane crystallization (MCr), one of the new technologies to treat brine, sharing similar mechanism to MD, has been recently introduced to treat seawater brine and mine valuable resources during operation. Drioli and his colleagues presented a new concept indicating that desalination plants as a mineral production plant instead of the freshwater production plant from seawater (as mineral resources are more valuable than water) (Drioli, Ali & Macedonio 2015).

The aim of MCr is to achieve a “zero-liquid-discharge” and “total raw materials utilization”. MCr, which can be considered as an extension of MD, concentrates the solution at super-saturation state to recover some of the compounds in the feed solution (Quist-Jensen et al. 2016). Benefits of MCr include a well-controlled nucleation and grown kinetics, reduced crystal induction time, controllable super-saturation rate, and faster speed of crystallization, which leads to narrow size and high purity crystals (Drioli, Ali & Macedonio 2015). However, in terms of maintenance, MCr should overcome several operation issues like membrane fouling and membrane pore wetting due to its high concentration of the salts in the feed (Kim et al. 2017).

2.6.11.2 MD/PRO hybrid process

Another new hybrid process integrating MD with PRO process to treat RO brine as well as generate energy is being investigated and coined as the GMVP project in South Korea (Drioli, Ali & Macedonio 2015). The main goals of the project are to minimize the disposal of produced brine, further decrease the energy consumption, generate renewable energy, and recover mineral resources. The capacity of the SWRO, MD, and PRO hybrid process in the pilot plant to produce freshwater and renewable energy is 1,000 m^3/d, 400 m^3/d, and 240 m^3/d, respectively (**Fig. 2.16**). A lithium recovery system is also included in the plant.

In brief, the plant works via the following: 1) the brine from the SWRO process goes to the MD process to reduce its total volume and produce fresh water; 2) then, the concentrated brine from MD and treated water via pre-treatment of wastewater effluent flow to the PRO process as DS and feed solution (FS), respectively; 3) the concentrated brine and other by-products are then solidified, which can be used as construction materials, leading to reduction in the total volume of the brine and the by-products and thus achieve zero-liquid discharge.

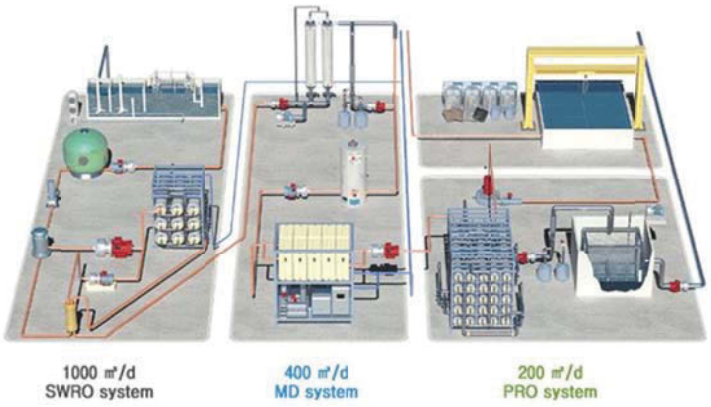

Figure 2.16. MD/PRO hybrid desalination demonstration plant (adapted from (Drioli, Ali & Macedonio 2015) and www.glovalmvp.org).

2.7 Concluding remarks

Recently, MD is rising as one of the most promising alternative membrane based technologies to produce freshwater. MD has potentials for various applications such as wastewater reclamation, desalination, and treatment of mining water and gas produced water. Although it is hard to replace RO technology in the current market, it is attractive considering its high water recovery for desalination. However, an ideally-designed suitable membrane is still needed to be developed for MD to improve water permeability and overcome several issues such as membrane pore wetting, fouling and scaling for commercial implementation. To address these challenges, electrospinning technique should be considered for MD application. In this study, several electrospinning techniques such as Janus-type hydrophobic/hydrophilic dual layer and hydrophobic one-dimensional and two-dimensional nano-materials embedded method and a surface modification like plasma modification were proposed to enhance membrane morphologies and characteristics, which lead to improving water vapor flux performance in MD. Thus, this chapter covers a brief overview of MD, its fundamentals, literature reviews of the different membrane fabrication method for MD process, the different types of fouling mechanisms that can be found in MD processes, and the possible fouling mitigation and cleaning methods to enhance the MD efficiency. This chapter also highlights the electrospinning membrane fabrication technique for better understanding.

CHAPTER 3

University of Technology Sydney
FACULTY OF ENGINEERING

MATERIALS AND METHODS

3.1 Introduction

The experimental work covers fabricated electrospun nanofiber membranes, phase-inverted membranes, surface modified membranes, evaluation performances of MD by laboratory MD set-ups and characterization techniques. Descriptions of the in detail methods can be found in the present chapter.

3.2 Experimental materials

Poly(vinylidene fluoride) (PVDF, Kynar® 761, Mw = 441,000 g/mol) and PVDF-*co*-HFP (Mw = 450,000 g/mol, Kynar Powerflex® LBG) (referred herein as PH) were purchased from Arkema Inc., Australia. N, N-dimethylformamide (DMF), acetone sodium dodecyl sulfate (SDS), diiodomethane, ethylene glycol, methanol, and lithium chloride (LiCl) were all purchased from Sigma-Aldrich. Multi-walled carbon nanotubes (referred generally herein as CNTs) (diameter = <8 nm, length ~ 10-30 μm, specific surface area ~ 500 m^2/g) were purchased from Cheap Tubes, Inc., USA and were used as received. The graphene used in the present study was xGNP-C500-grade material from XG-Science, USA, which has a particle diameter of 1 ~ 2 μm, an average thickness of 2 nm and an average surface area of 500 m^2/g. h-BN powders were purchased from Kojundo Korea Co., Ltd. Deionized (DI) water from a Millipore Milli-Q water system was used. A commercial PVDF membrane herein referred to as C-PVDF (Durapore® - GVHP, pore size of 0.22 μm) was purchased from Millipore. All chemicals were used as received.

3.3 Fabrication and modification techniques

3.3.1 Electrospinning device

The electrospinning set-up is described in detail in **Figure 3.1**. All of the fabricated membranes were controlled at an employed voltage, tip-to-collector distance, and feed flow rate depends on the polymer solution used. All nanofibers were directly fabricated onto a rotating drum collector covered with aluminium foil. A polymer solution was supplied in a 10 ml syringe attached with a needle (21G, inner diameter = 510 μm) that was mounted on an adaptor. The needle kept on oscillating sideways during electrospinning and was controlled by LabView software (National Instrument). The chamber humidity (40 ~ 50 %) and temperature (18 ~ 23°C) were maintained constant throughout the electrospinning process. After electrospinning, the as-spun membranes were peeled off from the aluminium foil and transferred onto a baking paper and kept in a dry oven (OTWMHD24, LABEC) at 50 °C for 1 day to remove the residual solvents.

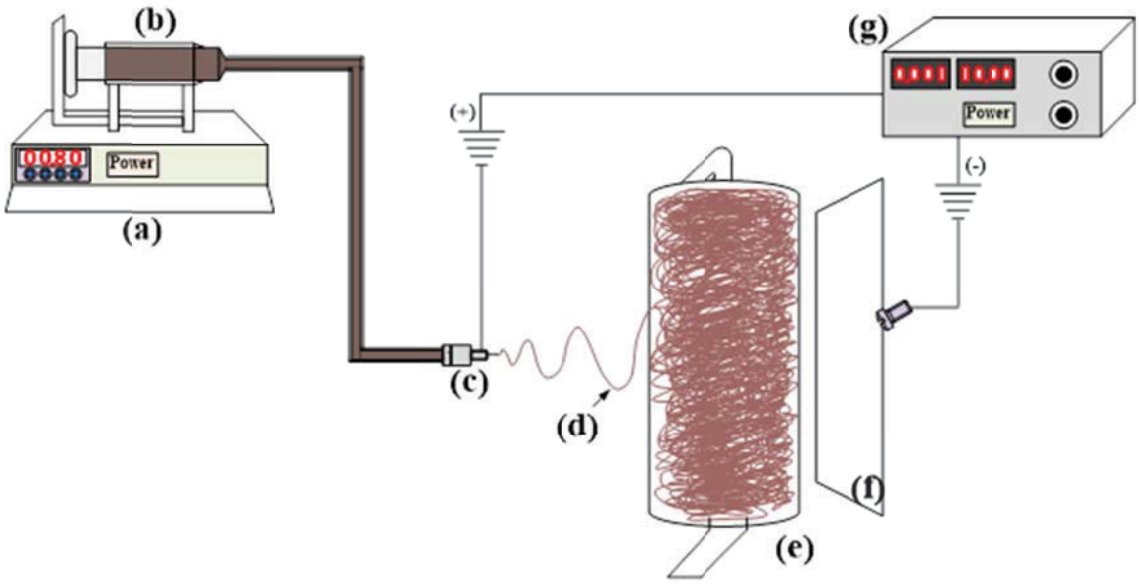

Figure 3.1. Schematic diagram of the electrospinning device: (a) syringe pump, (b) polymer solution, (c) tip, (d) nanofiber, (e) collector, (f) plate and (g) high voltage power supply.

3.3.2 CF_4 plasma modification

For plasma treatment, an IoN 40 plasma system (PVA TePla Co.Ltd.) equipped with parallel plate electrodes coupled with a radio frequency (RF) glow discharge system was utilized (Tian, Yin, et al. 2015). The membranes were first placed on the plates, then, CF_4 gas was introduced to the chamber at a flow rate of 250 standard cubic centimeter per minute (SCCM) (Yang et al. 2014b). RF glow discharge power was set at 150 W, and the treatment time was varied at 5, 10, 15, 20, 30, and 60 min (herein referred to as P/CF-5, P/CF-10, P/CF-15, P/CF-20, P/CF-30, and P/CF-60, respectively) to find the optimum treatment time (Wei et al. 2012). After the treatment, the chamber was purged with N_2 for around 10 min at atmospheric pressure to reduce the physical adsorption of CF_4 gas on the surfaces. Thereafter, the treated membrane was taken out from the chamber and was kept in a clean holder for 24 h before using for further tests and characterization.

3.4 Laboratory MD process

3.4.1 DCMD experiments

Figure 3.2 shows a schematic layout of the DCMD system used in the present study. The produced membranes were placed in a home-made module, and sealed tightly. Both feed and permeate streams had identical flow channels with dimensions (L x W x H): 77 mm x 26 mm x 3 mm. The effective surface area of the membrane was 20 cm^2. The feed and permeate streams were both cycled through the MD cell each at 400 ml/h forming a counter flow set-up. The feed stream was composed of either de-ionized (DI) water, 35 g/L NaCl or 70 g/L NaCl aqueous solutions, while DI with an initial conductivity of <5 µS/cm was used in the permeate stream. The inlet temperatures at the feed and permeate

streams were maintained at 60 ± 1°C and 20 ± 1°C, respectively. The permeate flux was calculated according to **eq.3.1**, which is based from the change in weight through time of the water at the permeate tank as automatically measured by a digital balance (PGW 4502e, Adam) connected to a personal computer. The conductivity of the feed and permeate solutions was monitored throughout the test using a portable conductivity meter (HQ40d, Hach). Salt rejection performance of DCMD was then calculated using **eq.3.2**, which is based from the measurements of the initial and final electrical conductivities to get the concentrations of the feed and permeate solutions. The DCMD performance of the membranes was compared to a commercial flat-sheet PVDF membrane (GVHP, Millipore).

$$\boldsymbol{J = \frac{\Delta g}{A \times \Delta t}} \qquad \textbf{(eq.3.1)}$$

$$\boldsymbol{SR = \frac{C_f - C_p}{C_f} \times 100} \qquad \textbf{(eq.3.2)}$$

In the above equations, *J, Δg, A, t,, SR, C_f,* and C_p represent the water permeate flux (L/m^{2}h or LMH), mass of permeate water (L), effective membrane area (m^2), sampling time (s), salt rejection (%), feed concentration (mg/L), and permeate concentration (mg/L), respectively.

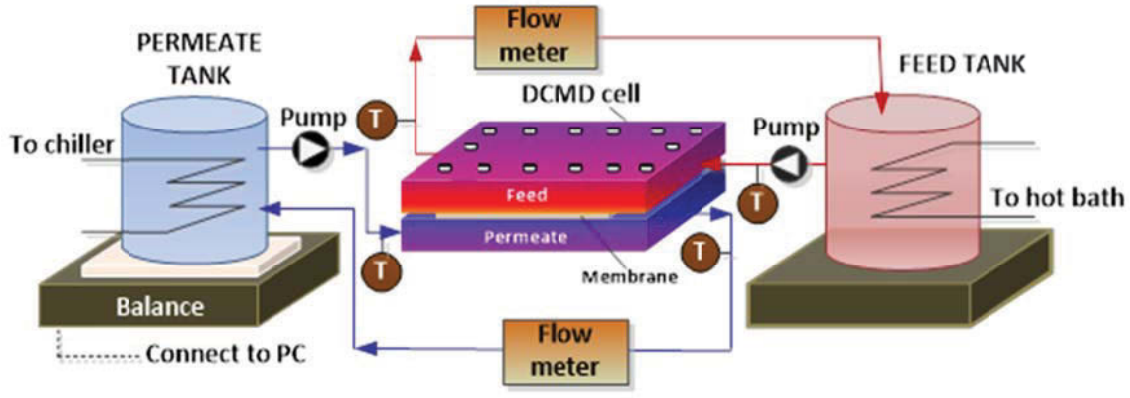

Figure 3.2. Schematic illustrations of the direct contact membrane distillation (DCMD) system

3.4.2 AGMD experiments

The commercial and fabricated membranes were also tested in a home-made AGMD set-up with an effective membrane area of 21 cm^2 and a feed channel dimension of 60 mm × 35 mm × 1 mm (L × W × H) (**Fig. 3.3**). The thickness of the air gap was 3 mm. The coolant plate was made of a stainless steel (SUS-316L) to condense the water vapor and produce pure water. The AGMD in a co-current flow set-up was carried out with constant inlet temperatures at the feed and the coolant sides of 60.0 ± 1.5°C and 20.0 ± 1.5°C, respectively. The feed solution was 3.5 wt% NaCl solution (conductivity of 62.0 ± 0.5 mS/cm). The feed and coolant circulation rates were both maintained at 24 L/h. The inlet and outlet temperatures on both feed and coolant sides were measured by thermocouples. The concentration of the feed and permeate water was constantly measured with electrical conductivity meters (HQ40d, Hach) throughout the tests. A commercial PVDF flat-sheet membrane (pore size = 0.22 μm, Durapore®-GVHP, Millipore) was used for comparison. The normalized flux was calculated according to the following equation (Woo et al. 2015):

$$J/J_o\ (\%) = \frac{Flux_E}{Flux_I} \times 100 \qquad \textbf{(eq.3.3)}$$

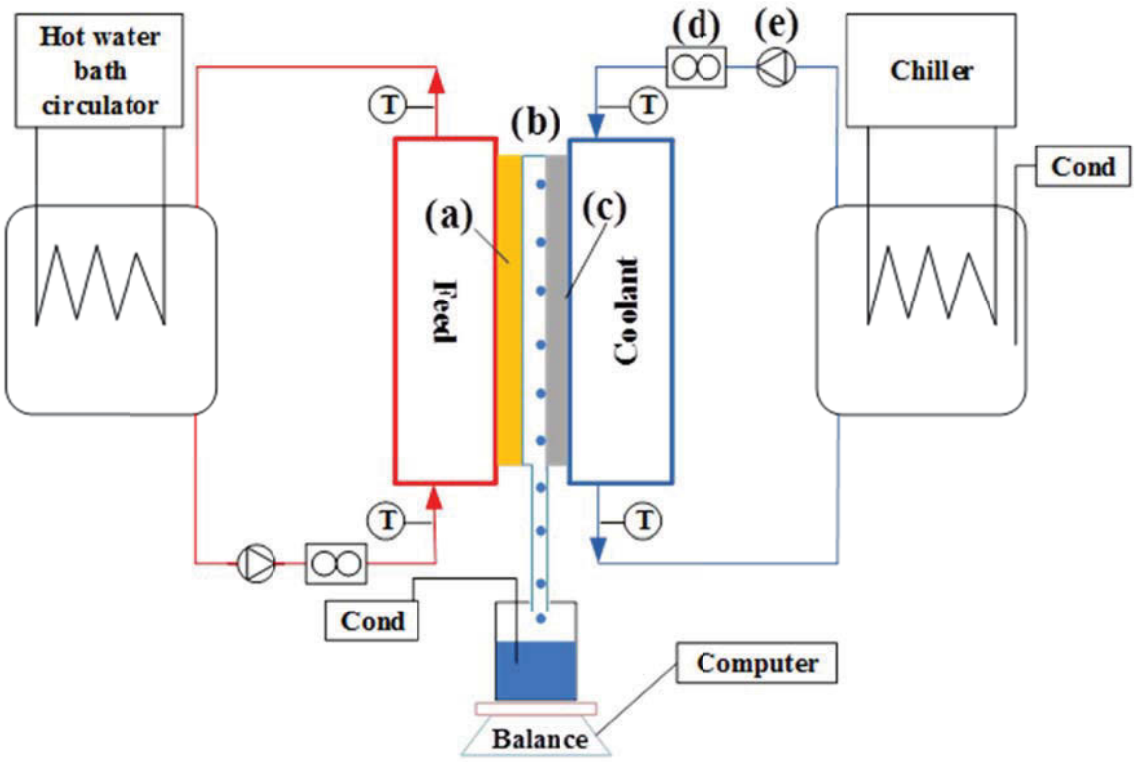

Figure 3.3. Schematic diagram of air gap membrane distillation (AGMD) process: (a) membrane, (b) air-gap, (c) condenser, (d) flow meter and (e) pump

3.5 Membrane characterization and measurements

3.5.1 Scanning Electron Microscope (SEM) and energy dispersive X-ray spectroscopy (EDX)

The surface and cross-sectional morphologies of the fabricated membranes were observed by scanning electron microscopy (SEM, Zeiss Supra 55VP, Carl Zeiss AG) and energy dispersive x-ray spectroscopy (EDX). Samples taken from each membrane were first lightly coated with Au/Pd. The SEM imaging was carried out at an accelerating voltage of 10 kV, and multiple image magnifications at various areas were taken for each sample.

3.5.2 Transmission electron microscopy (TEM)

The morphology of the pristine nanoparticles and the nanofibers was observed by transmission electron microscopy (TEM, Tecnai T20, FEI Tecnai^{TM}). The nanofibers and pristine nanoparticles were placed on 200 mesh copper grid (Ted Pella Inc., CA, USA) and examined with high resolution TEM.

3.5.3 Liquid entry pressure (LEP)

Liquid entry pressure (LEP) is the minimum pressure required to enable water to penetrate the membrane pores. LEP is affected by the membrane hydrophobicity, maximum pore size and pore shape, and can be calculated using the Laplace equation (Yao et al. 2016). In the present study, the LEP of the membrane was obtained using a home-made LEP apparatus as shown schematically in **Figure 3.4**. The reservoir was first filled with 25 mL distilled water and then a dry membrane sample (effective surface area = 7 cm^2) was tightly secured in the cell. Nitrogen gas was then supplied through the bottom of the water-filled chamber, raising the pressure step wise thereby pushing the water up to the membrane sample. The first sign of water bubble on the top of the membrane was regarded as the LEP. To reduce the error, triplicate measurements were taken and averaged.

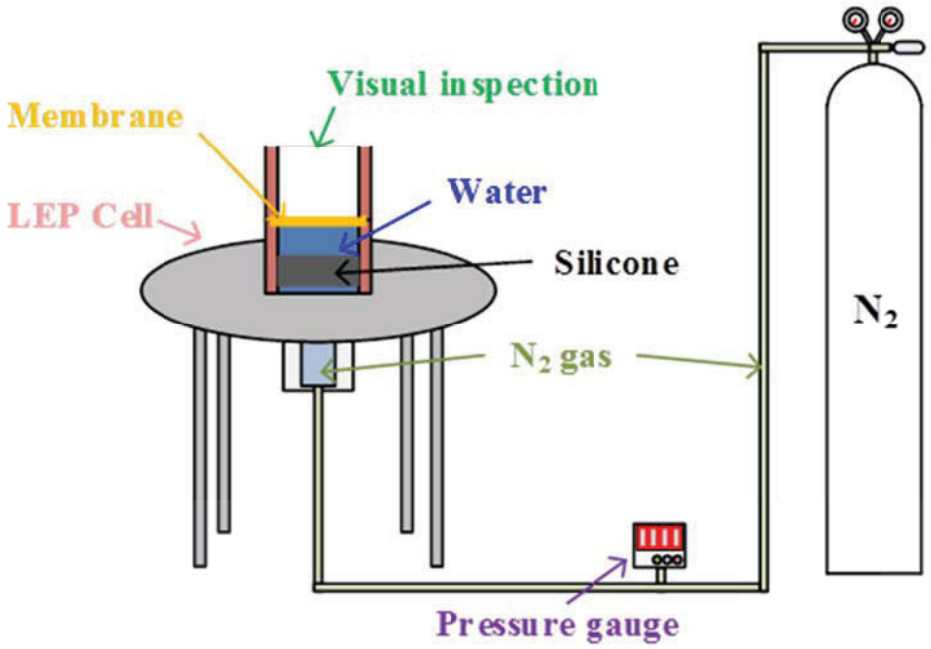

Figure 3.4. Schematic lay-out of the LEP apparatus (Woo et al. 2016).

3.5.4 Contact angle (CA)

The membrane contact angle (CA) was measured by the sessile drop method using an optical subsystem (Theta Lite 100) integrated with image-processing software. Sample membranes were placed on a platform, and droplets of 5-8 µL were dropped carefully on the membrane surface. A real-time camera captured the image of the droplet, and the CA was estimated by a computer. At least 5 measurements were taken for each membrane sample and the average value is reported here.

3.5.5 Sliding angle (SA)

Water sliding angle (SA) was measured using a tilting method as reported in other studies (Artus et al. 2006; Furstner & Barthlott 2005; Pierce, Carmona & Amirfazli 2008). SA shows the difference between advancing and receding CA, i.e., hysteresis

(Artus et al. 2006; Jin et al. 2005). A 10 μL water droplet was first placed on neat and modified membranes and the water droplet was then gradually tilted until the water droplet started to slide on the membrane surface, and that tilting angle was recorded as SA (Valk et al. 1983).

3.5.6 Surface free energy (SFE)

The surface free energy (SFE) of the membrane surface can be obtained via the contact angle measurements employing the Lifshitz van der Walls (non-polar, γ_m^{LW}) and Lewis acid-base (polar, γ_m^{AB}) approaches using three different liquids (two polar and one non-polar) of well-known surface tension (Zhao, Chen, et al. 2013). The total SFE of a membrane can be written as follow (van Oss 2007):

$$\gamma_m^T = \gamma_m^{LW} + \gamma_m^{AB} \qquad \textbf{(eq.3.4)}$$

$$\gamma_m^{AB} = 2\sqrt{\gamma_m^+ \gamma_m^-} \qquad \textbf{(eq.3.5)}$$

where, γ_m^T, γ_m^{LW}, γ_m^{AB}, γ_m^+, and γ_m^- represent the total SFE of the membrane, the Lifshitz van der Walls interactions of the membrane (dispersive component), the acid-base interactions of the membrane (polar component), the electron acceptor parameter and the electron donor parameter, respectively (Nishino et al. 1999).

3.5.7 Surface roughness by atomic force microscopy (AFM)

Membrane surface roughness was analyzed by atomic force microscopy (AFM) imaging. AFM was carried out under ambient conditions in non-contact mode with silicon probes (Dimension 3100 Scanning Probe Microscope, Bruker). All membranes were scanned three times, and each time the scan position was randomly selected (Kim, Lee, et al. 2015).

3.5.8 Tensile properties

The mechanical properties of the different membrane samples were measured using a Universal Testing Machine (UTM LS, Lloyd) equipped with a 1 kN load cell. The test was conducted using a constant elongation velocity of 5 mm/min under room temperature.

3.5.9 Pore size and pore size distribution (PSD)

The pore size of the fabricated and modified electrospun nanofiber membranes (ENMs) was measured by capillary flow porometry (Porolux 1000). All samples were firstly applied with N_2 gas to determine the gas permeability. Then the dry samples were wetted by Porefil (a wetting liquid with a low surface tension of 16 dynes/cm) and tested under the same condition (Tian, Yin, et al. 2015). The mean pore size of the samples was calculated at wet, dry and half dry conditions.

3.5.10 Porosity

The membrane porosity, defined as the volume of pores divided by the total volume of the membrane, was measured via a gravimetric method (Tijing, Woo, et al. 2014). Membrane samples with equal sizes of (2 cm x 2 cm) were first wetted by ethanol (Scharlau), after that, samples were immersed in DI water for replacing the ethanol within the ENM pores. The weight of the samples was measured before and after saturation of DI water, and the membrane porosity was determined by the following equation (Wei et al. 2012):

$$\rho = \frac{(W_1 - W_2)/D_e}{[(W_1 - W_2)/D_e] + W_2/D_p} \quad \textbf{(eq.3.6)}$$

where ρ is the porosity, W_1 is the weight (g) of the saturated membrane, W_2 is the weight (g) of the dry membrane, D_e is the density (g/m^3) of DI water and D_p is the overall density (g/m^3) of PVDF material.

3.5.11 X-ray diffraction (XRD)

X-Ray diffraction (XRD) (Siemens D5000) was carried out over Bragg angles ranging from 10° to 50° (Cu Kα, λ=1.54059Å). Membrane samples with equal sizes of (3 cm x 3 cm) were attached on sample holders.

3.5.12 X-ray photoelectron spectroscopy (XPS)

The chemical composition of the nanofiber and phase-inverted membranes was measured by X-ray photoelectron spectroscopy (ESCALAB250Xi, Thermo Scientific, UK) with a monochromated Al K alpha X-ray source (1486.68 eV), and the pressure in the analyzing vacuum chamber was higher than 2×10^{-9} mbar. Surface survey data was obtained by high resolution scans over C1s (281 - 298 eV), O1s (528 - 540 eV), Cl2p (196 - 208 eV), N1s (396 - 407 eV), Si2p (99 - 108 eV) and F1s (682 - 695 eV). Peak areas and relative peak area ratios were calculated by software (Avantage).

3.5.13 Attenuated total reflectance – Fourier transform infrared spect roscopy (ATR-FTIR)

The material analysis was done by attenuated total reflectance Fourier transform infrared spectroscopy (ATR-FTIR) via Paragon 1000 Spectrometer (PerkinElmer, USA)

in the range of 500-4000 cm^{-1} with a signal resolution of 1 cm^{-1} and a minimum of 16 scans.

3.5.14 Raman spectra

Raman spectra of the membranes were obtained via a Renishaw in Via Raman spectrometer system (Renishaw, Gloucestershire, UK) using a He-Ne laser source at 633 nm with a spectral resolution of 1 cm^{-1}.

3.5.15 The Brunauer-Emmett-Teller (BET)

In order to investigate the textural properties of membranes, the well-known nitrogen adsorption/desorption experiments were performed at 77 K using the nanoPOROSITY adsorption analyzer (Mirae SI, Korea). Before the test, the samples were degassed in vacuum for 24 h to eliminate the surface contaminants including the moisture. The textural properties including specific surface area, pore volume, pore size distributions were determined using the Brunauer–Emmett–Teller (BET) and the Barrett–Joyner–Halenda (BJH) methods. In addition, the nitrogen adsorption energy distributions were calculated using the generalized nonlinear regularization method (Nahm et al. 2012; Roths et al. 2001; Shim, Lee & Kim 2008).

3.5.16 Thermogravimetric analysis (TGA)

Thermogravimetric analysis (TGA) was carried out using a Q600 (TA Instuments). The fabricated membranes were heated to 1000°C at a rate of 10°C/min in N_2.

CHAPTER 4

University of Technology Sydney
FACULTY OF ENGINEERING

Hydrophobic/hydrophilic dual-layer electrospun nanofiber membrane for seawater desalination by membrane distillation application

4.1 Introduction

Currently, the membranes used for membrane distillation (MD) studies are usually microfiltration (MF) membranes, which are made of either polyvinylidene fluoride (PVDF), polytetrafluoroethylene (PTFE), or polypropylene (PP). However, some properties of MD are still needed to be enhanced. Moreover, for higher efficiency MD, better hydrophobicity, higher porosity, adequate pore size, and narrower pore size distribution are the main focuses to enhance the performance of the membranes. Thus, there is a need to improve the design and structure of current MD membranes.

Although phase inversion and melting are the usual techniques for MD membrane fabrication, in recent years, a number of research groups started to look into nanotechnology specifically the electrospinning technique to prepare novel membranes (Feng et al. 2013; Tijing, Choi, et al. 2014). Electrospinning is an excellent method in fabricating nanofiber membranes through the use of high electric fields applied on a polymer solution (Tijing et al. 2012). Among the advantages of electrospinning include the production of nanofiber membranes with high surface area, high hydrophobicity and surface porosity, and adjustable pore sizes and membrane thickness (Amarjargal et al. 2012), which make them an attractive candidate as MD membranes (Essalhi & Khayet 2013a; Feng et al. 2008). However, most of the previous research in literature using nanofiber membrane employed only single-layer membranes with or without a backing layer for direct contact MD (DCMD) application (Tijing, Choi, et al. 2014). Essalhi and Khayet (Essalhi & Khayet 2013a, 2013b) investigated the effect of different electrospinning duration on the characteristics and DCMD performance of single-layer self-standing PVDF nanofiber membranes. Su et al. (Su et al. 2012) utilized PVDF and polyvinylidene fluoride-co-hexafluoropropylene (PH) as polymers of electrospun

nanofiber membranes (ENM) for desalination by DCMD. Liao et al. fabricated single-layer ENM with and without heat-press treatment or surface modification and tested for DCMD performance (Liao, Wang & Fane 2014; Liao et al. 2013). Lalia et al. (Lalia, Guillen-Burrieza, et al. 2013) reported an increased DCMD performance of PH nanofibers after undergoing heat-press post-treatment. Tijing et al. (Tijing, Choi, et al. 2014) reported a comprehensive review of the recent progress of the use of nanofiber membrane for MD application.

Other studies reported on the use of dual-layer or triple-layer membrane for MD application. However, most of the dual-layer membrane reports used phase inversion, melting method, and wet spinning to fabricate flat-sheet or hollow fiber membranes, and not by electrospinning (Bonyadi & Chung 2007; Edwie, Teoh & Chung 2012; Su et al. 2010; Wang, Teoh & Chung 2011). Studies reported that using hydrophobic/hydrophilic dual-layer hollow fibre membrane for long-term DCMD operation showed less pore wetting problem. The group of Khayet (Essalhi & Khayet 2012, 2014; Khayet, Matsuura & Mengual 2005; Qtaishat, Khayet & Matsuura 2009a, 2009b) published several papers related to hydrophobic/hydrophilic dual-layer flat-sheet membrane by a casting method. They reported that an increase of the thermal conductivity of the hydrophilic support layer of a dual-layer membrane can result to an increase in the MD permeate flux. Additionally, a thin hydrophobic layer (i.e., the active layer) leads to better flux performance. Prince et al. (Prince et al. 2013) employed different membrane configurations from single-layer, dual-layer, and triple-layer membranes for air gap MD (AGMD) applications. They used electrospun nanofiber layer as the top layer (i.e., the active layer facing the feed), a cast middle layer and a commercial backing support. They reported that if nanofiber membranes were to be used for AGMD or vacuum MD

(VMD), the pore wetting problem would more likely be obtained due to the differential pressure across the membrane. **Table 4.1** shows some of the previous reports found in literature on the fabrication and investigation of dual-layer membranes for MD applications.

Table 4.1. Reports in literature on hydrophobic/hydrophilic dual-layer membrane for MD application (Inlet temperatures: feed = 60^{o}C, permeate = 20^{o}C).

MD application	Fabricating method	Layer format	Active layer	Support layer	Pore size (μm)	Porosity (%)	Contact angle of active-layer	Flux (L/m^2 h)	Salt rejection (%)	Reference
DCMD	Dry-jet wet phase inversion	Hollow fibre dual-layer	PVDF/MeOH/NMP	PVDF/PAN/Closite NA+/NMP/EG	0.47	75.4 ± 0.3	136.1	83.4 ± 3.7	99.99	(Edwie, Teoh & Chung 2012)
DCMD	Dry-jet wet-spinning	Hollow fibre dual-layer	PVDF/Closite 15A	PAN/Closite NA+/graphite/MWNT	0.41	80	-	66.9	-	(Su et al. 2010)
DCMD	Dry-jet wet-spinning	Hollow fibre dual-layer	PVDF/NMP/Closite 15A	PVDF/PAN/NMP/Closite NA+	0.41	80	137	55.2	-	(Bonyadi & Chung 2007)
DCMD	Dry-jet wet phase inversion	Hollow fibre dual-layer	PVDF/NMP/EG/PTFE	PVDF/NMP/EG/Closite 20A	-	84.0 ± 1.1	110 ± 2.9	98.6	99.99	(Wang, Teoh & Chung 2011)
DCMD AGMD	Phase inversion	Flat sheet dual-layer	SMM	PEI	0.03	-	-	13/6.2	99.90/99.70	(Essalhi & Khayet 2012)
AGMD LGMD	Phase inversion	Flat sheet dual-layer	SMM	PEI	0.02	-	94.8 ± 0.5	9/9.5	99.60/99.57	(Essalhi & Khayet 2014)
AGMD	Casting with electrospinning	Flat sheet triple-layer	PVDF/PVDF-PVP	PET	0.1	-	145.0 ± 1.2	15.2	99.98	(Prince et al. 2013)
DCMD	Electrospinning	Flat sheet dual-layer	PVDF/silica	PVDF	0.36	64	150	16 ~ 27	99.99	(Liao et al. 2014)

LGMD: liquid gap membrane distillation

In this chapter, a hydrophobic/hydrophilic nanofiber membrane was fabricated using an electrospinning technique and tested for their AGMD performance. Here, in contrast with the previous studies using flat sheet and hollow fiber membranes made by phase inversion and wet spinning, our fabricated membranes are wholly made of electrospun

nanofibers composed of two layers: the top (active) layer, which faces the feed side is made of hydrophobic nanofibers, and the lower layer, which faces the permeate side (in this case, the air gap) is made of hydrophilic nanofibers. Our previous study (Tijing, Woo, et al. 2014) on the use of a dual-layer nanofiber membrane using PH as the active membrane surface layer and polyacrylonitrile (PAN) as a support layer showed promising results in its DCMD performance. The main objective of this chapter was to investigate the effect on the AGMD flux and rejection performance of the different wettability (hydrophilicity) and characteristics of the bottom layer of a dual-layer hydrophobic/hydrophilic nanofiber membrane. The top layer (i.e., the active layer) was made of PH nanofibers, while the bottom support layer was made of either PAN, nylon-6 (N6) or polyvinyl alcohol (PVA) nanofibers. PH was used as the top (active) layer as PVDF-based membranes are usually used for commercial membrane separation applications due to their good mechanical, thermal and chemical stability (Park et al. 2014). Furthermore, PH was chosen due to its higher hydrophobicity and free volume properties than PVDF (Lalia, Guillen-Burrieza, et al. 2013). On the other hand, PAN, N6 and PVA are hydrophilic materials that have been employed as water filtration materials in many studies. They possess good thermal and chemical stability as well as good electrospinnability, so that they were chosen as support layer materials in this study.

Heat-press post-treatment was applied to the electrospun nanofibers to investigate its effect on the mechanical and physical properties of the dual-layer nanofiber membrane. Previous studies showed better pore size distribution and smaller pore sizes after exposing the membrane to heat pressing (Lalia, Guillen-Burrieza, et al. 2013). Improving the mechanical and physical properties of the membranes makes them more

attractive for long-term operation in MD process (Kim, Ahn & Choi 2010; Na et al. 2008). The present study provides a better understanding of the role of the support layer of the dual-layer electrospun nanofiber membranes for their performance in desalination by AGMD.

This chapter is an extension of the research article published by the author in Desalination.

4.2 Experimental

4.2.1 Materials

PH (Mw = 455,000 g/mol), PAN (Mw = 150,000 g/mol), N6 (Mw = 10,000 g/mol), PVA (Mw = 85,000-124,000 g/mol, hydrolysis = 87-89%), N,N-dimethylformamide (DMF), lithium chloride (LiCl), and Triton X-100 were all purchased from Sigma-Aldrich. The solvents formic acid and acetic acid were bought from Chem-Supply and Ajax Finechem Pty Ltd, respectively. All chemicals were used as received. In addition, a commercial PVDF membrane (Durapore®-GVHP, pore size of 0.22 μm) was purchased from Millipore.

4.2.2 Dope preparation

Neat PH solution was prepared by dissolving through overnight stirring of 20 wt% PH in a mixed solvent composed of DMF and acetone (4:1 by wt%). A small amount of LiCl was added to the PH solution to improve its electrospinnability (Tijing, Woo, et al. 2014). PAN (10 wt%) was dissolved in DMF by stirring for 1 h at 60^{o}C then followed by stirring at room temperature for 1 day. N6 pellets were dissolved in formic/acetic (4:1 v/v) solution for 1 day by vigorous stirring. PVA solution at 10 wt% was prepared

in distilled water as solvent with an addition of 0.6 v/wt% Triton X-100 to lower the surface tension by stirring for 3 h at 160^{o}C, then followed by stirring at room temperature for 1 day.

4.2.3 Electrospinning

The electrospinning parameters and conditions used in this study are listed in **Table 4.2**. As a baseline membrane, neat 20 wt% PH nanofibers were directly fabricated onto a rotating drum collector (termed here as as-spun membrane). To fabricate dual-layer electrospun nanofiber membranes, different kinds of support layer solutions (i.e, either PAN, N6 or PVA) were first electrospun directly to the collector covered with foil, followed by electrospinning of PH nanofibers on top of the support layer membrane. PH and support layer thickness ratio was maintained at 50/50. The nozzle mounted on an adaptor was kept on oscillating laterally controlled by LabView software (National Instrument) for a distance of 20 cm. The chamber humidity (40 ~ 45 %) and temperature (20 ~ 25 °C) were also maintained constant for all tests. After electrospinning, the fabricated membranes were dried in an oven at 60 °C for 2 days to remove the residual solvents. Heat-press post-treatment was then employed by pressing the dry nanofiber membranes between two flat-plates with a dead weight of 6.8 kg inside a dry oven at 170 °C for 1.5 h. Since PVA was water soluble, a cross-linking process was carried out to make it more stable. Electrospun PVA nanofibers were cross-linked by immersing them in 0.05 M glutaraldehyde (GA) and 0.02 M hydrochloric acid (HCl) in acetone solution for 1 day. After cross-linking, the PVA nanofibers were washed several times with acetone and then kept in water before use (Yoon, Hsiao & Chu 2009).

Table 4.2. Electrospinning conditions used in the present study

	Applied voltage (kV)	Polymer solution flow rate (ml/h)	Tip-to-collector distance (cm)
PH	21	0.8	20
PAN	18	1.2	20
N6	22	0.6	15
PVA	27	0.8	10

4.2.4 AGMD test

The commercial, single-layer and dual-layer electrospun nanofiber membranes were tested in a home-made AGMD set-up with an effective membrane area of 21 cm^2 and a feed channel dimension of 60 × 35 × 1 mm (L × W × H). The thickness of the air gap was 3 mm. The coolant plate was made of a stainless steel (SUS-316L) to condense the water vapour and produce pure water. The AGMD in a co-current flow set-up was carried out with constant inlet temperatures at the feed and the coolant sides of 60 ± 1.5 °C and 20 ± 1.5 °C, respectively. The feed solution was 3.5 wt% NaCl solution with conductivity of around 61.5 mS/cm and the coolant fluid was tap water. The feed and coolant circulation rates were both maintained at 12 L/h. The inlet and outlet temperatures on both feed and coolant sides were measured by thermocouples. The concentration of the feed and permeate water was constantly measured with electrical conductivity meters (HQ40d, Hach) throughout the tests. A commercial PVDF flat-sheet membrane (pore size = 0.22 μm, Durapore®-GVHP, Millipore,) was used for comparison.

4.3 Results and discussion

4.3.1 Morphology

The effect of the heat-press process on the membrane characteristics such as pore size, porosity, LEP, contact angle, membrane thickness, fibre diameter and mechanical properties of the electrospun nanofiber membranes are shown in **Table 4.3**. Heat pressing the nanofiber membrane at 170^{o}C (which is near the melting point of PH) for 1.5 h resulted in a decrease in pore size, porosity, membrane thickness and surface contact angle. However it led to an increase in mechanical strength, fibre size, and LEP. The trend of the results reported here is similar with previous studies (Lalia, Guillen-Burrieza, et al. 2013). **Figure 4.1** shows the surface and cross-sectional morphologies of the neat PH nanofiber with and without heat-press treatment. Neat PH nanofibers (M1) (**Fig. 4.1a**) showed cylindrical, beadless and uniform ultrafine fibers with an average fiber diameter of 239.3 ± 67 nm. Generally, the as-spun (non-heat-pressed) membrane is fluffier with sponge-like and irregular structure at the surface (Lalia, Guillen-Burrieza, et al. 2013). On the other hand, the heat-pressed M2 (**Fig. 4.1c**) exhibited bigger and flatter fibers with some melted and fused nodes (inset of **Fig. 4.1c**) forming connection points between the fibers. The heat pressing has increased the fibre diameter to 333.1 ± 104.2 nm or an increase of 39% compared to M1. The heat-pressing of nanofibers brought the fibers closer together and resulted to smaller pores and smoother surface with a much regular structure. The present results are in congruent with the previous studies employing heat press treatment (Bilad, Westbroek & Vankelecom 2011). Cross-sectional views of the M1 (**Fig. 4.1b**) and M2 (**Fig. 4.1d**) showed highly porous and interconnected structure through the depth of the nanofiber membrane. M2 clearly exhibited thinner thickness (a decrease of ~25%) and more compact structure compared to M1, while still maintaining a highly porous morphology (inset of **Fig. 4.1d**). Additionally, melting and flattening of the fibers as well as the compaction of the membrane due to heat press have reduced the mean pore size to 0.25 μm (from 0.34 μm

in M1) and the porosity to 78.6 ± 1.5% (from 89.6%) (Li, Hashaikeh & Arafat 2013). Although the porosity is reduced by heat press, it is still higher than that of the C-PVDF. The higher porosity presents more surface area for the vapour to pass through thereby increasing the permeate flux tendency.

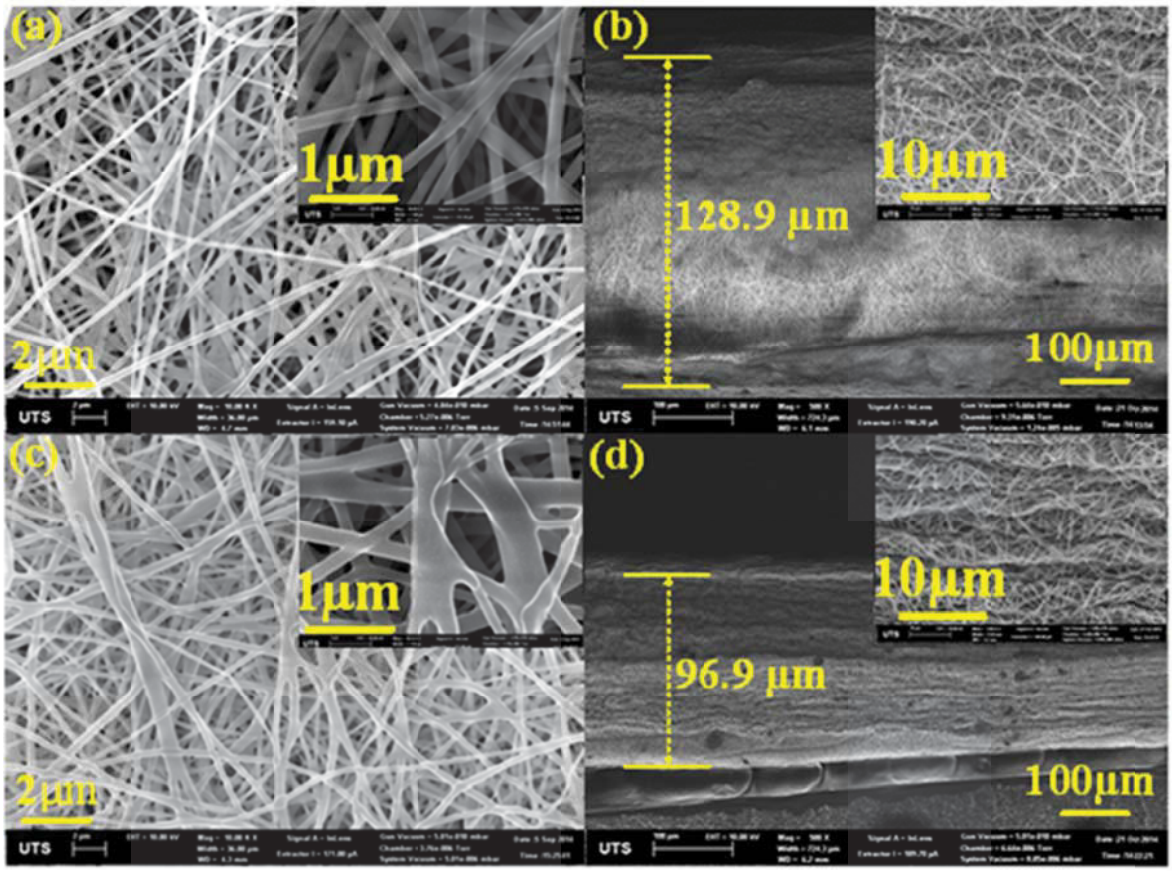

Figure 4.1. High and low magnification surface (a, c) and cross-sectional (b, d) SEM images of (a, b) neat PH (M1) and (c, d) heat-pressed PH (M2) membranes

Table 4.3. Characteristics of the membranes used in this study

Membrane type	Membrane code	Heat-pressed	Mean pore size (µm)	Maximum pore size (µm)	Membrane thickness (µm)	Porosity (%)	LEP (kPa)	Contact angle of the active-layer (deg)	Fibre diameter (nm)	Young's modulus (MPa)	Tensile strength (MPa)	Elongation at break (%)
As-spun neat PH	M1	No	0.34	0.51	128.9 ± 3.0	89.6 ± 0.3	122.3 ± 2.5	148.4 ± 1.6	239.3 ± 67.0	18.2 ± 4.4	9.0 ± 1.4	99.8 ± 5.2
Heat-pressed neat PH	M2	Yes	0.25	0.38	96.9 ± 3.1	78.6 ± 1.5	144.7 ± 1.7	128.6 ± 1.8	333.1 ± 104.2	124.3 ± 6.6	19.5 ± 2.6	59.7 ± 7.4
Dual-layer PH/PAN	M3	No	0.40	0.53	126.7 ± 2.1	90.5 ± 0.3[a]	123.0 ± 0.8	149.8 ± 2.6	270.1 ± 61.7/ 185.5 ± 41.5	52.8 ± 19.7	5.9 ± 0.6	52.1 ± 2.9
Heat-pressed dual-layer PH/PAN	M4	Yes	0.27	0.38	96.3 ± 2.7	81.1 ± 2.0[a]	140.3 ± 0.5	128.5 ± 1.2	333.3 ± 53.5 / 140.0 ± 18.5	129.4 ± 37.2	6.6 ± 0.9	27.6 ± 1.9
Dual-layer PH/N6	M5	No	0.22	0.29	108.3 ± 1.3	91.5 ± 0.7[a]	134.7 ± 3.1	148.9 ± 1.0	285.1 ± 79.5/ 124.3 ± 30.5	37.7 ± 1.4	6.2 ± 1.8	32.4 ± 0.7
Heat-pressed dual-layer PH/N6	M6	Yes	0.18	0.25	92.7 ± 1.0	85.3 ± 0.9[a]	184.7 ± 2.9	126.3 ± 1.5	329.7 ± 126.2 / 110.4 ± 17.6	91.6 ± 16.6	9.6 ± 0.4	28.8 ± 7.1
Dual-layer PH/PVA	M7	No	0.16	0.24	121.4 ± 4.1	92.8 ± 0.4	136.3 ± 1.7[a]	143.5 ± 2.1	168.0 ± 52.0 / 126.8 ± 22.3	58.8 ± 23.0	5.9 ± 2.6	28.0 ± 12.0
Heat-pressed dual-layer PH/PVA	M8	Yes	0.13	0.20	94.1 ± 1.6	86.7 ± 1.0	164.67 ± 2.6[a]	122.4 ± 3.0	302.4 ± 56.0 / 121.0 ± 18.2	117.6 ± 23.4	9.6 ± 1.3	18.4 ± 0.6
Commercial flat-sheet PVDF (GVHP)	C-PVDF	-	0.22	0.29	107.4 ± 1.6	70.3 ± 0.3	213.3 ± 2.1[a]	131.1 ± 3.1	-	183.2 ± 12.4	7.2 ± 0.2	36.3 ± 3.1

[a] Signifies dual-layer values

Figure 4.2 shows the surface and cross-sectional morphologies of the heat-pressed dual-layer nanofiber membranes and the summary is presented in **Table 4.3.** The active top layer of all dual-layer membranes was made of PH, while the support layer was made of either PAN, N6 or PVA. Similar morphologies were observed for the top PH layer showing fiber sizes >300 nm. The support layers showed much smaller diameters than PH nanofiber with N6 and PVA having similar neat fibre diameters of 124-126 nm,

while PAN had 185.5 nm (**Table 4.3**). The heat pressed dual-layer fibers: M4, M6 and M8 showed decreased thickness (about 110-140 μm) from their non-heat-pressed counterpart. Among the support layers, N6 showed the most uniform fiber sizes and smooth structure. As shown in **Fig. 4.2**, M6 has a continuous and fully intertwined fibers of the top PH layer and the bottom N6 layer. However, both M4 and M8 showed some loose overlapping structures between the top and bottom layers, which could allow the penetration and accumulation of small salt water drops (Liao et al. 2013). The accumulation of these drops in the gap/pores could result in a decrease in driving force across the membrane, thus lowering the permeate flux.

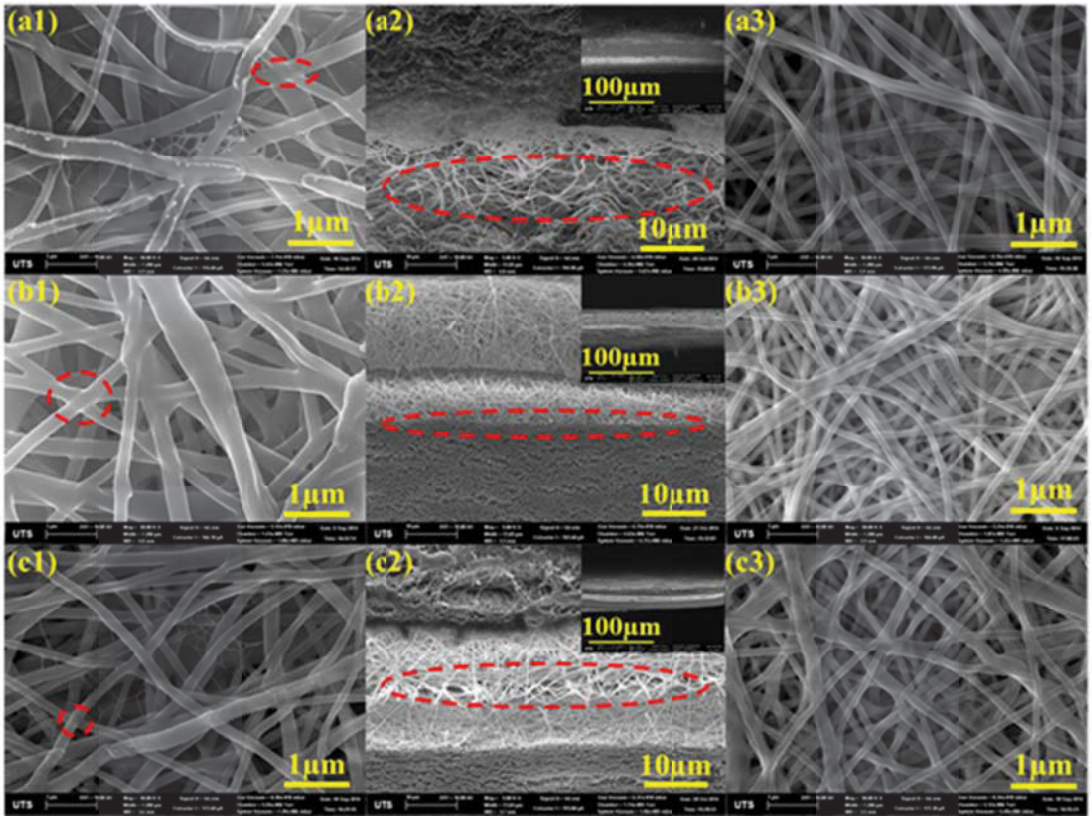

Figure 4.2. SEM images of the active layer made of PH (a1-c1), cross-section (a2-c2) and hydrophilic support layer (a3-c3) of the dual-layer membranes: (a) M4 (PH/PAN), (b) M6 (PH/N6), and M8 (PH/PVA).

4.3.2 Pore size and pore size distribution (PSD)

Figure 4.3 and **Table 4.3** show the pore size and pore size distribution (PSD) of the C-PVDF and nanofiber membranes with and without heat press. The C-PVDF exhibited narrow PSD with an average pore size of 0.22 μm (similar with the manufacturer's data), while M1 nanofiber showed bigger pore size of 0.34 μm, but still with narrow PSD. However, heat pressing of the neat PH nanofiber (M2) lowered the average pore size to 0.25 μm, which was similar with that of C-PVDF. This shows that heat-pressing could be employed to reduce the pore size and other characteristics of the membrane. Studies have reported that a MD membrane pore size of <0.60 μm is needed to lessen the occurrence of pore wetting for long term operation (Liao, Wang & Fane 2013). In this study, all the electrospun nanofiber membranes exhibited a maximum pore size of 0.53 μm, indicating that the fabricated nanofiber membranes have suitable maximum pore size for MD application. All dual-layer nanofiber membranes showed the same decreasing mean pore size trend upon employing heat press treatment to the membrane. PH/PAN nanofibers showed higher mean pore size and wider PSD compared to PH/N6 and PH/PVA nanofibers. This could be attributed to the bigger fibre diameter of the PAN fibers (**Table 4.3**). Among the dual-layer membranes, PH/N6 showed the smallest mean pore size as well as a sharp and narrow PSD, especially after heat press treatment. Interestingly, the M6 dual-layer membrane showed even smaller mean pore size than that of C-PVDF. Studies have shown than smaller pore sizes could lead to higher LEP values, which contributes to less membrane wetting tendency. Additionally, all dual-layer membranes still maintained high porosity (>80%) despite a slight decrease due to the effect of heat press.

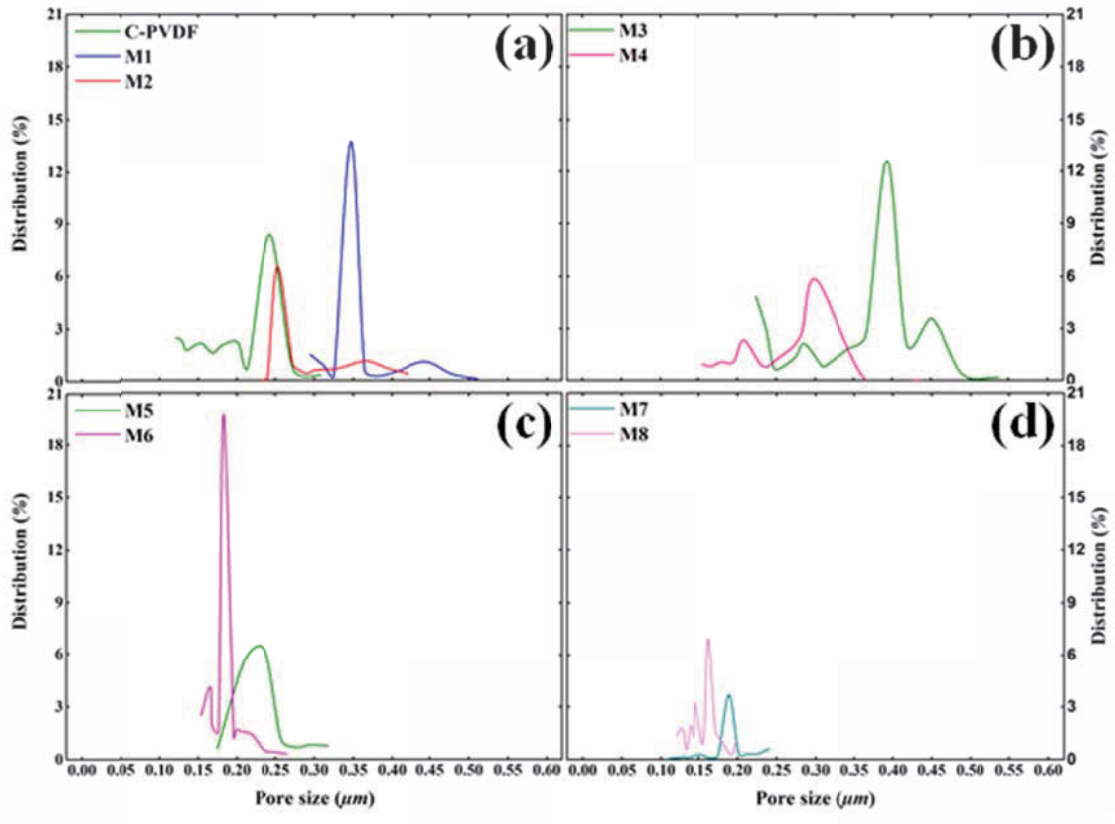

Figure 4.3. Pore size distribution of the membranes: (a) M1, M2 and C-PVDF, (b) M3 and M4, (c) M5 and M6, and (d) M7 and M8

4.3.3 Contact angle (CA)

The water CA results of the electrospun nanofiber membranes are presented in **Table 4.3**. Generally, nanofiber membranes are expected to have higher contact angles compared to the phase inversion sheets because of the overlapping structure of the nanofibers that make the surface rough. As can be seen in **Table 4.3**, the top active layer composed of neat PH nanofibers showed high hydrophobicity from 143.5 to 149.8°, but lowered to 122.4 to 128.6° after heat pressing. The support layers on the other hand have much lower CAs than PH. Heat-pressed PAN (M4) showed a CA of 110° after 10 s, while N6 and PVA had 56 and 70°, respectively. However, at longer duration, the CA of N6 proved to be more stable, which stayed constant at 45° after 150 s, while the other

support layers (M4 and M8), showed decreasing CAs with time. This could impact the wetting issue in AGMD if too hydrophilic support layer is used. For PH nanofiber, the decrease in CA due to heat-press treatment could be explained by the decrease in surface roughness of the surface. Due to the compaction of the membrane, the surface layer is flattened out, which decreases the surface roughness as shown schematically in **Fig. 4.4**. Similar observation was reported by other studies (Lalia, Guillen-Burrieza, et al. 2013). However, the heat-pressed nanofiber membranes still showed high hydrophobicity that is adequate for MD application.

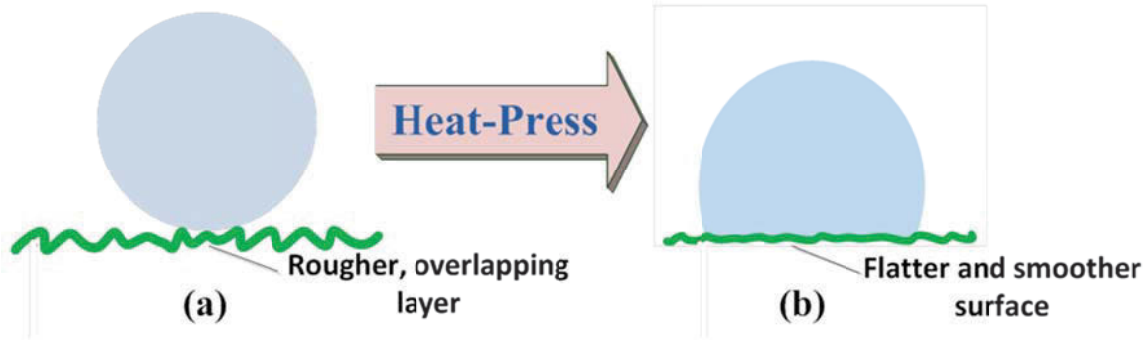

Figure 4.4. Schematic illustrations of water drops on the active-layer of the electrospun nanofiber membranes: (a) without heat-press process, and (b) with heat-press process.

4.3.4 Liquid entry pressure (LEP)

One of the most important membrane properties for MD application is the stability of membrane performance for long-term use, which can be evaluated by its LEP. LEP is the minimum pressure needed for water to penetrate the pores of the membrane, thereby wetting the membrane. For MD applications, higher membrane LEP is desirable to lessen the possibility of pore wetting. LEP measurements were conducted by a home-made set-up and the results are summarized in **Table 4.3**. The neat PH nanofiber (M1)

exhibited an LEP of 122 kPa, which is higher than those reported in literature for nanofiber membranes. The heat pressing process has increased the LEP to 144.7 kPa (M2), which is attributed to the compaction of the membrane and the decrease in pore sizes. LEP is known to be affected by the pore size, hydrophobicity, and thickness of the membrane (Tijing, Choi, et al. 2014). Similar trend was being observed for heat-pressed dual layer membranes compared to their non-pressed counterpart. Interestingly, the addition of hydrophilic support layers to the membrane has improved the overall LEP of the dual-layer membranes, with LEP values of 140, 185 and 165 kPa for M4, M6 and M8, respectively. This increased LEP is attributed to the decreased pore sizes from the heat-pressing, as well as the more uniform PSD, while maintaining a hydrophobic surface. Moreover, the more porous and small pore sizes with thin fiber diameters of the supporting hydrophilic layer have given an additional resistance to water passage. In comparison, C-PVDF has an LEP of 213 kPa, which is higher than all dual-layer nanofiber membranes, which could be because of the surface morphology of the C-PVDF membrane (not shown), where many dense areas exist (lower porosity), resulting to smaller surface area for water penetration. The present LEP values of our dual-layer nanofiber membranes are much higher compared to those reported in literature for nanofiber membranes.

4.3.5 Mechanical properties

The MD process generally operates at atmospheric pressure, thus the membrane has less requirements for mechanical integrity. However, for a long term operation, adequate mechanical properties are still needed to provide stable operation, and additionally, the membranes should withstand the stress from packing the membranes in modules (Essalhi & Khayet 2013a). **Figure 4.5** shows the stress-strain curves of the different

nanofiber membranes in comparison with C-PVDF, and the mechanical properties are summarized in **Table 4.3**. Neat PH nanofiber (M1) exhibited a tensile strength of 9 MPa and elongation of 99.8%, with a stress-strain plot showing a falling-rate curve until failure. Heat pressing of the neat PH membrane (M2) has drastically enhanced its tensile strength by 117% (from 9 to 19.5 MPa) with corresponding 40% decrease in elongation at break as expected when the material becomes stiffer. The modulus also increased drastically after heat-pressing, which makes the membrane more compact. The heat-press process of the electrospun nanofiber membranes has been reported to enhance mechanical properties of the membranes (Gopal et al. 2006; Liao et al. 2013; Na et al. 2008). M2 showed a steeper non-linear curve from 0-10% elongation, then to more linear trend thereafter. Interestingly, M2 obtained much higher tensile strength (19.5 MPa) and elongation at break (99.8%) than C-PVDF, where the latter had 7.2 MPa and 36.3%, respectively. During heat pressing, the nodes of the nanofiber are melted together creating a fusion and linking of nanofibers, thereby increasing the mechanical properties of the nanofiber membrane (Gopal et al. 2006). This suggests the good effect of heat pressing in improving the mechanical properties of the membrane, and the nanofiber membrane is adequate for MD application (Lalia, Guillen-Burrieza, et al. 2013). All heat-pressed dual-layer membranes (M4, M6 and M8) showed higher tensile strengths than that of C-PVDF, with M6 (PH/N6) showing the highest among the dual-layer membranes with tensile strength and elongation of 9.6 MPa and 28.8%. The good linking of the PH and N6 layers with interlocking fibers (see **Fig. 4.2b2**) could be the main reason behind the good mechanical performance of M6. With proper heat-press treatment, nanofiber membranes could be used as stand-alone membranes for MD due to its adequate mechanical properties (Gopal et al. 2006).

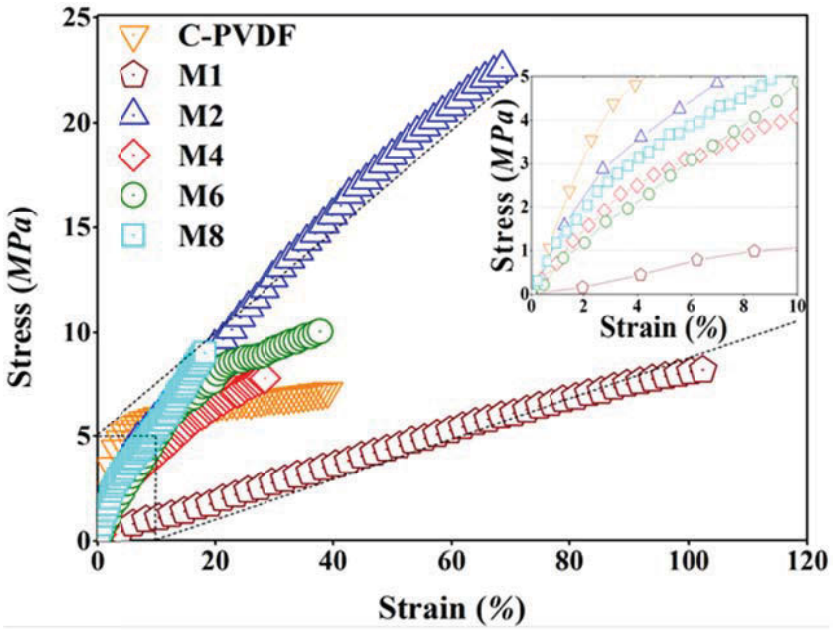

Figure 4.5. Stress-strain curves of the electrospun nanofiber membranes and commercial membrane

4.3.6 AGMD performances

4.3.6.1 Effect of different support layer

Desalination by AGMD was performed using the nanofiber membranes fabricated in this study. Only the heat-pressed membranes were used for AGMD tests because of their improved characteristics compared to non-heat-pressed membranes. The effect of the differences in wettability and characteristics of the support layer (i.e., PAN, N6 and PVA) was investigated. **Figure 4.6** shows the pure water flux and salt rejection performances of the heat-pressed neat PH and dual-layer nanofiber membranes and C-PVDF. The tests were carried out for 10 h with 3.5 wt% NaCl solution as feed under a temperature of 60°C and 20°C at the feed and coolant sides, respectively. For a fair comparison, all membranes have similar thickness between 90 and 110 µm including C-PVDF. All membranes showed similar decreasing trend from their initial fluxes. After

10 h of test, all nanofiber membranes showed higher permeate fluxes compared to that of C-PVDF with a flux trend of M6 (15.5 L/m^{2}h or LMH) > M8 (13 LMH) > M4 (10 LMH) > M2 (7 LMH) > C-PVDF (5 LMH). The better performance of the nanofiber membranes compared to C-PVDF could be attributed to their greater void volume fraction, which allows more surface area for vapour to pass through. Moreover, the higher porosity reduces the conduction heat transfer since air trapped in the voids has much lower conductivity than the polymer (Essalhi & Khayet 2012). Also, the higher hydrophobicity of nanofibers at the surface compared to C-PVDF could have provided more resistance to water penetration. As can be seen in **Fig. 4.2**, the overlapping structure and interconnected pores through the depth of the membrane provide less resistance for vapour to pass through. The dual-layer membranes performed higher flux performance than M2 and C-PVDF depending on the type of support layer. It should be noted that the thickness of the active PH layer of all dual-layer membranes was half of the total membrane thickness. Thus, when compared with M2, the dual-layer membranes provide shorter path for the vapour to pass through, and the other half of membrane, which is the hydrophilic support layer provides lower mass transfer resistance (Su et al. 2010) and lower conduction heat transfer resulting to faster flux rate. The differences in flux performance between the dual-layer membranes could be explained by investigating the characteristics of the support layers, since the top active layer (PH nanofiber) was basically the same conditions for all dual-layer membranes. M6 exhibited the highest flux at 15.5 LMH compared to M4 and M8. The smaller fiber diameter of N6 (thus, higher porosity) should have contributed to the smaller overall mean pore size of the membrane as shown in **Table 4.3**, which led to the highest LEP value and flux performance. The overall PSD of the membrane has also affected the flux performance of the dual-layer membranes. As shown in **Fig. 4.3**, the PSD was

mainly affected by the characteristics of the support layer and the heat-pressing process. The sharp and very narrow PSD of M6 helped in the uniform distribution of the vapour through the membrane, thus making more stable flux and salt rejection performances. On the other hand, M4 showed a wider PSD and bigger pore sizes. The bigger fiber diameter of PAN results to lower porosity, thus affecting the permeate flux and salt rejection performances of the membrane. Eventually, M4 exhibited membrane partial pore wetting problem in AGMD application, which seemed to be not practical membrane for MD. Additionally, it was found that the wettability of N6 was more stable through time compared to PAN and PVA, thus a more stable salt rejection was obtained. The salt rejection was within 98-99.5% for all the membranes, where M2, M6 and C-PVDF have similar rejection of >99%. Based from the results, the better performance of the dual-layer membranes is attributed to the thinner active layer thickness and less mass transfer resistance of the hydrophilic support layer compared to the heat pressed PH membrane (M2). M6 showed the best performance from all the membranes, which could be due to the more uniform fiber diameter of N6, smaller mean pore size and consequently, more uniform and narrow PSD of M6. Additionally, the high porosity of N6 as support layer significantly contributed to the increased flux. These properties led to high LEP for M6, which resulted to more stable and high salt rejection and permeate flux.

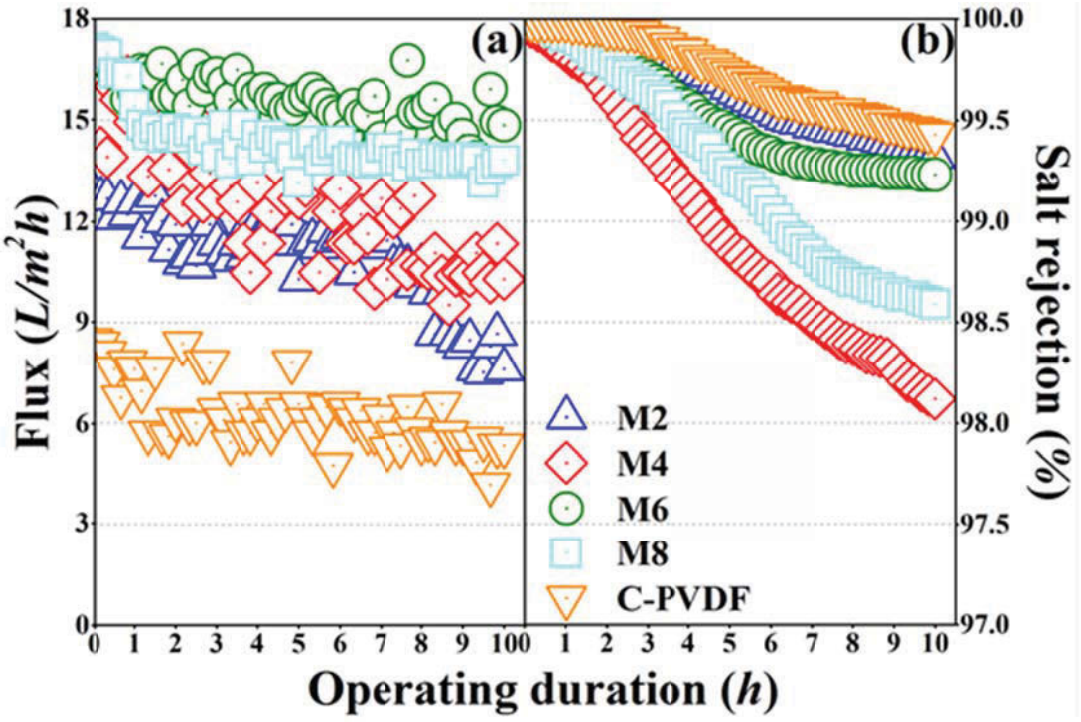

Figure 4.6. (a) Flux and (b) salt rejection performance of the commercial PVDF membrane and the heat-pressed electrospun nanofiber membranes.

4.3.6.2 Effect of feed temperature

In order to study the effect of feed temperature on AGMD flux and rejection performance, we varied the feed temperature from 50 to 80°C and maintained the coolant temperature at 20°C. M6 membrane was chosen in these tests as it previously showed the optimum AGMD performance among all the tested membranes in the present study. The AGMD tests were carried out for a 20-h duration using the same set-up used previously. **Figure 4.7** shows that increasing the feed temperature also increased the permeate flux as similarly observed by other studies (Khayet, Matsuura & Mengual 2005; Prince et al. 2012). The flux obtained was 5, 15, 20, and 25 LMH for a feed temperature of 50, 60, 70 and 80°C, respectively after 20 h. This increasing trend is related to the Antoine equation, where there is an exponential relation between vapour

pressure and temperature (Chiam & Sarbatly 2013). However, the flux trend through time was different for each feed temperature. At lower temperatures (i.e., 50 and 60°C), the permeate flux was very stable for a 20 h period. However, when the feed temperature was increased to 70 and 80°C, the flux curves showed decreasing trend from their initial values. The gradual decrease in flux at higher feed temperatures could be due to the initial expansion of the surface pore sizes at high temperature, and then a faster deposition of salt crystals on the pores, which could have partially clogged up the passage way resulting to lower flux.

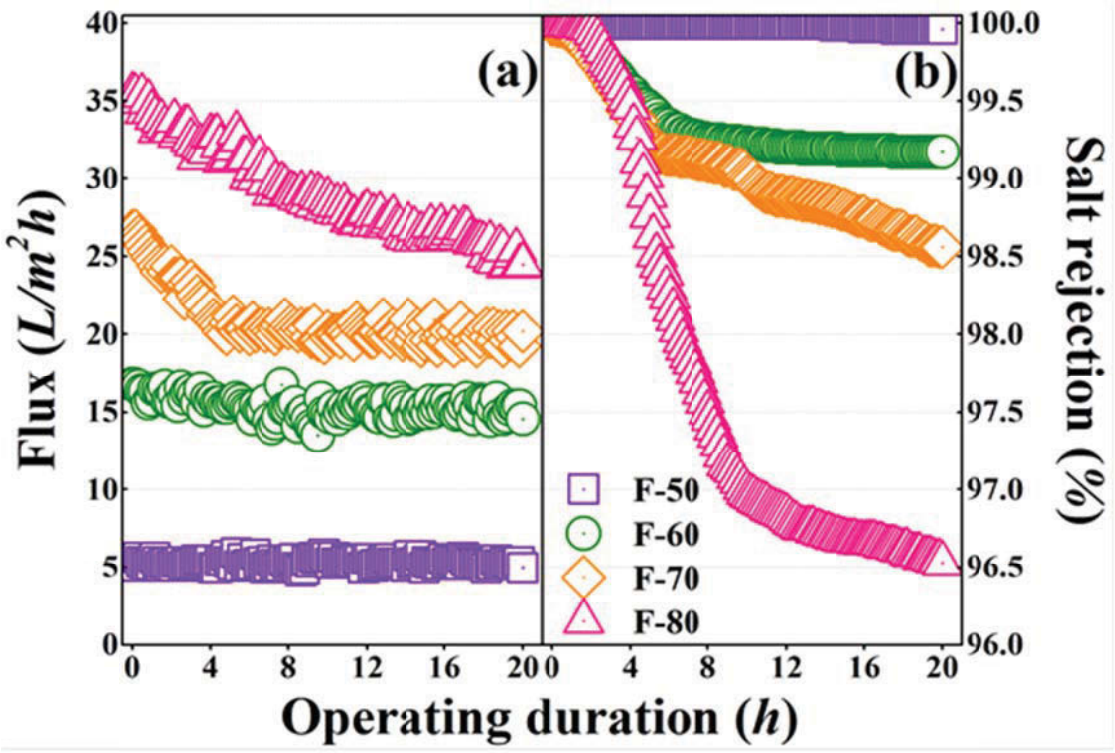

Figure 4.7. (a) Flux and (b) salt rejection performance of the different temperature using the PVDF-HFP/Nylon-6 membrane.

Indeed, NaCl salt crystals were seen on the membrane surface after 20 h test at feed temperature of 70 and 80°C (**Fig. 4.8**). Additionally, the high temperature has led to

higher feed concentration as the evaporation rate of water in the feed tank is faster at high temperature, taking into acount that the feed stream was not refilled with new feed solution during each test (Martinez-Diez, Florido-Diaz & V~quez-GonzS.lez 1999). After 20 h, the conductivity of the remaining feed solution (initial conductivity ~ 61.5 mS/cm) at the tank was 71, 94, 124, and 203 mS/cm, which clearly shows the much increased feed concentration at higher temperatures and it may contribute to concentration polarization (Peng, Fane & Li 2005). Other factors that led to decreasing flux trend are due to a decrease in bulk temperature of the feed with the decrease in feed volume (Alkhudhiri, Darwish & Hilal 2012) and also due to increased permeate temperature as operational time progressed (Alklaibi & Lior 2005). The salt rejection performance corresponded well with the flux profiles, wherein a high salt rejection (99.2 to 99.99%) with good stability was obtained at lower feed temperatures (50 and 60^{o}C). Increasing the feed temperature has resulted to partial pore wetting, especially at the highest feed temperature of 80^{o}C decreasing to 96.5%, where the increase in driving force (i.e., higher temperature difference), could induce the pore wetting phenomena. The results suggest that M6 membranes could be potentially used for desalination by AGMD with stable flux and salt rejection in the feed temperature range of 50 to 60^{o}C based from test range of our present study.

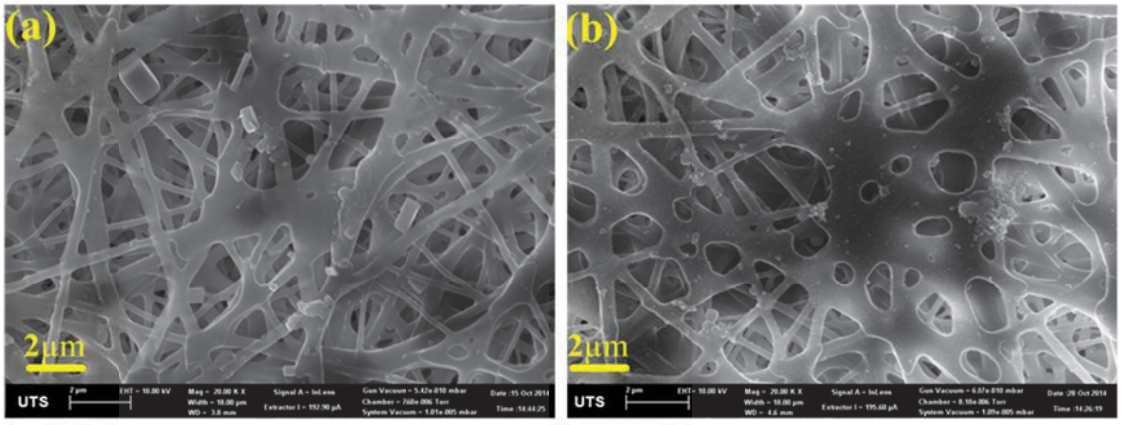

Figure 4.8. Surface SEM images of the membrane after 20 h of test at feed site temperature of: (a) feed – 70 ˚C and (b) feed – 80 ˚C.

4.3.6.3 Comparison with other AGMD flat-sheet membrane

The AGMD performance of the M6 membrane was compared with commercial (GVHP) and other AGMD membranes are produced by different fabrication methods reported in literature (**Table 4.4**). The present dual-layer nanofiber membrane M6 (heat-pressed PH/N6) showed a high flux AGMD performance compared to other reports. Though the flux was comparable with that of Prince et al. (Prince et al. 2013), it should be noted that we used a lower feed temperature of 60^{o}C and a much lower flow rate. The presence of a hydrophilic support layer under an adequate thickness of active hydrophobic top layer has definitely improved the performance of the nanofiber membrane with good and stable flux and salt rejection by AGMD. Based on **Table 4.4**, the flux of the heat-pressed PH/N6 (M6) membrane was better than that of other flat-sheet membranes test under similar conditions. The results demonstrate the potential of the heat-pressed PH/N6 dual-layer nanofiber membrane as a new membrane for AGMD desalination that can be fabricated via a simple electrospinning technique.

Table 4.4. Comparison of results using different membranes in AGMD application

Membrane	Method	Air gap (mm)	Membrane thickness (µm)	Mean pore size (µm)	Contact angle of the active-layer (deg)	Porosity (%)	Feed parameter			Coolant parameter		Permeate flux (L/m^2h)	References
							Solution	Flow rate (L/h)	Feed inlet temperature (°C)	Flow rate (L/h)	Coolant inlet temperature (°C)		
PVDF nanofibre	Electrospinning	2	-	-	-	-	3.5 wt % NaCl	21	62	72	22	4.2	(Feng et al. 2008)
Triple layer membrane	Casting with electrospinning	3	175	0.10	145.0 ± 1.2	-	3.5 wt % NaCl	108	80	108	15 ~ 20	15.2	(Prince et al. 2013)
Composite membrane	Phase inversion	4.4	64.7 ± 6.3	0.03	94.8 ± 0.5	-	3.0 wt % NaCl	100	80	-	20	7.8	(Essalhi & Khayet 2014)
Modified clay ceramic membrane	Grafting modification	10	-	0.18	180	-	0.5 mol/L NaCl	-	95	-	5	7.2	(Khemakhem & Amar 2011)
GVHP (commercial membrane)	-	3	107.4 ± 1.6	0.22	131.1 ± 3.1	70.3 ± 0.3	3.5 wt % NaCl	12	60	12	20	6.2	Present study
M6	Electrospinning	3	92.7 ± 1.0	0.18	126.3 ± 1.5	85.3 ± 0.9	3.5 wt % NaCl	12	60	12	20	15.5	Present study

4.4 Concluding remarks

In the present study, heat-pressed dual-layer nanofiber membranes were fabricated by an electrospinning technique and their performance in desalination by air gap membrane distillation (AGMD) was investigated. The dual-layer nonwoven nanofiber membranes composed of a polyvinylidene fluoride-co-hexapropylene (PH) active top layer and a bottom support layer made of either polyacrylonitrile (PAN), nylon-6 (N6), or polyvinyl alcohol (PVA) have been evaluated and compared with a single-layer nanofiber membrane and a commercial PVDF flat-sheet membrane (C-PVDF). The following are the summary and conclusions drawn from this chapter:

- As-spun neat PH and dual-layer nanofiber membranes showed high porosity, slightly larger mean pore size than commercial GVHP membrane, good pore size distribution, and highly-hydrophobic rough surfaces.
- The heat-press post-treatment of the nanofiber membrane has resulted to:
  - fusion of nanofiber nodes and has increased the mechanical properties of the membrane. The dual-layer nanofiber membranes also showed comparable mechanical properties with C-PVDF.
  - smoother surface resulting to decreased contact angle but still comparable with commercial membrane.
  - decreased but more uniform pore size and narrow pore size distribution (PSD).
  - thinner but more compact membrane, while maintaining high porosity (>80%)
  - increased liquid entry pressure (LEP)
- From among the dual-layer membranes, M6 (heat-preseed PH/N6) showed the best properties with completely intertwined and linked PH-N6 interface, with good PSD and smaller pore size than C-PVDF.
- AGMD test results showed the highest and most stable flux (15 LMH) and salt rejection (>99%) obtained using M6, which was 1.5 times higher flux than that of C-PVDF.
- A support layer that is hydrophilic such as N6 with high porosity, uniform and small fiber diameter, coupled with porous hydrophobic active layer results to high flux performance as it provides reduced mass transfer resistance and less heat transfer loss; a thinner hydrophobic active layer led to increased water permeate flux.

- Increasing the feed temperature resulted to increased permeate flux, but has also increased the tendency of pore wetting.
- Feed temperature at higher than 60^{o}C while maintaining a coolant temperature of 20^{o}C for AGMD process using a dual-layer membrane could be more prone to partial pore wetting. More stable flux and salt rejection was obtained at 50 to 60^{o}C feed temperature.

The results suggest that M6 membranes could be potentially used for desalination by AGMD with stable flux and salt rejection in the feed temperature range of 50 to 60^{o}C.

CHAPTER 5

University of Technology Sydney
FACULTY OF ENGINEERING

SUPERHYDROPHOBIC NANOFIBER MEMBRANE CONTAINING CARBON NANOTUBES FOR HIGH-PERFORMANCE MEMBRANE DISTILLATION

5.1 Introduction

The membrane properties and pore structure play a major role in the selectivity and the permeability of MD (Roy, Bhadra & Mitra 2014), which are dependent on the preparation and synthesis method of the membrane, and the kind of polymer and/or additives used. However, appropriate membranes specifically designed for MD is still lacking, wherein mostly commercially-available microfiltration (MF) membranes made by phase inversion, stretching, sintering or thermally-induced phase separation are currently utilized (Dong et al. 2014). These MF membranes have sub-optimal performance (i.e., low permeability) and wetting issues during the MD process. Hence, a need to develop new membranes specifically designed for MD is imperative to increase its potential for practical applications.

In recent years, electrospun membranes have attracted considerable interest for membrane-based desalination especially MD application (Huang et al. 2003). Although there has been good progress in the preparation of superhydrophobic electrospun membranes for MD application, there are still concerns on the membrane durability and robustness, mechanical stability, and simplicity of preparation. It has been reported that carbon-based membranes or composites particularly utilizing carbon nanotubes (CNTs) can drastically improve the membrane properties and performance. CNTs are extensively studied these days as stand-alone or filler materials of polymer composites for different applications (Goh, Ismail & Ng 2013). CNTs are considered to be ideal nanofillers as they possess high aspect ratio, high thermal and mechanical stabilities, and are light weight (Xiao et al. 2010). They are inherently hydrophobic, thus their application for MD as stand-alone buckypaper or CNT-coated membrane has recently been investigated (Dumée et al. 2011; Dumée et al. 2010; Gethard, Sae-Khow & Mitra

2011; Roy, Bhadra & Mitra 2014). However, stand-alone CNT membranes are prone to damage and delamination, while coated CNTs on polymer membranes usually do not have strong adhesion to the polymer matrix. Preventing or minimizing CNTs from leaking out to the process fluids, which could become a secondary foulant is one important consideration when using CNTs for water treatment and desalination. The CNTs should be robust enough to remain in the membrane, and at the same time add new functionalities to the membrane. The challenge still remains on how to immobilize CNTs on supports without being carried away by fluid flow.

Nanofibers can serve as ideal substrates to immobilize CNTs as they provide very high surface areas. With the combination of the attractive properties of electrospun membrane and the interesting properties of CNTs, a CNT/polymer composite nanofiber via a simple solution blend or colloid electrospinning could provide the optimal membrane properties for MD application. Herein, this chapter describes a facile strategy via one-step colloid electrospinning to fabricate robust, superhydrophobic, and mechanically-strong nanofiber membranes. The unique design includes a two-layer electrospun membrane in the chapter 4, wherein the top thin layer is composed of CNT/polymer nanofiber with increased roughness, and the thick bottom layer is composed of smooth, highly porous neat polymer nanofibers. Benefitting from the incorporation of pristine CNTs, micro/nano beads with CNT protrusions are formed on the top layer, which increases the surface roughness leading to superhydrophobic surface. The two layer design ensures the provision of superhydrophobicity while maintaining desirable characteristics and quality mechanical properties for the whole membrane. To the best of our knowledge, the potential of CNTs as nano-reinforcements to polymeric nanofiber membrane to provide enhanced properties for MD process has

never been studied. The one-step electrospinning process of CNT-incorporated PH nanofibers in this study provides a scalable approach for potential mass manufacturing. This chapter is an extension of the research article published by the author in Journal of Membrane Science.

5.2 Experimental methods

5.2.1 Materials

Polyvinylidene fluoride-co-hexafluoropropylene or PH (Sigma-Aldrich, Mw = 455,000 g mol^{-1}), lithium chloride (powder, Sigma), N,N dimethylformamide (DMF, 99.8% anhydrous, Aldrich), and acetone (analytical grade, Scharlau) were used as received. Polypropylene membrane (spunbond, Hollytex) served as the support layer for the nanofibers and was purchased from Ahlstrom. Multi-walled carbon nanotubes (referred generally herein as CNTs) (diameter = <8 nm, length ~ 10-30 μm, specific surface area ~ 500 m^2/g) were purchased from Cheap Tubes, Inc., USA and were used as received.

5.2.2 Dope preparation

Two solutions were prepared for electrospinning; one was neat PH solution and the other one contained 1 to 5 wt% CNTs w.r.t. to the amount of PH. Neat 20 wt% PH solution was prepared by dissolving a certain amount of PH pellets in DMF/acetone (80/20 by wt%) solvent solution by overnight stirring at room temperature. **Table 5.1** shows the contents of the different dope solutions and their respective codes used in this paper. To prepare the CNT/PH solution, CNTs were first dispersed in a certain amount of DMF for at least 1 h by bath sonication (Soniclean). After sonication, the CNT/DMF solution was mixed with a neat 15 wt% PH solution by rapidly stirring overnight at

room temperature. Before electrospinning, the CNT/PH solution was sonicated for 30 min to disperse the CNTs.

Table 5.1. Dope compositions used for electrospinning in the present study.

Dope/Membrane code	[a]PH (wt%)	DMF (wt%)	Acetone (wt%)	[b]CNT (wt%)
PH	20	64	16	0
1CNT	15	68	17	1
3CNT	15	68	17	3
5CNT	15	68	17	5

[a] Polyvinylidene fluoride-co-hexafluropropylene

[b]Amount of CNTs added to dope solution w.r.t. to the total weight of PH.

5.2.3 Electrospinning parameters

Electrospinning device was composed of a DC voltage power supply (NanoNC, Korea), a plastic syringe (10 ml, Lock-Lauer) with a metallic nozzle (inner diameter of 0.510 mm), a programmable syringe pump (New Era Pump Systems, Inc.), and a cylindrical collector (d = 20 cm) covered with aluminum foil. A voltage of 20-22 kV was applied to the polymer solution, which elongates and travel through the air space between the nozzle and collector (tip-to-collector distance, TCD = 20 cm), and solidify on the rotating collector in the form of nanofibers. The flow rate was maintained at 0.8 ml/h and 0.5 ml/h for the neat PH and CNT/PH solutions, respectively. For the CNT-incorporated composite nanofibers, a two-layer membrane was composed of a thin CNT/PH electrospun layer as top selective layer (~20 μm) and a thick neat PH electrospun layer as bottom support layer (~60 μm). Based from our previous study, this two -layer configuration with high hydrophobicity/less hydrophobicity membrane

configuration could result to improved MD performance (Tijing, Woo, et al. 2014). This CNT/PH membrane was prepared by electrospinning first the neat PH porous membrane on the drum collector covered with aluminium foil for a specified time, and then the CNT/PH solution was directly electrospun over it.

5.3 Results and discussion

5.3.1 Morphology

Based from our initial tests, the optimum neat PH concentration for electrospinning in this study was 20 wt% to produce cylindrical and bead-free membrane. Incorporation of CNTs in 20 wt% PH solution has increased the solution viscosity to the point that it was not easy to electrospin. So that, for CNT/PH solutions, a lower PH concentration (i.e., 15 wt%) was used for adequate dispersion of CNTs as well as for good electrospinnability. The morphologies of the electrospun nanofibers and the commercial flat-sheet membrane are characterized by SEM imaging as shown in **Fig. 5.1**.

All nanofibers showed ultrafine, randomly-oriented, and interconnected nonwoven fibers and pore structure(Li & Xia 2004). The neat PH nanofibers (**Fig. 5.1a**) show bead-free surface, with smooth and cylindrical nanofibers at an average fiber diameter of 296 ± 70 nm. The surface morphology of the nanofiber membrane shows large amounts of protrusions, and hills and valleys, providing microscale and nanoscale roughness that could possibly increase the hydrophobicity of the surface (Liao et al. 2014).

The CNT/PH nanofibers resulted to thinner fibers (257 to 290 nm, see **Table 5.2**), which could be due to the lower PH concentration and the increased conductivity with increasing CNT content (Huang et al. 2008). This led to more charges of the solution

and consequently more elongation and thinner fibers. Beads were formed on the membrane when CNTs were incorporated with increasing bead formation at increasing CNT concentration. Hence, the highest concentration of 5 wt% CNT (**Fig. 5.1b**) showed the most amount of beads-on-string. These beads are attributed to the lower concentration of PH (i.e., at 15 wt%) as well as on the agglomeration of CNTs during the nanofiber formation. The presence of beads has increased the surface roughness through microscopic inspection. Many studies have demonstrated that porous beaded fibers exhibit increased hydrophobicity (Yoon et al. 2008; Zhan et al. 2010) due to increased surface roughness.

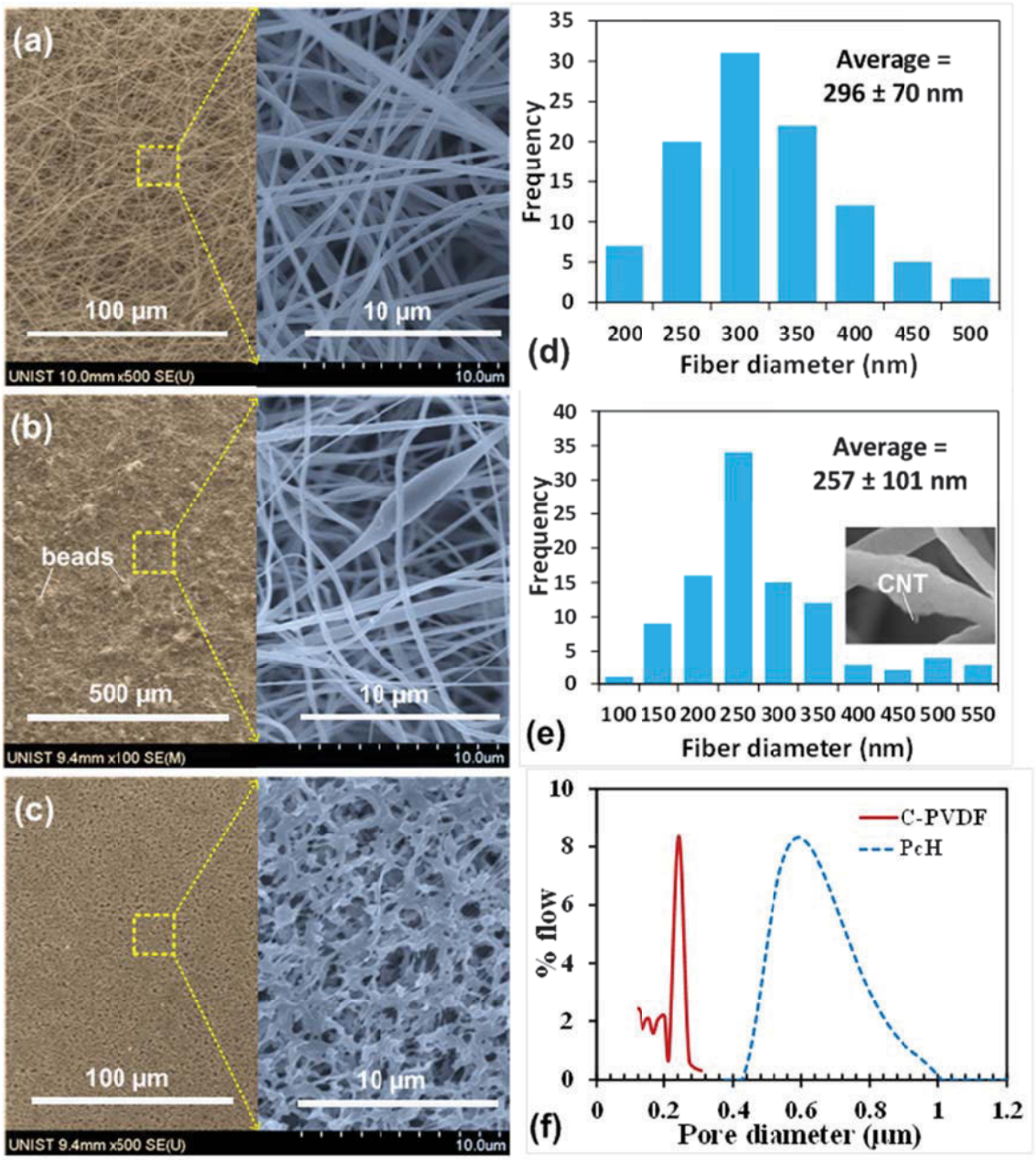

Figure 5.1. Morphological images and corresponding fiber size distributions of (a, d) PH and (b, e) 5CNT nanofiber, and (c) commercial PVDF membranes. Also shown is the (f) pore size distribution of PH and C-PVDF as measured by porometry

Table 5.2. Properties of the commercial and fabricated nanofiber membranes

Membrane code	Material	Thickness (µm)	Porosity (%)	Mean pore size (µm)	Contact angle (deg)	Fiber diameter (nm)
PH	Pure PVDF-co-HFP nanofiber	82 ± 1.3	89 ± 1.0	0.58 ±0.01[a] (0.52 ± 0.14[b])	149 ± 1.21	296 ± 70
1CNT	PH nanofiber containing 1 wt% CNT	70 ± 2.2	85 ± 1.3	(0.550 ± 0.08 [b])	151.4 ± 1.52	290 ± 60
3CNT	PH nanofiber containing 3 wt% CNT	78 ± 2.3	84 ± 1.22	(0.555 ± 0.07 [b])	152.2 ± 1.25	287 ± 88
5CNT	PH nanofiber containing 5 wt% CNT	81 ± 1.8	84 ± 1.36	0.29 ±01[a] (0.570 ± 0.10 [b])	158.5 ± 1.42	257 ± 101
C-PVDF	PVDF unbacked (GVHP, Millipore)	107 ±1.6	75 ± 1.27	0.24 ±0.01[a] (0.435 ± 0.01[b])	131 ± 3.1	-

[a] measured through capillary flow porometry

[b] measured through analysis of at least 60 pore sizes based from the SEM images.

It should be noted that no surfactant or surface modification was carried out on the CNTs during the preparation of the CNT solution, as we wanted to maintain the hydrophobic nature of the CNTs. Coating them with surfactants will help in the dispersion, however, it also renders the CNTs hydrophilic. As one of our main aims was to produce superhydrophobic surface, producing a rough surface through the beaded and protuberant structure would help in this regard without compromising the porosity and pore sizes. The formation of beads with CNTs in/on the surface increases the surface roughness at a nanoscale level, which affects the wettability of the surface and increases its hydrophobicity (Zhan et al. 2010). Similar effect was found when graphene was

added into electrospun nanofibers as reported by other studies (Moradi et al. 2015). Additionally, beads were also observed through the depth of the 5CNT layer, while smooth, beadless fibers were observed at the bottom layer of the 5CNT membrane (**Fig. 5.2**), which was made of neat PH. Beads are generally considered as demerits in an electrospun membrane as they provide additional stress points that can affect the membrane's mechanical properties. However, if properly designed, the micro or nanobeads on the electrospun membrane can serve as additional roughness to the membrane surface that can enhance the membrane hydrophobicity. In the present study, it was strategically designed that the beads are only formed on the top layer (the 5CNT layer) of the electrospun membrane which constitutes only about 25% of the total thickness of the membrane. The remaining membrane thickness (~75%) was made of beadless and smooth PH nanofibers to provide the bulk of the mechanical properties of the electrospun membrane. This unique design enables the provision of superhydrophobicity of the top membrane surface facing the feed side while maintaining high mechanical properties as explained in **Sec. 5.3.5**. In addition, it has to be noted that the beads on the top surface had not negatively affected the other membrane properties such as porosity and pore sizes. Other study has combined bead-on-string and microfiber morphology via multi-nozzle electrospinning process and obtained a superhydrophobic membrane without sacrificing the mechanical properties (El-Bourawi et al. 2006). The top thin CNT/PH layer was found to be entangled and nicely adhered to the bottom neat PH layer forming good interfacial connection, as both layers are mainly made of PH host matrix. This ensures robustness of the design of this membrane. One can notice obvious differences in morphology of the nanofibers compared to the commercial membrane. The commercial PVDF membrane (**Fig. 5.1c**) showed a sponge-like structure with more dense areas on the top surface. Looking at the

SEM images, it can be seen that the surface pore sizes of the nanofiber membranes are larger than C-PVDF.

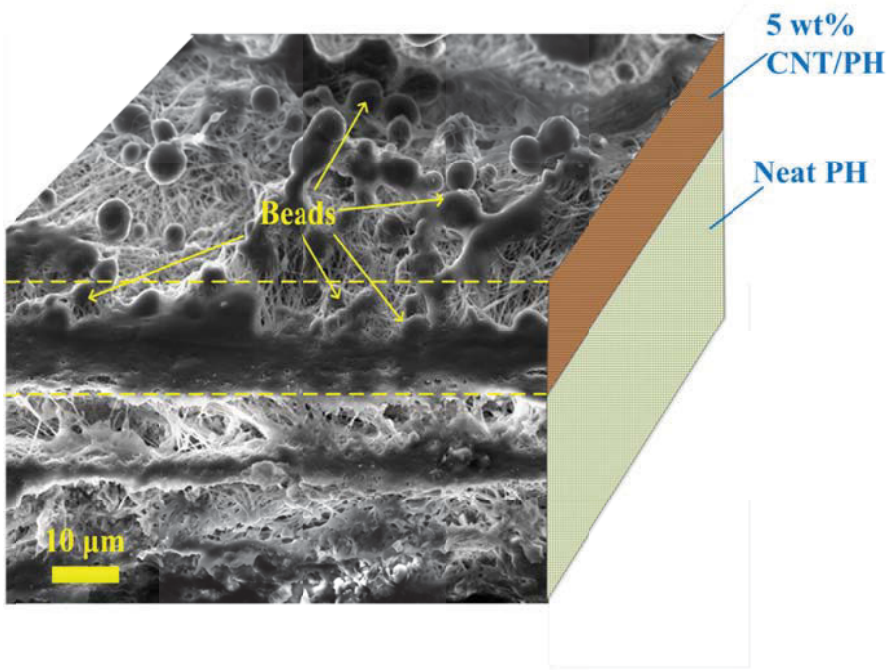

Figure 5.2. Cross-sectional SEM image of the 5CNT nanofiber composed of a thin top 5wt% CNT/PH electrospun layer and a thicker bottom neat PH electrospun layer

Pore size, PSD and porosity are important parameters affecting the MD performance of a membrane. The pore size should be adequate enough to allow higher fluxes but small enough to maintain a high LEP. The PSD should also be as narrow as possible to allow uniformity in the permeation of the water vapour and to lessen membrane wetting (El-Bourawi et al. 2006). From literature, nanofiber membranes were found to have slightly wider PSD compared to the commercial flat-sheet membrane by phase inversion or stretching (Tijing, Choi, et al. 2014). Our present results also suggested similar trend, wherein the nanofiber membranes had slightly wider PSD (see **Figure 5.1d**). It is also generally accepted that higher porosity leads to higher MD permeate flux due to the

availability of more surface area and that the presence of more voids lessens the conductive heat loss to the surroundings. **Table 5.2** shows the porosity and pore size measurements of the commercial and nanofiber membranes. Two methods were utilized to measure the membrane pore sizes: capillary flow porometry (CFP) and SEM image analysis using ImageJ. CFP measures the pore throat in the bulk of the material compared to the surface pore or pore mouth measurement using SEM image analysis. One can see differences in the measured pore sizes between the two methods. Generally, the result showed bigger pore sizes at the surface as indicated by SEM image analysis, which is consistent with the observation of other studies (AlMarzooqi et al. 2015; Dumée et al. 2010). The CNT/PH nanofiber membranes showed similar surface pore sizes (~0.52-0.57 μm**)** regardless of the CNT concentration, while the C-PVDF had a smaller surface pore size of 0.435 μm**.** However, when considering the bulk of the material, the pore size through CFP yielded almost similar pore sizes for 5CNT and C-PVDF at 0.29 and 0.24 μm, respectively. The small pore size of C-PVDF, which is close to its manufacturer's data (i.e., 0.22 μm), is attributed to its sponge-like and tortuous structure (Liao et al. 2014). Meanwhile, the presence of beads through the depth of the 5CNT membrane has helped in constricting the gap between neighboring fibers, hence resulting to smaller pore sizes compared to its surface pores. This smaller pore sizes could help in increasing the LEP value. On the other hand, the neat PH membrane still showed large pore sizes due to the fact that no beads were formed on/in the membrane. Similar pore sizes with the present neat PH membrane were also obtained from other nanofiber membrane studies for MD (Liao, Wang & Fane 2014; Prince et al. 2012). The nanofiber membrane pore size can be decreased by increasing the thickness of the membrane or by heat-press treatment process as recently reported by our previous work (Yao et al. 2016). The generally bigger pore sizes of the nanofiber

membranes could be attributed to the overlapping fiber structure of the membrane, which also resulted to higher porosity (>85%) compared to that of the commercial membrane (70%). The porosity of the nanofiber membranes did not change much after incorporation of different CNT contents, as the fiber size difference was also not drastically different, which led to similar porosities. The higher porosity of the nanofiber membranes could lead to less mass transfer resistance in the MD process, and consequently more available surface areas for water vapour to pass through.

5.3.2 Liquid entry pressure (LEP)

In MD, the LEP, i.e., the pressure needed for water to overcome in order to penetrate the membrane, should be as high as possible to prevent membrane wetting. Once the hydraulic pressure exceeds the LEP of the membrane, the feed solution could overcome the surface tension of the membrane surface and penetrate the pores leading to wetting and contamination of the permeate. There are two possible ways to improve LEP, namely: (1) by improving the hydrophobicity of the membrane, and (2) by making the pore size smaller with uniform pore size distribution (Alkhudhiri, Darwish & Hilal 2012). One of the ways to improve the hydrophobicity of the membrane is by surface modification techniques such as layer-by-layer assembly, sol-gel coating, and plasma treatment. New materials with superhydrophobic properties (i.e., low surface energy) are also synthesized and fabricated. The incorporation of hydrophobic nanoparticles into polymeric surfaces has also resulted to improved hydrophobicity and LEP values. LEP is an important parameter of an MD membrane as it provides information on the anti-wetting ability of the membrane.

Figure 5.3a shows the LEP test results. The nanofiber membranes posted lower LEP values (91-99 kPa) compared to the commercial PVDF membrane (~213 kPa), which is mainly due to the bigger pore sizes of the nanofiber membranes (**Table 5.2**). The neat PH and 5CNT nanofiber posted LEPs of 91 kPa and 99 kPa, respectively. The increase in LEP of the composite membrane is attributed to the increased surface hydrophobicity of the CNT/PH membrane as checked by the CA measurement (see **Fig. 5.3a**). The present LEP results are comparable with the reported LEPs of nanofiber membranes of other studies (Essalhi & Khayet 2013a; Liao, Wang & Fane 2013) which are considered to be adequate for MD application. Even though the nanofiber membranes posted lower LEPs than the commercial membrane, they are still adequate enough to obtain high and stable salt rejection as reported in **Sec. 5.3.7.**

5.3.3 Membrane hydrophobicity

The wettability of the surface depends on the surface energy and the roughness of the surface (McHale, Shirtcliffe & Newton 2004). The effect of different CNT concentrations on the hydrophobicity of the composite nanofiber surface was investigated. **Figure 5.3a** shows the CA measurements of the different fabricated and commercial membranes in the present study. The commercial PVDF membrane showed a CA of 134^{o}, which is consistent with the measurement of other studies. On the other hand, the neat PH nanofiber had a CA of 149^{o}, which is higher than the commercial PVDF membrane that is mainly attributed to the rougher surface structure of the overlapping layers of nanofibers. The fibers form layers on top of each other, which creates hills and valley regions on the surface and air pockets are formed thereby reducing the surface area for water to contact with leading to increased CA (Wang et al. 2011). When CNTs (**Fig. 5.3d**) were incorporated, beads were formed on the membrane

surface, which further increase the surface roughness of the membrane thereby increasing the CA as schematically depicted in **Fig. 5.3b**. A closer look at the beads and on the fiber surface shows protruding CNTs (**Figure 5.3c**), which further adds to the roughness of the surface at the nano scale. Similar results were obtained in a previous study when modified silica nanoparticles were electrosprayed on the surface of nanofibers forming beads on the surface (Liao, Wang & Fane 2014).

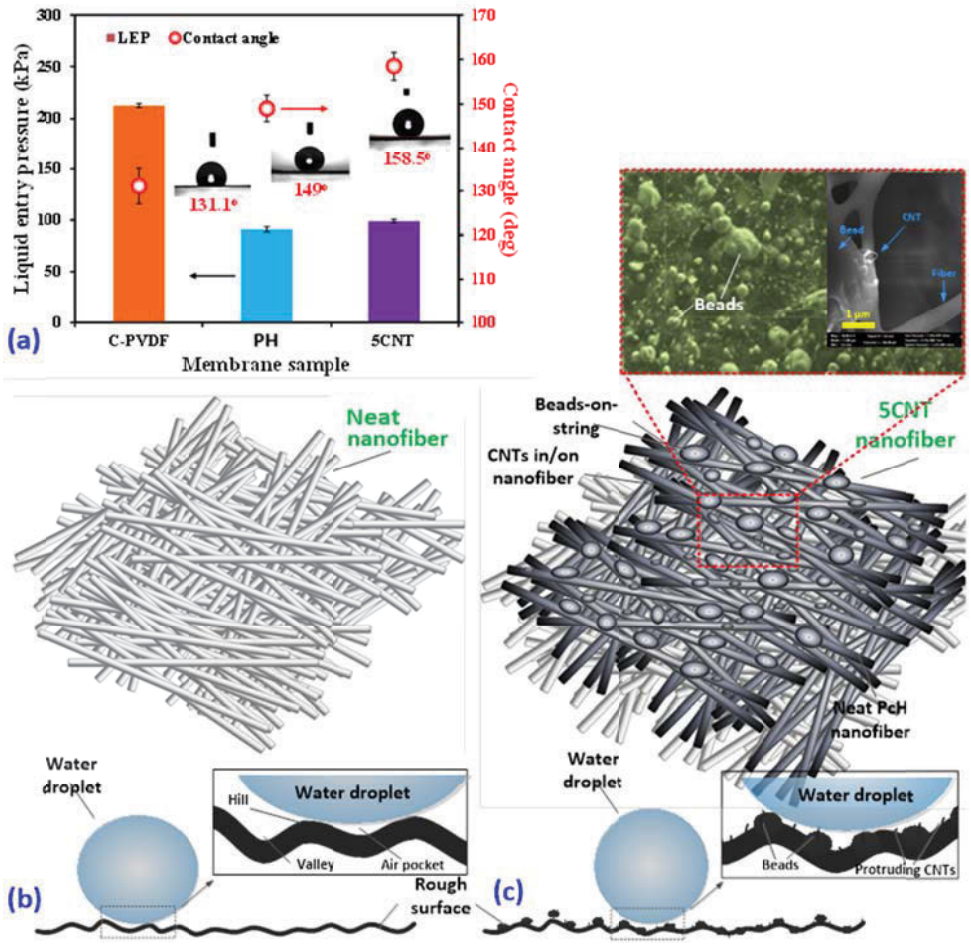

Figure 5.3. (a) Liquid entry pressure and contact angle measurements, and (b) schematic representation of the structure of the neat and CNT-incorporated nanofiber structures, (c) SEM images showing the beads and CNTs on the fiber, and (d) SEM image of the pristine CNTs used in this study

5.3.4 Membrane topography and roughness

To support the discussions above, the surface topography and roughness of the different membranes were measured using a non-contact mode AFM. The 2D and 3D profiles and their corresponding average roughness (R_a) values are presented in **Fig. 5.4** for a scan size of 10 µm x 10 µm. The AFM images show that nanofiber membranes (**Fig. 5.4a-c**) are generally rougher than the commercial PVDF flat sheet membrane (**Fig. 5.4d**). Here, it is confirmed that the overlapping structure of nanofibers has created hills and valleys that produce rough surfaces, which is consistent with the SEM images in **Fig. 5.1**. The incorporation of CNTs in/on the nanofiber has given additional roughness, which are attributed to the bumps from the beads on the nanofiber surface as well as to the CNT protrusions on the surface of the fiber. Moreover, increasing roughness was obtained at higher CNT loadings. Here, the neat PH nanofiber posted R_a = 358.8 nm, while the 1CNT and 5CNT showed much higher roughness at 415.1 and 455.1 nm, respectively. Compared to the commercial membrane which showed smooth surface with cellular holes (R_a=154.6 nm), the electrospun membranes have much rougher surfaces. The AFM images strongly support the CA and SEM measurements giving more hydrophobicity at 5CNT due to much rougher surface roughness.

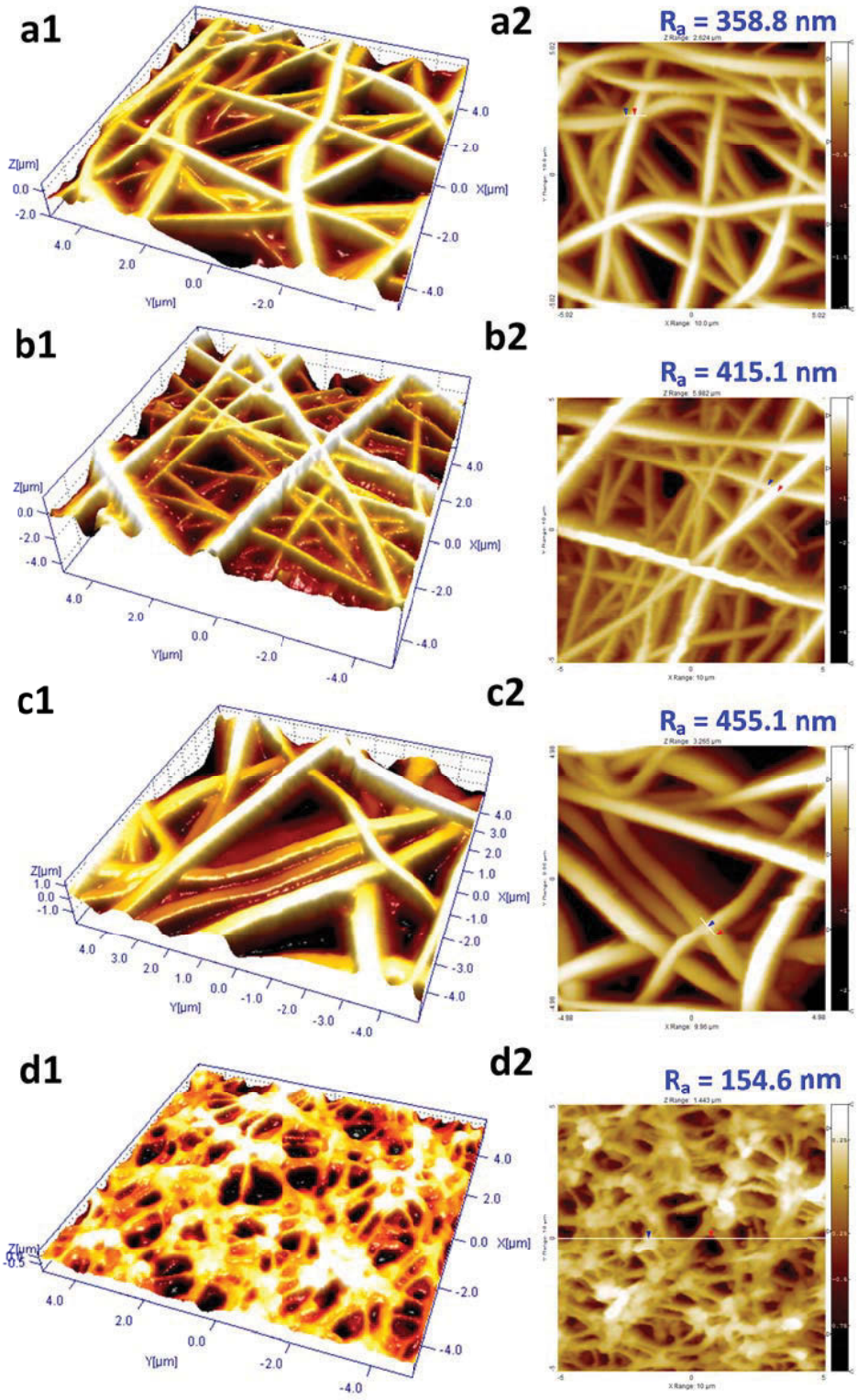

Figure 5.4. AFM (2D and 3D) images of the (a) neat, (b) 1CNT and (c) 5CNT nanofibers and (d) the commercial flat sheet membrane

5.3.5 Mechanical properties

MD has less membrane mechanical integrity requirements compared to pressure-driven membrane separation processes, however, adequate mechanical properties are still needed for long term operation and to withstand the stress from packing in modules (Essalhi & Khayet 2013b). Hence, the mechanical properties of the fabricated nanofiber membranes and C-PVDF were investigated. Due to their very small sizes, nanoparticles are ideal filler materials for polymer substrates to impart additional functionalities and improve the overall properties of the composite material. **Figure 5.5 and Table 5.3** show the typical stress-strain curves and the summary of mechanical properties of the fabricated nanofibers and C-PVDF. C-PVDF showed a steep increase in tensile strength in the first 5% of strain and then proceeded with a falling rate mode until rupture (**Figure 5.5**). The tensile strength and strain of C-PVDF was 7.2 ± 0.2 MPa and 36.3 %, respectively. Interestingly, both neat PH and 5CNT nanofiber membranes showed increased tensile and elongation properties compared to C-PVDF. The neat PH nanofibers showed higher tensile strength (25% higher) and higher strain at break (an increase of 175%) compared to C-PVDF. This difference could be explained by examining their morphologies. While the C-PVDF membrane depicts a sponge-like structure with more dense areas, the nanofibers are in nonwoven form composed of multidirectional fibers, wherein upon stretching during tensile test, the fibers oriented on the principal strain were stretched uniaxially, while the fibers in other orientation experienced rotation and align themselves to the strain direction (Xu et al. 2006) as depicted in the low stress and the low strain region of the neat PH (inset of **Fig. 5.5**). This resulted to higher elongation for the nanofibers. The addition of CNTs has drastically increased the tensile strength by 176% and 121% compared to C-PVDF and neat PH nanofiber, respectively, without the loss of elongation. In fact, 5CNT nanofiber

still showed higher elongation compared to C-PVDF (79.6 compared to 36.3%). This could be attributed to the good load transfer of the PH polymer to the CNTs (Chen, Tao & Liu 2006), wherein a good interfacial interaction was found between CNTs and PH as discussed in the next section. Additionally, the increase in mechanical strength could also be due to micromechanical locking of the walls of CNT and the host polymer, weak van der Waals bonding between PH and CNTs, and some point-bond structure of the nanofibers upon the incorporation of CNTs (Jeong et al. 2007; Tijing et al. 2013). CNT incorporation also resulted to higher modulus compared to neat PH. Although there are many beads formed on the 5CNT membrane surface, it seems that other CNTs were well encapsulated by the PH nanofiber, so that they were not easily visible through SEM imaging. In this study, even though no surfactant was used for the dispersion of CNTs in the solution, it still resulted to improved mechanical properties, which signifies that CNTs have successfully provided reinforcement to the composite material. To elucidate the effect of CNT fillers in the composite, chemical characterizations were carried out.

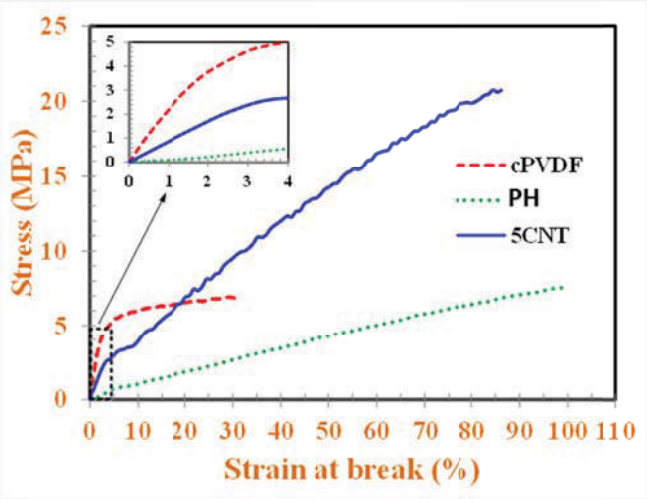

Figure 5.5. (a) Typical stress-strain curves of the neat (i) PH, (ii) 5CNT, and (iii) C-PVDF membranes

Table 5.3. Mechanical properties of the neat and 5 wt% CNT/PH nanofiber membranes, and the commercial PVDF membrane

Membrane sample	Tensile strength (MPa)	Young's modulus (MPa)	Strain at break (%)
C-PVDF	7.2 ± 0.2	183.2 ± 12.4	36.3 ± 3.1
Neat PH	9.0 ± 1.4	18.2 ± 4.4	99.8 ± 5.2
5CNT	19.9 ± 1.43	83.7 ± 15.9	79.6 ± 8.7

5.3.6 Structural and chemical analysis

To further prove the successful incorporation of CNTs in/on the nanofibers and their interaction, spectroscopic and X-ray diffraction characterizations were carried out. **Figure 5.6** shows the Raman, XRD, FTIR, and EDX spectra of the nanofiber membranes. The Raman spectra of 5CNT (**Fig. 5.6a**) show prominent peaks at 1350 and 1584 cm^{-1}, which are associated with the D-band (defect-induced mode), and the G-band (in-plane vibration of the sp^2-bonded carbon atoms in a hexagonal lattice) (Ke et al. 2014), respectively, indicating the successful incorporation of CNTs in the PVDF nanofiber. The peaks at 800, 1436, and 2969 cm^{-1} correspond to CF_2 symmetrical stretching, CH_2 bending, and CH_2 stretching vibrations, respectively of the PVDF host matrix (Ke et al. 2014).

Figure 5.6b shows the XRD spectra of the different samples. PVDF is known to crystallize into three main structures, namely: α, β, and γ types (Cao, Zhu & Xu 2006). In **Fig. 5.6b**, it shows that the PH is crystalline in nature wherein the peak at 20.3^o ((2 0 0)/(1 1 0)) is indicative of the polar β-crystalline phase (Baji et al. 2013; Liu et al. 2010) , while the peaks at 24.8 (120) and 26.8^o (0 2 1) indicates the α crystal phase (Ma, Zhang & Wang 2008). The results indicate the co-existence of both α and β crystal

phases. For 5CNT membrane, the peak at 20.3^{o} showed slight broadening, while the peaks at 24.8 and 26.8^{o} have weakened, which indicates interfacial interaction between CNTs and PH. The XRD results are corroborated by the FTIR spectra (**Fig. 5.6c**). The α crystal phase of PH shows characteristic peaks at 881 and 1400 cm^{-1} corresponding to CH_2 in-plane bending or rocking (Shao et al. 2015) and C-F stretching vibrations, respectively (Baji et al. 2013). The peaks at 841 (CH_2 in-plane bending or rocking/CF_2 asymmetrical stretching) and 1277 cm^{-1} (C-F stretching vibrations) correspond to the β phase (Bormashenko et al. 2004) and the strong peak at 1180 cm^{-1} corresponds to the C-C band (Rahimpour et al. 2009). Broader peak at 1180 cm^{-1} as well as slight shifting of the peaks at 1072, 881, and 841 cm^{-1} of 5CNT indicates interfacial interaction (physical adsorption or weak chemical bonding) between the PH and CNT (Ke et al. 2014). Surface elemental analysis was further carried out on the nanofiber membranes using EDX. The element C showed higher content in 5CNT compared to neat PH, showing increased C/F ratio of 0.69 compared to 0.54 of neat PH, which could be attributed to the presence of CNTs on/in the nanofiber (**Fig. 5.6d**). Visual inspection of the fabricated membranes showed a change in color from white for neat PH to black for 5CNT, further indicating the successful incorporation of the CNTs in/on the nanofibers.

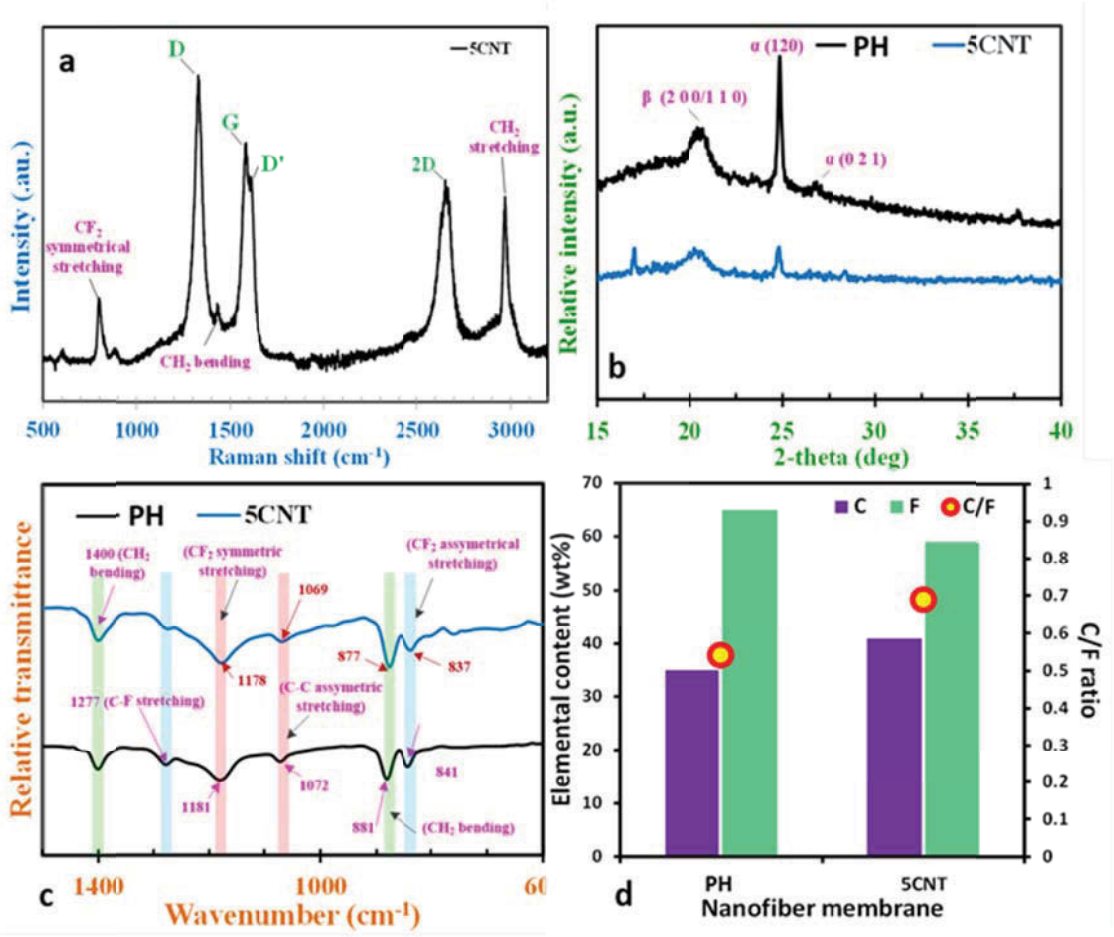

Figure 5.6. (a) Raman, (b) XRD, (c) FTIR, and (d) EDX spectra results of the PH and 5CNT nanofiber membranes

5.3.7 DCMD performance

5.3.7.1 Effect of CNT concentration

In the present study, the incorporation of different amounts (1 to 5 wt%) of CNTs in/on the PH nanofiber has resulted to changes in the nanofiber morphology and properties. These changes could exhibit the differences in the performance of such membranes for DCMD application. **Figure 5.7** shows the variation of flux over time of the different fabricated membranes. Both DI and 35 g/L NaCl solutions were used as feed. Using DI as feed (**Figure 5.7a**), the flux showed very constant curve for over 60 min for all

membranes. The commercial PVDF membrane obtained a flux of 20 L/m^{2}h or LMH, which was the lowest from among the tested membranes. The neat PH posted a flux of 26 LMH, while the composite membranes containing 1, 3, and 5 wt% CNTs obtained fluxes of 28, 32, and 35 LMH, respectively. This signifies an increase of 40-75% and 12-40% when compared to the commercial PVDF and neat PH nanofibers, respectively. As one can see, adopting neat PH nanofiber membrane alone has already enhanced the DCMD flux performance with respect to the commercial PVDF membrane. This could be attributed to the higher porosity of the nanofiber membrane and its superhydrophobic surface property. Additionally, the bigger pore sizes but increased hydrophobicity also led to the increased permeate fluxes as also observed by other studies (Liao et al. 2014). The incorporation of CNTs in/on the polymeric PH nanofiber has definitely improved the flux performance of the neat PH nanofiber. This is attributed to the higher hydrophobicity of the membrane, which resulted to increased LEP values at increasing CNT concentration. It should be noted that the CNT/PH nanofiber only forms a skin-layer (about 25% of the total membrane thickness) on the membrane, and the rest of the layers were composed of neat PH nanofiber.

When 35 g/l NaCl solution was used as feed (**Figure 5.7b**), a gradual decrease in the permeate flux curve was observed through time for the nanofiber membranes. This decrease is attributed to the bigger pore size of the nanofibers, wherein some salts could have deposited on the surface but not through the depth of the membrane, thereby lowering the pore sizes leading to decreasing flux. Additionally, the increase in feed concentration through time, and the lowering of the feed bulk temperature due to the decrease in feed volume as the test went on have also resulted to the gradual decrease of permeate flux as also observed by other studies (Alklaibi & Lior 2005). The commercial

PVDF membrane still showed constant curve throughout the duration of the test with a flux of 18.5 LMH. However, the nanofiber membranes obtained much higher fluxes compared to the commercial membrane. Increasing CNT content in the nanofiber resulted to increasing flux performances, wherein the highest flux from among all membranes was obtained for 5CNT at 29.5 LMH after 5 h. This is a 59% and 34% increase from those of C-PVDF (18.5 LMH) and neat PH membranes (22 LMH), respectively. The salt rejection was very high at 99.99% for both C-PVDF and 5CNT and 99.98% for PH membrane. The final permeate concentration was <1 mg/L and <6 mg/L for C-PVDF and 5CNT, and neat PH, respectively. The much better flux and salt rejection performance of 5CNT could be attributed to its bigger pore sizes but with increased hydrophobicity compared to other membranes especially C-PVDF. However, one concern with bigger pore sizes could be its possible rapid scaling and wetting at higher salt concentration, thus we tested the effect of different salt concentrations in our succeeding tests.

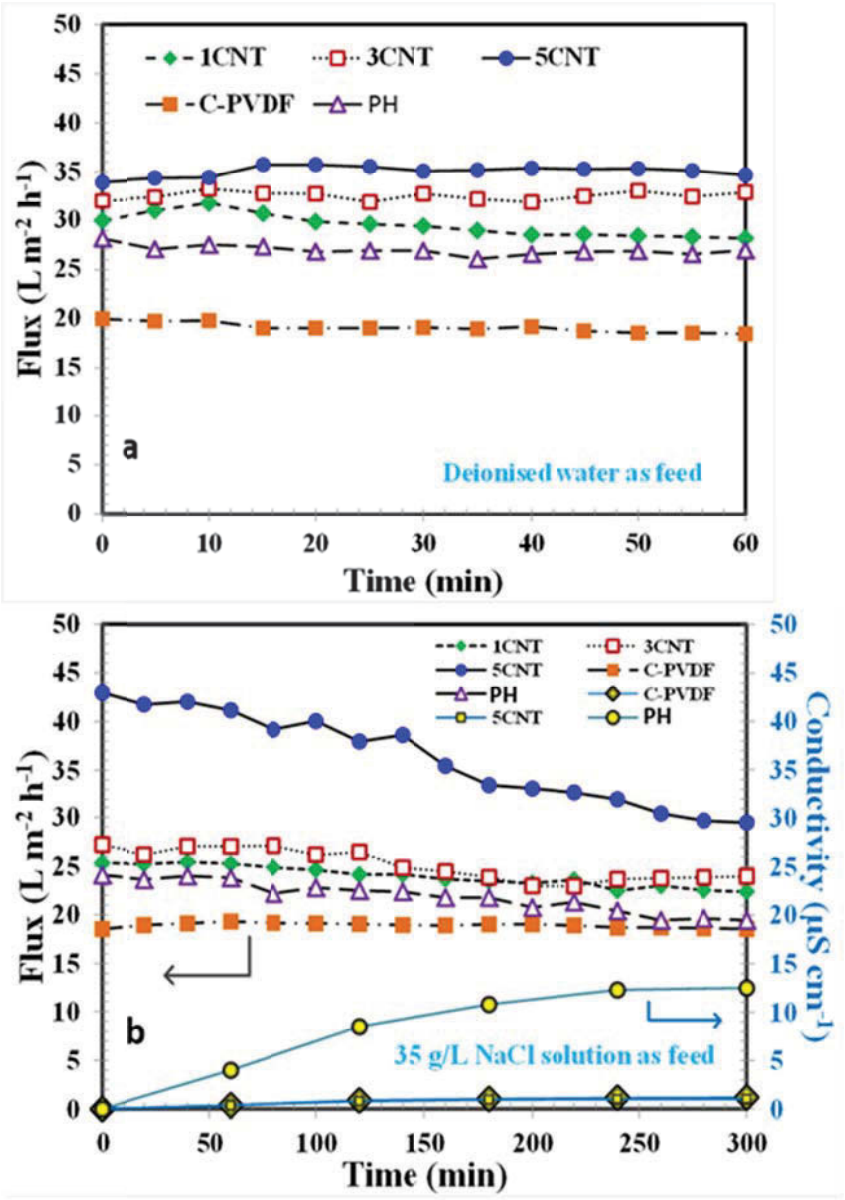

Figure 5.7. Flux performance of the commercial PVDF membrane and the electrospun nanofibrous membranes at different CNT concentrations using (a) deionised water and (b) 35 g/L feed

5.3.7.2 Effect of salt concentration

Figure 5.8 shows the effect of different NaCl feed concentrations on the permeate flux and salt rejection performance of different membranes. For each feed type, the 5CNT nanofiber membrane showed consistently the highest flux from among the three

membrane types tested. As expected, the feed using DI water (**Fig. 5.8a**) showed higher fluxes for each corresponding membrane using different NaCl solutions. The increase in NaCl solution from 35 (**Fig. 5.8b**) to 70 g/L (**Fig. 5.8c**) resulted to decreasing flux trend for all membranes. But even at the highest NaCl solution of 70 g/L, both neat PH and 5CNT nanofiber membranes showed higher flux (19.5 and 24 LMH, respectively) compared to the commercial PVDF membrane (18 LMH). In fact, both nanofiber membranes posted even higher fluxes at 70 g/L compared to C-PVDF at lower feed concentration of 35 g/L. The flux trend was as follows: 5CNT > PH > C-PVDF (commercial membrane). As the feed concentration was increased, the flux correspondingly decreased but still maintained the same trend for the three membranes. The membrane characteristics, feed flow rate and solution temperatures are important factors in the selective permeation of vapour through the membrane pores. Temperature affects the both vapour pressure and diffusion coefficient, wherein the vapour pressure exponentially increases with temperature based from Antoine's equation, while the diffusion coefficient is related with temperature through Arrhenius type expression (Al-Obaidani et al. 2008; Gethard, Sae-Khow & Mitra 2012). The decrease in flux at higher concentration could be attributed to the increased temperature polarization effect at higher concentration as also observed by other studies (Martínez-Díez & Vázquez-González 1999; Yun et al. 2006), as well as on the slightly smaller vapour pressure (driving force) of NaCl solution compared to pure water (Roy, Bhadra & Mitra 2014). Since there was not much changes in the permeate conductivity during the operation, the lower flux at higher NaCl concentration could also be due to pore blocking from NaCl crystallization on the surface. This reduces the membrane area available for vaporization to occur, hence the reduced flux.

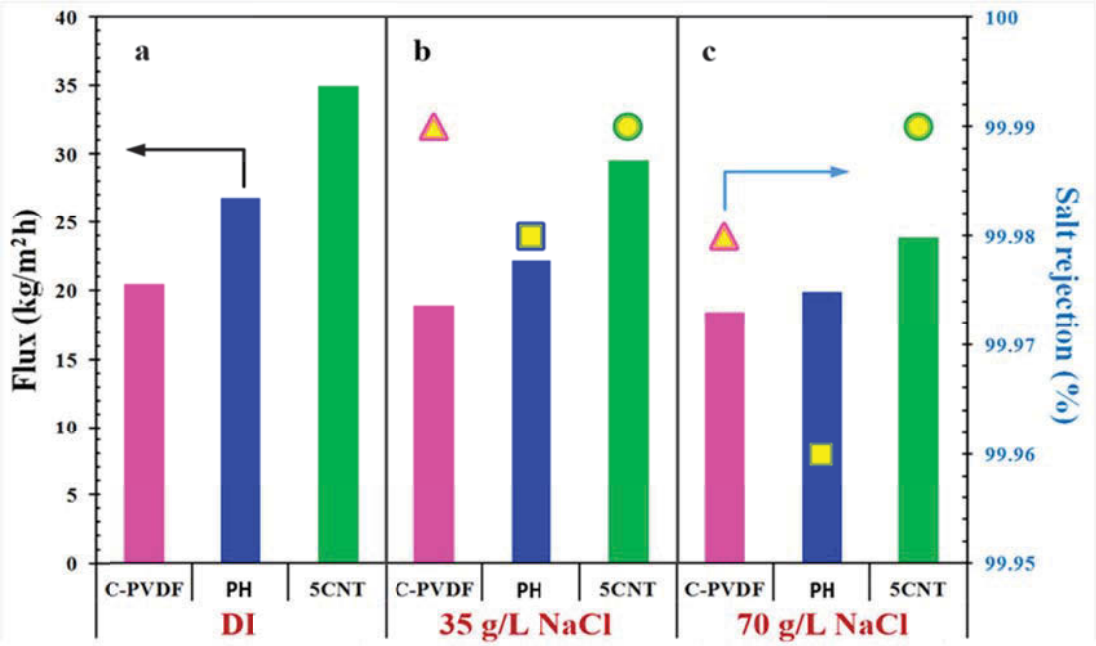

Figure 5.8. Effect of feed type on the DCMD performance of different membranes tested in the present study: (a) deionised water, (b) 35 g/L NaCl and (c) 70 g/L NaCl

5.3.7.3 Role of CNTs in the DCMD performance

The incorporation of CNTs in the composite nanofiber has resulted to multi-level roughness on the surface. This multi-level roughness (micro and nano) is a requirement to achieve superhydrophobicity. **Figure 5.3c** shows schematically how CNTs affect the roughness of the surface. CNTs have strong van der Waals attraction thus agglomeration could not be avoided as no surfactant or surface modification was used, which resulted to bead formation on the surfaces. The large aspect ratio of the CNTs could lead to protrusion of the ends of the CNTs onto the nanofiber surfaces and even on the bead surfaces, forming hierarchical structure with nano and micro roughness, which add to the overall roughness of the surface. One important aspect of the one-step electrospinning of CNT-incorporated nanofiber is the ease of preparation and the assurance that CNTs will not wear off from the membrane as a portion of the CNT

structure is well encapsulated in the polymer. The better DCMD performance could be explained through the working mechanism schematically depicted in **Fig. 5.9**. When feed water is exposed to the membrane surface, the increased hydrophobicity of the 5CNT membrane prevents the water from penetrating through the pores (Fig. 10a). The protrusion of CNTs on the nanofiber and bead surface decreases the tendency of the pores to be wetted and offers more exchange surface available due to the added hydrophobicity of CNTs, thereby leading to more pure water vapour transport (**Fig. 5.9b**) (Al-Obaidani et al. 2008). The beads-on-string are not only limited on the surface, but are also found through the depth of the 5CNT layer. The increase in flux due to increase in hydrophobicity is also observed by other studies (Dumée et al. 2011; Martínez et al. 2003). Moreover, the rapid adsorption/desorption capacity of CNTs could allow the vapour molecules to follow diffusion along the surface of the protruded CNTs, resulting to increased overall vapour transport (**Fig. 5.9c**) (Gethard, Sae-Khow & Mitra 2011; Hussain, Saridara & Mitra 2009). Other studies have shown that CNTs can enhance the permeability of water in water desalination. Gethard et al. (Gethard, Sae-Khow & Mitra 2011) immobilized CNTs in the pores of a hydrophobic membrane by vacuum filtration, and found that the presence of immobilized CNTs has promoted vapour permeability and at the same time has prevented membrane wetting.

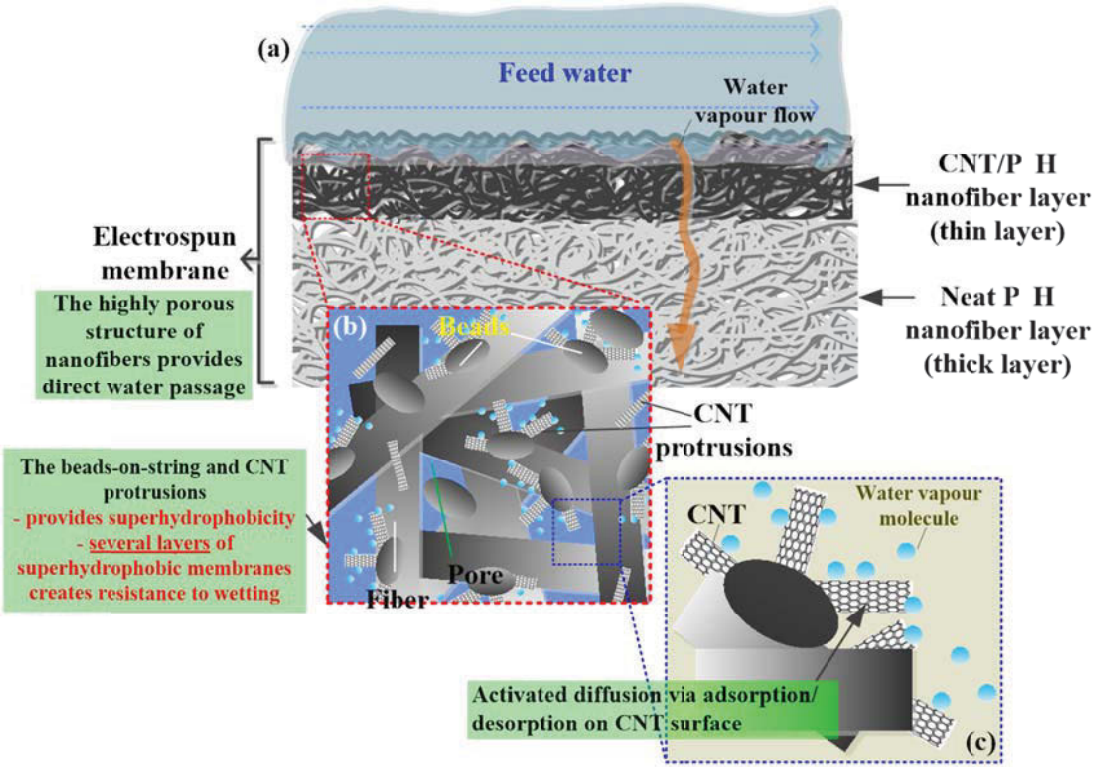

Figure 5.9. Schematic depiction of the working mechanism of CNT/PH nanofiber membrane for MD application in the present study

5.3.7.4 Comparison with other studies

The potential of the present 5CNT nanofiber membrane for DCMD application is compared with the performance of nanofiber membranes from literature. **Table 5.4** shows the flux and salt rejection performances of different membranes for DCMD test using 35 g/L NaCl feed and with inlet temperatures of 60 and 20°C at the feed and permeate streams, respectively. The present electrospun 5CNT membrane achieved a high salt rejection of 99.99% in addition to a very high flux of 29.5 LMH, which is much higher compared to other reported PVDF nanofiber membranes. The increased hydrophobicity of the selective layer of the membrane with high porosity and adequate pore sizes is the main reason for this improved performance. Moreover, the present electrospun membrane showed much better mechanical properties compared to other

nanofiber membranes, which is attributed to the good load transfer effect of the polymer to the CNT nanofillers as well as on the overall design of the two-layer electrospun membrane.

Table 5.4. MD performance of the present study in comparison with other reports in literature at the following DCMD conditions: Feed/permeate inlet temperatures: 60/20^{o}C; 35 g/L NaCl feed solutions.

Membrane type	**Polymer**	**Pore size (µm)**	**Porosity (%)**	**Thickness (µm)**	**Contact angle (^{o})**	**LEP (kPa)**	**Flux (kg/m^{2}h)**	**Salt rejection (%)**
Flat sheet/nanofiber (Liao, Wang & Fane 2014)	SiO_2-PVDF	0.69	82 ± 2	102 ± 15	156.3 ± 2.0	175 ± 5	18.9	-
Flat sheet/nanofiber (Francis, Maab, et al. 2013)	Matrimid 5218	2.15	-	-	130	-	23[b]	99.99
Flat sheet/nanofiber (Essalhi & Khayet 2013a)	PVDF	2.9 – 5.2	85 – 93	144.4-1529.3	137.4-141.1	63-112	7.2-28.8[c]	-
Flat sheet/nanofiber (Liao et al. 2013)	PVDF Kynar HSV 900, PVDF Kynar 761	0.18 – 0.91	71.4	71	136 – 142	24, 35	20.6	-
Flat sheet/nanofiber (Liao, Wang & Fane 2013)	PVDF Kynar HSV 900	0.18 – 0.34	68 – 79	48 – 52	138 – 158	41 – 146	31.8[d]	-
Flat sheet/nanofiber (Prince et al. 2012)	PVDF Kynar 761	0.58 ± 0.23 0.60 ± 0.17 0.63 ± 0.15 0.64 ± 0.22	82±3 82 ±3 81.5±3 81±3	-	128.0±1.5 134.4±2.1 142.4±1.9 154.2±3.0	90±2 130±3 170±5 200±6	< 5[e]	98.27 99.95 99.99 99.97
Flat sheet/nanofiber (Prince et al. 2014)	PVDF Kynar 761	0.05 – 0.63	-	-	84.6 – 151.4	110 - 470	3-10	< 99.98
Flat sheet/GVHP commercial membrane (Yang et al. 2014a)	PVDF modified by CF_4 treatment	0.246	-	-	162.4	310	< 25.0	99.98
Flat sheet/nanofiber (Tijing, Woo, et al. 2014)	PVDF-HFP/PAN[a]	0.6 – 2.5	90	82	150	94	30	98.5

Flat sheet/nanofiber (Liao et al. 2014)	Silica-PVDF/PVDF	0.32 – 0.36	~ 80	72 - 76	150 – 154	50 ~ 150	21	99.99
Flat-sheet/nanofiber (Present study)	CNT/PVDF-co-HFP	0.52	>85	82	158.5	99	29.5	99.99

[a] PAN: polyacrylonitrile

[b] based from figure in paper

[c] at 30 g/L NaCl solution

[d] multi-step modification process

[e] at 55 and 17°C feed and permeate temperature

Our approach of one-step electrospinning makes sure the stability of CNTs in the membrane as the CNTs are either embedded in the host nanofiber matrix or are protruding, with the lower end being fully embedded in the nanofiber ensuring their stability. Additionally, the process used here is much simpler and can be easily scaled-up compared to other multiple-step fabrication.

5.4 Concluding remarks

Superhydrophobic nanofiber membranes containing carbon nanotubes (CNTs) were fabricated by a one-step colloidal electrospinning process for DCMD application. The hydrophobicity of electrospun PH membrane was further enhanced by the incorporation of CNTs in/on the nanofibers reaching a contact angle (CA) of 158.5°, which was much higher than that of a commercial PVDF membrane. The presence of CNTs in/on the nanofibers produced beads on the surface of the membrane and some protruding CNTs were also observed on the nanofiber surface, which increases the overall roughness of the membrane surfaces leading to increased CA. Different characterization and measurement techniques have proven the successful incorporation of CNTs in/on the membrane, wherein a change to black color (from white for neat PH) was observed for

the CNT/PH membranes. Incorporating 5 wt% CNTs in/on the nanofibers has also improved the overall mechanical properties of the composite membrane, with an increase of 121% and 360% in tensile strength and modulus, respectively with respect to the neat PH. The electrospun membranes showed higher porosity (>85%) than a commercially-available PVDF membrane (70%), however, the LEP values were still lower than C-PVDF mainly because of the bigger pore sizes and thinner thickness of the nanofiber membranes. The 5 wt% CNT/PH nanofiber membrane showed the best flux performance (24-29.5 LMH) from all the membranes tested including that of the commercial PVDF membrane (18-18.5 LMH), while maintaining a high salt rejection of >99.99%. The incorporation of CNTs in/on PH nanofibers could definitely provide additional functionalities that can enhance the DCMD performance. Thus, there is high potential of the present mixed-matrix nanofiber membranes as membrane material for desalination by membrane distillation.

CHAPTER 6

University of Technology Sydney
FACULTY OF ENGINEERING

WATER DESALINATION USING GRAPHENE-ENHANCED ELECTROSPUN NANOFIBER VIA MEMBRANE DISTLLATION

6.1 Introduction

Electrospun membranes possess high hydrophobicity, high porosity, high surface area-to-volume ratio and interconnected pore structure. The overlapping structure of the nanofiber provides rough nano-scale surface which leads to increased hydrophobicity that is ideal for the MD process. In recent years, a number of research studies are reported using electrospinning for MD application (Li, Wang, et al. 2014; Liao et al. 2014; Liao, Wang & Fane 2014; Tijing, Woo, et al. 2014). However, to date, continuous research efforts are still being undertaken to manufacture a robust electrospun membrane for long term efficient MD performance. Superhydrophobic membranes are being sought out as an appropriate membrane for MD (Sahoo & Kandasubramanian 2014; Tian, Yin, et al. 2015; Wei et al. 2012; Yang et al. 2014b). At having superhydrophobicity, it can lead to less wetting problem, enhanced liquid entry pressure (LEP), improved water vapour flux and high salt rejection (Lee, An, et al. 2016; Tijing, Choi, et al. 2014). Incorporation of nanofillers such as silica and carbon nanotubes (CNTs) in/on nanofibers is reported to lead to superhydrophobic electrospun membranes.

Recently, increasing interest is given to graphene as a unique nanofiller material that has interesting properties that could provide additional functionalities to the host material. Graphene is two-dimensional (2D), single carbon atom composed of sp^2 arranged in a honeycomb structure, and is an emerging new material used in various research fields including water treatment and purification processes (Perreault, Fonseca de Faria & Elimelech 2015; Wang & Karnik 2012; Woo et al. 2016). It has high thermal stability and electrical conductivity, high mechanical stiffness, low permeability to water, and is low cost (Cohen-Tanugi & Grossman 2012; Li & Kaner 2008). The very high aspect

ratio and high specific surface area make graphene ideal filler that could promote better interaction with the host polymer. Water and vapour molecules cannot penetrate via pure graphene pore due to its unique nature (Celebi et al. 2014). Graphene is particularly attractive for MD application due to its hydrophobic nature, selective sorption of water vapours, and anti-fouling properties (Celebi et al. 2014; Mi 2014; Surwade et al. 2015). Recent progress on the much cheaper synthesis of graphene provides better potential for its wider use (Polat et al. 2015).

Together with the attractive properties of nanofibers, the incorporation of graphene provides additional properties to the composite membrane such as added roughness and hydrophobicity that leads to robust and highly efficient MD membrane. In the present study, we exploited the unique properties of graphene to enhance the overall properties of a polymeric nanofiber membrane towards the production of a robust superhydrophobic membrane for long-term AGMD application. To the best of our knowledge, no one has reported yet on the use of graphene-incorporated electrospun nanofiber membrane for AGMD desalination. Realizing the excellent properties of graphene and electrospun nanofiber membranes, their combination as MD membrane is worth exploring. Hence, the objective of this chapter was to determine the optimal concentration of graphene in/on the electrospun nanocomposite membrane to lead to a robust and high AGMD performance desalination membrane. A series of measurements, characterization and AGMD tests were performed to determine the most suitable graphene loading and membrane composition for AGMD desalination.

This chapter is an extension of the research article published by the author in Journal of Membrane Science.

6.2 Model development

6.2.1 Two-dimensional dynamic model for AGMD module

A comprehensive two dimensional (2D) mathematical AGMD model was developed for the transport of water vapor through the hydrophobic membrane. The AGMD system configuration was composed of hot feed channel, porous (or hydrophobic) membrane, air gap, condensing plate, and cooling feed channel as shown in **Figure 6.1**. In this study, the following assumptions are made in the 2D AGMD mathematical model for flat sheet module: i) non steady state ii) constant physical properties of fluids, membrane and plate, iii) a parabolic velocity profile developed in the channels, iv) constant pressure inside the channel, v) forming a film type condensation on the cooling plate iv) negligible membrane fouling due to deposition (or adsorption) of solutes, v) no chemical reaction, vi) negligible heat loss from the module, and vii) only pure water in the air gap layer and the coolant channel.

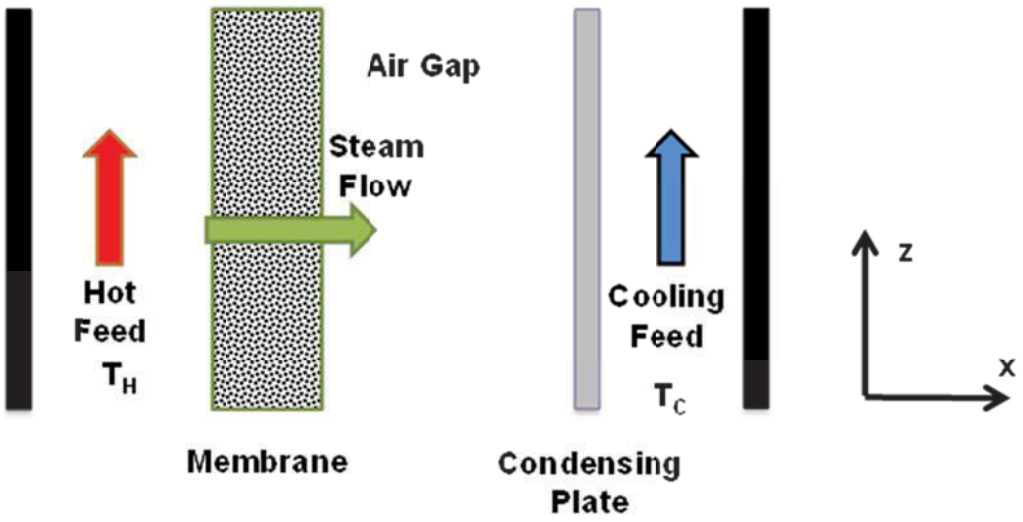

Figure 6.1. Schematic diagram of the AGMD module structure

6.2.2 Heat transfer in the hot and coolant channels

The comprehensive 2D AGMD energy balance equations, based on the above described assumptions, with the initial and boundary conditions can be written in the following forms (refer to the nomenclature for definition of symbols used):

$$\frac{\partial T_i}{\partial t} = \frac{k_z}{\rho C_p}\frac{\partial^2 T_i}{\partial z^2} - u_i(x)\frac{\partial T_i}{\partial z} + \frac{k_x}{\rho C_p}\frac{\partial^2 T_i}{\partial x^2} \qquad i = H \text{ or } C \qquad \textbf{(eq.6.1)}$$

$$T_i(0, x_i, z) = T_{i,in} \qquad \textbf{(eq.6.2)}$$

$$k_x \left.\frac{\partial T_i}{\partial x}\right|_{x=di} = \pm\frac{\alpha\beta}{(\alpha + k_{eq})}\left(J\lambda + k_{eq}(T_H - T_C)\right) \qquad \textbf{(eq.6.3)}$$

$$\left.\frac{\partial T_i}{\partial x}\right|_{x=0} = 0 \qquad \textbf{(eq.6.4)}$$

$$k_z \left.\frac{\partial T_i}{\partial z}\right|_{z=0} = -\rho C_p u_i\left(T_i|_{z=0^-} - T_i|_{z=0^+}\right) \qquad \textbf{(eq.6.5)}$$

$$\left.\frac{\partial T_i}{\partial z}\right|_{z=L} = 0 \qquad \textbf{(eq.6.6)}$$

In addition, the parameters included in equation (**eq.6.3**) have the following forms (Dehesa-Carrasco, Pérez-Rábago & Arancibia-Bulnes 2013):

$$\alpha = \frac{h_{cp}k_{cp}}{\delta_{cp}h_{cp} + k_{cp}} \qquad \textbf{(eq.6.7)}$$

$$\beta = \frac{h_{eq}}{k_{eq} + h_{eq}} \qquad \textbf{(eq.6.8)}$$

$$k_{eq} = \frac{k_m k_{gap}}{\delta_{ga}k_m + \delta_m k_{gap}} \qquad \textbf{(eq.6.9)}$$

$$h_{eq} = \frac{h_f h_{cf}}{h_f + h_{cf}} \qquad \textbf{(eq.6.10)}$$

Moreover, the heat transfer coefficients used in this work are determined using the following empirical correlations (Bird, Steward & Lightfoot 1976; Dehesa-Carrasco, Pérez-Rábago & Arancibia-Bulnes 2013; Khayet 2011; M. Gryta 2001):

$$\mathrm{h_f} = 0.13\,\mathrm{Re}^{0.64}\,\mathrm{Pr}^{0.38} \qquad \textbf{(eq.6.11)}$$

$$\mathrm{h_{cp}} = 3.66 + \frac{0.0668\left(\mathrm{Re\,Pr}\,\frac{\mathrm{d_h}}{\mathrm{L}}\right)}{1 + 0.0450\left(\mathrm{Re\,Pr}\,\frac{\mathrm{d_h}}{\mathrm{L}}\right)^{2/3}} \qquad \textbf{(eq.6.12)}$$

$$h_{cf} = \frac{4}{3}\left(\frac{k_f^3 \rho_{fl}^2 g}{3\mu_{fl}\Gamma}\right)^{1/3} \qquad \textbf{(eq.6.13)}$$

$$\mathrm{k_m} = \varepsilon \mathrm{k_{air}} + (1-\varepsilon)\mathrm{k_{si}} \qquad \textbf{(eq.6.14)}$$

In order to solve the preceding set of 2D AGMD equations numerically, the orthogonal collocation method (OCM) was first applied to discretize the partial differential equations (PDEs) into a set of ordinary differential equations (ODEs) and then these resulting ODEs were integrated in time using the variable coefficients ordinary differential equation (VODE) algorithm (Brown, Byrne & Hindmarsh 1989; Shim et al. 2015; Villadsen & Michelsen 1978).

6.2.3 Mass transfer

In general, the permeate water vapor flux through the membrane pores can be expressed as the function of vapor pressure difference representing the following form (Drioli, Ali & Macedonio 2015; Geng et al. 2014; Khayet & Matsuura 2011):

$$J = C_m\left(P_H - P_C\right) \qquad \textbf{(eq.6.15)}$$

In the AGMD process, the total mass transfer resistance, R_{AGMD}, can be written as follows:

$$R_{AGMD} = R_K + R_M + R_{M-air} \quad \textbf{(eq.6.16)}$$

where R_K, R_M, and $R_{M\text{-}air}$ are the Knudsen diffusion resistance, the molecular diffusion resistance and the molecular diffusion resistance in the air gap, respectively (Drioli, Ali & Macedonio 2015; Geng et al. 2014; Khayet & Matsuura 2011).

These corresponding resistances can be calculated by using the following equations (Drioli, Ali & Macedonio 2015; Geng et al. 2014):

Knudsen diffusion resistance: $$R_K = \left(1.064 \frac{r\varepsilon}{\delta_m \tau_m} \sqrt{\frac{M_w}{R\left(T_{avg,m} + 273.15\right)}}\right)^{-1} \quad \textbf{(eq.6.17)}$$

Molecular diffusion resistance: $$R_M = \left(\frac{P_T D_{AB}}{P_{avg,m}} \frac{\varepsilon}{\delta_m \tau_m} \frac{M_w}{R\left(T_{avg,m} + 273.15\right)}\right)^{-1} \quad \textbf{(eq.6.18)}$$

Molecular diffusion resistance in the air gap:

$$R_{M-air} = \left(\frac{P_T D_{AB}}{P_{avg,ma}} \frac{\varepsilon}{\delta_a} \frac{M_w}{R\left(T_{avg,a} + 273.15\right)}\right)^{-1} \quad \textbf{(eq.6.19)}$$

On the other hand, the Poiseuille flow can be ignored in AGMD system due to low operating temperature (< 100 ^{o}C).

Based on this expression, the net water flux, J_{AGMD}, can be written as follows:

$$J_{AGMD} = C_{AGMD}\left(P_H - P_C\right) = \frac{1}{R_{AGMD}}\left(P_H - P_C\right) \quad \textbf{(eq.6.20)}$$

where C_{AGMD} is the mass transfer coefficient.

6.3 Materials & methods

6.3.1 Materials

PVDF-*co*-HFP (Mw = 450,000 g/mol, Kynar Powerflex® LBG) (referred herein as PH) and N, N-dimethylformamide (DMF) solvent were purchased from Arkema Inc., Australia and Sigma-Aldrich, respectively. The graphene used in the present study was xGNP-C500-grade material from XG-Science, USA, which has a particle diameter of 1 ~ 2 μm, an average thickness of 2 nm and an average surface area of 500 m^2/g. Ethanol was purchased from Ajax Finechem Pty Ltd. For AGMD performance test, sodium chloride (NaCl, Chem-supply) and deionized (DI) water were used.

6.3.2 Dope preparation

Neat PH solution (referred herein as PH18) was prepared by dissolving 18 wt% PH in DMF/acetone solvent (4:1 ratio) via magnetic stirring overnight. For graphene/PH solutions, a given amount of graphene (1, 3, 5, 7, and 10 wt% relative to PH; referred herein as G1PH, G3PH, G5PH, G7PH and G10PH, respectively) was first dispersed in a certain amount of DMF/acetone solution by bath sonication (Thermoline Scientific) for 1 hour and then mixed with 18 wt% PH solution by magnetic stirring at 80^oC for another hour followed by stirring at room temperature for 24 h.

6.3.3 Electrospinning

The electrospinning set-up is explained in detail in **Chapter 3**. All of the fabricated membranes were electrospun at an employed voltage, tip-to-collector distance, and feed flow rate of 10 kV, 100 mm, and 1.0 ml/hour, respectively (**Table 6.1**).

Table 6.1. Electrospinning conditions of the G/PH and neat PH nanofiber membranes

Membrane type		As-spun neat PH	1 wt % graphene/PH	3 wt % graphene/PH	5 wt % graphene/PH	7 wt % graphene/PH	10 wt % graphene/PH
Membrane code		PH18 (neat PH)	G1PH	G3PH	G5PH	G7PH	G10PH
Solution	Graphene (%)	0	1	3	5	7	10
	PVDF-co-HFP (%)	18	18	18	18	18	18
Solvent	DMF (%)	65.6	65.6	65.6	65.6	65.6	65.6
	Acetone (%)	16.4	16.4	16.4	16.4	16.4	16.4
Electrospinning	Voltage (kV)	10	10	10	10	10	10
	Flow rate (ml/h)	1.0	1.0	1.0	1.0	1.0	1.0
	TCD[a] (cm)	15	15	15	15	15	15

6.4 Results and discussion

6.4.1 Membrane characteristics and morphology

The characteristics and morphologies of the neat and G/PH electrospun nanofiber membranes are shown in **Table 6.2** and **Fig. 6.2**. All of the fabricated membranes showed highly-porous, non-woven and overlapping nanofiber structures and had a similar thickness of about 100 μm. The mean and maximum pore sizes of the electrospun membranes did not change much even with the incorporation of different graphene concentrations. However, it could be seen that the fiber diameter decreased with the incorporation of graphene compared with the neat PH until 3wt% graphene concentration, and then increased slightly at higher concentrations. This decreasing fiber diameter trend could be attributed to the increased conductivity of the graphene/PH

solutions, which increased the likelihood of more electrostatic repulsion leading to increased stretching, hence smaller fibers. At higher graphene concentration (>3 wt%), this could have led to increased viscosity and more agglomeration among graphene particles (Woo et al. 2016), which led to bigger fiber diameters, as also observed by other studies (Drew et al. 2003; Moradi et al. 2015).

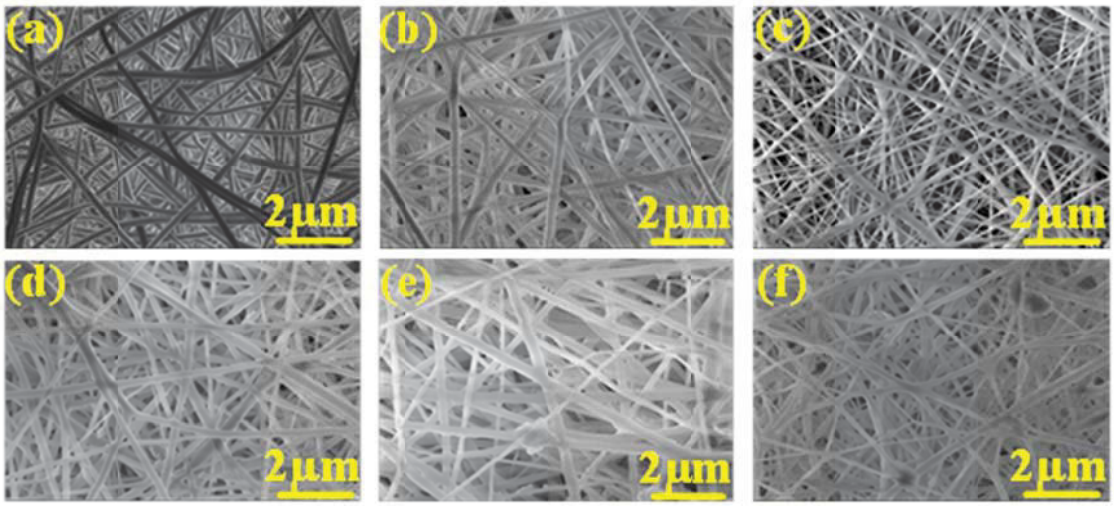

Figure 6.2. Surface SEM images of the G/PH and neat PH electrospun nanofiber membranes: (a) neat PH, (b) G1PH, (c) G3PH, (d) G5PH, (e) G7PH and (f) G10PH

Table 6.2. Characteristics of the neat and G/PH electrospun membranes and commercial membrane

	Membrane thickness (µm)	Mean pore size (µm)	Maximum pore size (µm)	Porosity (%)	LEP (kPa)	Fiber diameter (nm)	Average contact angle (deg)	Tensile strength (MPa)	Elongation at break (%)
PH18	100.1 ± 1.6	0.87 ± 0.03	1.37 ± 0.02	94.7 ± 1.2	139.1 ± 2.5	613.0 ± 130.6	142.3 ± 1.3	2.3 ± 0.2	85.2 ± 0.7
G1PH	100.4 ± 1.9	0.86 ± 0.01	1.38 ± 0.02	92.2 ± 2.8	163.2 ± 2.2	557.1 ± 210.8	149.3 ± 2.0	2.8 ± 0.3	68.2 ± 1.4
G3PH	100.2 ± 0.7	0.83 ± 0.02	1.34 ± 0.03	90.4 ± 1.5	165.8 ± 1.9	359.5 ± 179.5	151.2 ± 4.1	6.3 ± 0.6	146.4 ± 2.2
G5PH	100.2 ± 1.2	0.86 ± 0.02	1.36 ± 0.03	88.7 ± 1.8	186.9 ± 2.4	378.6 ± 144.1	162.7 ± 2.1	12.2 ± 1.2	146.8 ± 2.3
G7PH	100.3 ± 2.4	0.84 ± 0.01	1.35 ± 0.04	84.7 ± 2.4	188.7 ± 3.1	409.1 ± 118.9	159.9 ± 3.0	5.6 ± 0.5	137.8 ± 1.9
G10PH	100.3 ± 1.8	0.85 ± 0.02	1.33 ± 0.03	82.3 ± 2.1	190.3 ± 4.2	429.7 ± 186.4	159.3 ± 1.9	4. 7 ± 0.3	127.1 ± 1.6
C-PVDF	107.4 ± 1.6	0.22 ± 0.02	0.29 ± 0.02	70.3 ± 0.3	213.3 ± 3.1	-	131.1 ± 3.1	7.2 ± 0.2	36.3 ± 3.1

The decreasing porosity from 94.7% for neat PH to 82.3% for G10PH was mainly because of the existence of aggregated graphene and some bead formation on the membrane surface at increasing graphene concentrations (**Figs. 6.2** and 6.**3**). However, it should be noted that regardless of the decreasing porosity of the graphene/PH membranes, they still have much higher porosity compared with the commercial PVDF membrane (~70%). This high porosity of nanofiber membrane is an attractive asset for MD application as higher porosity indicates more surfaces for vapour to pass through, hence enhanced flux rate (Liao, Wang & Fane 2014). Though the mean pore and

maximum pore sizes were similar for all electrospun membranes, the graphene-loaded membranes showed increasing LEP values from 163 kPa for G1PH to 190 kPa for G10PH, compared with 139 kPa for neat PH. This clearly shows that graphene has enhanced the anti-wetting property of the membrane, which could be attributed to the added hydrophobicity of the incorporated graphene, as confirmed by contact angle (CA) measurements (**Table 6.2** and **Fig. 6.4**), showing increased CAs (149 to 162^{o}) with increasing graphene contents up to 5 wt%.

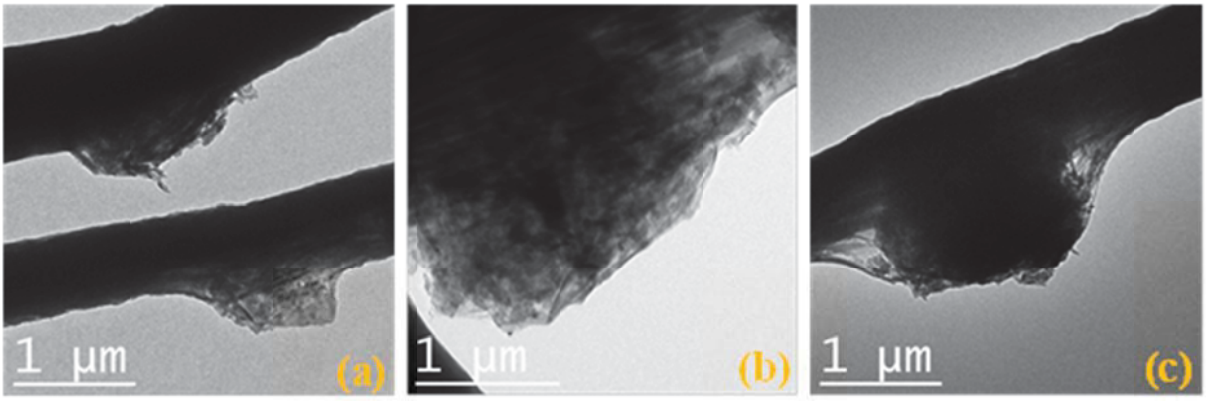

Figure 6.3. TEM images of the G/PH electrospun nanofiber membranes: (a) G5PH, (b) G7PH and (c) G10PH

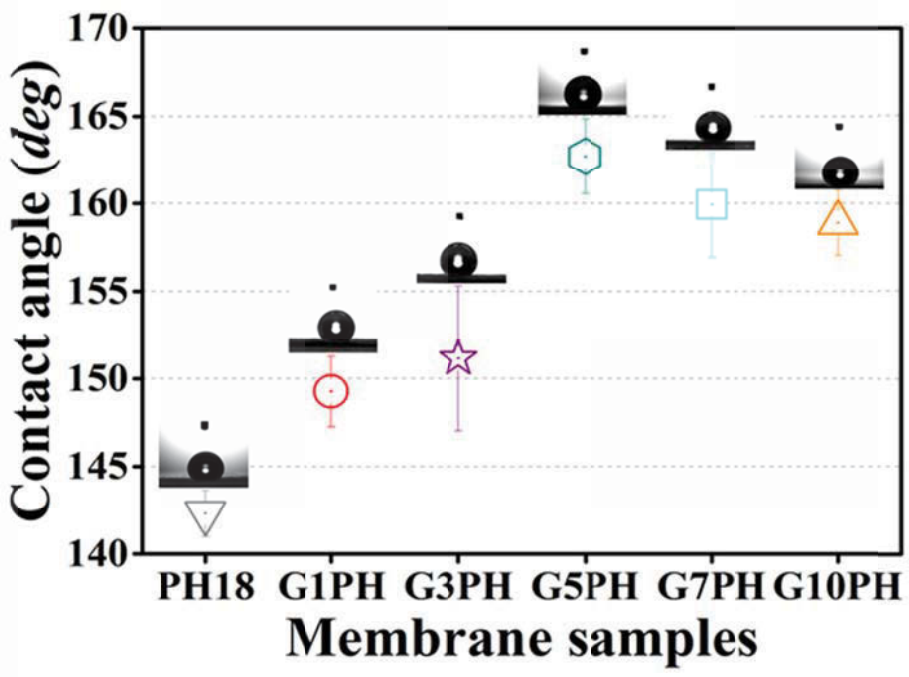

Figure 6.4. Average contact angle of the fabricated G/PH and neat PH electrospun nanofiber membranes

In **Fig. 6.5**, AFM results of the nanofiber membranes revealed that G5PH membrane had much rougher mean surface roughness (R_a= 0.719 ± 0.03 µm) compared with that of neat PH18 membrane (R_a= 0.623 ± 0.013 µm), which is attributed to the added roughness from the graphene nanoparticles in/on the nanofiber. Slight decrease in CA was observed at >5wt% graphene content which could be due to more agglomeration of graphene that led to less and non-uniform dispersion of graphene on the membrane surface (**Fig. 6.3**). Though some researchers noted that the ideal pore size for MD membrane should be <0.6 µm to avoid wetting problems, however, this is not the case with our present study, as also observed by other researchers utilising nanofiber membranes mainly due to increased hydrophobicity of electrospun membrane. For example, Liao et al. observed no wetting problems for 50 h of their nanofiber membranes despite having bigger pores (i.e., >0.6 µm) (Liao, Wang & Fane 2014). It

should be noted that the wetting phenomenon is not only affected by the pore size, but by different membrane properties such as hydrophobicity, pore size distribution, and operating parameters. Based from **Table 6.2**, the optimal graphene concentration was found to be 5 wt%, obtaining the highest CA and favourable porosity and LEP values.

Further checking of G5PH (see **Fig. 6.6(a)** and **Fig. 6.6(b)**) showed interconnected and overlapping fibers, with graphene sheets protruding at the surface. Characterization by TEM (**Fig. 6.6(c)**) also revealed the successful incorporation of graphene with many protruding on the surface leading to nano surface roughness and higher hydrophobicity.

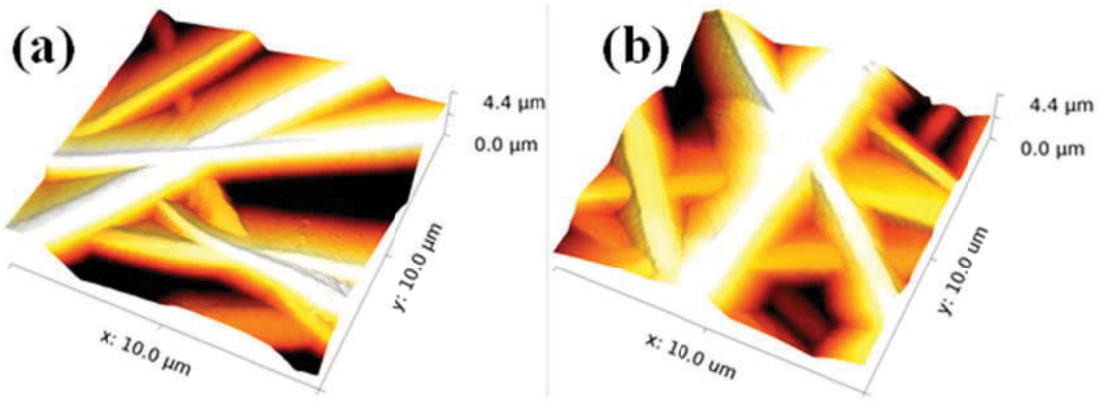

Figure 6.5. AFM images of (a) the PH18 and (b) the G5PH membranes. The mean roughness (Ra) of the PH18 and G5PH membranes was 0.623 ± 0.01 µm and 0.719 ± 0.03 µm, respectively.

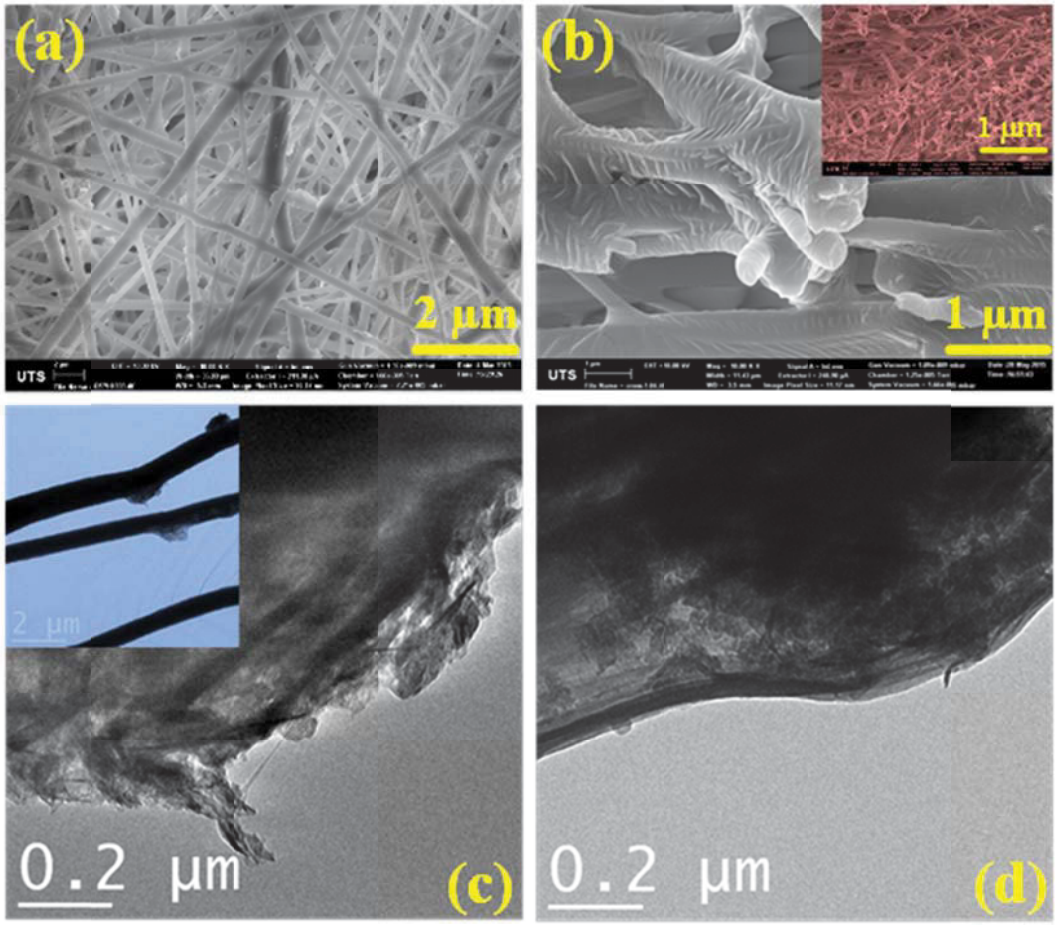

Figure 6.6. Surface and cross-section morphologies of the G5PH electrospun nanofiber membrane (a and b) by SEM and (c and d) surface morphology of the G5PH electrospun nanofiber membrane by TEM

EDX measurement was carried out to further confirm the successful incorporation of graphene in/on the nanofiber **(Fig. 6.7). Figure 6.7(a)** indicates increasing atomic carbon concentration with the increase in the amount of graphene incorporated in/on the membrane, suggesting the presence of more graphene at increasing concentration. The atomic carbon to fluorine (C/F) ratio (**Fig. 6.7(b)**) also showed increasing values with the increase in graphene contents, further confirming the proper dispersion and incorporation of graphene.

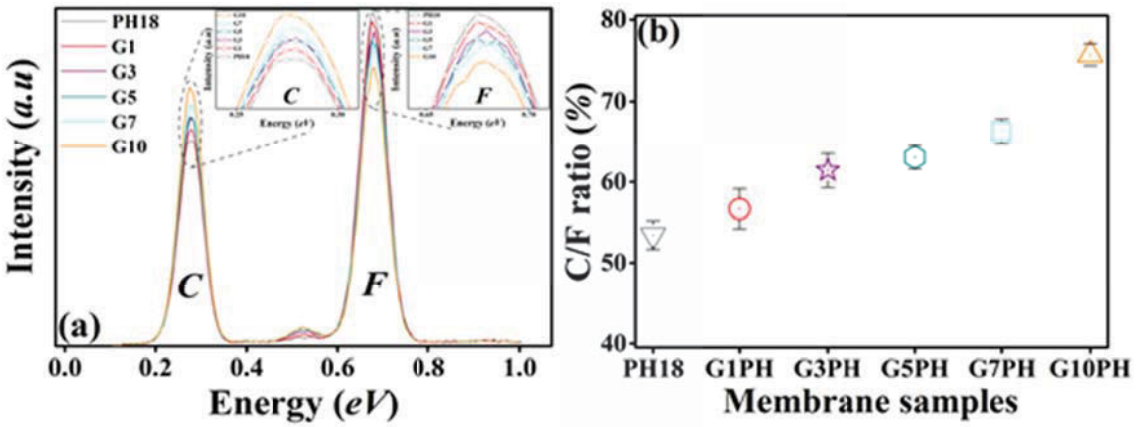

Figure 6.7. (a) EDX and (b) C/F ratio by EDX of the G/PH and neat PH electrospun nanofiber membranes

6.4.2 Structural and chemical characterization

Figure 6.8 shows the results of XRD, FT-IR and Raman spectroscopy measurements of the fabricated membranes. XRD crystallographic analyses (**Fig. 6.8(a)**) reveal that PH is crystalline showing peaks at 18.5º and 20.5º, which correspond to α (0 2 0) and β ((2 0 0)/(1 1 0)) crystal phases, respectively (Baji et al. 2013). This indicates the existence of both α and β phases. Meanwhile, G5PH membrane showed an additional peak at 26.4º (An et al. 2014), which is the characteristic peak of graphene (see **Fig. 6.8(b)**), indicating the presence of graphene in the composite membrane. G5PH showed slight shifting of the peaks to the left which suggests the interaction between the polymer matrix and graphene nanofiller.

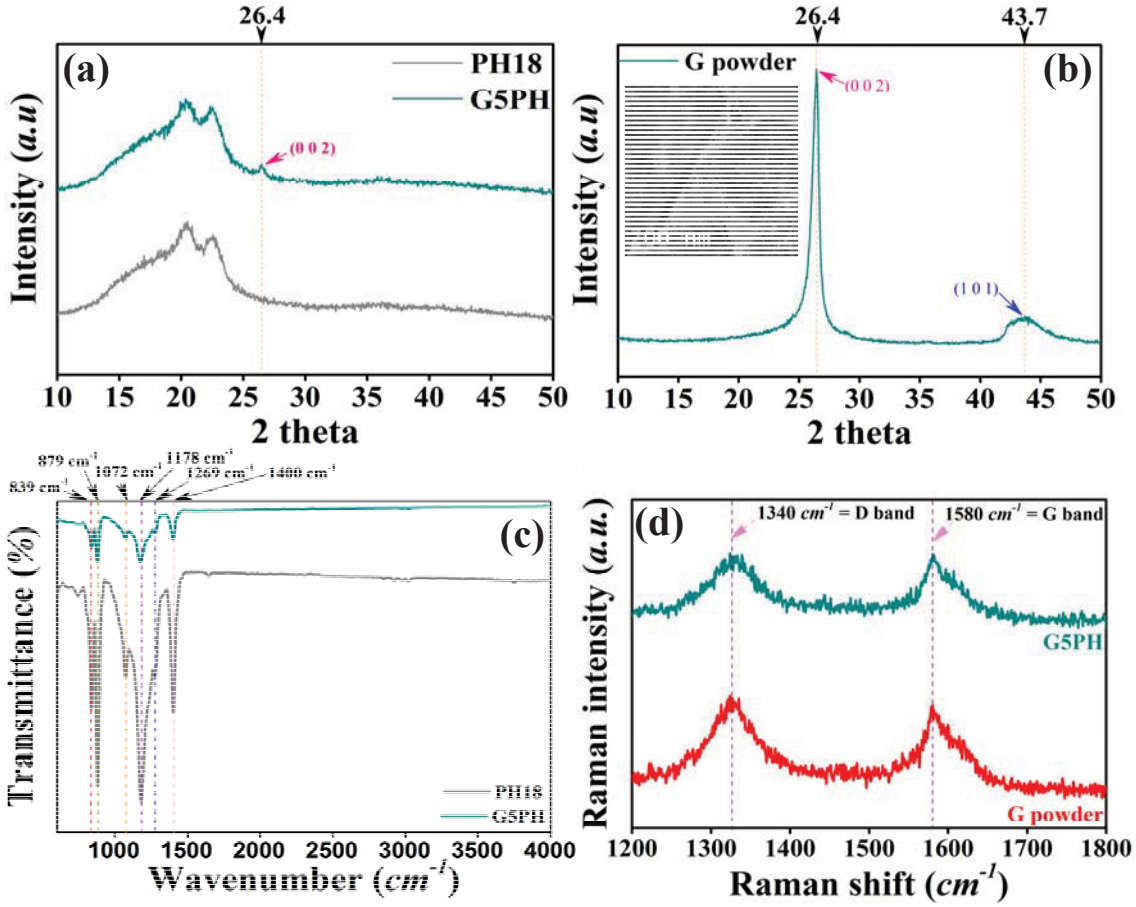

Figure 6.8. XRD spectra of (a) neat PH and G5PH membranes, and (b) graphene powder; (c) FTIR peaks of neat PH and G5PH membranes, and; (d) Raman spectra of the G5PH membrane and graphene powder

Fig. 6.8(c) shows the FT-IR spectra of the different fabricated membranes. All neat and G/PH nanofibers showed the same absorption bands attributed to the basic structural characteristics of PVDF-HFP at 839 cm^{-1}, 879 cm^{-1}, 1072 cm^{-1}, 1178 cm^{-1}, 1269 cm^{-1}, and 1400 cm^{-1}, which correspond to CH_2 rocking and CF_2 asymmetric stretch (the β phase), CH_2 in plane bending or rocking (the α phase), C-C asymmetric stretch, C-C asymmetric stretch and CF_2 symmetric stretching, CF out of plane deformation (the β phase), and CF stretching vibrations or CH_2 wagging (the α phase), respectively (Woo et al. 2015). Similar spectra were observed for the G/PH electrospun membranes but at

lower intensities, which signify the presence of interfacial interaction (physical adsorption or weak chemical bonding) between PH and graphene particles.

The Raman spectra of G5PH electrospun membrane (**Fig. 6.8(d)**) showed two prominent peaks at 1340 and 1580 cm^{-1}, which are indicative of the D (defect-induced region) and G (ordered lattice or in-plane vibrations of carbon atoms) bands of graphene, respectively (Surwade et al. 2015). This suggests the presence of graphene in the membrane. The D and G band intensity ratio (I_D/I_G) or the R-value of the graphene powder and that of G5PH was very similar (0.86 and 0.95, respectively) indicating that graphene in the composite membrane has maintained its chemical structure and crystallinity (Tuinstra & Koenig 1970).

6.4.3 Thermal and mechanical properties of the G/PH nanofiber

The thermal and mechanical properties of the samples were measured by TGA and tensile tester, respectively, and the results are shown in **Fig. 6.9** and **Table 6.2**. It is general knowledge that when nanofillers are properly dispersed in a host polymer, they can spread the load transfer of the composite material, thereby improving its thermal and mechanical properties. In the present study, the incorporation of 5 wt% graphene in/on PH nanofiber has resulted to improved thermal and mechanical properties. Based from the TGA curves in **Fig. 6.9(a)**, the neat PH membrane showed two prominent weight losses at ~ 146ºC and at ~ 400ºC, which are consistent with the degradation pattern of PVDF-*co*-HFP (Cao et al. 2005). For G5PH membrane, a shift of thermal decomposition towards higher temperature (about 14ºC higher) was observed, which confirms enhancement in thermal stability. The weight loss of the neat PH and the G5PH electrospun nanofiber membranes at 480ºC was 38.6% and 46.5%, at 600ºC was

30.8% and 36.1%, and at 700ºC was 28.3% and 33.0%, respectively. Higher residual mass was observed for G5PH compared with neat PH at 1000°C indicating the good dispersion of graphene in the composite membrane that resulted to improved thermal properties. As observed in SEM and TEM, graphene was either fully enveloped in the polymer matrix or protruding while the tail end is embedded onto the nanofiber (Gethard, Sae-Khow & Mitra 2011).

The MD process is commonly employed under atmospheric pressure so that the membrane for MD has lower requirements for tensile properties; however, adequate tensile properties are still needed to guarantee successful packing in modules and provide stable operation (Essalhi & Khayet 2012). Thus, the mechanical properties of the membranes were investigated.

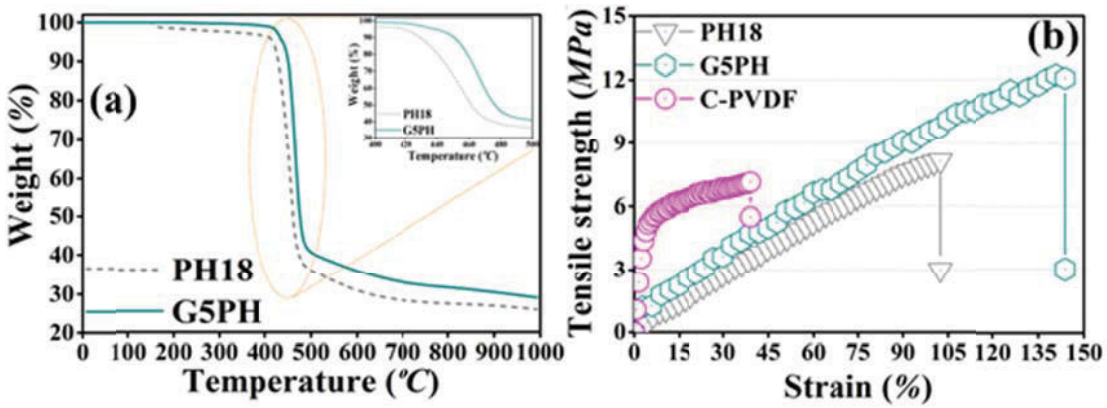

Figure 6.9. (a) TGA and (b) stress-strain curves of the G5PH and neat PH electrospun nanofiber membranes.

Fig. 6.9(b) shows the stress-strain curves of the commercial and electrospun membranes. Neat PH nanofiber exhibited a tensile strength and elongation of 8.1 MPa and 102.4%, respectively. Meanwhile, G5PH exhibited tensile strength and elongation of 12.2 MPa

and 143.9%, respectively, or an increase of 51% in tensile strength when graphene was incorporated. Even elongation has increased for G5PH compared with neat PH. This clearly indicates the good interaction of graphene and PH polymer matrix that resulted to good load transfer from PH to graphene. Membranes with higher graphene loading (> 7 wt%) have decreased mechanical properties compared with the G5PH membrane, which shows that the graphene loading of 5 wt% is optimum (**Table 6.2**). Additionally, the increased mechanical property of G5PH could be due to good interfacial interaction between graphene and polymer matrix, weak van der Waals bonding between PH and graphene, and some micromechanical locking of fibers and graphene. Interestingly, the nanofiber membranes posted much better tensile strength and elongation compared with the commercial PVDF flat-sheet membrane (7.2 MPa and 36.3%, respectively). The stress-strain curves of the nanofiber membrane and commercial membrane presented different trends. The commercial membrane had a steep increase in tensile strength in the first 10% elongation, and then gradually increased thereafter until failure. However, the nanofiber membrane showed a linear mode of stress-strain curve, which could be attributed to the nonwoven porous structure of the nanofibers as compared with a denser structure of the commercial membrane.

6.4.4 BET of the G/PH membrane

Nitrogen adsorption/desorption analysis was used to further characterize the neat PH and graphene composite membrane, G5PH. As shown in **Fig. 6.10(a)**, both neat PH and G5PH represent typical type II or III isotherms with type H3 (or H4) hysteresis loop and sharp increase in adsorption at a high relative pressure of 0.9-0.99, representing the existence of the numerous meso and macropores in the sample (Lowell et al. 2004; Rouquerol, Rouqueorol & Sing 1999). This nitrogen adsorption analysis reveals that the

graphene composite membrane, G5PH, has a relatively larger surface area and pore volume compared with those of neat PH, revealing appreciable development of the porosity after introducing the graphene into membrane. Namely, G5PH represent a specific surface area of 163 m^2/g with a total pore volume of 0.379 cm^3/g, which is about 2 to 3 times greater than those of PH (78 m^2/g and 0.131 cm^3/g). However the specific surface area of G5PH is approximately 16 times smaller than the theoretical value (2620 m^2/g) of single layer graphene sheets.

Figure 6.10(b) compares the Barrett–Joyner-Halenda (BJH) pore size distribution curves derived from the desorption branches of the isotherms. These curves also indicate that G5 has more plentiful amounts of meso pores than those of PH, which are closely related to the graphene sheets (See **Fig. 6.6(b)**, wavy wrinkles). The obtained PSD curves are uniformly distributed at 2.5 nm for G5PH and 2.9 nm for PH, respectively.

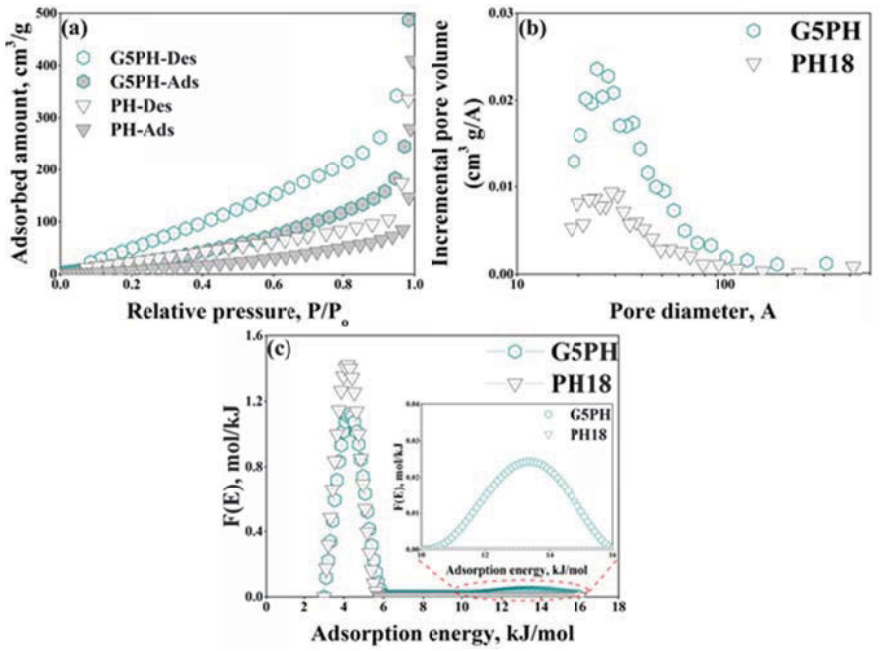

Figure 6.10. Nitrogen adsorption-desorption isotherms (a) BJH pore size distributions and (b) for G5PH and neat PH membranes and (c) nitrogen adsorption energy distributions on G5PH and neat PH membranes

In order to comparatively examine the surface energetic heterogeneity for model membranes, nitrogen adsorption energy distribution (AED) functions were calculated using a regularization method. In this work, the Flower-Guggenheim isotherm model was used as a kernel function because this equation can generally explain the localized adsorption with lateral interactions (Jaroniec & Madey 1988; Nahm et al. 2012; Rudzinski & Everett 1991; Shim, Lee & Kim 2008). As compared in **Fig. 6.10(c)**, the shapes of AED function curve for neat PH and G5PH differ slightly, providing further evidence of the existence of different types of surface energy. The G5PH represent two pronounced peaks at 4.3 and 13.4 kJ/mol (see inset) but the neat PH shows only a single peak at 4.2 kJ/mol. No appreciable high energy peak is obtained in the neat PH. These results clearly indicate that the G5PH have mainly two different types of surface energetic heterogeneity for nitrogen. In particular, the high-energy peak observed in G5PH can be explained with the existence of the graphene nanosheets in the composites, which can provide more suitable pores and available adsorption sites for target ion. Thus it is reasonable to suggest that the graphene composite, G5PH, seems to be more heterogeneous than that of neat PH.

6.4.5 AGMD performance of the G/PH membrane

Figure 6.11 presents the AGMD performances of the different fabricated neat and composite membranes. Initial AGMD tests for 20 h reveal that neat PH (PH18) and G1PH membranes had wetting problems in less than 3 h of operation. However, at higher graphene loadings (>5 wt%), nearly stable fluxes were observed. The highest flux was obtained using G5PH, which was stable for 20 h at 22.91 L/m^{2}h or LMH, followed by G7PH (~18 LMH) and G10PH (~13.5 LMH), and their salt rejection was

>99.99%. The difference in their performance could be explained by investigating their morphologies and properties. Although G10PH had the highest LEP among all nanofiber membranes, many agglomerations on the membrane surface could have constricted the membrane pores (which explains the high LEP) thereby decreasing the surface area for vapour transport. Similarly, G7PH showed some agglomerations at the surface but at a lesser extent compared with G10PH. The G5PH seemed to have the good dispersion of graphene in/on the surface with adequate roughness and surface pore size and porosity, thereby attaining the highest flux and high rejection.

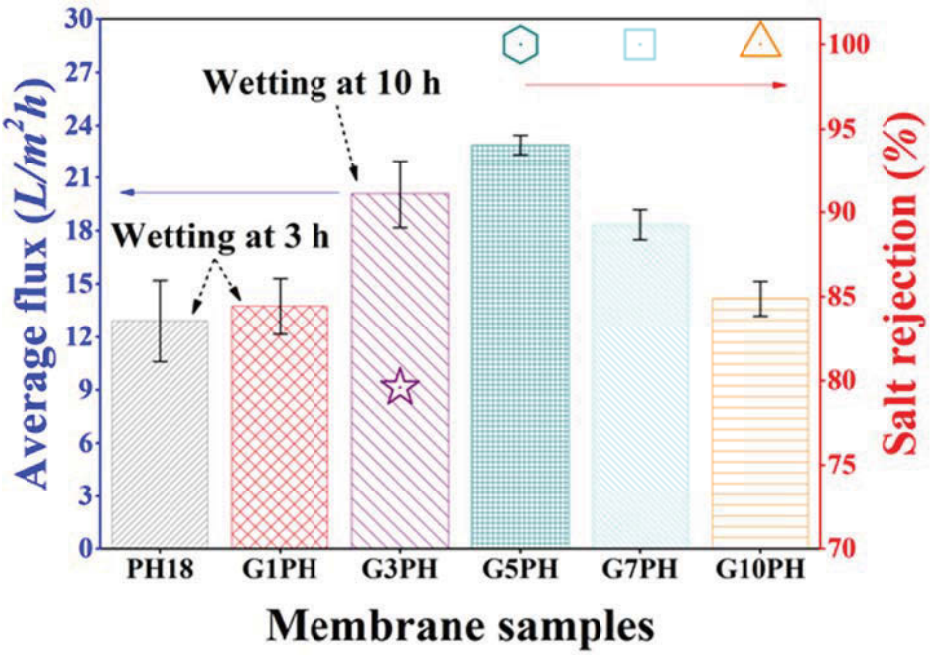

Figure 6.11. Flux and salt rejection performances of the G/PH and neat PH membranes for 20h operation (Inlet temp at feed = 60°C; Inlet temperature at coolant = 20°C)

Based from the result of the short term AGMD performance, G5PH membrane was compared to a commercial PVDF membrane for 60 h of operation and the results are shown in **Fig. 6.12.** The water vapour flux of the commercial membrane showed an

initial value of 6 LMH and declined slightly until 15 h, then maintained constant until 60 h at 4.75 LMH. On the other hand, G5PH membrane remained stable for 60 h at 22.91 LMH. This flux is five times higher than that of the commercial membrane while maintaining a 99.99% salt rejection (compared with 99.2% for the commercial membrane). This better performance is attributed to the greater void volume fraction of G5PH, bigger pore sizes yet with high LEP values primarily due to superhydrophobicity, and the presence of graphene.

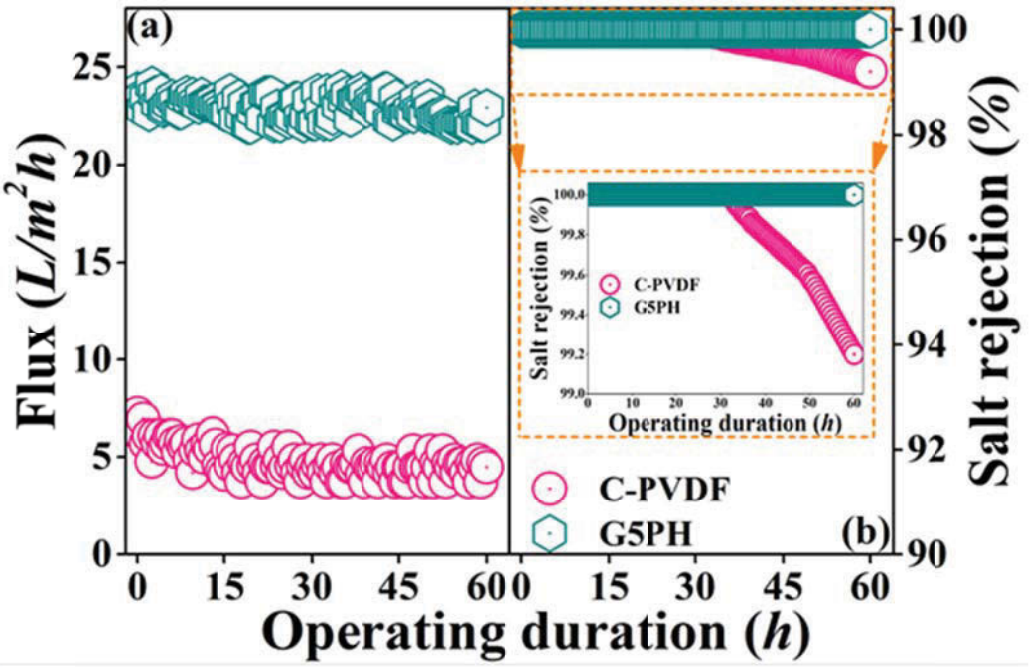

Figure 6.12. (a) Flux and (b) salt rejection of the G5PH electrospun nanofiber membrane and commercial PVDF membrane

As shown in **Fig. 6.6** and depicted in **Fig. 6.13,** graphene addition produces multi-level roughness on the membrane surface, which helps in increasing the hydrophobicity and consequently the LEP. The large aspect ratio of graphene leads to protrusion on the surface of the nanofibers after electrospinning. When the membrane is exposed to the

feed solution (see **Fig. 6.13**), the nano and micro-level thickness and superhydrophobicity prevent the penetration of water molecules into the membrane pores, and with the high volume fraction of electrospun membrane, allows more water vapour to pass through. Additionally, the protruded graphene provides diffusion path for water vapour due to its rapid adsorption/desorption capacity. This adds to the overall water vapour transport across the membrane.

To further explain the role of graphene in the enhancement of AGMD performance, an experimental and theoretical evaluation is presented in the next section.

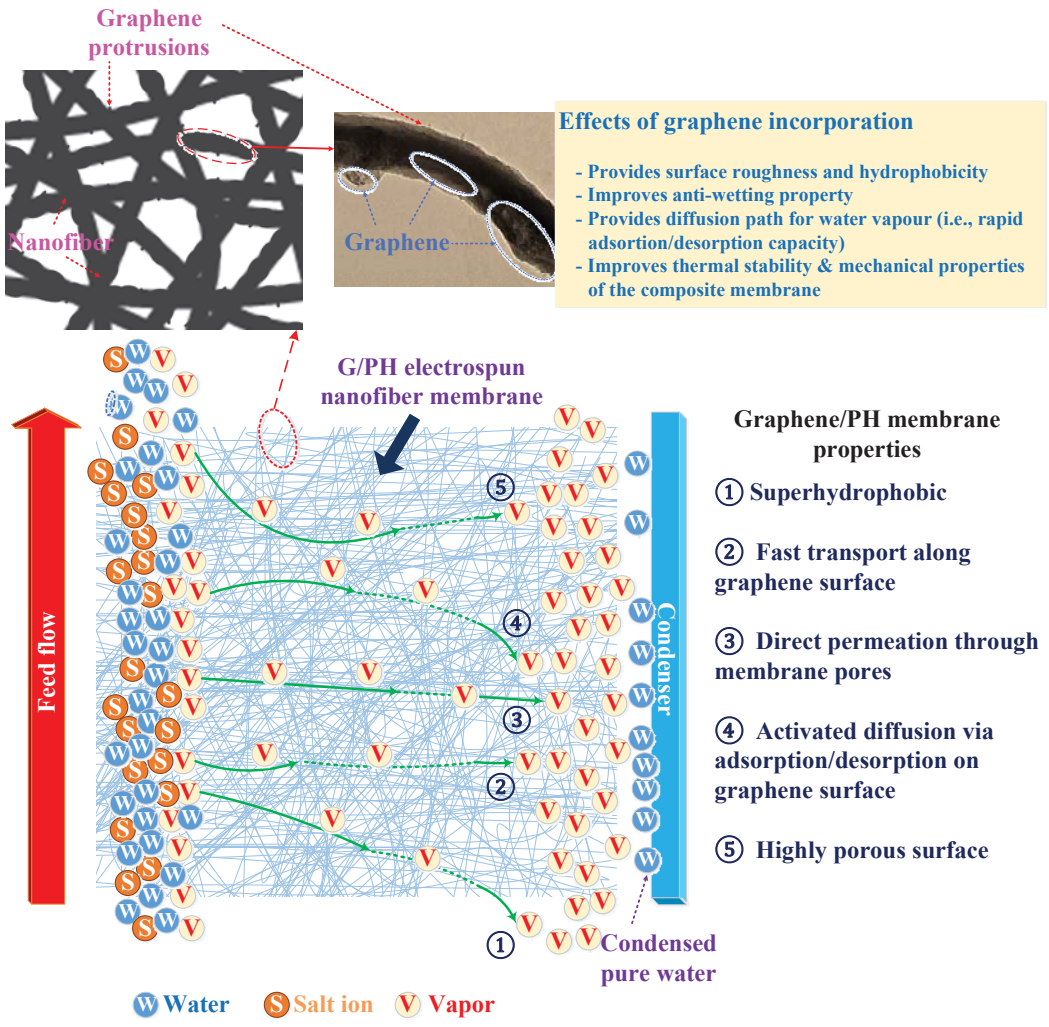

Figure 6.13. Schematic of the effect of graphene on the membrane for AGMD process

6.4.6 AGMD performance of the G/PH membrane

Fig. 6.14 compares the experimental and simulation results for G5PH and commercial PVDF. A considerable improvement in flux enhancement was obtained from G5PH. As shown in this figure, the average flux (22.91 L/m^{2}h) through G5PH is approximately 4.8 times greater than that (4.75 L/m^{2}h) of the commercial PVDF sample, which is closely related to the existence of graphene. This enhanced flux performance of G5PH can be explained by its high hydrophobicity, high thermal conductivity, large available surface area and pore volume.

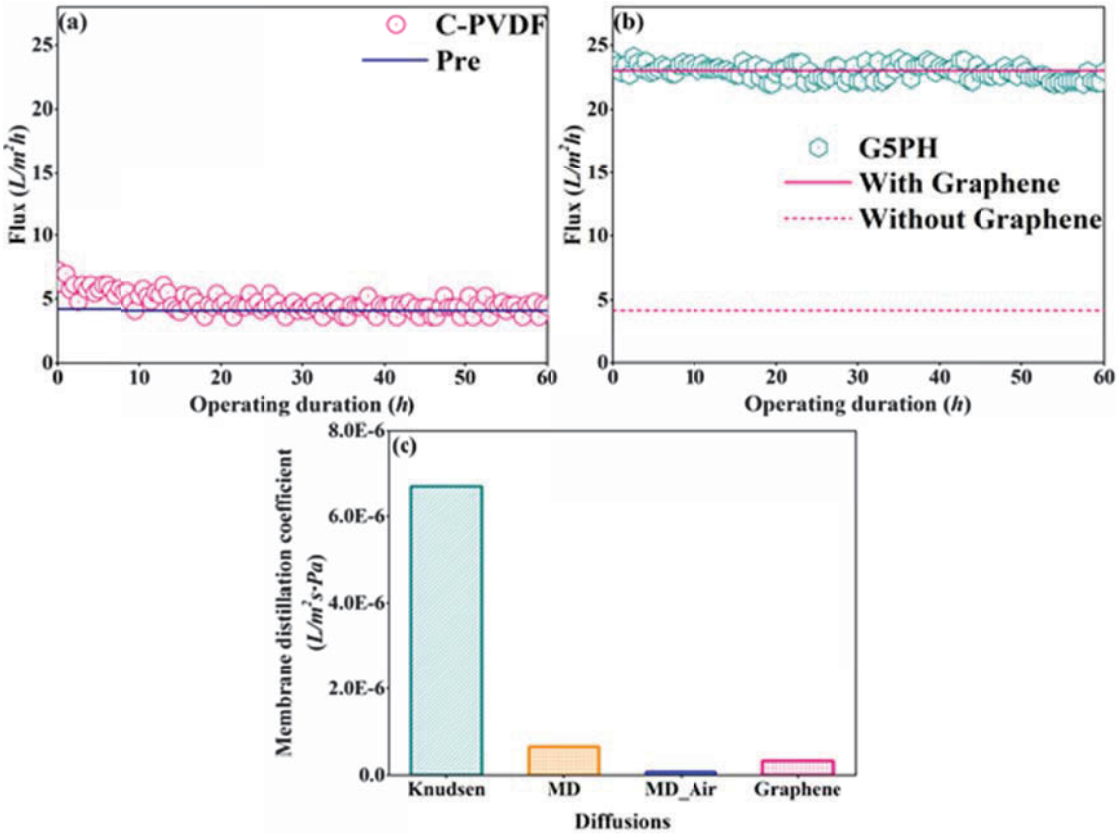

Figure 6.14. Experimental and predicted flux for commercial PVDF, (b) Predictions for G5PH flux by the AGMD models with and without the presence of graphene sheet and (c) comparison of membrane distillation coefficients for G5PH

The total mass transfer resistance in AGMD system, R_{AGMD}, can be expressed in terms of the combined membrane resistance and air gap resistance (Drioli, Ali & Macedonio 2015). Then the net water flux, J_{AGMD}, can be described as follows,

$$J_{AGMD} = C_{AGMD}\left(P_H - P_C\right) = \frac{1}{R_{AGMD}} = \left(\frac{1}{\left(R_K + R_M + R_{M-air}\right)}\right)\left(P_H - P_C\right) \quad \textbf{(eq.6.21)}$$

where C_{AGMD}, R_K, R_M, and $R_{M\text{-}air}$ are the mass transfer coefficient, the Knudsen diffusion resistance, the molecular diffusion resistance and the molecular diffusion resistance in the air gap, respectively.

Based on the heat and mass transfer equations suggested in this area, the experimental flux behavior of commercial PVDF can be well explained as shown in **Fig. 6.14(a)**. However, the general AGMD model could not fit the flux pattern of G5PH properly (See **Fig. 6.14(b)** dashed line). A considerable difference was noted between the experimental data and the predicted one, indicating the limitation of the general AGMD model. Thus in order to explain the flux behavior, in this work, we introduce the net water flux, $J_{AGMD\text{-}G}$, which consider the existence of graphene sheets as follows,

$$J_{AGMD-G} = C_{AGMD-G}\left(P_H - P_C\right) = \frac{1}{R_{AGMD-G}} = \left(\frac{1}{\left(R_K + R_M + R_{M-air}\right)} + \frac{1}{R_G}\right)\left(P_H - P_C\right)$$

(eq.6.22)

where $C_{AGMD\text{-}G}$ and R_G are the mass transfer coefficient and the molecular diffusion resistance related with the graphene sheets, respectively. Here we used the coefficient R_G as adjustable parameter to fit the experimental flux data. As shown in **Fig. 6.14(b)**, a reasonable fitting to the data could be obtained using this approach, which indicates that the suggested model can describe the mass transfer process well. Moreover, **Fig. 6.14(c)** compares the determined membrane distillation coefficient (MDC) values for different

mass transfer models, which shows the following order: Knudsen diffusion > molecular diffusion > graphene sheet > molecular air gap diffusion-air. It is clear from this result that the influence of graphene sheet on the AGMD process is larger than that of molecular air gap diffusion.

Herein, we have shown the positive effect of the incorporation of 5 wt% graphene into PH electrospun membrane for AGMD application. For further improvement, optimization of the membrane thickness and pore size distribution could be carried out in future research.

6.5 Concluding remarks

In summary, graphene/PVDF-HFP (G/PH) membranes were successfully fabricated by a one-step electrospinning technique and evaluated by air gap membrane distillation (AGMD) using 3.5 wt% NaCl solution as feed. Graphene nanoparticles have been dispersed well in/on the nanofiber, which was confirmed by FT-IR, XRD, EDX and Raman spectroscopy. Further, there was an increase in hydrophobicity of G/PH electrospun nanofiber membrane compared with the as-spun neat PH membrane. Several protruding graphene nanoparticles were observed on the nanofiber by SEM and TEM, which leads to increased contact angle. The nanofiber membrane with 5 wt% graphene loading (G5PH) showed an adequate porosity (88.7%), pore size (0.86 μm), contact angle (162.7°) and LEP (186.9 kPa) for AGMD application. For 60 h AGMD test, G5PH nanofiber membrane showed more stable flux (22.9 LMH) and better salt rejection performances (99.99%) compared with commercial PVDF membrane (flux of 4.75 LMH and salt rejection of 99.20%). Additionally, the effect of graphene on the flux performance was corroborated by theoretical models as suggested in the present study.

The present results suggest that the graphene-incorporated nanofiber membrane has good potential as a robust MD membrane for water desalination by AGMD process.

CHAPTER 7

University of Technology Sydney
FACULTY OF ENGINEERING

BORON NITRIDE EMBEDDED MEMBRANE BY ELECTROSPINNING FOR SEAWATER DESALINATIO BY MEMBRANE DISTILLATION

7.1 Introduction

Conventionally, membranes are fabricated by several techniques such as phase inversion and wet spinning method (Woo et al. 2016). Recently, electrospinning has been applied as one of the alternative techniques to fabricate MD membranes with suitable properties. Currently, a number of studies on MD membrane fabrication have been reported using electrospinning technique (Li, Wang, et al. 2014; Liao et al. 2014; Liao, Wang & Fane 2014). However, these membranes are still not robust enough for long term operation of MD process. Some of the most desirable properties of the MD membrane include superhydrophobicity to reduce membrane wetting problem, high liquid entry pressure (LEP) (allowing higher operating pressure) and high porosity (higher water vapor flux) as well as high salt rejection for long-term MD process. Incorporation of nanoparticles such as carbon nanotubes (CNTs) and silica nanoparticles in/on nanofibers has been studied to enhance the hydrophobicity of electrospun nanofiber membranes. Even though CNT and silica nanoparticle embedded nanofiber membranes were successfully fabricated and also shown much higher hydrophobicity compared to an as-spun nanofiber membrane, their performances significantly decreases during the long-term MD operation. Therefore, further strategies are essential for the development of MD membranes that can provide a stable water vapor flux and salt rejection performances during the long-term MD operation.

This chapter used a scalable method for exfoliating hexagonal boron nitride (h-BN) by using a hydroxide-assisted ball milling process, similar to our previous work (Lee et al. 2015). The two-dimensional h-BN (so called ‘white graphene’) is isostructural to graphene and has received considerable attention due to its good mechanical properties,

chemical stability and potential applications including superhydrophobic coatings (Lee et al. 2013; Lei et al. 2013; Oh et al. 2014).

The incorporation of h-BN is expected to provide additional properties to the electrospun nanofiber membrane such as improved roughness and hydrophobicity thereby improving the robustness of the MD membrane. In this study, we exploited the unique properties of the h-BN to enhance the overall properties of a polymeric nanofiber membrane in obtaining a robust superhydrophobic membrane for improved long-term performance of air gap MD (AGMD). The unique properties of BN nanoparticles are expected to improve the characteristics of MD membrane favourably and their incorporation into the electrospun membrane is therefore worth exploring. The study also includes a series of measurements, characterization and AGMD performance tests with seawater as feed.

7.2 Materials and methods

7.2.1 Materials

h-BN powders were purchased from Kojundo Korea Co., Ltd. Sodium hydroxide (NaOH), and hydrochloric acid (HCl) were purchased from Junsei Chemical Co., Ltd. Isopropanol (IPA) was purchased from Merck. PVDF-co-HFP (Mw = 450,000 g/mol, Kynar powerflex® LBG) (referred herein as PH) and N, N-dimethylformamide (DMF) solvent were purchased from Arkema Inc., Australia and Sigma-Aldrich, respectively. Ethanol was purchased from Ajax Finechem Pty Ltd. For AGMD performance test, sodium chloride (NaCl, Chem-supply) and deionized (DI) water were used. All chemicals were used as received. Commercial PVDF membrane (Durapore®-GVHP,

pore size = 0.22 μm) received from Merck Millipore was used as a reference for AGMD flux and salt rejection performance comparison.

7.2.2 Fabrication of OH-BNNPs by hydroxide-assisted ball milling

A horizontal planetary mill (Fritsch Pulverisette 5) was used for the exfoliation. Micron-sized h-BN powder (2 g) and 2 M aqueous NaOH solution were loaded into a steel grinding bowl with 8-mm-diameter steel balls at a ball:powder ratio of 50:1. The rotational speed of the planetary mill was set to 200 rpm, and the mixture was milled for 24 h. The milled product was rinsed with aqueous HCl to remove the remaining residual Fe ion and washed with deionized water until the pH close to neutral. Then, the samples were dried and dispersed in IPA. The dispersed BN solution was centrifuged at 2,000 rpm for 30 min to remove any thick flakes and aggregates. Detailed descriptions of all of the experimental procedures are addressed in our previous research (Lee et al. 2015).

7.2.3 Dope preparation

Neat PH solution was prepared by dissolving 15 wt% PH in DMF/acetone solvent (4:1 ratio) and homogeneous solution was obtained by magnetic stirring overnight. For BN-PH solutions, a given amount of the OH-BNNP (5 wt% relative to PH) was first dispersed in a certain amount of DMF/acetone solution by bath sonication (Thermoline Scientific) for 3 h, and then the pre-dissolved solution was mixed with 15 wt% PH solution by magnetic stirring at 80^{o}C for two hours followed by stirring at room temperature for 24 h.

7.2.4 Electrospinning of superhydrophobic BN-PH nanofiber

The electrospinning set-up has been explained in detail in the chapter 3. Consistent electrospinning conditions were applied to all of the fabricated membranes at an employed voltage, tip-to-collector distance, and feed flow rate of 10 kV, 15 cm, and 1.0 ml/hour, respectively. All nanofibers were directly fabricated onto a rotating drum collector covered with aluminum foil. The polymer solution was supplied in a 12 ml syringe attached to a needle (21G, inner diameter = 510 μm) mounted on an adaptor. The needle kept on oscillating sideways during electrospinning, controlled by LabView software (National Instrument). After electrospinning, the as-spun membranes were peeled off from the aluminum foil, transferred onto a baking paper, and kept in a dry oven (OTWMHD24, LABEC) at 50 °C for 1 day for removal of the residual solvents.

7.2.5 Evaluation of the BN-PH nanofiber membrane by AGMD

The commercial PVDF, and neat PH and BN-PH electrospun nanofiber membranes were operated in a home-made AGMD set-up with a feed channel dimension of 60 × 35 × 1 mm (L × W × H), an effective membrane area of 21 cm^2 and an air gap thickness of 3 mm. The coolant plate was made of a stainless steel to condense the water vapor. The AGMD in a co-current flow set-up was carried out with constant inlet temperatures at the feed and the coolant sides of 60 ± 1.5 °C and 20 ± 1.5 °C, respectively. The feed solution was 3.5 wt% NaCl solution (conductivity of 62.0 ± 0.5 mS/cm) and the coolant fluid was tap water. The feed and coolant circulation rates were both maintained at 12 L/h. The concentration of the feed and permeate water was constantly measured with electrical conductivity meters (HQ40d, Hach) throughout the tests.

7.2.6 Characterization and measurements

The morphologies of the PVDF-*co*-HFP (PH), OH-BNNP, and BN-PH were investigated by field-emission scanning electron microscopy (FE-SEM) (Hitachi S4800). TEM (FEI Tecnai F30) analyses were also carried out. The surface functional groups were measured by Fourier transform infrared (FT-IR) spectroscopy (Jasco FT/IR-4100 Type-A) and X-ray photoelectron spectroscopy (XPS, Sigma Probe, Al Kα; Thermo Scientific, Hudson, NH, USA). The contact angle measurements of the prepared nanofiber membranes were conducted using a Contact Angle Analyzer (Theta Lite 100) to investigate the surface wetting characteristics of membrane. The measurements were carried out using distilled water at room temperature. The contact angle values were obtained with the average of five measurements to minimized experimental error. The crystallographic structures of the samples were analyzed by X-ray diffraction (XRD, D/MAX-2500 (18kW)) with Cu Kα radiation (λ=1.518 Å). The response to tensile loading was measured using a universal testing machine (Instron 8848 Microtester) with a crosshead speed of 5 mm min^{-1} and gauge distance of 30 mm. The test specimens consisted of strips of uniform width (10 mm) and length (50 mm). The pore size and pore size distribution of the fabricated PH and BN-PH were measured by capillary flow porometry (CFP-1200-AEXL). All samples were firstly applied with N_2 gas to determine the gas permeability. Then the dry samples were wetted by Porefil (a wetting liquid with a low surface tension of 15.9 dynes/cm) and tested under the same condition. Membrane surface roughness was analyzed by atomic force microscopy (AFM) imaging, AFM was carried out under ambient conditions in tapping mode with silicon probes (TT-AFM, AFM workshop) (Woo et al. 2016). Liquid entry pressure (LEP), which is a measurement of the ability of a hydrophobic membrane against pore wetting, was investigated by a homemade LEP set-up. The reservoir was firstly filled with 25 mL distilled water and then a dry membrane sample (effective surface area = 7

cm^2) was tightly secured in the cell. Nitrogen gas was then supplied and pressed through the bottom of the water-filled chamber, raising the pressure step wise and thereby pushing the water up to the membrane sample. The first sign of bubble on the top of the membrane was regarded as the LEP. To reduce the error, triplicate measurements were taken and averaged. The membrane porosity, defined as the volume of pores divided by the total volume of the membrane, was measured via a gravimetric method (Tijing, Woo, et al. 2014). Membrane samples with equal sizes of (2 cm x 2 cm) were wetted by ethanol. After that, samples were immersed in DI water to replace the ethanol within the fabricated PH and NP-PH membrane pores. The dry and wet weight of the samples was measured before and after saturation of DI water respectively.

7.3 Results and discussion

7.3.1 Morphology of the BN nanoparticles and BN-PH nanofiber

The morphology of OH-BNNPs was examined using transmission electron microscopy (TEM). **Fig. 7.1a** shows low-magnification TEM images indicating that OH-BNNPs had structure of thin 2D nanoplatelets. The OH-BNNPs existed as few-layer nanoplatelets and the spacing of the folded edges was observed to be about 0.33 nm, which corresponded to the theoretical layer to layer distance of h-BN as shown in **Fig. 7.1b**. **Fig. 7.1c** is the selected area electron diffraction (SAED) pattern measured along the [0001] zone axis, which exhibited typical 6-fold symmetry of h-BN, suggesting that the hexagonal lattices of the OH-BNNPs were not damaged during the exfoliation processes. The surface morphology of the neat PVDF-co-HFP (referred herein as PH) nanofiber and BN-PH nanofiber was observed by SEM analysis. **Figs. 7.1d** and 7.**1e** exhibit the surface morphology of nano-sized nanofibers with network-like porous

structures. The average fiber diameter of the neat PH and BN-PH membranes was 336.32 nm and 307.58 nm, respectively, which showed that the BNNP dispersed well in the PH solution (**Table 7.1** and **Fig. 7.2**). BNNPs were implanted or wrapped within a PH nanofiber as shown by the SEM image in **Fig. 7.1e**. The microstructure of BN-PH nanofibers was further examined by TEM and the energy dispersive X-ray spectrometry (EDX) mapping analysis. **Fig. 7.1f** shows the typical microstructure of a single BN-PH nanofiber. TEM image and EDS mapping (**Fig. 7.1f**) reveal that BNNP are dispersed well in/on the PH nanofibers.

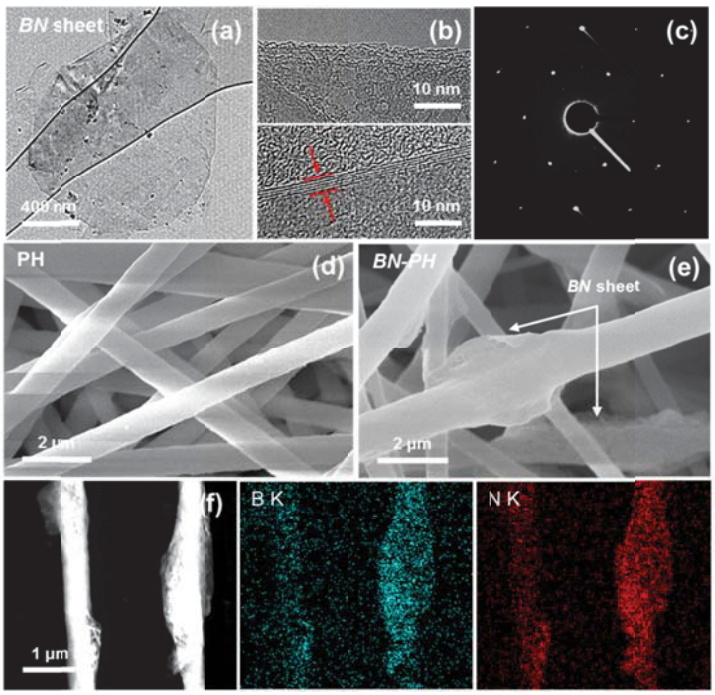

Figure 7.1. (a) Low-magnification TEM image of OH-BNNPs, (b) layer to layer distance of OH-BNNPs, (c) selected-area diffraction (SAED) patterns, (d, e) surface SEM images of the as-spun neat PH and the BN-PH electrospun nanofiber membranes, respectively and (f) the corresponding EDX elemental distribution of B and K in the BN-PH nanofiber samples.

Table 7.1. Characteristics of the neat PH and BN-PH electrospun nanofiber membranes used in the present study

Sample	Thickness [μm]	Fiber size (μm)	Minimum pore size (μm)	Mean pore size (μm)	Maximum pore size (μm)	Contact angle (deg)	LEP (kPa)	Porosity (%)
As spun neat PH	130 ± 2.4	336.32 ± 69.63	0.40	0.72	1.18	142.3 ± 2.1	140.42 ± 2.13	88.2 ± 0.3
BN-PH	130 ± 1.9	307.58 ± 73.97	0.41	0.72	1.21	153.2 ± 1.6	214.18 ± 1.57	84.7 ± 0.1

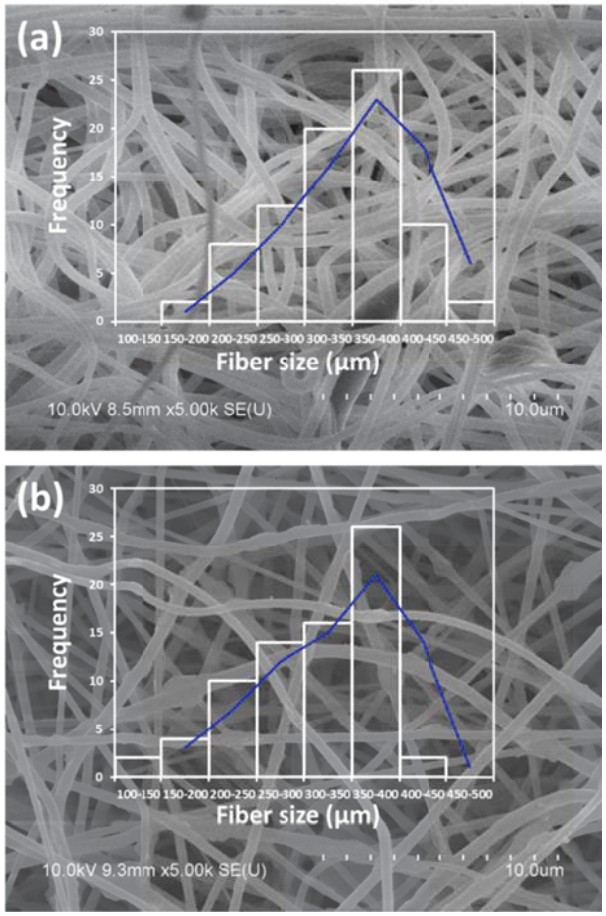

Figure 7.2. SEM images of (a) the neat PH and (b) the BN-PH electrospun nanofiber membranes and corresponding fiber size distributions.

The porosity, mean pore size and pore size distribution of the neat PH and BN-PH membranes are shown in **Table 7.1** and **Fig. 7.3**. The porosity and mean pore size of the BN-PH nanofiber membrane did not change significantly compared to the neat PH membrane. The BN-PH membrane also had a similar pore size of 0.72 µm as the neat PH membrane showed similar porosity. In general, high membrane porosity has lower mass transfer resistance and hence can lead to higher water vapor flux performance in the MD process. Additionally, the pore size distribution data in **Fig. 7.3** indicates that the highest average pore size distribution of the BN-PH membrane was below 0.7 µm due to its smaller fiber size compared to the neat PH membrane. This shows that the BN-PH membrane can have less wetting issues compared to the neat PH membrane. Both the neat PH and BN-PH electrospun nanofiber membranes presented higher porosity and mean pore size compared to the commercial PVDF membrane (70.3% and 0.22 µm, respectively). It is expected that, membranes with higher porosity and larger pore size could lead to higher MD water vapor flux due to reduced mass transfer resistance and also reduction in conductive heat loss through the membrane.

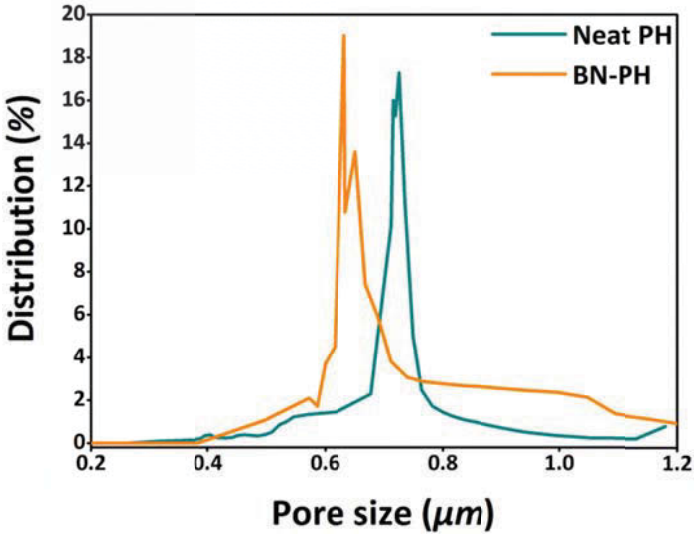

Figure 7.3. Pore size distribution of the neat PH and BN-PH electrospun nanofiber membranes. The mean pore sizes of the neat PH and BN-PH are both 0.72 µm.

The surface contact angles of the neat PH and BN-PH nanofiber membrane were measured using sessile drop observation method. As shown in **Table 7.1**, the surface contact angles of the BN-PH nanofiber membrane was 153.2° higher than the neat PH nanofiber membrane with 142.3°. This improved hydrophobicity of the BN-PH membrane can be ascribed to the hydrophobic nature of the OH-BNNP material. The other potential contribution to enhanced hydrophobicity of the BN-PH membrane may also be partly aided by the enhanced surface roughness. It is believed that multiple beads of the BNNPs are formed on/in the nanofiber, which increases the roughness of the BN-PH membrane compared to the neat PH membrane (Lalia, Guillen-Burrieza, et al. 2013). This increased surface roughness of the BN-PH membranes was confirmed by atomic force microscopy (AFM) as shown in **Fig. 7.4.** The mean roughness (R_a) of the BN-PH membrane (515 nm) was much higher than the neat PH membrane (353 nm) due to the presence of incorporated BNNPs in/on the nanofiber.

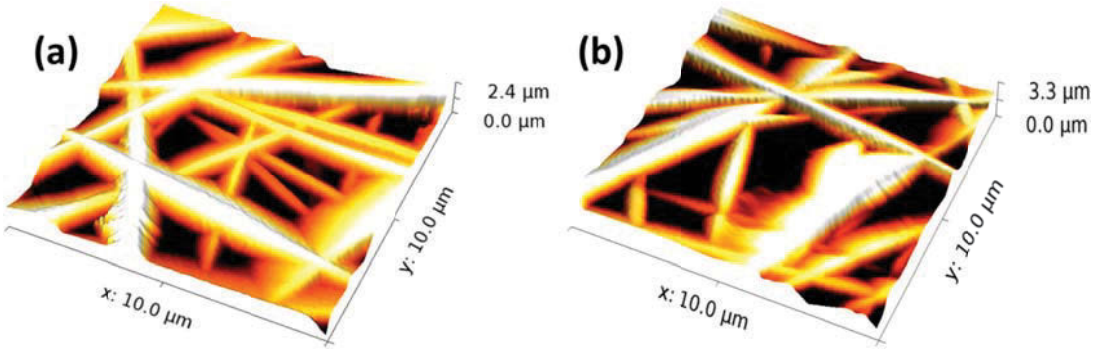

Figure 7.4. Atomic force microscopy (AFM) images of (a) the neat PH and (b) the BN-PH electrospun nanofiber membranes. The mean roughness (R_a) of the neat PH and BN-PH membranes was 353.0 ± 14 nm and 515 ± 21 nm, respectively. The maximum

vertical distance between the highest data points (R_{max}) of the neat PH and BN-PH membranes was 2233.5 ± 208.5 nm and 4170.5 ± 236.5 nm, respectively.

The long-term stability of MD membrane is one of the critical aspects of performance for application, determined indirectly by the liquid entry pressure (LEP) of the membrane which is affected by the membrane hydrophobicity and maximum pore size. LEP higher than 150 kPa is usually desirable for MD membranes to reduce the wetting problem (Ahmed, Lalia & Hashaikeh 2015). The LEP of the BN-PH membrane (214.2 kPa) was higher than that of the neat PH membrane which was only 140.4 kPa (**Table 7.1**) indicating that the wetting problem is less likely for the BN-PH membrane during the long term MD operation. This higher LEP was attributed to the improved membrane hydrophobicity ascribed to the incorporation of BNNPs. It is important to note that, the LEP of the BN-PH nanofiber membrane is the highest among those reported nanofiber membranes in literature so far (Boo, Lee & Elimelech 2016; Lalia, Guillen-Burrieza, et al. 2013; Lee et al. 2017; Lee, An, et al. 2016; Lee, Boo, et al. 2016; Liao et al. 2014; Liao, Wang & Fane 2013; Liao, Wang & Fane 2014; Liao et al. 2013; Tijing, Woo, et al. 2014).

7.3.2 Chemical analysis

In order to confirm the existence of the BNNP in the nanofiber, Raman, XRD, FT-IR and XPS analyses were carried out. **Fig. 7.5a** shows typical Raman spectra taken from the samples of BNNP and BN-PH nanofiber. The dominant peak near 1365 cm^{-1} which shows up intensely in both the BNNP and BN-PH samples is attributed to the B-N vibrational mode (E2g) within h-BN layers (Song et al. 2010). In the XRD spectra (**Fig. 7.5b**), the (002) plane peak of BN (26.7°) was preserved on the samples after

electrospinning process. The XPS spectra of the BNNP and BN-PH nanofiber for the B and N edges are presented in **Figs. 7.5c** and **d**. In the XPS spectra, the peak at 190.0 eV is attributed to B 1s in the OH-BNNPs, and the peak at 397.6 eV to N 1s from the OH-BNNPs, resembling the peaks in h-BN bulk phase (Park et al. 1997). **Fig. 7.5e** shows FT-IR spectra of the BN-PH together with that of the OH-BNNPs. OH-BNNP samples exhibited strong absorption at 1348 cm^{-1}, which was attributed to B−N stretching (in-plane ring vibration, the E1u mode) and at 782 cm^{-1}, which is attributed to B−N bending (out-of-plane vibration, A2u mode); these spectra are consistent with previously reported ones (Lee et al. 2015; Shi et al. 2010). However in the BN-PH sample these two peaks shift to higher frequency compared with that in the OH-BNNP. We speculate that the FTIR peaks shift to higher frequency due to interaction between BNNP and PH (but unclear). From the Raman spectroscopy, XRD, XPS, and FTIR results it could be concluded that the BNNP was successfully incorporated within the PH nanofiber.

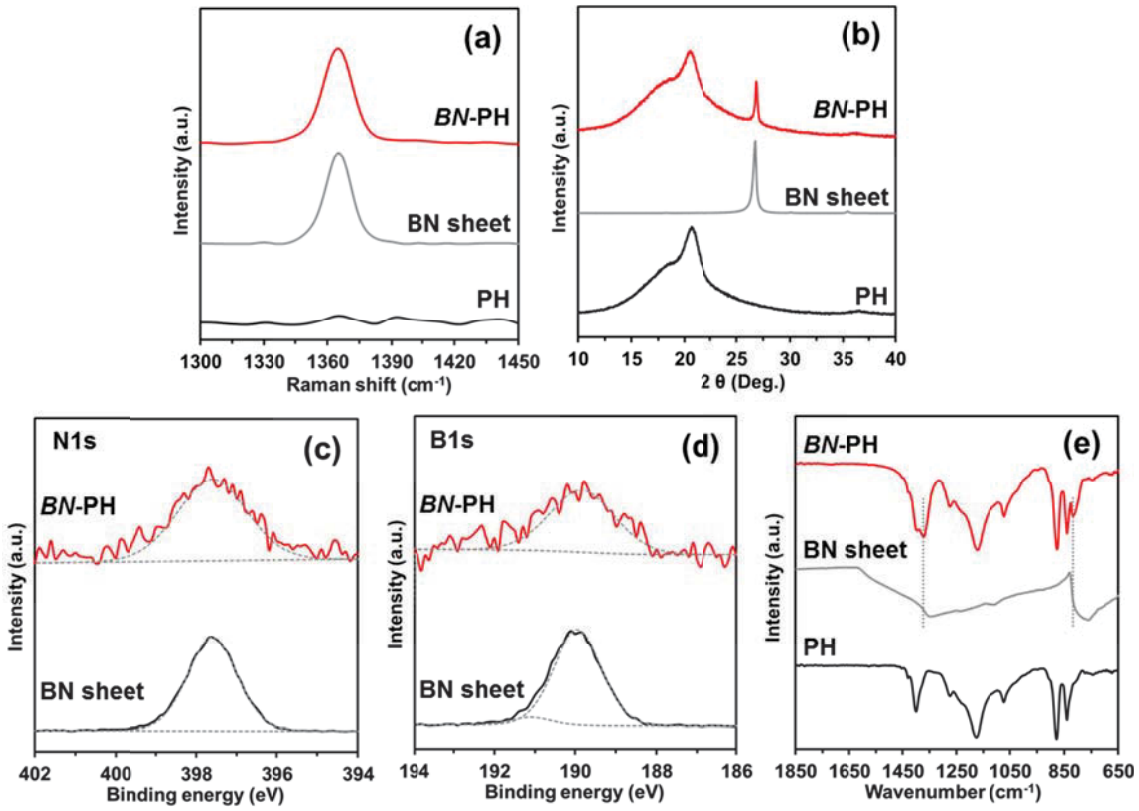

Figure 7.5. (a) Raman spectroscopy, (b) XRD patterns of the OH-BNNPs, neat PH and BN-PH electrospun nanofibers, (c, d) N1s and B1s narrow XPS scan of the OH-BNNPs and BN-PH electrospun nanofiber and (e) FT-IR of the OH-BNNPs, neat PH and BN-PH electrospun nanofibers.

7.3.3 Mechanical properties

The mechanical properties of the nanofiber membranes were measured by universal testing machine. The results in **Fig. 7.6** show that the incorporation of the BNNPs in/on PH nanofiber has resulted in enhanced mechanical properties. Representative stress-strain curves for the neat PH and BN-PH nanofiber are plotted in **Fig. 7.6a**. For the neat PH, the ultimate tensile strength (UTS) and tensile modulus are 6.81 MPa and 16.8 MPa, respectively. The addition of the OH-BNNP enhanced the UTS and the modulus of the BN-PH membrane to 7.72 MPa and 17.0 MPa, an effective increase of 13.4% and 1.2%,

respectively, compared to the neat membrane (**Fig. 7.6b**). This slightly enhanced mechanical strength is presumably caused due to hydrogen bond and physical bond interaction between the OH-BNNP and PH nanofiber. The applied mechanical load might have been effectively transferred to OH-BNNP through the interfacial interactions (Lee et al. 2013).

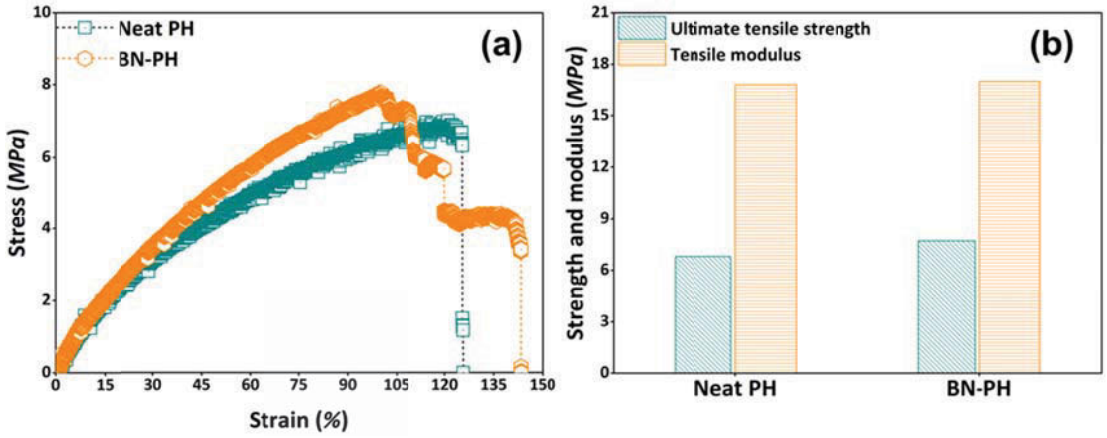

Figure 7.6. (a) Stress-strain curves and (b) ultimate tensile strength and tensile modulus of the neat PH and BN-PH electrospun nanofiber membranes

7.3.4 Long-term AGMD performances

The long-term performance of the BN-PH membrane was tested and compared with the neat PH and commercial PVDF membranes through the operation of AGMD for 280 h and the results are shown in **Fig. 7.7**. The initial water vapor flux of the neat PH membrane was 11.42 $L \cdot m^{-2}h^{-1}$ (LMH), however, it suffered wetting problem in less than 4 h of AGMD operation, as indicated by a rapid flux and permeate conductivity increase (**Fig. 7.7(a)**). The initial water vapor flux of the commercial PVDF membrane was 6.13 LMH which gradually declined reaching a stable flux of 4.53 LMH after about 28 h (**Fig. 7.7(b)**). The membrane wetting was evident after 212 h of operation for

commercial PVDF membrane. On the other hand however, the BN-PH membrane showed a stable water vapor flux performance of 18 LMH even when operated up to 280 h (**Fig. 7.7(c)**). The flux performance of the BN-PH membrane was approximately four times higher than that of the commercial PVDF membrane maintaining a high salt rejection at 99.99%. This greatly improved flux performance for the BN-PH membrane could be explained by its unique morphologies and properties. Additionally, thermal conductivity of BN-PH membrane showed 0.009 W/mK, which was lower than that of the neat PH membrane (0.025 W/mK). The low thermal conductivity led to improved water vapor flux performance (Tijing, Choi, et al. 2014). It was observed earlier that the pore size and porosity of the BN-PH or PH membrane were slightly larger than the commercial PVDF membrane responsible for higher water vapor flux than the commercial PVDF membrane. In general, the ideal pore size for MD membrane should be less than 0.6 μm to avoid pore wetting problems and point is supported by the fact that the neat PH membrane suffered severe wetting issues (Alkhudhiri, Darwish & Hilal 2012).

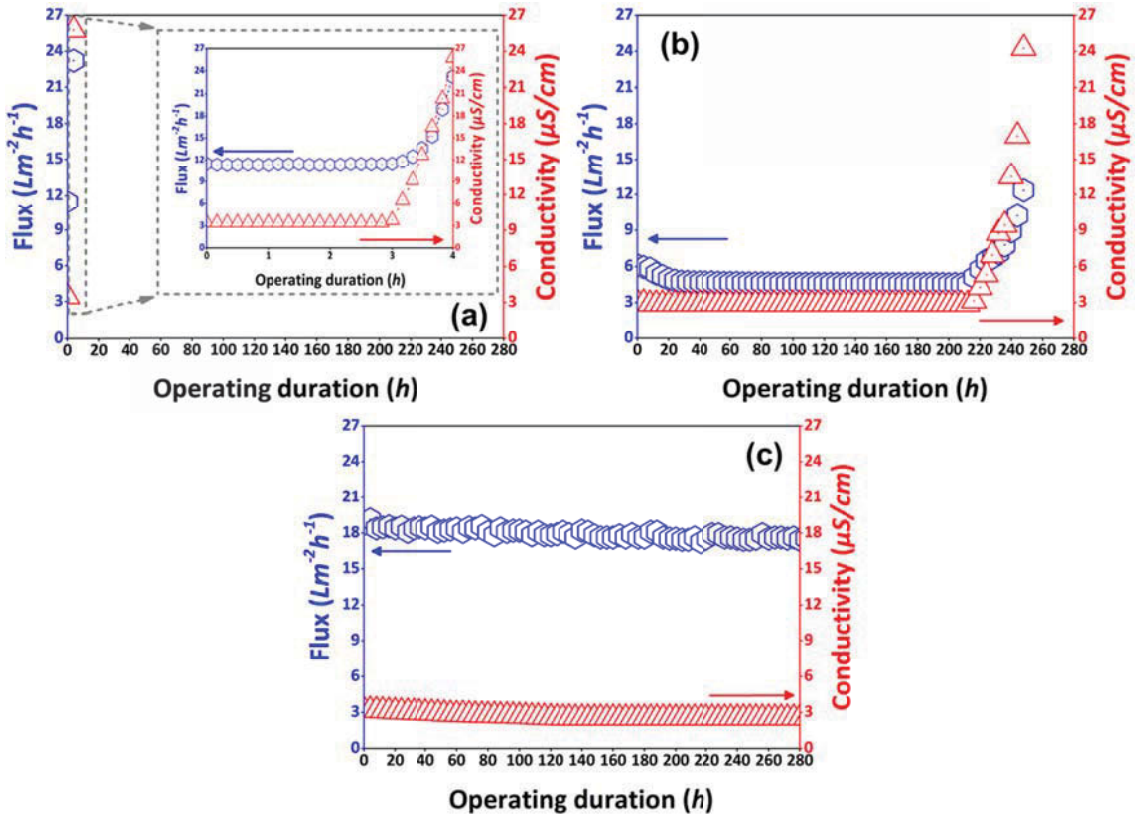

Figure 7.7. Water vapor flux and conductivity performances of (a) the neat PH electrospun nanofiber, (b) the commercial PVDF and (c) the BN-PH nanofiber membranes with feed solution containing 3.5 wt% NaCl in the AGMD tests. The feed and coolant temperatures were 60°C and 20°C, respectively. The flow rates of all AGMD tests were both maintained at 12 L/h in the feed and coolant stream. The initial water vapor flux of the neat PH, commercial PVDF and BN-PH membranes were 11.42 LMH, 6.13 LMH and 18.76 LMH, respectively.

However, in other studies, it was also noted that superhydrophobic membranes shows lower wetting issues even at pore sizes larger than 0.6 μm (Liao et al. 2014; Liao, Wang & Fane 2014). This is evident in this study where the BN-PH membrane with pore size larger than 0.6 μm showed no wetting problem during AGMD operation. Besides, the contact angle and LEP of the BN-PH membrane were much higher than 153.2° and

214.2 kPa, respectively. The LEP of the BN-PH was even slightly higher than the commercial PVDF membrane (213.3 kPa) (Woo et al. 2016).

In conclusion, the incorporation of BN into electrospun nanofiber membrane significantly improved its LEP and hydrophobicity thereby reducing the wetting problem while maintaining higher pore size and porosity of the electrospun membrane contributing to higher flux performance. Future interest in this study may be to find a mechanism for the improved water vapor flux performance of the BNNPs enabled electrospun nanofiber MD membrane.

7.4 Concluding remarks

In this chapter, boron nitride nanoparticle (BNNP) was incorporated in the poly(vinylidene fluoride-co-hexafluoropropylene) (PH) nanofiber fabricated by simple electrospinning technique. The hexagonal lattices of the OH-BNNPs were successfully modified by hydroxide-assisted ball milling without damage during the exfoliation processes. The OH-BNNPs have been dispersed in/on the nanofiber as confirmed by TEM, XPS, EDX mapping, FT-IR, XRD and Raman spectroscopy. The BN-PH nanofiber membrane showed higher high hydrophobicity, higher liquid entry pressure (LEP) and improved thermal and mechanical properties compared to the neat PH membrane. During the air gap membrane distillation (AGMD) process, BN-PH membrane exhibited significantly higher and also stable water vapor flux and, salt rejection performances when operated up to 280 h. This study clearly shows that, incorporation of the BNNPs in the electrospun PH nanofiber membrane could significantly improve the membrane properties suitable for long-term AGMD process. Therefore, this chapter suggests that the BNNPs embedded PH nanofiber is a good

potential candidate as a robust MD membrane for the treatment of seawater for the long-term AGMD application.

CHAPTER 8

University of Technology Sydney
FACULTY OF ENGINEERING

CF_4 PLASMA-MODIFIED OMNIPHOBIC ELECTROSPUN NANOFIBER MEMBRANE FOR TREATMENT OF RO BRINE FROM COAL SEAM GAS PRODUCED WATER

8.1 Introduction

The presence of some low surface tension components such as oil and surfactants that are usually present in challenging water sources (e.g., coal seam gas produced water) can cause membrane wetting and/or fouling issues which can pollute the permeate water. The membrane characteristics therefore play a very important role in the separation efficiency of the MD process (Lin et al. 2014). However, the currently used membranes for research and pilot-scale studies are usually made of polyvinylidene fluoride (PVDF), polypropylene (PP) or polytetrafluoroethylene (PTFE) hydrophobic microfiltration membranes which suffer from low flux and wetting problems as they are not specifically designed for MD operation (Zuo & Wang 2013). Therefore, given the high prospects of MD process for different applications including those for gas and industrial wastewater treatment, there is a need to develop MD membranes with adequate flux without wetting issues for the long-term operation. Membranes with omniphobic properties that provide anti-wetting capability for both water and low surface tension components are particularly attractive for treatment of challenging waters including RO brine from coal seam gas (CSG) produced water.

Recently, increasing number of research has been focused on the development of new MD membranes. The design and fabrication of new hollow fiber and flat-sheet MD membranes using spinning, stretching and phase inversion technique have been recently reported (Nejati et al. 2015; Wang & Chung 2013; Woo et al. 2016). Other studies focused on modifying commercial and lab-fabricated membranes to improve their anti-wetting and other membrane properties. Though many of these studies indicated improvement of flux and salt rejection, most of them mainly tested their membranes on relatively “clean” water or at seawater quality, while a few considered higher salt

concentrations without the presence of organics and low surface tension contaminants like oil and surfactants. CSG, also known as coal bed methane (CBM), is a natural gas located in the coal seams underground (300 ~ 1,000 m) (Nghiem et al. 2015; Woo et al. 2016). The CSG exploration involves the treatment and management of huge volume of produced water most of which are highly saline. In many cases, this CSG produced water is treated by RO process before reuse or environmental discharge. The RO brine from CSG produced water usually contains varying amounts of low surface tension contaminants, which need to be removed from the RO brine. MD membranes possessing high hydrophobicity, adequate pore size, narrow pore size distribution and high liquid entry pressure (Woo et al. 2016) are ideal for treating any saline water. However, for highly challenging water such as CSG produced water containing low surface tension contaminants, MD membrane with omniphobic properties are more suitable. Therefore, different groups have tried various approaches for developing new MD membranes (Boo, Lee & Elimelech 2016; Lee, Boo, et al. 2016; Lin et al. 2014).

In recent years, membranes fabricated by electrospinning have gained attention as a promising membrane for MD application (Tijing, Woo, et al. 2014). Among the many applications, electrospun membranes have recently been utilized as a potential stand-alone or as a support-membrane material for desalination, water and wastewater treatment processes. Reports in literature signify the potential of nanofiber membranes for MD application.

Providing omniphobicity to the electrospun nanofiber membrane is an attractive strategy to exploit its highly porous and multi-layered structure with relatively rough surface. Among the many surface modification methods, plasma treatment is a scalable approach to provide resistant coatings on the membrane surface (Park et al. 2016; Yang et al.

2014b). In particular, tetrafluoromethane (CF_4) plasma modification enables etching, replacement or polymer modification of the membrane, enhancing its anti-wetting properties. Several previous studies noted that CF_4 plasma was able to make fluorinated polymer surfaces exhibiting desirable properties of low surface free energy and low coefficient of friction, hence improving surface wettability (Cuddy & Fisher 2012; Hopkins & Badyal 1996; Riekerink et al. 1999; Wei et al. 2012; Yan, Chan-Park & Yue 2005; Yang et al. 2014b; Yoon et al. 2009). Wei et al (Wei et al. 2012) reported that fluorination and deposition layer formation on the membrane surface were the main reasons for the wettability change of the membrane surface. Recently, few research groups reported CF_4 plasma modification of phase inversion (Tian, Yin, et al. 2015) and commercial (Wei et al. 2012; Yang et al. 2014b; Yang et al. 2015) membranes and detailed their improved membrane characteristics and desalination performance via direct contact MD (DCMD) process. However, no study has been reported on the potential of CF_4 plasma modified nanofiber membranes. The overlapping nanofiber structure already provides relatively rough surface that gives increased hydrophobicity to the membrane. When this membrane is further exposed to CF_4 plasma treatment, the fluorination and modifying the surface into having much lower surface energy further improves the anti-wetting properties of the membrane probably by making the membrane omniphobic. This could be interesting and worth investigating for its application to challenging waters containing organic contaminants. In this study, we investigated the modification of the nanofiber membranes by CF_4 plasma treatment to improve its hydrophobic and omniphobic properties, and evaluated their performance via air gap MD (AGMD). The morphology, wetting properties for water and low surface tension liquids, and AGMD performance using real RO brine from CSG

produced water with the addition of surfactant as feed of the neat and plasma modified nanofiber membranes were evaluated and compared.

This chapter is an extension of the research article published by the author in Journal of Membrane Science.

8.2 Materials and methods

8.2.1 Dope preparation and electrospinning conditions

Homogenous PVDF solution with a concentration of 15 wt% was prepared by overnight stirring in a mixed solvent composed of DMF and acetone (4:1 by wt%). A small amount of LiCl (0.004 wt%) was added to the PVDF solution to improve its electrospinnability. Details of the electrospinning system are reported in Chapter 3. PVDF solution placed in a syringe was pushed at a flow rate of 1.5 ml/h. Continuous flow of nanofibers was obtained at an applied voltage of 18 kV and a tip-to-collector distance (TCD) of 15 cm. The nanofibers were directly collected on a grounded rotating drum collector covered with aluminum foil. The chamber humidity and temperature were maintained at 40-45% and 20-25^{o}C, respectively for all tests. After electrospinning, the fabricated electrospun nanofiber membranes (ENMs) were dried in an oven at 60°C for 2 days to remove the residual solvents.

8.2.2 CF_4 plasma modification

For plasma treatment, an IoN 40 plasma system (PVA TePla Co.Ltd.) equipped with parallel plate electrodes coupled with a radio frequency (RF) glow discharge system was utilized (Tian, Yin, et al. 2015). The electrospun membranes were first placed on

the plates, then, CF_4 gas was introduced to the chamber at a flow rate of 250 standard cubic centimeter per minute (SCCM) (Yang et al. 2014b).

8.2.3 Air gap membrane distillation performance test

The AGMD was operated in a co-current flow set-up with constant inlet temperatures of 60 ± 1.5°C and 20 ± 1.5°C at the feed and the coolant sides, respectively. The feed solution was RO brine from CSG produced water (from Gloucester Basin located along the lower north coast of New South Wales, Australia) with electrical conductivity and dissolved solid concentration of around 22.6 mS/cm and 15,354 mg/L, respectively with tap water as the coolant fluid (Woo et al. 2016). Key characteristics of the CSG RO brine are shown in **Table 8.1**.

To check the performance of CF_4 plasma-modified PVDF electrospun membranes in separating salt and low surface tension components from the feed solution, SDS was continuously added every 2 h to the CSG RO brine feed from 0.1 mM up until 0.7 mM for a total test duration of 10 h and the same AGMD test was repeated as above.

Table 8.1. Characteristics of RO brine from CSG produced water

Parameter	RO brine from CSG produced water	Parameter	RO brine from CSG produced water
pH	9.07 ± 0.00	Sulfate (mg/L SO_4^{2-})	23.72 ± 2.46
Conductivity (mS/cm)	22.58 ± 0.01	Chloride / Sulfate ratio	204.26 ± 21.70
Total dissolved salts (TDS, mg/L)	15,354.40 ± 9.62	Total coliforms (cfu/100 ml)	480.00 ± 84.85
Turbidity	0.86 ± 0.12	Ecoli faecal bacteria (cfu/100 ml)	8.00 ± 4.24
Alkalinity (mg/L $CaCO_3$ equivalent)	6,466.67 ± 47.14	Aluminum (mg/L)	<0.001
Water hardness (mg/L $CaCO_3$ equivalent)	151.12 ± 0.99	Arsenic (mg/L)	<0.003
Orthophosphate (mg/L P)	5.21 ± 0.14	Cadmium (mg/L)	<0.001
Nitrate (mg/L N)	<0.005	Chromium (mg/L)	<0.002
Ammonia (mg/L N)	0.04 ± 0.01	Copper (mg/L)	0.09 ± 0.01
Sodium (mg/L)	6,088.67 ± 39.36	Iron (mg/L)	0.02 ± 0.01
Potassium (mg/L)	28.50 ± 0.16	Manganese (mg/L)	0.03 ± 0.00
Calcium (mg/L)	36.33 ± 0.57	Nickel (mg/L)	<0.004
Magnesium (mg/L)	14.67 ± 0.26	Lead (mg/L)	<0.001
Sodium Absorption Ratio (SAR)	215.29 ± 1.07	Zinc (mg/L)	0.01 ± 0.00
Chloride (mg/L)	4,792.67 ± 71.00	Silicon (mg/L)	23.5 ± 0.73

8.2.4 Contact angle (CA), sliding angle (SA) and surface free energy (SFE)

In order to compare the wetting and omniphobic properties of neat and modified ENMs, surface contact angle (CA) was measured. The CA of the membranes was measured by using the sessile drop method with an optical subsystem (Theta Lite 100) integrated with image-processing software. Membrane samples were placed on a flat platform, and

5 µL droplets of water, methanol, diiodomethane, mineral oil, or ethylene glycol were carefully dropped on the membrane surface. A real-time camera captured the image and video of the droplet on the sample and the CA was calculated with the aid of software. At least 5 measurements were taken for each membrane sample and the average value is reported here. The wettability of a membrane surface can be expressed in terms of the contact angle (θ), which is governed by Young's equation (Zuo & Wang 2013) as follows:

$$\gamma_m = \gamma_{ml} + \gamma_l \cos\theta \qquad \textbf{(eq.8.1)}$$

where, γ_m, γ_{ml}, and γ_l represents the surface tensions of membrane in contact with air, membrane in contact with liquid, and liquid in contact with air, respectively.

Water sliding angle (SA) was measured using a tilting method as reported in other studies (Artus et al. 2006; Furstner & Barthlott 2005; Pierce, Carmona & Amirfazli 2008). SA shows the difference between advancing and receding CA, i.e., hysteresis (Artus et al. 2006; Jin et al. 2005). A 10 µL water droplet was first placed on neat and modified membranes and the water droplet was then gradually tilted until the water droplet started to slide on the membrane surface, and that tilting angle was recorded as SA (Valk et al. 1983).

The surface free energy (SFE) of the membrane surface can be obtained via the contact angle measurements employing the Lifshitz van der Walls (non-polar, γ_m^{LW}) and Lewis acid-base (polar, γ_m^{AB}) approaches using three different liquids (two polar and one non-polar) of well-known surface tension (Zhao, Chen, et al. 2013). The total SFE of a membrane can be written as follow (van Oss 2007):

$$\gamma_m^T = \gamma_m^{LW} + \gamma_m^{AB} \qquad \textbf{(eq.8.2)}$$

$$\gamma_m^{AB} = 2\sqrt{\gamma_m^+ \gamma_m^-} \qquad \textbf{(eq.8.3)}$$

where, γ_m^T, γ_m^{LW}, γ_m^{AB}, γ_m^+, and γ_m^- represent the total SFE of the membrane, the Lifshitz van der Walls interactions of the membrane (dispersive component), the acid-base interactions of the membrane (polar component), the electron acceptor parameter and the electron donor parameter, respectively (Nishino et al. 1999).

For SFE calculations, various liquids with different surface tensions were used, such as methanol (γ= 22.70 mN/m), diiodomethane (γ = 50.80 mN/m), ethylene glycol (γ = 47.70 mN/m) and water (γ = 72.80 mN/m) (Zuo & Wang 2013).

8.3 Results and discussion

8.3.1 Morphologies and characteristics of the fabricated membranes

The morphologies as observed by SEM and the membrane characteristics of the fabricated and CF_4 plasma modified ENMs are shown in **Figure 8.1** and **Table 8.2**, respectively. It can be seen from **Figure 8.1** that the neat PVDF and the modified membranes did not show significant differences in terms of surface structure and morphology indicating that CF_4 plasma modification did not significantly alter the membrane characteristics compared to the neat PVDF membrane. The neat electrospun PVDF membranes showed nanofibers with diameter of 296.36 ± 76.14 nm, while the modified membranes have similar fiber diameter in the range of 290 – 299 nm. All fabricated nanofiber membranes exhibited a porosity of around 86% and mean pore size of 0.81 μm regardless of different plasma treatment conditions. Though no drastic changes in morphologies and physical properties were observed, it is anticipated that the chemical structure of the nanofibers might change through plasma modification as discussed below (Yang et al. 2014b).

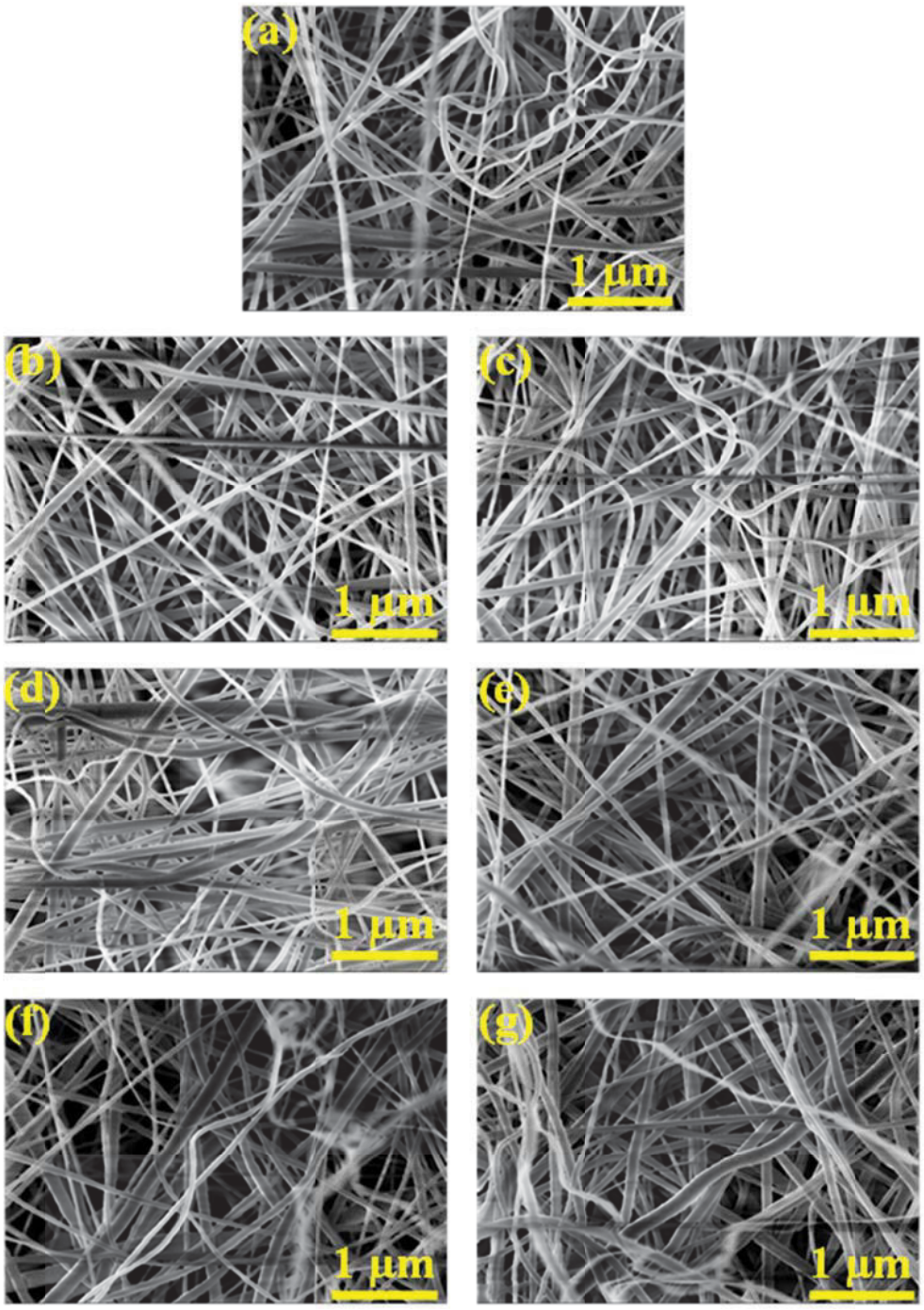

Figure 8.1. Surface SEM images of the neat and CF_4 modified electrospun nanofiber membranes: (a) Neat, (b) P/CF-5, (c) P/CF-10, (d) P/CF-15, (e) P/CF-20, (f) P/CF-30 and (g) P/CF-60

Table 8.2. Membrane codes and characteristics of the neat and CF_4 modified electrospun nanofiber membrane

CF_4 treatment duration (min)	Membrane code	Thickness (μm)	Porosity (%)	Mean pore size (μm)	Maximum pore size (μm)	Fiber diameter (nm)
0	Neat	150.0 ± 1.6	86.4 ± 1.2	0.82 ± 0.02	1.03 ± 0.03	296.36 ± 76.14
5	P/CF-5	150.0 ± 1.2	86.3 ± 0.9	0.82 ± 0.01	1.02 ± 0.02	290.48 ± 85.61
10	P/CF-10	150.0 ± 1.4	86.5 ± 1.0	0.81 ± 0.03	1.04 ± 0.01	291.26 ± 62.53
15	P/CF-15	150.0 ± 0.6	86.4 ± 1.3	0.80 ± 0.02	1.02 ± 0.02	297.69 ± 48.41
20	P/CF-20	150.0 ± 1.1	86.5 ± 0.4	0.82 ± 0.02	1.01 ± 0.02	293.35 ± 90.66
30	P/CF-30	150.0 ± 1.2	86.3 ± 0.7	0.80 ± 0.01	1.01 ± 0.01	298.80 ± 79.84
60	P/CF-60	150.0 ± 0.9	86.4 ± 0.6	0.82 ± 0.02	1.03 ± 0.03	295.15 ± 72.33

8.3.2 Plasma polymerization and deposition

The surface chemical compositions of the neat and CF_4 plasma modified ENMs were examined by XPS measurements. XPS survey scans revealed that C and F are the major components on the surface of the neat and CF_4 modified ENMs (**Table 8.3** and **Fig. 8.2(a, c, e)**). The C atomic concentration of the neat, P/CF-15 and P/CF-60 ENMs was 48.5 %, 37.63 %, and 33.52 %, respectively. It is obvious that the C atomic concentration decreased with the increase in the treatment duration of CF_4 plasma modification, while the F atomic concentration increased (**Table 8.3**). The F/C ratio increased from 1.04 for the neat to 1.94 for the P/CF-60 (see **Table 8.3**) indicating that CF_4 plasma modification has brought a fluorinated layer onto the membrane surface, which is reported to change in the wettability of the membrane surface (Wei et al. 2012). This indicates that CF_4 plasma modification affects the membrane surface by etching and insertion of F atom on the membrane surface thereby improving its surface

hydrophobicity. As the CF_4 plasma was applied to the membrane in the gaseous form, it is possible that the gas might penetrate inside the membrane pores thereby enabling the modification to occur even within the inner porous surfaces of the membrane (Wei et al. 2012). This is expected to results in a more uniform surface modification across the depth of the electrospun membrane especially with the increase in the duration of plasma treatment.

As shown in **Fig. 8.2(b)**, the neat ENM surface showed carbon atoms in the form of C-C/C=C (284.33 eV), C-H (286.68 eV), C=O (288.66 eV), and CF_2-CH_2 (289.48 eV) bonds, while those of the modified membranes showed new C atom bond formations: C-F (287.30 eV), CF_2-CF_2 (291.58 eV) and CF_3 (293.87 eV) (**Fig. 8.2(d, f)**) (Hopkins & Badyal 1996; Woodward et al. 2003; Yan, Chan-Park & Yue 2005). Carbon atoms on the surface of the neat ENM was mainly in the form of CF_2-CH_2 status, while those after CF_4 plasma modification were mostly changed to CF_2-CF_2 status, which existed on the membrane as a deposited layer. In addition, a new CF_3 peak appeared after modification, which gives lower surface free energy on the membrane surface compared to -CF_2 and -CH_2, hence, higher hydrophobicity was observed for modified membranes (Alexander et al. 2016). The CF_3 content increased from 0% for neat membrane to 5.31% for the plasma modified membrane treated for 60 min.

Table 8.3. Surface compositions of the neat and CF_4 treated electrospun nanofiber membranes (at. %)

Membrane code	C1s							F1s	O1s	F/C
	C-C/C=C	C-H	C=O	C-F	CF_2-CH_2	CF_2-CF_2	CF_3			
Neat	1.28	23.96	0.78	0	22.48	0	0	50.41	0.66	1.04
P/CF - 15	0.79	6.42	0	2.51	4.86	19.94	3.11	58.57	3.27	1.56
P/CF - 60	0.19	0.35	0	1.21	5.99	20.47	5.31	65.17	1.21	1.94

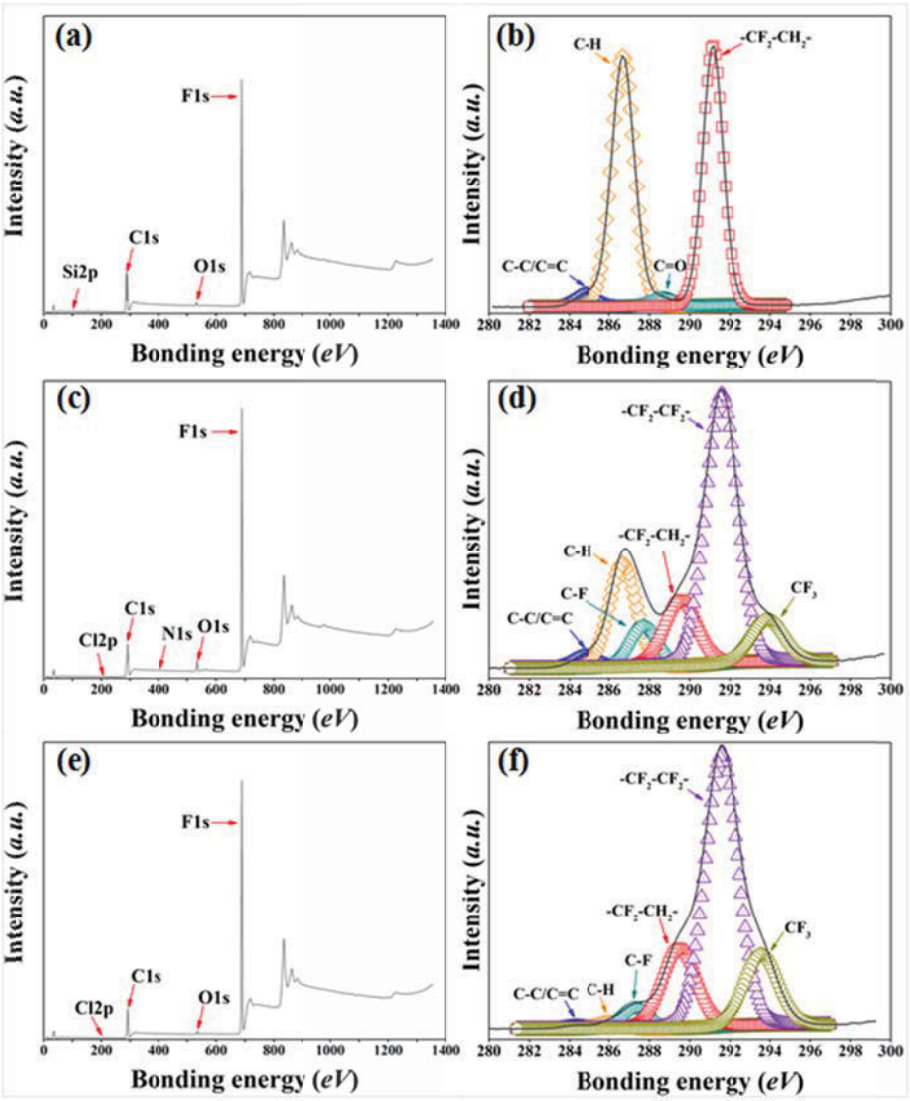

Figure 8.2. (a, c, e) XPS survey scans and (b, d, f) carbon spectra of (a, b) the neat, (c, d) P/CF-15 and (e, f) P/CF-60 electrospun nanofiber membranes

8.3.3 Plasma polymerization and deposition

The contact angle (CA) and sliding angle (SA) of the neat and CF_4 modified ENMs in water were investigated and the results are shown in **Figure 8.3**. The addition of fluorinated layer via CF_4 plasma modification on the ENM led to an increase in hydrophobicity. The CA measured for 600s of the neat ENM was 133.6 ± 1.8 deg, while

those of P/CF-5, P/CF-10, P/CF-15, P/CF-20, P/CF-30 and P/CF-60 were 140.8 ± 2.0, 144.6 ± 5.7, 160.6 ± 4.5, 160.7 ± 3.8, 160.8 ± 2.6, and 160.9 ± 0.9 deg, respectively. CF_4 plasma treatment above 15 min however did not result in further improvement in the CA value (i.e., about 160^o indicating superhydrophobicity), which is primarily attributed to reaching its saturation from plasma modification on the membrane surface (Wei et al. 2012). This means that the whole membrane surface area was already fully covered after 15 min of treatment; hence further increasing the treatment time did not further change the surface energy. As explained previously, the CF_4 plasma treatment produced C atoms in the deposited layer in the form of CF_2 - CF_2 and CF_3 (fluoropolymer) (**Table 8.4**) lowering the surface energy and thereby increasing the contact angle (i.e., hydrophobicity) (Hare, Shafrin & Zisman 1954; Nishino et al. 1999; Wei et al. 2012).

Figure 8.3 also shows the sliding angle of the different membranes. The neat unmodified nanofiber membrane showed a 'petal' surface effect, wherein the water droplet did not roll off the surface even if it was turned upside down. This is the normal surface property of PVDF material including the commercial flat-sheet membrane used in the present study. Similar phenomenon was also observed for CF_4 treatment below 10 min, which indicates the non-homogenous plasma treatment of the membrane surface. However, for membranes treated at longer treatment duration (P/CF-15, P/CF-20, P/CF-30 and P/CF-60), water droplets started rolling off at similar sliding angle of around 51-52^o indicating that the CF_4 plasma treatment enhances a 'lotus' surface effect (Bhushan & Jung 2011; Marmur 2004). This is attributed to the fully saturated CF_4 treatment of the entire membrane surface. Having a lotus-like surface property could provide a self-cleaning effect as the rolling of the drops can carry with them some impurities on the

surface (Bhushan & Jung 2011). Further, the lotus effect can also help in mitigating fouling and wetting problems of the MD membrane. Hence, this additional lotus effect property of the CF_4-treated membrane has the potential for enhancing the long-term MD application with more anti-wetting property and fouling resistance.

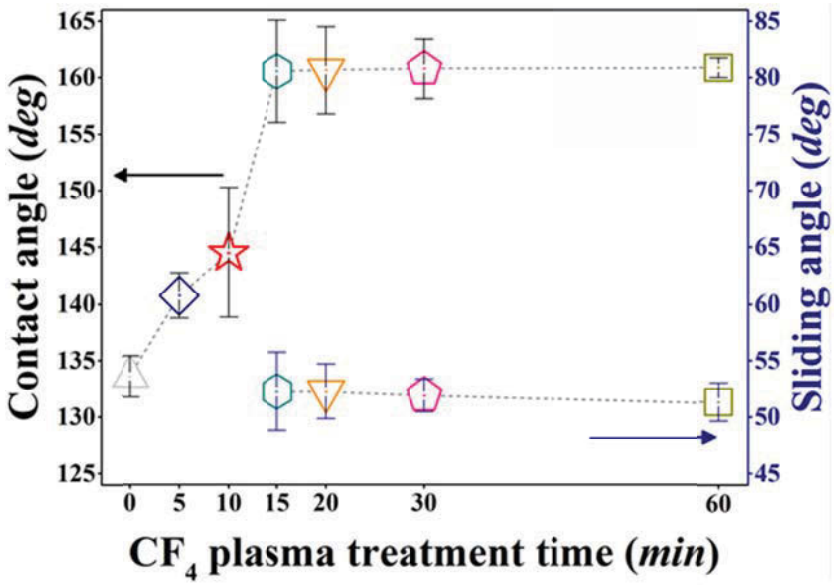

Figure 8.3. Contact and sliding angle measurements of the neat and CF_4 modified electrospun nanofiber membranes at different treatment times

In addition, the CAs of the fabricated membranes were also investigated when exposed to low surface tension liquids such as methanol (γ = 22.70 mN/m), mineral oil ($\gamma \approx$ 30 mN/m), and ethylene glycol (γ = 47.70 mN/m). Though the pristine ENM showed relatively high hydrophobicity due to the innate hydrophobicity of PVDF material, and its overlapping nanofiber structure and high membrane porosity, it was not able to retain all low surface tension liquids and instant wicking was observed (**Figs. 8.4** and **8.5**) which is attributed to the relatively high surface energy of PVDF. Similar observation was made for P/CF-5 membrane. However, CF_4 treatment above 15 min showed high CAs (147-149^o) for ethylene glycol, mineral oil and methanol, and along with their high

CAs in water, this indicates good oleophobic property of the membrane after CF_4-treatment above 15 min duration. The improvement in wetting properties of the modified membrane to both water and low surface tension liquids is mainly attributed to the successful homogenous fluorination of the membrane surface due to CF_4 treatment resulting to low surface energy of the modified membranes (see **Table 8.4** using diiodomethane as low surface tension liquid to calculate surface energy), and the overlapping nanofiber structures leading to rougher surface of the membrane. The CF_4 treated membranes showed decreasing surface energy with the increase in CF_4 treatment time (from SFE = 1.966 mN/m for P/CF-10 to 0.3000 mN/m for P/CF-60). These SFEs were much lower than that of PVDF at 25 mN/m as given in literature (Liu et al. 2011). Clearly, the plasma treatment has helped lower the surface energy of the nanofiber membranes, which gives them wetting resistance to both water and low surface tension liquids.

Table 8.4. Contact angle of diiodomethane and surface free energy (SFE) of the CF_4 modified and neat electrospun nanofiber membranes

Membrane code	Diiodomethane (deg)	γ_m^T (mN/m)	γ_m^{LW} (mN/m)	γ_m^{AB} (mN/m)	γ_m^+ (mN/m)	γ_m^- (mN/m)
Neat	-	25[a,(Valk et al. 1983)]	-	-	-	-
P/CF-5	127.4 ± 1.4	-	-	-	-	-
P/CF-10	131.4 ± 0.2	1.966	1.455	0.511	0.179	0.364
P/CF-15	157.2 ± 4.4	0.503	0.076	0.427	0.351	0.13
P/CF-20	157.8 ± 4.9	0.482	0.070	0.412	0.332	0.128
P/CF-30	158.0 ± 0.4	0.454	0.067	0.387	0.337	0.111
P/CF-60	158.1 ± 2.7	0.333	0.066	0.267	0.344	0.052

[a] Surface energy given in literature for PVDF

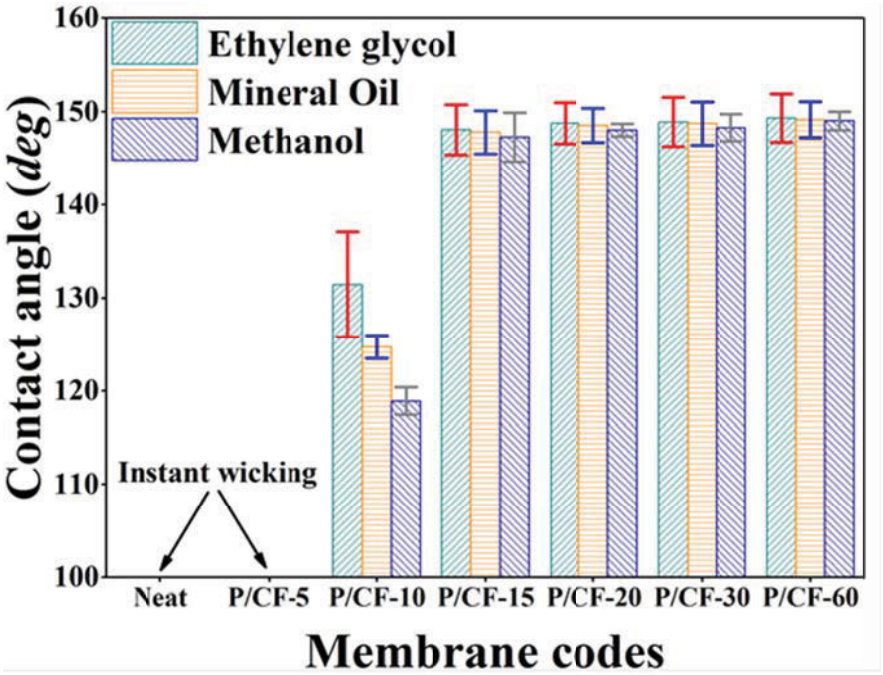

Figure 8.4. Contact angles of the neat and CF_4 modified electrospun nanofiber membranes by ethylene glycol (γ = 47.7 mN/m), mineral oil (γ = 30.0 mN/m) and methanol (γ = 22.7 mN/m)

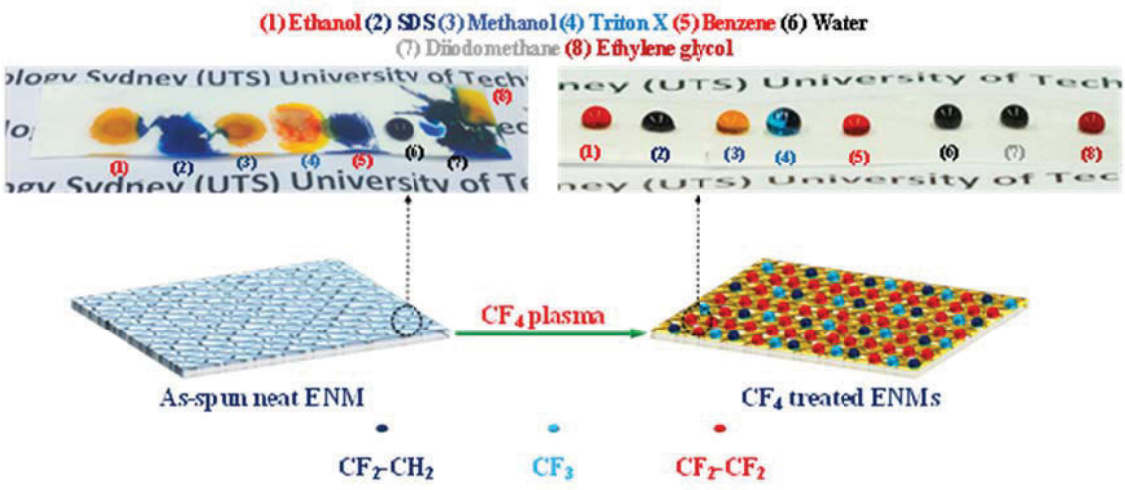

Figure 8.5. Schematic illustrations of the neat and CF_4 plasma modified electrospun nanofiber membranes

The Lifshitz-van der Waals (LW) and Lewis acid-base (AB) parameters of the modified membranes, referring to the non-polar (dispersive) and polar values, respectively, are very low indicating less chance of organic and inorganic foulants adsorbing on the surface. Therefore, by applying the P/CF ENMs in MD process a stable water vapor flux and rejection performances would be maintained. **Figure 8.5** shows a schematic illustration of the formation of fluorinated compounds on the membrane surface and the photographic images of the behavior of different solutions including water and low-surface tension liquids on the neat and CF_4-treated membranes. Except for water, all other solutions were not retained on the neat nanofiber surface while after CF_4 treatment; spherical to semi-spherical droplets were retained on the surface indicating the omniphobic property of the plasma modified membranes.

The LEP of the fabricated membranes was also investigated. Higher LEP is desirable for MD applications so as to provide wetting resistance for long-term MD operation. **Figure 8.6** shows the LEP results of the neat and CF_4 plasma-modified membranes. The neat ENM exhibited an LEP of 142.7 ± 1.2 kPa, while those of CF_4-plasma treated membrane showed higher LEP that increases with the increase in plasma treatment duration. However, beyond 15 min treatment, no appreciable differences in LEP were obtained for the modified membranes. For P/CF-15 ENM, the LEP was 186.7 ± 1.6 kPa, or an increase of 31% compared with that of neat membrane. As there was not much change in the overall morphology and structure of the CF_4 plasma treated membranes compared to the neat ENM membranes, this improved LEP that is mainly attributed to the increase in hydrophobicity of the treated membranes, which is consistent with the trend in hydrophobicity and surface energy results. This makes the CF_4 modified

membrane treated above 15 min (i.e., P/CF-15) suitable for long-term operation by AGMD process.

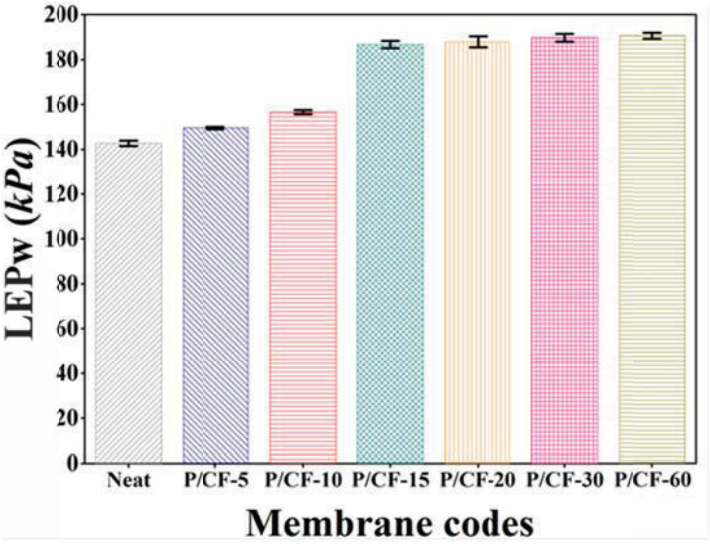

Figure 8.6. LEP of the neat and CF_4 modified electrospun nanofiber membranes

8.3.4 AGMD performance of omniphobic membrane

The omniphobic membranes fabricated in the present study were tested for their performance in the saline and more challenging (containing organic contaminants) feed solutions. In the first part, the flux and salt rejection performance of the neat and CF_4 plasma-modified nanofibers were evaluated and compared for 24 h test duration using real RO brine from CSG produced water as feed. After determining the individual performances of the modified membranes, the membrane with optimal performance was chosen and further evaluated using a more challenging feed solution – RO brine from CSG produced water containing different concentrations of surfactants (i.e., SDS).

In **Fig. 8.7**, all CF_4-plasma modified membranes showed much higher flux performance (10.5-15.3 LMH) compared to the neat nanofiber membrane (8.5 LMH). This signifies

an increase of 23 to 80% in flux performance after CF_4-plasma modification. The water flux improved with the increase in the plasma treatment time up to 15 min and beyond this treatment duration, the flux steadily declined. The highest water vapor flux was observed for P/CF-15 ENM membrane (15.3 ± 0.8 LMH) amongst all the fabricated membranes. The decrease in the water vapor flux for the membranes treated over 15 min is likely attributed to the increasing deposition of fluorinated layer and depth of deposition through the membrane. It is also likely that, at longer treatment duration, the fluorinated compounds are formed on the inner depth of the membrane, which decreases its internal layer surface energy, hence resulting to higher hydrophobicity and consequently more resistance to mass transfer. Similar results were obtained from previous studies, indicating decreased gas permeability at much longer CF_4 plasma treatment duration (Yang et al. 2014b; Yang et al. 2015). For P/CF-15 treated membrane, the treatment duration of 15 min was optimum that resulted only in added hydrophobicity and oleophobicity at the upper surface of the membrane, while maintaining more wettability at the inner layers, which is desirable to enhance the mass transfer of the water vapor. At an optimum treatment duration, it provides a highly omniphobic thin active surface, and less omniphobic inner pore surfaces, leading to good flux performance.

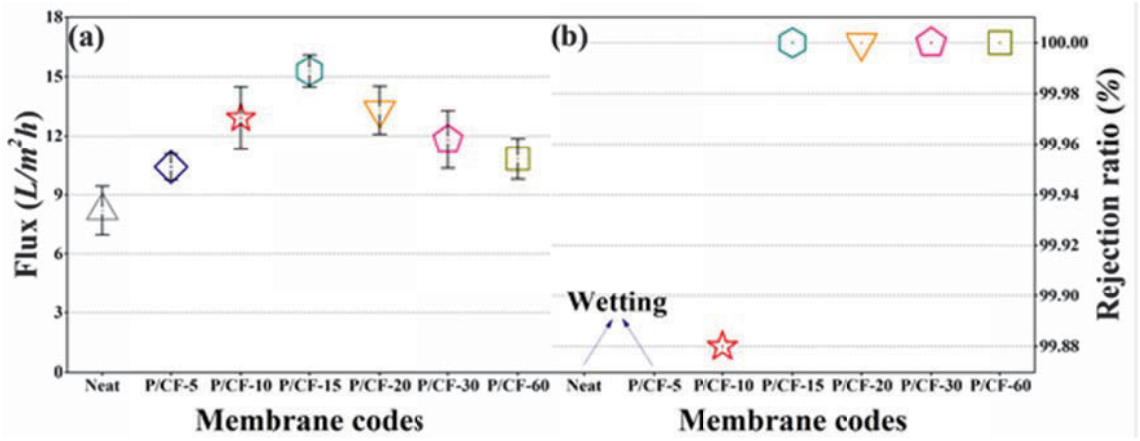

Figure 8.7. (a) Flux and (b) rejection performances of the neat and CF_4 modified electrospun nanofiber membranes by AGMD process using RO brine from CSG produced water as feed for 24 h

Aside from obtaining high flux performance, a stable and high salt rejection is also equally if not more important for MD application with good balance between these two performances. The CF_4 plasma modified membranes with treatment 15 min and above obtained similar final permeate electrical conductivity of 1.2 µS/cm after 24 h of test, indicating almost 100% salt rejection performance. On the other hand, both neat and P/CF-5 nanofiber membranes suffered the wetting problem after 5 h of operations (**Fig. 8.7b**). This behavior could be due to the presence of some organic contaminants in the real RO brine from CSG produced water feed that might have leaked through the membrane inducing membrane wetting. As observed in **Fig. 8.5**, the neat membrane was not able to retain some organic contaminants on the membrane surface. For the P/CF-5 membrane, the treatment duration was quite short to achieve full plasma treatment on the membrane surface hence resulting in the same wetting problem as with the neat membrane.

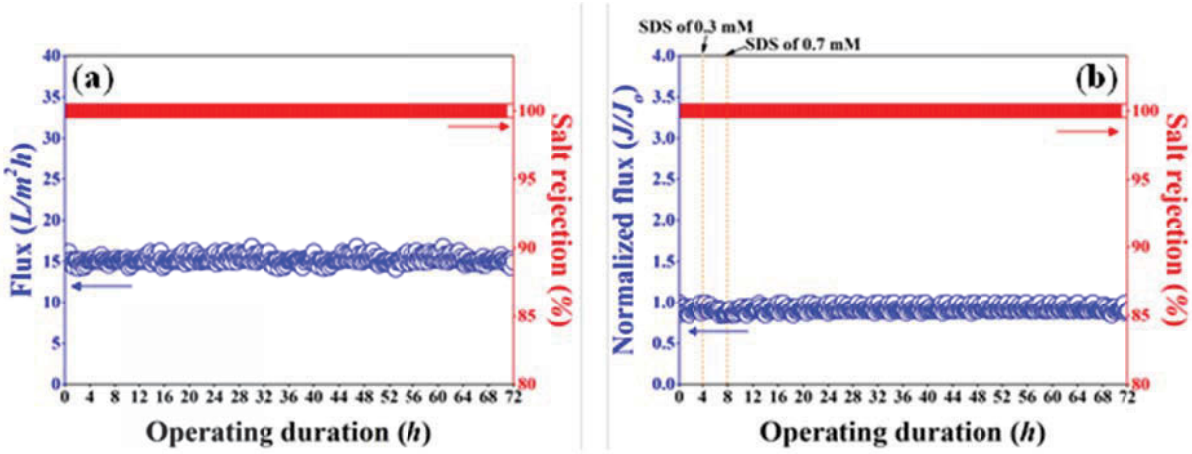

Figure 8.8. (a) Flux and salt rejection performances of the P/CF-15 nanofiber membrane by AGMD process using RO brine from CSG produced water as feed for 72 h and (b) normalized flux and salt rejection performances of the P/CF-15 nanofiber membrane by AGMD process using RO brine from CSG produced water with SDS additives as feed for 72 h.

Similarly, for P/CF-10, partial wetting was observed leading to 99.88% rejection ratio, which is primarily attributed to unsaturated treatment condition of the membrane surface. Based from the results, P/CF-15 membrane showed the optimal flux and salt rejection performance consistent with the improvement in membrane characteristics and properties explained in the previous sections. To further check the robustness of our CF_4-plasma treated membrane, long term test up to 72 h was carried out, and the P/CF-15 membrane still maintained very stable flux of 15 LMH and salt rejection of almost 100% (see **Fig. 8.8(a)**).

To further evaluate the reliability of the plasma modified omniphobic nanofiber membrane in treating challenging waters, different concentrations (from 0.1 to 0.7 mM) of SDS, an anionic surfactant, was added to the real RO brine from CSG produced water feed solution (**Fig. 8.9**). During AGMD operation using P/CF-15 membrane, SDS

was added to the feed every 2 h until arriving at a maximum concentration of 0.7 mM. The AGMD performance of P/CF-15 was compared to that of commercial PVDF membrane (C-PVDF). The initial water vapor flux of the P/CF-15 membranes (15.28 LMH) was almost three times higher than the initial flux of the C-PVDF membrane (5.24 LMH) which is likely attributed to the bigger pore sizes, higher porosity and high anti-wetting properties of the P/CF-15. The C-PVDF membrane showed decreasing salt rejection performance and sudden increase in the water vapor flux on adding 0.3 mM SDS after 4 hours of operation while the P/CF-15 membrane showed stable flux and salt rejection performances. On adding 0.5 mM and 0.7 mM SDS after 6 h and 8 h of operations, respectively, the salt rejection rapidly decreased along with the water flux reaching the water flux almost twice the initial flux and the salt rejection of 98.82%, indicating the wetting of the C-PVDF membrane. The presence of surfactant in the feed solution could have rendered the membrane surface hydrophilic, reducing the LEP and facilitating the leakage of raw salt water through the membrane (Lin et al. 2014). On the other hand, the P/CF-15 ENM membrane maintained a stable water vapor flux and high rejection ratio of 100% even after 0.7 mM of SDS addition, indicating its high resistance to wetting from low surface tension liquid. After the performance tests, the CA and LEP of the used membranes were evaluated and the results are shown in **Table 8.5**. It is evident from the results that the plasma modified membrane has maintained similar CA and LEP values as with the initial values as its virgin membrane while the CA and LEP values of the C-PVDF membrane had drastically dropped after the performance test. This demonstrated the robustness of the plasma modified omniphobic ENM membrane and hence its high potential for the treatment of challenging waters containing low surface tension contaminants.

We also conducted long-term AGMD experiments using CSG RO brine with SDS additives as feed (**Fig. 8.8(b)**). SDS was dosed into the feed solution after 4 h and 8 h of operation, leading to concentrations of 0.3 mM and 0.7 mM, respectively. The normalized flux performance indicates that CF_4-treated nanofiber membrane was very stable after 72 h of operation, while also maintaining very high salt rejection (~100%) even with the presence of surfactants in the feed solution, signifying the high potentiality of the present membranes for AGMD treatment for challenging water.

The behavior of the CF_4 plasma treated membrane could potentially be depicted as schematically presented in **Fig. 8.10.** The modification of the nanofiber membrane by CF_4 plasma treatment is expected to provide fluorinated layers on the surface of the nanofibers, leading to the decrease in its surface energy and consequently providing both hydrophobicity and oleophobicity and hence increased in anti-wetting property. Plasma gas is a mixture of highly active and energetic anions, cations and radicals, which can react drastically when applied onto the membrane surface. The radicals were expected to be allocated in the channels via pores when the plasma gas penetrated the membrane pores, which could lead to higher wetting resistance during MD operation (Wei et al. 2012; Yang et al. 2014b). Such plasma treated membrane can adequately prevent the leakage of salts and even low surface tension liquids through the pores of the membrane. This clearly shows the potential of the CF_4 plasma treated omniphobic nanofiber membrane in treating challenging waters especially containing high salinity and organic contaminants. Based from the results, the present omniphobic ENM can also be possibly used for the treatment of other challenging waters such as from textile, food and oily wastewater by MD applications.

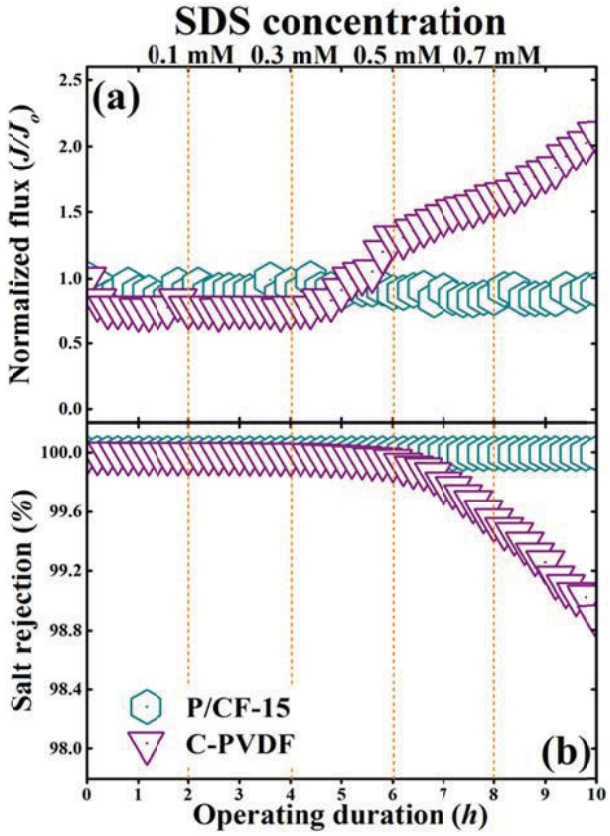

Figure 8.9. Normalized flux and (b) salt rejection of the C-PVDF and P/CF-15 electrospun nanofiber membranes by RO brine from CSG produced water with SDS as feed. The Porosity, mean pore size, membrane thickness, contact angle and LEP of the C-PVDF were 70.3%, 0.22 μm, 107.4 μm, 131.1° and 213.3 kPa, respectively.

Table 8.5. Contact angle and LEP of the electrospun nanofiber membranes before and after operations by AGMD using RO brine from CSG produced water containing SDS as feed

Membrane code	CA (deg)			LEP (kPa)		
	Virgin	After operation	Dried membrane	Virgin	After operation	Dried membrane
C-PVDF	130.9 ± 2.4	33.4 ± 2.4	105.2 ± 1.5	214.2 ± 2.5	78.5 ± 1.2	136.3 ± 3.7
P/CF-15	160.6 ± 4.5	151.2 ± 1.2	157.4 ± 0.7	186.7 ± 1.6	179.6 ± 0.9	184.2 ± 1.3

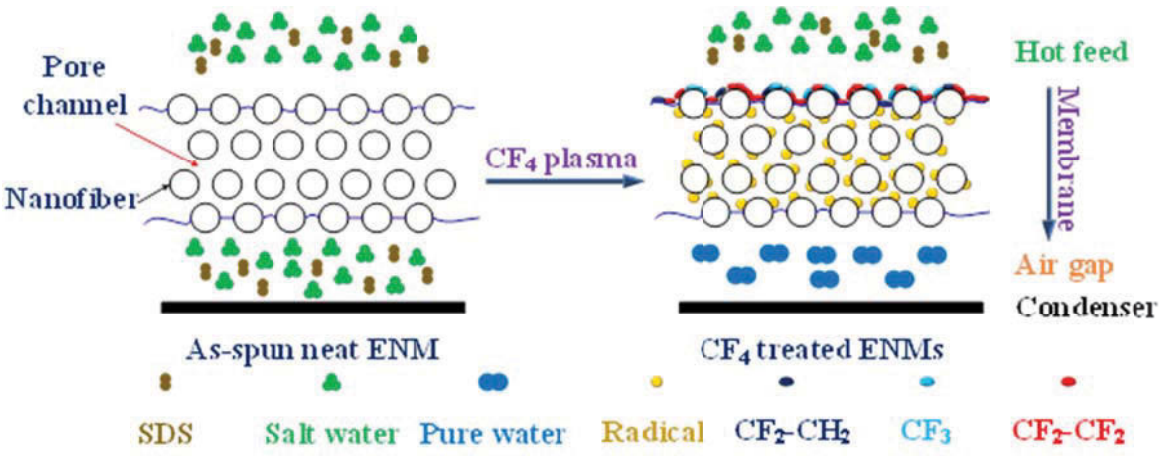

Figure 8.10. Comparison between the behavior of as-spun neat and CF_4 plasma modified electrospun nanofiber membranes in AGMD process.

8.4 Concluding remarks

In the present chapter, poly(vinylidene fluoride) (PVDF) membranes were successfully fabricated by electrospinning and modified by CF_4 plasma treatment. The fabricated and modified electrospun nanofiber membranes (ENMs) were evaluated by air gap membrane distillation (AGMD) process using real reverse osmosis (RO) brine from coal seam gas (CSG) produced water as feed. Results suggest the successful chemical modification of the membrane by plasma treatment without significantly altering the morphology and its physical properties, providing increased fluorination especially through the formation of CF_3 and CF_2-CF_2 bonds, with the treatment duration. This led to the improvement in wetting properties of the modified membrane, as the plasma treatment lowered its surface energy and gave omniphobic property to the membrane. The optimal treatment duration was found to be 15 min in the present study (the P/CF-15 membrane), obtaining the highest hydrophobicity and high wetting resistance to low surface tension liquids such as methanol, mineral oil and ethylene glycol, and

consequently high liquid entry pressure (187 kPa). These improved properties translate to high flux (15.28 L/m^2h) and salt rejection (~100%) performances of P/CF-15 even with the addition of up to 0.7 mM sodium dodecyl sulfate (SDS) in the real RO brine feed during AGMD operation. The results signify the high potential of the current CF_4 plasma modified nanofiber membrane in treating challenging feed solutions that may contain organic contaminants such as wastewater from CSG exploration.

CHAPTER 9

University of Technology Sydney
FACULTY OF ENGINEERING

CONCLUSIONS AND RECOMMENDATIONS

9.1 Conclusions

Membrane distillation (MD) is considered as an alternative technology to produce freshwater from seawater and other water resources. However, the lack of a proper membrane is a critical issue for MD. Thus, this thesis aimed to develop a suitable membrane for MD applications and evaluate its performances such as water vapor permeability and salt rejection ratio. To fabricate a suitable membrane in terms of prevention of the wetting problem and enhancement of water vapor flux performance in MD, several electrospinning techniques and surface modification methods were investigated. Eventually, this study achieved its objective of fabrications of a specially-designed MD electrospun nanofiber membrane, which showed a high water vapor flux performance and prevented wetting problems in MD. The fabricated and modified electrospun nanofiber membranes exhibited some advantages in terms of membrane properties like superhydrophobicity and anti-wetting property, leading to the improvement of water vapor flux and salt rejection performances. This study has the implications of fabricate electrospun nanofiber membranes with a high water vapor flux compared with previous studies. The summary and recommendations for further development of a high-performance commercial membrane in MD applications are addressed as follows.

9.1.1 Janus-type electrospun nanofiber membrane

To reduce the mass transfer resistance and improve water vapor flux performance, Janus-type electrospun nanofiber membranes were developed. In MD, Janus-type membrane consists of two major parts, which are hydrophobic active layer and hydrophilic or less hydrophobic support layer. The hydrophilic or less hydrophobic

support layer can reduce the mass transfer resistance, thereby improving water vapor flux performance. Thus, Chapter 4 investigates the heat-pressed dual-layer nanofiber membranes that were fabricated by electrospinning technique, and their performance in desalination by air gap membrane distillation (AGMD) is conducted. The dual-layer nonwoven nanofiber membranes composed of a polyvinylidene fluoride-co-hexapropylene (PH) active top layer and a bottom support layer made of either polyacrylonitrile (PAN), nylon-6 (N6), or polyvinyl alcohol (PVA) have been evaluated and compared with a single-layer nanofiber membrane and a commercial PVDF flat-sheet membrane (C-PVDF). Based on the results, as-spun neat PH and dual-layer nanofiber membranes showed high porosity, slightly larger mean pore size than C-PVDF membrane, good pore size distribution, and highly-hydrophobic rough surfaces. The heat-press post-treatment of the nanofiber membrane has indicated that fusion of nanofiber nodes and has increased the mechanical properties of the membrane. The dual-layer nanofiber membranes also showed comparable mechanical properties with C-PVDF. The heat-pressed nanofiber membrane showed smoother surface resulting to decreased contact angle but still comparable with commercial membrane and decreased but more uniform pore size and narrow pore size distribution (PSD) as well as increased liquid entry pressure (LEP). In addition, the heat-pressed nanofiber membrane was thinner but more compact membrane, while maintaining high porosity (>80%). From among the dual-layer membranes, M6 (heat-pressed PH/N6) showed the best properties with completely intertwined and linked PH-N6 interface, with good PSD and smaller pore size than C-PVDF. AGMD test results showed the highest and most stable flux (15 LMH) and salt rejection (>99%) obtained using M6, which was 1.5 times higher flux than that of C-PVDF. A support layer that is hydrophilic such as N6 with high porosity, uniform and small fiber diameter, coupled with porous hydrophobic active layer results

to high flux performance as it provides reduced mass transfer resistance and less heat transfer loss; a thinner hydrophobic active layer led to increased water permeate flux. Increasing the feed temperature resulted to increased permeate flux, but has also increased the tendency of pore wetting. Feed temperature at higher than 60^{o}C while maintaining a coolant temperature of 20^{o}C for AGMD process using a dual-layer membrane could be more prone to partial pore wetting. More stable flux and salt rejection was obtained at 50 to 60^{o}C feed temperature. The results suggest that M6 membranes could be potentially used for desalination by AGMD with stable flux and salt rejection in the feed temperature range of 50 to 60^{o}C.

9.1.2 Nanomaterials-incorporated electrospun nanofiber membranes

In the present study, three different types of nanomaterials were applied for fabrication of superhydrophobic electrospun nanofiber membranes to improve their water permeability and LEP. The three nano-materials, carbon nanotubes (CNTs), graphene, and hexagonal boron nitride (h-BN), were investigated and results are presented in Chapters 5, 6 and 7.

To enhance water vapor permeability and anti-wetting properties, hydrophobicity of MD membranes needs to be improved. Therefore, the aim of Chapter 5 achieves highly hydrophobic property electrospun nanofiber membranes by incorporating carbon nanotubes (CNTs) into polymeric solution. The hydrophobicity of the neat PH electrospun membrane was further enhanced by the incorporation of CNTs in/on the nanofibers reaching a contact angle (CA) of 158.5^{o}, which was higher than that of the C-PVDF membrane. The presence of CNTs in/on the nanofibers produced beads on the surface of the membrane and some protruding CNTs were also observed on the

nanofiber surface, which increases the overall roughness of the membrane surfaces leading to increased CA. Different characterization and measurement techniques have proven the successful incorporation of CNTs in/on the membrane, wherein a change to black color (from white for neat PH) was observed for the CNT/PH membranes. The electrospun membranes showed higher porosity (>85%) than a commercially-available PVDF membrane (70%), however, the LEP values were still lower than C-PVDF mainly because of the bigger pore sizes and thinner thickness of the nanofiber membranes. The 5 wt% CNT/PH nanofiber membrane showed the best flux performance (24-29.5 LMH) from all the membranes tested including that of the C-PVDF membrane (18-18.5 LMH), while maintaining a high salt rejection of >99.99%. The incorporation of CNTs in/on PH nanofibers could definitely provide additional functionalities that can enhance the direct contact MD (DCMD) performance. Thus, there is high potential of the present CNT-loaded nanofiber membranes as membrane material for desalination by membrane distillation.

Another attractive carbon-based nanomaterial is graphene, which is particularly attractive for MD application due to its hydrophobic nature and selective sorption of water vapors. Recently, graphene has been recognized for its better potentials of wide applications. Thus, the objective of Chapter 6 was to determine the optimal concentration of graphene in/on the electrospun nanocomposite membrane to lead to a robust and high AGMD performance desalination membrane. To summarize of this chapter, graphene/PH (G/PH) membranes were successfully fabricated by a one-step electrospinning technique and evaluated by AGMD using 3.5 wt% NaCl solution as feed. Graphene nanoparticles have been dispersed well in/on the nanofiber, which was confirmed by EDX, Raman spectroscopy, FT-IR and XRD. Further, there was an

increase in hydrophobicity of G/PH electrospun nanofiber membrane compared with the as-spun neat PH membrane. Several protruding graphene nanoparticles were observed on the nanofiber by SEM and TEM, which leads to increased contact angle. The nanofiber membrane with 5 wt% graphene loading (G5PH) showed an adequate porosity (88.7%), pore size (0.86 μm), CA (162.7°) and LEP (186.9 kPa) for AGMD application. For 60 h AGMD test, G5PH nanofiber membrane showed more stable flux (22.9 LMH) and better salt rejection performances (99.99%) compared with commercial PVDF membrane (flux of 4.75 LMH and salt rejection of 99.20%). Additionally, the effect of graphene on the flux performance was corroborated by theoretical models as suggested in this chapter. The present results suggest that the graphene-incorporated nanofiber membrane has good potential as a robust MD membrane for water desalination by MD process.

In order to compare with CNT and graphene nanoparticles, another hydrophobic nanoparticle, the hexagonal boron nitride (h-BN), was embedded into electrospun nanofiber membranes and then evaluated for its MD performance. The h-BN is a two-dimensional structure, which is isostructural to graphene, and has received considerable attention due to its superhydrophobic property. In Chapter 7, the researcher exploited the unique properties of the h-BN to enhance the overall properties of a polymeric membrane in obtaining a superhydrophobic membrane for enhanced long-term MD operation. The h-BN nanoparticle (BNNP) was incorporated in the PH nanofiber fabricated by the electrospinning technique. The hexagonal lattices of the OH-BNNPs were successfully modified by hydroxide-assisted ball milling without damage during the exfoliation processes. The OH-BNNPs had been dispersed in/on the nanofiber as confirmed by TEM, XPS, EDX mapping, FT-IR, XRD, and Raman spectroscopy. The

BN-PH nanofiber membrane showed higher hydrophobicity, LEP, and improved mechanical properties compared with the neat PH membrane. Besides, thermal conductivity of BN-PH membrane showed 0.009 W/mK, which was lower than that of the neat PH membrane (0.025 W/mK). Low thermal conductivity of BN-PH membrane can lead to improved water vapor permeability and maintain it during MD operation. BN-PH membrane exhibited significantly higher and stable water vapor flux, and salt rejection performances when operated up to 280 h. This study clearly shows that, incorporation of the BNNPs in the electrospun PH nanofiber membrane could significantly improve the membrane properties suitable for long-term MD process. Therefore, this chapter suggests that the BNNPs embedded PH nanofiber is a strong potential candidate of a robust MD membrane for the treatment of seawater in the long-term MD application.

Based from the results, CNT, graphene and BN nanoparticles incorporated PH electrospun nanofiber membranes showed higher hydrophobic properties than the neat PH membrane, due to the added more hydrophobic property of the incorporated nanoparticles. In general, two-dimensional nanomaterials such as graphene and BN had much larger surface area and pore volume than one-dimensional nanomaterial like CNT. These characteristics increased the surface pore volume and area of the two-dimensional nanoparticle embedded electrospun nanofiber membranes, leading to increased amounts of the vapor transport via membranes from the feed side to the permeate side. Two-dimensional nanoparticles embedded nanofiber membranes therefore exhibited a high water flux performance in MD.

9.1.3 CF_4 plasma modified electrospun nanofiber membrane

In this study, the fabrication of omniphobic membrane was proposed for treatment of reverse osmosis (RO) brine from coal seam gas (CSG) produced water containing a low surface tension liquid. To generate the omniphobic property, CF_4 plasma modification was applied on the membrane surface. In Chapter 8, poly(vinylidene fluoride) (PVDF) membranes were successfully fabricated by electrospinning and modified by CF_4 plasma treatment. The fabricated and modified electrospun nanofiber membranes were evaluated by AGMD process using real RO brine from CSG produced water as feed. Results suggest the successful chemical modification of the membrane by plasma treatment without significantly altering the morphology and its physical properties, providing increased fluorination especially through the formation of CF_3 and CF_2-CF_2 bonds, with the treatment duration. This led to the improvement in wetting properties of the modified membrane, as the plasma treatment lowered its surface energy and gave omniphobic property to the membrane. The optimal treatment duration was found to be 15 min in the present study (the P/CF-15 membrane), obtaining the highest hydrophobicity and high wetting resistance to low surface tension liquids such as methanol, mineral oil and ethylene glycol, and consequently high liquid entry pressure (187 kPa). These improved properties translate to high flux (15.28 L/m^2h) and salt rejection (~100%) performances of P/CF-15 even with the addition of up to 0.7 mM sodium dodecyl sulfate (SDS) in the real RO brine feed during AGMD operation. The results signify the high potential of the current CF_4 plasma modified nanofiber membrane in treating challenging feed solutions that may contain organic contaminants such as wastewater from CSG exploration.

In conclusion, this study successfully fabricated dual-layer (hydrophobic/hydrophilic) nanofiber membrane, two-dimensional carbon-based nanoparticles incorporated

nanofiber membranes, and plasma modified nanofiber membrane for MD applications. Due to several benefits of electrospinning technique in membrane fabrication, these nanofiber membranes show a high vapor flux and stable salt rejection performances in the treatment of seawater, seawater RO brine and CSG RO brine by MD application. Additionally, this study may provide helpful insight to the industries for future commercialization of membrane fabrication for MD applications using the electrospinning technique. However, the membrane fabrication by electrospinning still require improvement in terms of the stability in MD applications although the fabricated and modified nanofiber membranes have achieved better performances than commercial membranes.

9.2 Recommendations

In this study, the electrospinning technique is utilized for development of a suitable membrane for MD application. The proposed electrospun nanofiber membrane was successfully fabricated by i) hydrophobic/hydrophilic Janus-type (dual-layer) electrospinning to reduce total mass transfer resistance of the membrane, ii) nano-materials embedded on/in the polymeric nanofiber membrane to enhance its hydrophobic property, and iii) surface modification by CF_4 plasma treatment for achievement of omniphobic property to treat challenging feed solutions containing a low surface tension liquid. However, several issues need to be addressed to further improve the membrane properties and performance and possibly enable the commercialization of electrospun nanofiber membrane for MD.

Firstly, the heat-pressed hydrophobic/hydrophilic dual-layer membrane can improve water permeability due to a low mass transfer resistance of the hydrophilic support layer

compared with the heat-pressed hydrophobic single layer membrane. However, there is complicated in its preparation and fabrication. In addition, LEP is still not that high. A possible new nanofiber membrane design could be having internal interpenetrated pores on each nanofiber, which can increase its porosity while maintaining high LEP. In addition, the internally-porous morphologies on nanofiber membranes can lead to a much higher surface area to volume ratio than commonly fabricated nanofiber membranes. Thus, the internal interpenetrated nanofiber membranes can possibly result to enhanced water vapor flux performance and maintain anti-wetting properties in MD application.

Secondly, the present study achieved to decrease thermal conductivity with the h-BN nanoparticle embedded nanofiber membrane. Low thermal conductivity of the h-BN nanofiber membrane led to improvement of water permeability during 280 h MD operation. However, the h-BN nanoparticle is still expensive to synthesize even though it can promise high performances. Thus, to solve the problem, other nanoparticles should be considered other than h-BN. One of the possible nanoparticles is silica aerogel, which can be applied for the membrane fabrication for MD to improve its high MD performances. Silica aerogel is a low-priced material and has showed high hydrophobicity as it contains methyl and methoxy groups. It also exhibits a low thermal conductivity (below 0.05 W/mK), which is lower than PVDF (0.22 W/mK) and PP (0.25 W/mK). Thus, incorporation of silica aerogel may reduce the conductive heat losses, which leads to maintenance of water permeability during MD operation.

Lastly, a fabricated PVDF electrospun nanofiber membrane was modified by CF_4 plasma treatment to enhance hydrophobic property and even acquire omniphobic property for the membrane surface. This study optimised the operation conditions of the

CF_4 plasma treatment such as duration and power to evaluate their effect on the water vapor permeability of the modified membranes in MD application. The CF_4 plasma treated nanofiber membrane indicated high and stable flux and salt rejection performances. The study also showed the formation of new CF_3 and CF_2-CF_2 bonds after plasma treatment by application of various measurements, which contributed to highly hydrophobic property. However, the modification technique is hard to apply for the fabrication of a commercial membrane because of high modification cost and energy usage and limitations of the technique, like size of facilities and usage of hazardous plasma gas. For these reasons, another electrospinning technique, co-axial electrospinning, may be a better approach to achieve similar results in simple procedures. Via this technique, it is possible to fabricate a MD membrane and to modify it simultaneously. It is also a much more efficient technique to fabricate a superhydrophobic and omniphobic MD membrane by forming three-dimensional structures compared with the CF_4 plasma treatment. Thus, the co-axial electrospinning technique may have more potential for upscaling and possible commercialisation of the MD membranes fabrication than the CF_4 plasma modification technique.

REFERENCES

Abdallah, H., Moustafa, A.F., AlAnezi, A.A. & El-Sayed, H.E.M. 2014, 'Performance of a newly developed titanium oxide nanotubes/polyethersulfone blend membrane for water desalination using vacuum membrane distillation', *Desalination*, vol. 346, pp. 30-6.

Adnan, S., Hoang, M., Wang, H. & Xie, Z. 2012, 'Commercial PTFE membranes for membrane distillation application: Effect of microstructure and support material', *Desalination*, vol. 284, no. 0, pp. 297-308.

Ahmed, F.E., Lalia, B.S. & Hashaikeh, R. 2015, 'A review on electrospinning for membrane fabrication: Challenges and applications', *Desalination*, vol. 356, pp. 15-30.

Al-Amoudi, A. & Lovitt, R.W. 2007, 'Fouling strategies and the cleaning system of NF membranes and factors affecting cleaning efficiency', *Journal of Membrane Science*, vol. 303, no. 1-2, pp. 4-28.

Al-Amoudi, A.S. & Farooque, A.M. 2005, 'Performance restoration and autopsy of NF membranes used in seawater pretreatment', *Desalination*, vol. 178, no. 1–3, pp. 261-71.

Al-Obaidani, S., Curcio, E., Macedonio, F., Di Profio, G., Al-Hinai, H. & Drioli, E. 2008, 'Potential of membrane distillation in seawater desalination: Thermal efficiency, sensitivity study and cost estimation', *Journal of Membrane Science*, vol. 323, no. 1, pp. 85-98.

Al-Shammiri, M., Safar, M. & Al-Dawas, M. 2000, 'Evaluation of two different antiscalants in real operation at the Doha research plant', *Desalination*, vol. 128, no. 1, pp. 1-16.

Alexander, S., Eastoe, J., Lord, A.M., Guittard, F. & Barron, A.R. 2016, 'Branched Hydrocarbon Low Surface Energy Materials (LSEMs) for Superhydrophobic Nanoparticle Derived Surfaces', *ACS Appl Mater Interfaces*, vol. 8, pp. 660-6.

Alkhudhiri, A., Darwish, N. & Hilal, N. 2012, 'Membrane distillation: A comprehensive review', *Desalination*, vol. 287, pp. 2-18.

Alkhudhiri, A., Darwish, N. & Hilal, N. 2013, 'Produced water treatment: Application of air gap membrane distillation', *Desalination*, vol. 309, pp. 46-51.

Alklaibi, A.M. & Lior, N. 2005, 'Membrane-distillation desalination: Status and potential', *Desalination*, vol. 171, no. 2, pp. 111-31.

Alklaibi, A.M. & Lior, N. 2006, 'Heat and mass transfer resistance analysis of membrane distillation', *Journal of Membrane Science*, vol. 282, no. 1–2, pp. 362-9.

AlMarzooqi, F., Bilad, M.R., Mansoor, B. & Arafat, H. 2015, 'A comparative study of image analysis and porometry techniques for characterization of porous membranes', *Journal of Materials Science*, pp. 1-16.

Alves, V.D. & Coelhoso, I.M. 2006, 'Orange juice concentration by osmotic evaporation and membrane distillation: A comparative study', *Journal of Food Engineering*, vol. 74, no. 1, pp. 125-33.

Amarjargal, A., Tijing, L.D., Ruelo, M.T.G., Lee, D.H. & Kim, C.S. 2012, 'Facile synthesis and immobilization of Ag–TiO2 nanoparticles on electrospun PU nanofibers by polyol technique and simple immersion', *Mater Chem Phys*, vol. 135, pp. 277-81.

An, Q., Lv, F., Liu, Q., Han, C., Zhao, K., Sheng, J., Wei, Q., Yan, M. & Mai, L. 2014, 'Amorphous vanadium oxide matrixes supporting hierarchical porous

Fe3O4/graphene nanowires as a high-rate lithium storage anode', *Nano Lett*, vol. 14, no. 11, pp. 6250-6.

Artus, G.R.J., Jung, S., Zimmermann, J., Gautschi, H.P., Marquardt, K. & Seeger, S. 2006, 'Silicone Nanofilaments and Their Application as Superhydrophobic Coatings', *Advanced Materials*, vol. 18, no. 20, pp. 2758-62.

AWWA 1999, 'Water Quality and Treatment: A handbook of Community Water Supplies', McGraw-Hill, New York.

Baghbanzadeh, M., Rana, D., Matsuura, T. & Lan, C.Q. 2015, 'Effects of hydrophilic CuO nanoparticles on properties and performance of PVDF VMD membranes', *Desalination*, vol. 369, pp. 75-84.

Bai, Y., Huang, Z.-H., Yu, X.-L. & Kang, F. 2014, 'Graphene oxide-embedded porous carbon nanofiber webs by electrospinning for capacitive deionization', *Colloids and Surfaces A: Physicochemical and Engineering Aspects*, vol. 444, pp. 153-8.

Baji, A., Mai, Y.-W., Abtahi, M., Wong, S.-C., Liu, Y. & Li, Q. 2013, 'Microstructure development in electrospun carbon nanotube reinforced polyvinylidene fluoride fibers and its influence on tensile strength and dielectric permittivity', *Composites Science and Technology*, vol. 88, no. 0, pp. 1-8.

Baji, A., Mai, Y.-W., Wong, S.-C., Abtahi, M. & Chen, P. 2010, 'Electrospinning of polymer nanofibers: Effects on oriented morphology, structures and tensile properties', *Composites Science and Technology*, vol. 70, no. 5, pp. 703-18.

Banat, F., Al-Asheh, S. & Qtaishat, M. 2005, 'Treatment of waters colored with methylene blue dye by vacuum membrane distillation', *Desalination*, vol. 174, no. 1, pp. 87-96.

Banat, F., Jwaied, N., Rommel, M., Koschikowski, J. & Wieghaus, M. 2007, 'Desalination by a “compact SMADES” autonomous solarpowered membrane distillation unit', *Desalination*, vol. 217, no. 1, pp. 29-37.

Banat, F.A. & Simandl, J. 1996, 'Removal of benzene traces from contaminated water by vacuum membrane distillation', *Chemical Engineering Science*, vol. 51, no. 8, pp. 1257-65.

Ben Abdallah, S., Frikha, N. & Gabsi, S. 2013, 'Design of an autonomous solar desalination plant using vacuum membrane distillation, the MEDINA project', *Chemical Engineering Research and Design*, vol. 91, no. 12, pp. 2782-8.

Bhushan, B. & Jung, Y.C. 2011, 'Natural and biomimetic artificial surfaces for superhydrophobicity, self-cleaning, low adhesion, and drag reduction', *Progress in Materials Science*, vol. 56, no. 1, pp. 1-108.

Bilad, M.R., Westbroek, P. & Vankelecom, I.F.J. 2011, 'Assessment and optimization of electrospun nanofiber-membranes in a membrane bioreactor (MBR)', *Journal of Membrane Science*, vol. 380, no. 1-2, pp. 181-91.

Bird, R.B., Steward, W.E. & Lightfoot, E.n. 1976, *Transport phenomena*, Wiley, New York.

Bonyadi, S. & Chung, T.S. 2007, 'Flux enhancement in membrane distillation by fabrication of dual layer hydrophilic–hydrophobic hollow fiber membranes', *Journal of Membrane Science*, vol. 306, no. 1-2, pp. 134-46.

Boo, C., Lee, J. & Elimelech, M. 2016, 'Engineering Surface Energy and Nanostructure of Microporous Films for Expanded Membrane Distillation Applications', *Environ Sci Technol*.

Bormashenko, Y., Pogreb, R., Stanevsky, O. & Bormashenko, E. 2004, 'Vibrational spectrum of PVDF and its interpretation', *Polymer Testing*, vol. 23, no. 7, pp. 791-6.

Bott, T.R. 1995, *Fouling of heat exchangers*, Elsevier Science B.V., Netherlands.

Brown, P.N., Byrne, G.D. & Hindmarsh, A.C. 1989, 'Vode: A variable-coeeficient ODE solver', *Siam Journal on Scientific Computing*, vol. 10, pp. 1038-51.

Cao, J.-H., Zhu, B.-K. & Xu, Y.-Y. 2006, 'Structure and ionic conductivity of porous polymer electrolytes based on PVDF-HFP copolymer membranes', *Journal of Membrane Science*, vol. 281, no. 1–2, pp. 446-53.

Cao, J., Zhu, B., Ji, G. & Xu, Y. 2005, 'Preparation and characterization of PVDF–HFP microporous flat membranes by supercritical CO2 induced phase separation', *Journal of Membrane Science*, vol. 266, no. 1-2, pp. 102-9.

Celebi, K., Buchheim, J., Wyss, R.M., Droudian, A., Gasser, P., Shorubalko, I., Kye, J.-I., Lee, C. & Park, H.G. 2014, 'Ultimate Permeation Across atomically thin porous graphene', *Science*, vol. 344, p. 289.

Chekli, L., Phuntsho, S., Kim, J.E., Kim, J., Choi, J.Y., Choi, J.-S., Kim, S., Kim, J.H., Hong, S., Sohn, J. & Shon, H.K. 2016, 'A comprehensive review of hybrid forward osmosis systems: Performance, applications and future prospects', *Journal of Membrane Science*, vol. 497, pp. 430-49.

Chen, G., Yang, X., Lu, Y., Wang, R. & Fane, A.G. 2014, 'Heat transfer intensification and scaling mitigation in bubbling-enhanced membrane distillation for brine concentration', *Journal of Membrane Science*, vol. 470, pp. 60-9.

Chen, G., Yang, X., Wang, R. & Fane, A.G. 2013, 'Performance enhancement and scaling control with gas bubbling in direct contact membrane distillation', *Desalination*, vol. 308, no. 0, pp. 47-55.

Chen, W., Tao, X. & Liu, Y. 2006, 'Carbon nanotube-reinforced polyurethane composite fibers', *Composites Science and Technology*, vol. 66, no. 15, pp. 3029-34.

Chew, J.W., Krantz, W.B. & Fane, A.G. 2014, 'Effect of a macromolecular- or bio-fouling layer on membrane distillation', *Journal of Membrane Science*, vol. 456, pp. 66-76.

Chiam, C.-K. & Sarbatly, R. 2013, 'Vacuum membrane distillation processes for aqueous solution treatment—A review', *Chemical Engineering and Processing: Process Intensification*, vol. 74, pp. 27-54.

Choi, J., Lee, H. & Hong, S. 2016, 'Capacitive deionization (CDI) integrated with monovalent cation selective membrane for producing divalent cation-rich solution', *Desalination*, vol. 400, pp. 38-46.

Choi, S.-H. 2016, 'On the brine re-utilization of a multi-stage flashing (MSF) desalination plant', *Desalination*, vol. 398, pp. 64-76.

Choi, W., Choi, J., Bang, J. & Lee, J.H. 2013, 'Layer-by-layer assembly of graphene oxide nanosheets on polyamide membranes for durable reverse-osmosis applications', *ACS Appl Mater Interfaces*, vol. 5, no. 23, pp. 12510-9.

Choi, W., Jeon, S., Kwon, S.J., Park, H., Park, Y.-I., Nam, S.-E., Lee, P.S., Lee, J.S., Choi, J., Hong, S., Chan, E.P. & Lee, J.-H. 2017, 'Thin film composite reverse osmosis membranes prepared via layered interfacial polymerization', *Journal of Membrane Science*, vol. 527, pp. 121-8.

Choi, Y., Vigneswaran, S. & Lee, S. 2016, 'Evaluation of fouling potential and power density in pressure retarded osmosis (PRO) by fouling index', *Desalination*, vol. 389, pp. 215-23.

Christensen, K., Andresen, R., Tandskov, I., Norddahl, B. & du Preez, J.H. 2006, 'Using direct contact membrane distillation for whey protein concentration', *Desalination*, vol. 200, no. 1–3, pp. 523-5.

Cohen-Tanugi, D. & Grossman, J.C. 2012, 'Water desalination across nanoporous graphene', *Nano Lett*, vol. 12, no. 7, pp. 3602-8.

Criscuoli, A., Zhong, J., Figoli, A., Carnevale, M., Huang, R. & Drioli, E. 2008, 'Treatment of dye solutions by vacuum membrane distillation', *Water Research*, vol. 42, no. 20, pp. 5031-7.

Cuddy, M.F. & Fisher, E.R. 2012, 'Contributions of CF and CF2 Species to fluorocarbon film composition and properties for C(x)F(y) plasma-enhanced chemical vapor deposition', *ACS Appl Mater Interfaces*, vol. 4, no. 3, pp. 1733-41.

Cui, Z., Drioli, E. & Lee, Y.M. 2014, 'Recent progress in fluoropolymers for membranes', *Progress in Polymer Science*, vol. 39, no. 1, pp. 164-98.

Cui, Z.F., Chang, S. & Fane, A.G. 2003, 'The use of gas bubbling to enhance membrane processes', *Journal of Membrane Science*, vol. 221, no. 1–2, pp. 1-35.

Curcio, E., Ji, X., Di Profio, G., Sulaiman, A.O., Fontananova, E. & Drioli, E. 2010, 'Membrane distillation operated at high seawater concentration factors: Role of the membrane on CaCO3 scaling in presence of humic acid', *Journal of Membrane Science*, vol. 346, no. 2, pp. 263-9.

Daels, N., De Vrieze, S., Decostere, B., Dejans, P., Dumoulin, A., De Clerck, K., Westbroek, P. & Van Hulle, S.W.H. 2010, 'The use of electrospun flat sheet nanofibre membranes in MBR applications', *Desalination*, vol. 257, no. 1-3, pp. 170-6.

Dahdah, T.H. & Mitsos, A. 2014, 'Structural optimization of seawater desalination: I. A flexible superstructure and novel MED–MSF configurations', *Desalination*, vol. 344, pp. 252-65.

Dehesa-Carrasco, U., Pérez-Rábago, C.A. & Arancibia-Bulnes, C.A. 2013, 'Experimental evaluation and modeling of internal temperatures in an air gap membrane distillation unit', *Desalination*, vol. 326, pp. 47-54.

Derjaguin, B.V. & Landau, L. 1941, 'Theory of the stability of strongly charged lyophobic sols and of the adhesion of strongly charged particles in solutions of electrolytes', *Acta Phys. Chim. URSS*, vol. 14, pp. 633-62.

Devi, S., Ray, P., Singh, K. & Singh, P.S. 2014, 'Preparation and characterization of highly micro-porous PVDF membranes for desalination of saline water through vacuum membrane distillation', *Desalination*, vol. 346, pp. 9-18.

Ding, Z., Liu, L., Liu, Z. & Ma, R. 2010, 'Fouling resistance in concentrating TCM extract by direct contact membrane distillation', *Journal of Membrane Science*, vol. 362, no. 1–2, pp. 317-25.

Ding, Z., Liu, L., Liu, Z. & Ma, R. 2011, 'The use of intermittent gas bubbling to control membrane fouling in concentrating TCM extract by membrane distillation', *Journal of Membrane Science*, vol. 372, no. 1–2, pp. 172-81.

Dong, Z.-Q., Ma, X.-H., Xu, Z.-L. & Gu, Z.-Y. 2015, 'Superhydrophobic modification of PVDF–SiO2electrospun nanofiber membranes for vacuum membrane distillation', *RSC Adv.*, vol. 5, no. 83, pp. 67962-70.

Dong, Z.-Q., Ma, X.-h., Xu, Z.-L., You, W.-T. & Li, F.-b. 2014, 'Superhydrophobic PVDF–PTFE electrospun nanofibrous membranes for desalination by vacuum membrane distillation', *Desalination*, vol. 347, pp. 175-83.

Dong, Z.Q., Wang, B.J., Ma, X.H., Wei, Y.M. & Xu, Z.L. 2015, 'FAS Grafted Electrospun Poly(vinyl alcohol) Nanofiber Membranes with Robust Superhydrophobicity for Membrane Distillation', *ACS Appl Mater Interfaces*, vol. 7, no. 40, pp. 22652-9.

Dotremont, C., Kregersman, B., Sih, R., Lai, K.C., Koh, K. & Seah, H. 2010, 'Seawater desalination with memstill technology - a sustainable solution for the industry', *Water Practice and Technology*, vol. 5, no. 2, pp. wpt2010026-wpt.

Drew, C., Wang, X., Samuelson, L.A. & Kumar, J. 2003, 'The Effect of Viscosity and Filler on Electrospun Fiber Morphology', *Journal of Macromolecular Science, Part A*, vol. 40, no. 12, pp. 1415-22.

Drioli, E., Ali, A. & Macedonio, F. 2015, 'Membrane distillation: Recent developments and perspectives', *Desalination*, vol. 356, pp. 56-84.

Drioli, E., Ali, A., Simone, S., Macedonio, F., Al-Jlil, S.A., Al Shabonah, F.S., Al-Romaih, H.S., Al-Harbi, O., Figoli, A. & Criscuoli, A. 2013, 'Novel PVDF hollow fiber membranes for vacuum and direct contact membrane distillation applications', *Separation and Purification Technology*, vol. 115, pp. 27-38.

Drioli, E. & Macedonio, F. 2010, 'Integrated Membrane Systems for Desalination', *Membrane Technology*, Wiley-VCH Verlag GmbH & Co. KGaA, pp. 93-146.

Drioli, E., Stankiewicz, A.I. & Macedonio, F. 2011, 'Membrane engineering in process intensification—An overview', *Journal of Membrane Science*, vol. 380, no. 1-2, pp. 1-8.

Dumée, L., Germain, V., Sears, K., Schütz, J., Finn, N., Duke, M., Cerneaux, S., Cornu, D. & Gray, S. 2011, 'Enhanced durability and hydrophobicity of carbon nanotube bucky paper membranes in membrane distillation', *Journal of Membrane Science*, vol. 376, no. 1-2, pp. 241-6.

Dumée, L.F., Sears, K., Schütz, J., Finn, N., Huynh, C., Hawkins, S., Duke, M. & Gray, S. 2010, 'Characterization and evaluation of carbon nanotube Bucky-Paper membranes for direct contact membrane distillation', *Journal of Membrane Science*, vol. 351, no. 1–2, pp. 36-43.

Dydo, P., Turek, M., Ciba, J., Wandachowicz, K. & Misztal, J. 2004, 'The nucleation kinetic aspects of gypsum nanofiltration membrane scaling', *Desalination*, vol. 164, no. 1, pp. 41-52.

Ebrahim, S., Abdel-Jawad, M., Bou-Hamad, S. & Safar, M. 2001, 'Fifteen years of R&D program in seawater desalination at KISR part I. Pretreatment technologies for RO systems', *Desalination*, vol. 135, no. 1–3, pp. 141-53.

Ebrahim, S., Jawad, M.A., Hamad, S.B. & Safar, M. 2001, 'Fifteen years of R&D program in seawater desalination at KISR Part I. Pretreatment technologies for RO systems', *Desalination*, vol. 135, pp. 141-53.

Edwie, F., Teoh, M.M. & Chung, T.-S. 2012, 'Effects of additives on dual-layer hydrophobic–hydrophilic PVDF hollow fiber membranes for membrane distillation and continuous performance', *Chemical Engineering Science*, vol. 68, no. 1, pp. 567-78.

Efome, J.E., Baghbanzadeh, M., Rana, D., Matsuura, T. & Lan, C.Q. 2015, 'Effects of superhydrophobic SiO2 nanoparticles on the performance of PVDF flat sheet membranes for vacuum membrane distillation', *Desalination*, vol. 373, pp. 47-57.

El-Abbassi, A., Hafidi, A., Khayet, M. & García-Payo, M.C. 2013, 'Integrated direct contact membrane distillation for olive mill wastewater treatment', *Desalination*, vol. 323, no. 0, pp. 31-8.

El-Bourawi, M.S., Ding, Z., Ma, R. & Khayet, M. 2006, 'A framework for better understanding membrane distillation separation process', *Journal of Membrane Science*, vol. 285, no. 1–2, pp. 4-29.

Elimelech, M. & Phillip, W.A. 2011, 'The Future of Seawater desalination- energy, technology, and the environment', *Science*, vol. 333, pp. 712-7.

Essalhi, M. & Khayet, M. 2012, 'Surface segregation of fluorinated modifying macromolecule for hydrophobic/hydrophilic membrane preparation and application in air gap and direct contact membrane distillation', *Journal of Membrane Science*, vol. 417-418, pp. 163-73.

Essalhi, M. & Khayet, M. 2013a, 'Self-sustained webs of polyvinylidene fluoride electrospun nanofibers at different electrospinning times: 1. Desalination by direct contact membrane distillation', *Journal of Membrane Science*, vol. 433, pp. 167-79.

Essalhi, M. & Khayet, M. 2013b, 'Self-sustained webs of polyvinylidene fluoride electrospun nanofibers at different electrospinning times: 2. Theoretical analysis, polarization effects and thermal efficiency', *Journal of Membrane Science*, vol. 433, pp. 180-91.

Essalhi, M. & Khayet, M. 2014, 'Application of a porous composite hydrophobic/hydrophilic membrane in desalination by air gap and liquid gap membrane distillation: A comparative study', *Separation and Purification Technology*, vol. 133, pp. 176-86.

Fan, H. & Peng, Y. 2012, 'Application of PVDF membranes in desalination and comparison of the VMD and DCMD processes', *Chemical Engineering Science*, vol. 79, pp. 94-102.

Fang, H., Gao, J.F., Wang, H.T. & Chen, C.S. 2012, 'Hydrophobic porous alumina hollow fiber for water desalination via membrane distillation process', *Journal of Membrane Science*, vol. 403-404, pp. 41-6.

Farrell, E., Hassan, M.I., Tufa, R.A., Tuomiranta, A., Avci, A.H., Politano, A., Curcio, E. & Arafat, H.A. 2017, 'Reverse electrodialysis powered greenhouse concept for water- and energy-self-sufficient agriculture', *Applied Energy*, vol. 187, pp. 390-409.

Feng, C., Khulbe, K.C., Matsuura, T., Gopal, R., Kaur, S., Ramakrishna, S. & Khayet, M. 2008, 'Production of drinking water from saline water by air-gap membrane distillation using polyvinylidene fluoride nanofiber membrane', *Journal of Membrane Science*, vol. 311, no. 1-2, pp. 1-6.

Feng, C., Khulbe, K.C., Matsuura, T., Tabe, S. & Ismail, A.F. 2013, 'Preparation and characterization of electro-spun nanofiber membranes and their possible applications in water treatment', *Separation and Purification Technology*, vol. 102, pp. 118-35.

Feng, X., Jiang, L.Y., Matsuura, T. & Wu, P. 2017, 'Fabrication of hydrophobic/hydrophilic composite hollow fibers for DCMD: Influence of dope formulation and external coagulant', *Desalination*, vol. 401, pp. 53-63.

Filella, M. 2007, 'Colloidal properties of submicon particles in natural waters ', in K.J. Wilkinson & J.R. Lead (eds), *Environmental colloids and particles: behaviour, separation and characterisation*, vol. 10, John Wiley and Sons, England, pp. 17-93.

Fisher, L.R. & Israelachvili, J.N. 1981, 'Experimental studies on the applicability of the Kelvin equation to highly curved concave menisci', *Journal of Colloid and Interface Science*, vol. 80, no. 2, pp. 528-41.

Fragkou, M.C. & McEvoy, J. 2016, 'Trust matters: Why augmenting water supplies via desalination may not overcome perceptual water scarcity', *Desalination*, vol. 397, pp. 1-8.

Francis, L., Ghaffour, N., Alsaadi, A.A. & Amy, G.L. 2013, 'Material gap membrane distillation: A new design for water vapor flux enhancement', *Journal of Membrane Science*, vol. 448, pp. 240-7.

Francis, L., Maab, H., AlSaadi, A., Nunes, S., Ghaffour, N. & Amy, G.L. 2013, 'Fabrication of electrospun nanofibrous membranes for membrane distillation application', *Desalination and Water Treatment*, vol. 51, no. 7-9, pp. 1337-43.

Furstner, R. & Barthlott, W. 2005, 'Wetting and Self-Cleaning Properties of Artificial Superhydrophobic Surfaces', *Langmuir*, vol. 21, pp. 956-61.

Gagliardo, P., Adham, S., Trussell, R. & Olivieri, A. 1998, 'Water repurification via reverse osmosis', *Desalination*, vol. 117, pp. 73-8.

Galaverna, G., Di Silvestro, G., Cassano, A., Sforza, S., Dossena, A., Drioli, E. & Marchelli, R. 2008, 'A new integrated membrane process for the production of concentrated blood orange juice: Effect on bioactive compounds and antioxidant activity', *Food Chemistry*, vol. 106, no. 3, pp. 1021-30.

Gao, W., Liang, H., Ma, J., Han, M., Chen, Z.-l., Han, Z.-s. & Li, G.-b. 2011, 'Membrane fouling control in ultrafiltration technology for drinking water production: A review', *Desalination*, vol. 272, no. 1–3, pp. 1-8.

Garcia, X. & Pargament, D. 2015, 'Reusing wastewater to cope with water scarcity: Economic, social and environmental considerations for decision-making', *Resources, Conservation and Recycling*, vol. 101, pp. 154-66.

Ge, Q., Wang, P., Wan, C. & Chung, T.S. 2012, 'Polyelectrolyte-promoted forward osmosis-membrane distillation (FO-MD) hybrid process for dye wastewater treatment', *Environ Sci Technol*, vol. 46, no. 11, pp. 6236-43.

Geng, H., Wu, H., Li, P. & He, Q. 2014, 'Study on a new air-gap membrane distillation module for desalination', *Desalination*, vol. 334, no. 1, pp. 29-38.

Gethard, K., Sae-Khow, O. & Mitra, S. 2011, 'Water desalination using carbon-nanotube-enhanced membrane distillation', *ACS Applied Materials & Interfaces*, vol. 3, no. 2, pp. 110-4.

Gethard, K., Sae-Khow, O. & Mitra, S. 2012, 'Carbon nanotube enhanced membrane distillation for simultaneous generation of pure water and concentrating pharmaceutical waste', *Separation and Purification Technology*, vol. 90, no. 0, pp. 239-45.

Ghaffour, N., Missimer, T.M. & Amy, G.L. 2013, 'Technical review and evaluation of the economics of water desalination: Current and future challenges for better water supply sustainability', *Desalination*, vol. 309, pp. 197-207.

Gilron, J., Song, L. & Sirkar, K.K. 2007, 'Design for Cascade of Crossflow Direct Contact Membrane Distillation', *Industrial & Engineering Chemistry Research*, vol. 46, no. 8, pp. 2324-34.

Gleick, P.H. & Palaniappan, M. 2010, 'Peak water limits to freshwater withdrawal and use', *Proc Natl Acad Sci U S A*, vol. 107, no. 25, pp. 11155-62.

Goh, P.S., Ismail, A.F. & Ng, B.C. 2013, 'Carbon nanotubes for desalination: Performance evaluation and current hurdles', *Desalination*, vol. 308, no. 0, pp. 2-14.

Goh, S., Zhang, J., Liu, Y. & Fane, A.G. 2013, 'Fouling and wetting in membrane distillation (MD) and MD-bioreactor (MDBR) for wastewater reclamation', *Desalination*, vol. 323, no. 0, pp. 39-47.

Goh, S., Zhang, Q., Zhang, J., McDougald, D., Krantz, W.B., Liu, Y. & Fane, A.G. 2013, 'Impact of a biofouling layer on the vapor pressure driving force and performance of a membrane distillation process', *Journal of Membrane Science*, vol. 438, no. 0, pp. 140-52.

Gopal, R., Kaur, S., Ma, Z., Chan, C., Ramakrishna, S. & Matsuura, T. 2006, 'Electrospun nanofibrous filtration membrane', *Journal of Membrane Science*, vol. 281, no. 1-2, pp. 581-6.

Greenberg, G., Hasson, D. & Semiat, R. 2005, 'Limits of RO recovery imposed by calcium phosphate precipitation', *Desalination*, vol. 183, no. 1-3, pp. 273-88.

Griebe, T. & Flemming, H.-C. 1998, 'Biocide-free antifouling strategy to protect RO membranes from biofouling', *Desalination*, vol. 118, no. 1–3, pp. 153-IN9.

Gryta, M. 2005a, 'Long-term performance of membrane distillation process', *Journal of Membrane Science*, vol. 265, no. 1–2, pp. 153-9.

Gryta, M. 2005b, 'Osmotic MD and other membrane distillation variants', *Journal of Membrane Science*, vol. 246, no. 2, pp. 145-56.

Gryta, M. 2007, 'Influence of polypropylene membrane surface porosity on the performance of membrane distillation process', *Journal of Membrane Science*, vol. 287, no. 1, pp. 67-78.

Gryta, M. 2008, 'Fouling in direct contact membrane distillation process', *Journal of Membrane Science*, vol. 325, no. 1, pp. 383-94.

Gryta, M. 2010a, 'Application of membrane distillation process for tap water purification', *Membrane Water Treatment*, vol. 1, no. 1, pp. 1-12.

Gryta, M. 2010b, 'Desalination of thermally softened water by membrane distillation process', *Desalination*, vol. 257, no. 1–3, pp. 30-5.

Gryta, M., Grzechulska-Damszel, J., Markowska, A. & Karakulski, K. 2009, 'The influence of polypropylene degradation on the membrane wettability during membrane distillation', *Journal of Membrane Science*, vol. 326, no. 2, pp. 493-502.

Gryta, M. & Karakulski, K. 1999, 'The application of membrane distillation for the concentration of oil-water emulsions', *Desalination*, vol. 121, no. 1, pp. 23-9.

Gryta, M., Karakulski, K., Tomaszewska, M. & Morawski, A. 2005, 'Treatment of effluents from the regeneration of ion exchangers using the MD process', *Desalination*, vol. 180, no. 1–3, pp. 173-80.

Gryta, M., Tomaszewska, M. & Karakulski, K. 2006, 'Wastewater treatment by membrane distillation', *Desalination*, vol. 198, no. 1–3, pp. 67-73.

Guillén-Burrieza, E., Blanco, J., Zaragoza, G., Alarcón, D.-C., Palenzuela, P., Ibarra, M. & Gernjak, W. 2011, 'Experimental analysis of an air gap membrane distillation solar desalination pilot system', *Journal of Membrane Science*, vol. 379, no. 1, pp. 386-96.

Guillen-Burrieza, E., Ruiz-Aguirre, A., Zaragoza, G. & Arafat, H.A. 2014, 'Membrane fouling and cleaning in long term plant-scale membrane distillation operations', *Journal of Membrane Science*, vol. 468, no. 0, pp. 360-72.

Guillén-Burrieza, E., Zaragoza, G., Miralles-Cuevas, S. & Blanco, J. 2012, 'Experimental evaluation of two pilot-scale membrane distillation modules used for solar desalination', *Journal of Membrane Science*, vol. 409, pp. 264-75.

Gunko, S., Verbych, S., Bryk, M. & Hilal, N. 2006, 'Concentration of apple juice using direct contact membrane distillation', *Desalination*, vol. 190, no. 1–3, pp. 117-24.

Guo, F., Servi, A., Liu, A., Gleason, K.K. & Rutledge, G.C. 2015, 'Desalination by Membrane Distillation using Electrospun Polyamide Fiber Membranes with Surface Fluorination by Chemical Vapor Deposition', *ACS Appl Mater Interfaces*, vol. 7, no. 15, pp. 8225-32.

Hamzah, N. & Leo, C.P. 2017, 'Membrane distillation of saline with phenolic compound using superhydrophobic PVDF membrane incorporated with TiO 2 nanoparticles: Separation, fouling and self-cleaning evaluation', *Desalination*, vol. 418, pp. 79-88.

Han, G., Zhang, S., Li, X. & Chung, T.-S. 2013, 'High performance thin film composite pressure retarded osmosis (PRO) membranes for renewable salinity-gradient energy generation', *Journal of Membrane Science*, vol. 440, pp. 108-21.

Hao, J.-h., Dai, H.-p., Yang, P.-c., Wei, J.-m. & Wang, Z. 1996, 'Cellulose acetate hollow fiber performance for ultra-low pressure reverse osmosis', *Desalination*, vol. 107, pp. 217-21.

Hare, E.F., Shafrin, E.G. & Zisman, W.A. 1954, 'Properties of films of adsorbed fluorinated acids', *The Journal of Physical Chemistry*, vol. 58, no. 3, pp. 236-9.

Harris, C. 1999, 'Energy recovery for membrane desalination', *Desalination*, vol. 125, pp. 173-80.

He, F., Gilron, J., Lee, H., Song, L. & Sirkar, K.K. 2008, 'Potential for scaling by sparingly soluble salts in crossflow DCMD', *Journal of Membrane Science*, vol. 311, no. 1–2, pp. 68-80.

He, F., Sirkar, K.K. & Gilron, J. 2009a, 'Effects of antiscalants to mitigate membrane scaling by direct contact membrane distillation', *Journal of Membrane Science*, vol. 345, no. 1-2, pp. 53-8.

He, F., Sirkar, K.K. & Gilron, J. 2009b, 'Studies on scaling of membranes in desalination by direct contact membrane distillation: CaCO3 and mixed CaCO3/CaSO4 systems', *Chemical Engineering Science*, vol. 64, no. 8, pp. 1844-59.

He, T., Zhou, W., Bahi, A., Yang, H. & Ko, F. 2014, 'High permeability of ultrafiltration membranes based on electrospun PVDF modified by nanosized zeolite hybrid membrane scaffolds under low pressure', *Chemical Engineering Journal*, vol. 252, pp. 327-36.

Hoek, E.M.V., Allred, J., Knoell, T. & Jeong, B.-H. 2008, 'Modeling the effects of fouling on full-scale reverse osmosis processes', *Journal of Membrane Science*, vol. 314, no. 1–2, pp. 33-49.

Hopkins, J. & Badyal, J.P.S. 1996, 'CF_4 Plasma Treatment of Asymmetric Polysulfone Membranes', *Langmuir*, vol. 12, pp. 3666-70.

Hou, D., Dai, G., Wang, J., Fan, H., Zhang, L. & Luan, Z. 2012, 'Preparation and characterization of PVDF/nonwoven fabric flat-sheet composite membranes for desalination through direct contact membrane distillation', *Separation and Purification Technology*, vol. 101, pp. 1-10.

Hou, D., Fan, H., Jiang, Q., Wang, J. & Zhang, X. 2014, 'Preparation and characterization of PVDF flat-sheet membranes for direct contact membrane distillation', *Separation and Purification Technology*, vol. 135, pp. 211-22.

Hou, D., Wang, J., Qu, D., Luan, Z. & Ren, X. 2009, 'Fabrication and characterization of hydrophobic PVDF hollow fiber membranes for desalination through direct contact membrane distillation', *Separation and Purification Technology*, vol. 69, no. 1, pp. 78-86.

Hou, D., Wang, J., Sun, X., Ji, Z. & Luan, Z. 2012, 'Preparation and properties of PVDF composite hollow fiber membranes for desalination through direct contact membrane distillation', *Journal of Membrane Science*, vol. 405-406, pp. 185-200.

Hsu, S.T., Cheng, K.T. & Chiou, J.S. 2002, 'Seawater desalination by direct contact membrane distillation', *Desalination*, vol. 143, no. 3, pp. 279-87.

Huang, C.-Y., Ko, C.-C., Chen, L.-H., Huang, C.-T., Tung, K.-L. & Liao, Y.-C. 2016, 'A simple coating method to prepare superhydrophobic layers on ceramic alumina for vacuum membrane distillation', *Separation and Purification Technology*.

Huang, H., Schwab, K. & Jacangelo, J.G. 2009, 'Pretreatment for low pressure membranes in water treatment: A review', *Environmental Science & Technology*, vol. 43, no. 9, pp. 3011-9.

Huang, S., Yee, W.A., Tjiu, W.C., Liu, Y., Kotaki, M., Boey, Y.C.F., Ma, J., Liu, T. & Lu, X. 2008, 'Electrospinning of polyvinylidene difluoride with carbon nanotubes: synergistic effects of extensional force and interfacial interaction on crystalline structures', *Langmuir*, vol. 24, no. 23, pp. 13621-6.

Huang, Y., Huang, Q.-L., Liu, H., Zhang, C.-X., You, Y.-W., Li, N.-N. & Xiao, C.-F. 2017, 'Preparation, characterization, and applications of electrospun ultrafine fibrous PTFE porous membranes', *Journal of Membrane Science*, vol. 523, pp. 317-26.

Huang, Z.-M., Zhang, Y.-Z., Kotaki, M. & Ramakrishna, S. 2003, 'A review on polymer nanofibers by electrospinning and their applications in nanocomposites', *Composites Science and Technology*, vol. 63, no. 15, pp. 2223-53.

Hussain, C.M., Saridara, C. & Mitra, S. 2009, 'Modifying the sorption properties of multi-walled carbon nanotubesvia covalent functionalization', *Analyst*, vol. 134, no. 9, pp. 1928-33.

Hwang, K.-J., Chan, C.-S. & Chen, F.-F. 2008, 'A comparison of hydrodynamic methods for mitigating particle fouling in submerged membrane filtration', *Journal of the Chinese Institute of Chemical Engineers*, vol. 39, no. 3, pp. 257-64.

Islam, M.S., McCutcheon, J.R. & Rahaman, M.S. 2017, 'A high flux polyvinyl acetate-coated electrospun nylon 6/SiO 2 composite microfiltration membrane for the separation of oil-in-water emulsion with improved antifouling performance', *Journal of Membrane Science*, vol. 537, pp. 297-309.

Jackson, R.B., Carpenter, S.R., Dahm, C.N., Mcknight, D.M., Naiman, R.J., Postel, S.L. & Running, S.W. 2001, 'Water in a Changing World', *Issues in Ecology*, no. 20, pp. 1-16.

Jansen, A.E., Assink, J.W., Hanemaaijer, J.H., van Medevoort, J. & van Sonsbeek, E. 2013, 'Development and pilot testing of full-scale membrane distillation modules for deployment of waste heat', *Desalination*, vol. 323, pp. 55-65.

Jaroniec, M. & Madey, R. 1988, *Physical Adsorption on Heterogeneous Solids*, Elsevier, Amsterdam.

Jeong, J.S., Moon, J.S., Jeon, S.Y., Park, J.H., Alegaonkar, P.S. & Yoo, J.B. 2007, 'Mechanical properties of electrospun PVA/MWNTs composite nanofibers', *Thin Solid Films*, vol. 515, no. 12, pp. 5136-41.

Jin, M., Feng, X., Xi, J., Zhai, J., Cho, K., Feng, L. & Jiang, L. 2005, 'Super-Hydrophobic PDMS Surface with Ultra-Low Adhesive Force', *Macromolecular Rapid Communications*, vol. 26, no. 22, pp. 1805-9.

Jin, X., Huang, X. & Hoek, E.M.V. 2009, 'Role of Specific Ion Interactions in Seawater RO Membrane Fouling by Alginic Acid', *Environmental Science & Technology*, vol. 43, no. 10, pp. 3580-7.

Karakulski, K. & Gryta, M. 2005, 'Water demineralisation by NF/MD integrated processes', *Desalination*, vol. 177, no. 1–3, pp. 109-19.

Ke, K., Pötschke, P., Jehnichen, D., Fischer, D. & Voit, B. 2014, 'Achieving β-phase poly(vinylidene fluoride) from melt cooling: Effect of surface functionalized carbon nanotubes', *Polymer*, vol. 55, no. 2, pp. 611-9.

Kharraz, J.A., Bilad, M.R. & Arafat, H.A. 2015, 'Flux stabilization in membrane distillation desalination of seawater and brine using corrugated PVDF membranes', *Journal of Membrane Science*, vol. 495, pp. 404-14.

Khayet, M. 2011, 'Membranes and theoretical modeling of membrane distillation: a review', *Adv Colloid Interface Sci*, vol. 164, no. 1-2, pp. 56-88.

Khayet, M., Godino, M.P. & Mengual, J.I. 2004, 'Study of asymmetric polarization in direct contact membrane distillation', *Separation Science and Technology*, vol. 39, pp. 125-47.

Khayet, M. & Matsuura, T. 2001, 'Preparation and Characterization of Polyvinylidene Fluoride Membranes for Membrane Distillation', *Industrial & Engineering Chemistry Research*, vol. 40, no. 24, pp. 5710-8.

Khayet, M. & Matsuura, T. 2011, *Membrane distillation: principles and applications*, Elsevier.

Khayet, M., Matsuura, T. & Mengual, J. 2005, 'Porous hydrophobic/hydrophilic composite membranes: Estimation of the hydrophobic-layer thickness', *Journal of Membrane Science*, vol. 266, no. 1-2, pp. 68-79.

Khemakhem, S. & Amar, R.B. 2011, 'Modification of Tunisian clay membrane surface by silane grafting: Application for desalination with Air Gap Membrane Distillation process', *Colloids and Surfaces A: Physicochemical and Engineering Aspects*, vol. 387, no. 1-3, pp. 79-85.

Kim, A.S., Lee, H.-S., Moon, D.-S. & Kim, H.-J. 2016, 'Performance control on adsorption desalination using initial time lag (ITL) of individual beds', *Desalination*, vol. 396, pp. 1-16.

Kim, C.H., Kim, B.-H. & Yang, K.S. 2012, 'TiO2 nanoparticles loaded on graphene/carbon composite nanofibers by electrospinning for increased photocatalysis', *Carbon*, vol. 50, no. 7, pp. 2472-81.

Kim, D.I., Kim, J., Shon, H.K. & Hong, S. 2015, 'Pressure retarded osmosis (PRO) for integrating seawater desalination and wastewater reclamation: Energy consumption and fouling', *Journal of Membrane Science*, vol. 483, pp. 34-41.

Kim, J., Kwon, H., Lee, S., Lee, S. & Hong, S. 2017, 'Membrane distillation (MD) integrated with crystallization (MDC) for shale gas produced water (SGPW) treatment', *Desalination*, vol. 403, pp. 172-8.

Kim, Y.-J., Ahn, C.H. & Choi, M.O. 2010, 'Effect of thermal treatment on the characteristics of electrospun PVDF−silica composite nanofibrous membrane', *European Polymer Journal*, vol. 46, no. 10, pp. 1957-65.

Kim, Y., Lee, S., Kuk, J. & Hong, S. 2015, 'Surface chemical heterogeneity of polyamide RO membranes: Measurements and implications', *Desalination*, vol. 367, pp. 154-60.

Knyazkova, T.V. & Maynarovich, A.A. 1999, 'Recognition of membrane fouling: testing of theoretical approaches with data on NF of salt solutions containing a

low molecular weight surfactant as a foulant', *Desalination*, vol. 126, no. 1–3, pp. 163-9.

Koschikowski, J., Wieghaus, M. & Rommel, M. 2003, 'Solar thermal-driven desalination plants based on membrane distillation', *Desalination*, vol. 156, no. 1, pp. 295-304.

Krivorot, M., Kushmaro, A., Oren, Y. & Gilron, J. 2011, 'Factors affecting biofilm formation and biofouling in membrane distillation of seawater', *Journal of Membrane Science*, vol. 376, no. 1–2, pp. 15-24.

Kühnl, W., Piry, A., Kaufmann, V., Grein, T., Ripperger, S. & Kulozik, U. 2010, 'Impact of colloidal interactions on the flux in cross-flow microfiltration of milk at different pH values: A surface energy approach', *Journal of Membrane Science*, vol. 352, no. 1–2, pp. 107-15.

Kurihara, M. & Hanakawa, M. 2013, 'Mega-ton Water System: Japanese national research and development project on seawater desalination and wastewater reclamation', *Desalination*, vol. 308, pp. 131-7.

Lai, W.-C. & Cheng, L.-T. 2014, 'Preparation and characterization of novel poly(vinylidene fluoride) membranes using self-assembled dibenzylidene sorbitol for membrane distillation', *Desalination*, vol. 332, no. 1, pp. 7-17.

Lalia, B.S., Guillen-Burrieza, E., Arafat, H.A. & Hashaikeh, R. 2013, 'Fabrication and characterization of polyvinylidenefluoride-co-hexafluoropropylene (PVDF-HFP) electrospun membranes for direct contact membrane distillation', *Journal of Membrane Science*, vol. 428, pp. 104-15.

Lalia, B.S., Guillen, E., Arafat, H.A. & Hashaikeh, R. 2014, 'Nanocrystalline cellulose reinforced PVDF-HFP membranes for membrane distillation application', *Desalination*, vol. 332, no. 1, pp. 134-41.

Lalia, B.S., Kochkodan, V., Hashaikeh, R. & Hilal, N. 2013, 'A review on membrane fabrication: Structure, properties and performance relationship', *Desalination*, vol. 326, pp. 77-95.

Lawson, K.W. & Lloyd, D.R. 1997, 'Membrane distillation', *Journal of Membrane Science*, vol. 124, pp. 123-33.

Lee, D., Lee, B., Park, K.H., Ryu, H.J., Jeon, S. & Hong, S.H. 2015, 'Scalable exfoliation process for highly soluble boron nitride nanoplatelets by hydroxide-assisted ball milling', *Nano Lett*, vol. 15, no. 2, pp. 1238-44.

Lee, D., Song, S.H., Hwang, J., Jin, S.H., Park, K.H., Kim, B.H., Hong, S.H. & Jeon, S. 2013, 'Enhanced mechanical properties of epoxy nanocomposites by mixing noncovalently functionalized boron nitride nanoflakes', *Small*, vol. 9, no. 15, pp. 2602-10.

Lee, E.-J., An, A.K., Hadi, P., Lee, S., Woo, Y.C. & Shon, H.K. 2017, 'Advanced multi-nozzle electrospun functionalized titanium dioxide/polyvinylidene fluoride-co-hexafluoropropylene (TiO 2 /PVDF-HFP) composite membranes for direct contact membrane distillation', *Journal of Membrane Science*, vol. 524, pp. 712-20.

Lee, E.-J., An, A.K., He, T., Woo, Y.C. & Shon, H.K. 2016, 'Electrospun nanofiber membranes incorporating fluorosilane-coated TiO2 nanocomposite for direct contact membrane distillation', *Journal of Membrane Science*, vol. 520, pp. 145-54.

Lee, H.J., Amy, G., Cho, J.W., Yoon, Y.M., Moon, S.-H. & KIM, I.S. 2001, 'Cleaning strategies for flux recovery of an ultrafiltration membrane fouled by natural organic matter', *Water Res*, vol. 35, no. 14, pp. 3301-8.

Lee, J.-Y., Tan, W.S., An, J., Chua, C.K., Tang, C.Y., Fane, A.G. & Chong, T.H. 2016, 'The potential to enhance membrane module design with 3D printing technology', *Journal of Membrane Science*, vol. 499, pp. 480-90.

Lee, J., Boo, C., Ryu, W.H., Taylor, A.D. & Elimelech, M. 2016, 'Development of Omniphobic Desalination Membranes Using a Charged Electrospun Nanofiber Scaffold', *ACS Appl Mater Interfaces*, vol. 8, no. 17, pp. 11154-61.

Lei, W., Portehault, D., Liu, D., Qin, S. & Chen, Y. 2013, 'Porous boron nitride nanosheets for effective water cleaning', *Nat Commun*, vol. 4, p. 1777.

Li, D. & Kaner, R.B. 2008, 'Graphene-Based Materials', *Science*, vol. 320, p. 1170.

Li, D. & Xia, Y. 2004, 'Electrospinning of nanofibers: reinventing the wheel?', *Advanced Materials*, vol. 16, no. 14, pp. 1151-70.

Li, H., Zou, L., Pan, L. & Sun, Z. 2010, 'Novel Graphene-Like Electrodes for CDI', *Environ Sci Technol*, vol. 44, pp. 8692-7.

Li, L., Hashaikeh, R. & Arafat, H.A. 2013, 'Development of eco-efficient micro-porous membranes via electrospinning and annealing of poly (lactic acid)', *Journal of Membrane Science*, vol. 436, pp. 57-67.

Li, X., Wang, C., Yang, Y., Wang, X., Zhu, M. & Hsiao, B.S. 2014, 'Dual-biomimetic superhydrophobic electrospun polystyrene nanofibrous membranes for membrane distillation', *ACS Appl Mater Interfaces*, vol. 6, no. 4, pp. 2423-30.

Li, Z., Peng, Y., Dong, Y., Fan, H., Chen, P., Qiu, L. & Jiang, Q. 2014, 'Effects of thermal efficiency in DCMD and the preparation of membranes with low thermal conductivity', *Applied Surface Science*, vol. 317, pp. 338-49.

Liao, Y., Loh, C.H., Wang, R. & Fane, A.G. 2014, 'Electrospun superhydrophobic membranes with unique structures for membrane distillation', *ACS Appl Mater Interfaces*, vol. 6, no. 18, pp. 16035-48.

Liao, Y., Wang, R. & Fane, A.G. 2013, 'Engineering superhydrophobic surface on poly(vinylidene fluoride) nanofiber membranes for direct contact membrane distillation', *Journal of Membrane Science*, vol. 440, pp. 77-87.

Liao, Y., Wang, R. & Fane, A.G. 2014, 'Fabrication of bioinspired composite nanofiber membranes with robust superhydrophobicity for direct contact membrane distillation', *Environ Sci Technol*, vol. 48, no. 11, pp. 6335-41.

Liao, Y., Wang, R., Tian, M., Qiu, C. & Fane, A.G. 2013, 'Fabrication of polyvinylidene fluoride (PVDF) nanofiber membranes by electro-spinning for direct contact membrane distillation', *Journal of Membrane Science*, vol. 425-426, pp. 30-9.

Lin, S., Nejati, S., Boo, C., Hu, Y., Osuji, C.O. & Elimelech, M. 2014, 'Omniphobic Membrane for Robust Membrane Distillation', *Environmental Science & Technology Letters*, vol. 1, no. 11, pp. 443-7.

Lin, S., Yip, N.Y. & Elimelech, M. 2014, 'Direct contact membrane distillation with heat recovery: Thermodynamic insights from module scale modeling', *Journal of Membrane Science*, vol. 453, pp. 498-515.

Liu, F., Hashim, N.A., Liu, Y., Abed, M.M. & Li, K. 2011, 'Progress in the production and modification of PVDF membranes', *Journal of Membrane Science*, vol. 375, no. 1, pp. 1-27.

Liu, H. & Wang, J. 2013, 'Treatment of radioactive wastewater using direct contact membrane distillation', *Journal of Hazardous Materials*, vol. 261, no. 0, pp. 307-15.

Liu, Y.-L., Li, Y., Xu, J.-T. & Fan, Z.-Q. 2010, 'Cooperative effect of electrospinning and nanoclay on formation of polar crystalline phases in poly(vinylidene fluoride)', *ACS Applied Materials & Interfaces*, vol. 2, no. 6, pp. 1759-68.

Low, Z.-X., Chua, Y.T., Ray, B.M., Mattia, D., Metcalfe, I.S. & Patterson, D.A. 2017, 'Perspective on 3D printing of separation membranes and comparison to related unconventional fabrication techniques', *Journal of Membrane Science*, vol. 523, pp. 596-613.

Lowell, S., Shields, J.E., Thomas, M.A. & Thommes, M. 2004, *Characterization of Porous Solids and Powders: Surface Area, Pore Size and Density*, Springer Netherlands.

Lu, K.-J., Zuo, J. & Chung, T.-S. 2016, 'Tri-bore PVDF hollow fibers with a super-hydrophobic coating for membrane distillation', *Journal of Membrane Science*, vol. 514, pp. 165-75.

Lu, K.-J., Zuo, J. & Chung, T.-S. 2017, 'Novel PVDF membranes comprising n-butylamine functionalized graphene oxide for direct contact membrane distillation', *Journal of Membrane Science*, vol. 539, pp. 34-42.

Lu, Y., Ding, Z., Liu, L., Wang, Z. & Ma, R. 2008, 'The influence of bubble characteristics on the performance of submerged hollow fiber membrane module used in microfiltration', *Separation and Purification Technology*, vol. 61, no. 1, pp. 89-95.

Luo, L., Wang, P., Zhang, S., Han, G. & Chung, T.-S. 2014, 'Novel thin-film composite tri-bore hollow fiber membrane fabrication for forward osmosis', *Journal of Membrane Science*, vol. 461, pp. 28-38.

M. Gryta, K.K., A. W. Morawski 2001, 'Purification of oily wastewater by hybrid UF,MD', *Water research*, vol. 35, pp. 3665-9.

Ma, W., Zhang, J. & Wang, X. 2008, 'Formation of poly (vinylidene fluoride) crystalline phases from tetrahydrofuran/N, N-dimethylformamide mixed solvent', *Journal of Materials Science*, vol. 43, no. 1, pp. 398-401.

Macedonio, F., Curcio, E. & Drioli, E. 2007, 'Integrated membrane systems for seawater desalination: energetic and exergetic analysis, economic evaluation, experimental study', *Desalination*, vol. 203, no. 1–3, pp. 260-76.

Marmur, A. 2004, 'The Lotus Effect: Superhydrophobicity and Metastability', *Langmuir*, vol. 20, no. 9, pp. 3517-9.

Martinez-Diez, L., Florido-Diaz, F.J. & V~quez-GonzS.lez, M.I. 1999, 'Study of evaporation efficiency in membrane distillation', *Desalination*, vol. 126, pp. 193-8.

Martínez-Díez, L. & Vázquez-González, M.I. 1999, 'Temperature and concentration polarization in membrane distillation of aqueous salt solutions', *Journal of Membrane Science*, vol. 156, no. 2, pp. 265-73.

Martínez, L., Florido-Díaz, F.J., Hernández, A. & Prádanos, P. 2003, 'Estimation of vapor transfer coefficient of hydrophobic porous membranes for applications in membrane distillation', *Separation and Purification Technology*, vol. 33, no. 1, pp. 45-55.

Martínez, L. & Rodríguez-Maroto, J.M. 2007, 'On transport resistances in direct contact membrane distillation', *Journal of Membrane Science*, vol. 295, no. 1–2, pp. 28-39.

McHale, G., Shirtcliffe, N.J. & Newton, M.I. 2004, 'Super-hydrophobic and super-wetting surfaces: Analytical potential?', *Analyst*, vol. 129, no. 4, pp. 284-7.

Meindersma, G.W., Guijt, C.M. & de Haan, A.B. 2006, 'Desalination and water recycling by air gap membrane distillation', *Desalination*, vol. 187, no. 1–3, pp. 291-301.

Meng, F., Chae, S.R., Drews, A., Kraume, M., Shin, H.S. & Yang, F. 2009, 'Recent advances in membrane bioreactors (MBRs): membrane fouling and membrane material', *Water Res*, vol. 43, no. 6, pp. 1489-512.

Meng, J., Lin, S. & Xiong, X. 2017, 'Preparation of breathable and superhydrophobic coating film via spray coating in combination with vapor-induced phase separation', *Progress in Organic Coatings*, vol. 107, pp. 29-36.

Meng, S., Ye, Y., Mansouri, J. & Chen, V. 2014, 'Fouling and crystallisation behaviour of superhydrophobic nano-composite PVDF membranes in direct contact membrane distillation', *Journal of Membrane Science*, vol. 463, pp. 102-12.

Mi, B. 2014, 'Graphene Oxide Membranes for ionic and molecular sieving', *Science*, vol. 343, p. 740.

Mitropoulos, A.C. 2008, 'The Kelvin equation', *Journal of Colloid and Interface Science*, vol. 317, no. 2, pp. 643-8.

Moradi, R., Karimi-Sabet, J., Shariaty-Niassar, M. & Koochaki, M. 2015, 'Preparation and Characterization of Polyvinylidene Fluoride/Graphene Superhydrophobic Fibrous Films', *Polymers*, vol. 7, no. 8, pp. 1444-63.

Mossad, M. & Zou, L. 2013, 'Study of fouling and scaling in capacitive deionisation by using dissolved organic and inorganic salts', *J Hazard Mater*, vol. 244-245, pp. 387-93.

Munirasu, S., Banat, F., Durrani, A.A. & Haija, M.A. 2017, 'Intrinsically superhydrophobic PVDF membrane by phase inversion for membrane distillation', *Desalination*, vol. 417, pp. 77-86.

Na, H., Zhao, Y., Zhao, C., Zhao, C. & Yuan, X. 2008, 'Effect of hot-press on electrospun poly(vinylidene fluoride) membranes', *Polymer Engineering & Science*, vol. 48, no. 5, pp. 934-40.

Nahm, S.W., Shim, W.G., Park, Y.-K. & Kim, S.C. 2012, 'Thermal and chemical regeneration of spent activated carbon and its adsorption property for toluene', *Chemical Engineering Journal*, vol. 210, pp. 500-9.

Nejati, S., Boo, C., Osuji, C.O. & Elimelech, M. 2015, 'Engineering flat sheet microporous PVDF films for membrane distillation', *Journal of Membrane Science*, vol. 492, pp. 355-63.

Nene, S., Kaur, S., Sumod, K., Joshi, B. & Raghavarao, K.S.M.S. 2002, 'Membrane distillation for the concentration of raw cane-sugar syrup and membrane clarified sugarcane juice', *Desalination*, vol. 147, no. 1–3, pp. 157-60.

Nghiem, L.D. & Cath, T. 2011, 'A scaling mitigation approach during direct contact membrane distillation', *Separation and Purification Technology*, vol. 80, no. 2, pp. 315-22.

Nghiem, L.D., Elters, C., Simon, A., Tatsuya, T. & Price, W. 2015, 'Coal seam gas produced water treatment by ultrafiltration, reverse osmosis and multi-effect distillation: A pilot study', *Separation and Purification Technology*, vol. 146, pp. 94-100.

Nishino, T., Meguro, M., Nakamae, K., Matsushita, M. & Ueda, Y. 1999, 'The lowest surface free energy based on -CF_3 alignment', *Langmuir*, vol. 15, pp. 4321-3.

Oh, K.H., Lee, D., Choo, M.J., Park, K.H., Jeon, S., Hong, S.H., Park, J.K. & Choi, J.W. 2014, 'Enhanced durability of polymer electrolyte membrane fuel cells by functionalized 2D boron nitride nanoflakes', *ACS Appl Mater Interfaces*, vol. 6, no. 10, pp. 7751-8.

Park, C.H., Lee, S.Y., Hwang, D.S., Shin, D.W., Cho, D.H., Lee, K.H., Kim, T.W., Kim, T.W., Lee, M., Kim, D.S., Doherty, C.M., Thornton, A.W., Hill, A.J., Guiver,

M.D. & Lee, Y.M. 2016, 'Nanocrack-regulated self-humidifying membranes', *Nature*, vol. 532, no. 7600, pp. 480-3.

Park, K.S., Lee, D.Y., Kim, K.J. & Moon, D.W. 1997, 'Observation of a hexagonal BN surface layer on the cubic BN film grown by dual ion beam sputter deposition', *Applied physics letters*, vol. 70, no. 3, pp. 315-7.

Park, M.J., Nisola, G.M., Beltran, A.B., Torrejos, R.E.C., Seo, J.G., Lee, S.-P., Kim, H. & Chung, W.-J. 2014, 'Recyclable composite nanofiber adsorbent for Li+ recovery from seawater desalination retentate', *Chemical Engineering Journal*, vol. 254, pp. 73-81.

Peining, Z., Nair, A.S., Shengjie, P., Shengyuan, Y. & Ramakrishna, S. 2012, 'Facile fabrication of TiO2-graphene composite with enhanced photovoltaic and photocatalytic properties by electrospinning', *ACS Appl Mater Interfaces*, vol. 4, no. 2, pp. 581-5.

Peng, P., Fane, A.G. & Li, X. 2005, 'Desalination by membrane distillation adopting a hydrophilic membrane', *Desalination*, vol. 173, pp. 45-54.

Peng, Y., Dong, Y., Fan, H., Chen, P., Li, Z. & Jiang, Q. 2013, 'Preparation of polysulfone membranes via vapor-induced phase separation and simulation of direct-contact membrane distillation by measuring hydrophobic layer thickness', *Desalination*, vol. 316, pp. 53-66.

Perreault, F., Fonseca de Faria, A. & Elimelech, M. 2015, 'Environmental applications of graphene-based nanomaterials', *Chem Soc Rev*.

Phattaranawik, J., Fane, A.G., Pasquier, A.C.S., Bing, W. & Wong, F.S. 2009, 'Experimental Study and Design of a Submerged Membrane Distillation Bioreactor', *Chemical Engineering & Technology*, vol. 32, no. 1, pp. 38-44.

Phattaranawik, J., Jiraratananon, R. & Fane, A.G. 2003, 'Effect of pore size distribution and air flux on mass transport in direct contact membrane distillation', *Journal of Membrane Science*, vol. 215, no. 1–2, pp. 75-85.

Phuntsho, S., Lotfi, F., Hong, S., Shaffer, D.L., Elimelech, M. & Shon, H.K. 2014, 'Membrane scaling and flux decline during fertiliser-drawn forward osmosis desalination of brackish groundwater', *Water Res*, vol. 57, pp. 172-82.

Pierce, E., Carmona, F.J. & Amirfazli, A. 2008, 'Understanding of sliding and contact angle results in tilted plate experiments', *Colloids and Surfaces A: Physicochemical and Engineering Aspects*, vol. 323, no. 1-3, pp. 73-82.

Polat, E.O., Balci, O., Kakenov, N., Uzlu, H.B., Kocabas, C. & Dahiya, R. 2015, 'Synthesis of Large Area Graphene for High Performance in Flexible Optoelectronic Devices', *Scientific Reports*, vol. 5, p. 16744.

Post, J.W., Goeting, C.H., Valk, J., Goinga, S., Veerman, J., Hamelers, H.V.M. & Hack, P.J.F.M. 2010, 'Towards implementation of reverse electrodialysis for power generation from salinity gradients', *Desalination and Water Treatment*, vol. 16, no. 1-3, pp. 182-93.

Prince, J.A., Anbharasi, V., Shanmugasundaram, T.S. & Singh, G. 2013, 'Preparation and characterization of novel triple layer hydrophilic–hydrophobic composite membrane for desalination using air gap membrane distillation', *Separation and Purification Technology*, vol. 118, pp. 598-603.

Prince, J.A., Rana, D., Singh, G., Matsuura, T., Jun Kai, T. & Shanmugasundaram, T.S. 2014, 'Effect of hydrophobic surface modifying macromolecules on differently produced PVDF membranes for direct contact membrane distillation', *Chemical Engineering Journal*, vol. 242, pp. 387-96.

Prince, J.A., Singh, G., Rana, D., Matsuura, T., Anbharasi, V. & Shanmugasundaram, T.S. 2012, 'Preparation and characterization of highly hydrophobic poly(vinylidene fluoride) – Clay nanocomposite nanofiber membranes (PVDF–clay NNMs) for desalination using direct contact membrane distillation', *Journal of Membrane Science*, vol. 397-398, pp. 80-6.

Privett, B.J., Youn, J., Hong, S.A., Lee, J., Han, J., Shin, J.H. & Schoenfisch, M.H. 2011, 'Antibacterial Fluorinated Silica Colloid Superhydrophobic Surfaces', *Langmuir*, vol. 27, no. 15, pp. 9597-601.

Qi, S., Wang, R., Chaitra, G.K.M., Torres, J., Hu, X. & Fane, A.G. 2016, 'Aquaporin-based biomimetic reverse osmosis membranes: Stability and long term performance', *Journal of Membrane Science*, vol. 508, pp. 94-103.

Qtaishat, M., Khayet, M. & Matsuura, T. 2009a, 'Guidelines for preparation of higher flux hydrophobic/hydrophilic composite membranes for membrane distillation', *Journal of Membrane Science*, vol. 329, no. 1-2, pp. 193-200.

Qtaishat, M., Khayet, M. & Matsuura, T. 2009b, 'Novel porous composite hydrophobic/hydrophilic polysulfone membranes for desalination by direct contact membrane distillation', *Journal of Membrane Science*, vol. 341, no. 1-2, pp. 139-48.

Qu, D., Wang, J., Wang, L., Hou, D., Luan, Z. & Wang, B. 2009, 'Integration of accelerated precipitation softening with membrane distillation for high-recovery desalination of primary reverse osmosis concentrate', *Separation and Purification Technology*, vol. 67, no. 1, pp. 21-5.

Quist-Jensen, C.A., Ali, A., Mondal, S., Macedonio, F. & Drioli, E. 2016, 'A study of membrane distillation and crystallization for lithium recovery from high-

concentrated aqueous solutions', *Journal of Membrane Science*, vol. 505, pp. 167-73.

Rahimpour, A., Madaeni, S.S., Zereshki, S. & Mansourpanah, Y. 2009, 'Preparation and characterization of modified nano-porous PVDF membrane with high antifouling property using UV photo-grafting', *Applied Surface Science*, vol. 255, no. 16, pp. 7455-61.

Raluy, R.G., Schwantes, R., Subiela, V.J., Peñate, B., Melián, G. & Betancort, J.R. 2012, 'Operational experience of a solar membrane distillation demonstration plant in Pozo Izquierdo-Gran Canaria Island (Spain)', *Desalination*, vol. 290, pp. 1-13.

Rangarajan, R., Desai, N.V., Daga, S.L., Joshi, S.V., Prakash Rao, A., Shah, V.J., Trivedi, J.J., Devmurari, C.V., Singh, K., Bapat, P.S., Raval, H.D., Jewrajka, S.K., Saha, N.K., Bhattacharya, A., Singh, P.S., Ray, P., Trivedi, G.S., Pathak, N. & Reddy, A.V.R. 2011, 'Thin film composite reverse osmosis membrane development and scale up at CSMCRI, Bhavnagar', *Desalination*, vol. 282, pp. 68-77.

Ratkovich, N., Chan, C.C.V., Berube, P.R. & Nopens, I. 2009, 'Experimental study and CFD modelling of a two-phase slug flow for an airlift tubular membrane', *Chemical Engineering Science*, vol. 64, no. 16, pp. 3576-84.

Razmjou, A., Arifin, E., Dong, G., Mansouri, J. & Chen, V. 2012, 'Superhydrophobic modification of TiO2 nanocomposite PVDF membranes for applications in membrane distillation', *Journal of Membrane Science*, vol. 415–416, no. 0, pp. 850-63.

Riekerink, M.B.O., Terlingen, J.G.A., Engbers, G.H.M. & Feijen, J. 1999, 'Selective Etching of Semicrystalline Polymers: CF4 Gas Plasma Treatment of Poly(ethylene)', *Langmuir*, vol. 15, pp. 4847-56.

Roths, T., M.Martha, Weesec, J. & Honerkamp, J. 2001, 'A generalized regularization method for nonlinear ill-posed', *Computer Physics Communications*, vol. 139, pp. 279–96.

Rouquerol, F., Rouqueorol, J. & Sing, K. 1999, *Adsorption by Powders and Porous Solids: Principles, methodology, and applications*, San Diego: Academic Press.

Roy, S., Bhadra, M. & Mitra, S. 2014, 'Enhanced desalination via functionalized carbon nanotube immobilized membrane in direct contact membrane distillation', *Separation and Purification Technology*, vol. 136, pp. 58-65.

Rudzinski, W. & Everett, D. 1991, *Adsorption of Gases on Heterogeneous Solid Surfaces*, Academic Press, London.

Sahin, O., Stewart, R.A. & Porter, M.G. 2015, 'Water security through scarcity pricing and reverse osmosis: a system dynamics approach', *Journal of Cleaner Production*, vol. 88, pp. 160-71.

Sahoo, B.N. & Kandasubramanian, B. 2014, 'Recent progress in fabrication and characterisation of hierarchical biomimetic superhydrophobic structures', *RSC Advances*, vol. 4, no. 42, p. 22053.

Schofield, R.W., Fane, A.G. & Fell, C.J.D. 1987, 'Heat and mass transfer in membrane distillation', *Journal of Membrane Science*, vol. 33, no. 3, pp. 299-313.

Scialdone, O., D'Angelo, A., De Lumè, E. & Galia, A. 2014, 'Cathodic reduction of hexavalent chromium coupled with electricity generation achieved by reverse-electrodialysis processes using salinity gradients', *Electrochimica Acta*, vol. 137, pp. 258-65.

Shahzad, M.W., Burhan, M., Ang, L. & Ng, K.C. 2017, 'Energy-water-environment nexus underpinning future desalination sustainability', *Desalination*, vol. 413, pp. 52-64.

Shalaby, S.M. 2017, 'Reverse osmosis desalination powered by photovoltaic and solar Rankine cycle power systems: A review', *Renewable and Sustainable Energy Reviews*, vol. 73, pp. 789-97.

Shannon, M.A., Bohn, P.W., Elimelech, M., Georgiadis, J.G., Marinas, B.J. & Mayes, A.M. 2008, 'Science and technology for water purification in the coming decades', *Nature*, vol. 452, no. 7185, pp. 301-10.

Shao, H., Fang, J., Wang, H. & Lin, T. 2015, 'Effect of electrospinning parameters and polymer concentrations on mechanical-to-electrical energy conversion of randomly-oriented electrospun poly(vinylidene fluoride) nanofiber mats', *Rsc Advances*, vol. 5, no. 19, pp. 14345-50.

Shenvi, S.S., Isloor, A.M. & Ismail, A.F. 2015, 'A review on RO membrane technology: Developments and challenges', *Desalination*, vol. 368, pp. 10-26.

Shi, Y., Hamsen, C., Jia, X., Kim, K.K., Reina, A., Hofmann, M., Hsu, A.L., Zhang, K., Li, H., Juang, Z.Y., Dresselhaus, M.S., Li, L.J. & Kong, J. 2010, 'Synthesis of few-layer hexagonal boron nitride thin film by chemical vapor deposition', *Nano Lett*, vol. 10, no. 10, pp. 4134-9.

Shiklomanov, I.A. 1993, 'World fresh water resources', in P.H. Gleick (ed.), *Water in Crisis: A Guide to the World's Fresh Water Resources*.

Shim, W.G., He, K., Gray, S. & Moon, I.S. 2015, 'Solar energy assisted direct contact membrane distillation (DCMD) process for seawater desalination', *Separation and Purification Technology*, vol. 143, pp. 94-104.

Shim, W.G., Lee, J.W. & Kim, S.C. 2008, 'Analysis of catalytic oxidation of aromatic hydrocarbons over supported palladium catalyst with different pretreatments based on heterogeneous adsorption properties', *Applied Catalysis B: Environmental*, vol. 84, no. 1-2, pp. 133-41.

Shirazi, M.M.A., Kargari, A. & Shirazi, M.J.A. 2012, 'Direct contact membrane distillation for seawater desalination', *Desalination and Water Treatment*, vol. 49, no. 1-3, pp. 368-75.

Shon, H.K., Kim, S.H., Vigneswaran, S., Ben Aim, R., Lee, S. & Cho, J. 2009, 'Physicochemical pretreatment of seawater: fouling reduction and membrane characterization', *Desalination*, vol. 238, no. 1-3, pp. 10-21.

Silva, T.L.S., Morales-Torres, S., Figueiredo, J.L. & Silva, A.M.T. 2015, 'Multi-walled carbon nanotube/PVDF blended membranes with sponge- and finger-like pores for direct contact membrane distillation', *Desalination*, vol. 357, pp. 233-45.

Simone, S., Figoli, A., Criscuoli, A., Carnevale, M.C., Alfadul, S.M., Al-Romaih, H.S., Al Shabouna, F.S., Al-Harbi, O.A. & Drioli, E. 2014, 'Effect of selected spinning parameters on PVDF hollow fiber morphology for potential application in desalination by VMD', *Desalination*, vol. 344, pp. 28-35.

Song, L., Ci, L., Lu, H., Sorokin, P.B., Jin, C., Ni, J., Kvashnin, A.G., Kvashnin, D.G., Lou, J., Yakobson, B.I. & Ajayan, P.M. 2010, 'Large scale growth and characterization of atomic hexagonal boron nitride layers', *Nano Lett*, vol. 10, no. 8, pp. 3209-15.

Song, L., Li, B., Sirkar, K.K. & Gilron, J.L. 2007, 'Direct Contact Membrane Distillation-Based Desalination: Novel Membranes, Devices, Larger-Scale Studies, and a Model', *Industrial & Engineering Chemistry Research*, vol. 46, no. 8, pp. 2307-23.

Song, L., Ma, Z., Liao, X., Kosaraju, P.B., Irish, J.R. & Sirkar, K.K. 2008, 'Pilot plant studies of novel membranes and devices for direct contact membrane distillation-based desalination', *Journal of Membrane Science*, vol. 323, no. 2, pp. 257-70.

Song, Z., Xing, M., Zhang, J., Li, B. & Wang, S. 2012, 'Determination of phase diagram of a ternary PVDF/γ-BL/DOP system in TIPS process and its application in preparing hollow fiber membranes for membrane distillation', *Separation and Purification Technology*, vol. 90, pp. 221-30.

Srisurichan, S., Jiraratananon, R. & Fane, A.G. 2005, 'Humic acid fouling in the membrane distillation process', *Desalination*, vol. 174, no. 1, pp. 63-72.

Srisurichan, S., Jiraratananon, R. & Fane, A.G. 2006, 'Mass transfer mechanisms and transport resistances in direct contact membrane distillation process', *Journal of Membrane Science*, vol. 277, no. 1–2, pp. 186-94.

Su, C.-I., Shih, J.-H., Huang, M.-S., Wang, C.-M., Shih, W.-C. & Liu, Y.-s. 2012, 'A study of hydrophobic electrospun membrane applied in seawater desalination by membrane distillation', *Fibers and Polymers*, vol. 13, no. 6, pp. 698-702.

Su, C., Chang, J., Tang, K., Gao, F., Li, Y. & Cao, H. 2017, 'Novel three-dimensional superhydrophobic and strength-enhanced electrospun membranes for long-term membrane distillation', *Separation and Purification Technology*, vol. 178, pp. 279-87.

Su, M., Teoh, M.M., Wang, K.Y., Su, J. & Chung, T.-S. 2010, 'Effect of inner-layer thermal conductivity on flux enhancement of dual-layer hollow fiber membranes in direct contact membrane distillation', *Journal of Membrane Science*, vol. 364, no. 1-2, pp. 278-89.

Suárez, F., Ruskowitz, J.A., Tyler, S.W. & Childress, A.E. 2015, 'Renewable water: Direct contact membrane distillation coupled with solar ponds', *Applied Energy*, vol. 158, pp. 532-9.

Sun, D., Liu, M.-Q., Guo, J.-H., Zhang, J.-Y., Li, B.-B. & Li, D.-Y. 2015, 'Preparation and characterization of PDMS-PVDF hydrophobic microporous membrane for membrane distillation', *Desalination*, vol. 370, pp. 63-71.

Surwade, S.P., Smirnov, S.N., Vlassiouk, I.V., Unocic, R.R., Veith, G.M., Dai, S. & Mahurin, S.M. 2015, 'Water desalination using nanoporous single-layer graphene', *Nat Nanotechnol*, vol. 10, no. 5, pp. 459-64.

Tang, C.Y., Chong, T.H. & Fane, A.G. 2011, 'Colloidal interactions and fouling of NF and RO membranes: A review', *Advances in Colloid and Interface Science*, vol. 164, no. 1–2, pp. 126-43.

Tang, N., Feng, C., Han, H., Hua, X., Zhang, L., Xiang, J., Cheng, P., Du, W. & Wang, X. 2016, 'High permeation flux polypropylene/ethylene vinyl acetate co-blending membranes via thermally induced phase separation for vacuum membrane distillation desalination', *Desalination*, vol. 394, pp. 44-55.

Tang, Y., Li, N., Liu, A., Ding, S., Yi, C. & Liu, H. 2012, 'Effect of spinning conditions on the structure and performance of hydrophobic PVDF hollow fiber membranes for membrane distillation', *Desalination*, vol. 287, pp. 326-39.

Technology, N.R.C.C.o.A.D. 2008, *Desalination: A National Perspective*, National Academies Press, Washington D. C.

Tedesco, M., Scalici, C., Vaccari, D., Cipollina, A., Tamburini, A. & Micale, G. 2016, 'Performance of the first reverse electrodialysis pilot plant for power production from saline waters and concentrated brines', *Journal of Membrane Science*, vol. 500, pp. 33-45.

Teoh, M.M., Bonyadi, S. & Chung, T.-S. 2008, 'Investigation of different hollow fiber module designs for flux enhancement in the membrane distillation process', *Journal of Membrane Science*, vol. 311, no. 1–2, pp. 371-9.

Teoh, M.M., Chung, T.-S. & Yeo, Y.S. 2011, 'Dual-layer PVDF/PTFE composite hollow fibers with a thin macrovoid-free selective layer for water production via membrane distillation', *Chemical Engineering Journal*, vol. 171, no. 2, pp. 684-91.

Thomas, R., Guillen-Burrieza, E. & Arafat, H.A. 2014, 'Pore structure control of PVDF membranes using a 2-stage coagulation bath phase inversion process for application in membrane distillation (MD)', *Journal of Membrane Science*, vol. 452, pp. 470-80.

Thu, K., Kim, Y.-D., Shahzad, M.W., Saththasivam, J. & Ng, K.C. 2015, 'Performance investigation of an advanced multi-effect adsorption desalination (MEAD) cycle', *Applied Energy*, vol. 159, pp. 469-77.

Tian, M., Qiu, C., Liao, Y., Chou, S. & Wang, R. 2013, 'Preparation of polyamide thin film composite forward osmosis membranes using electrospun polyvinylidene fluoride (PVDF) nanofibers as substrates', *Separation and Purification Technology*, vol. 118, pp. 727-36.

Tian, M., Wang, R., Goh, K., Liao, Y. & Fane, A.G. 2015, 'Synthesis and characterization of high-performance novel thin film nanocomposite PRO membranes with tiered nanofiber support reinforced by functionalized carbon nanotubes', *Journal of Membrane Science*, vol. 486, pp. 151-60.

Tian, M., Wang, Y.-N., Wang, R. & Fane, A.G. 2017, 'Synthesis and characterization of thin film nanocomposite forward osmosis membranes supported by silica

nanoparticle incorporated nanofibrous substrate', *Desalination*, vol. 401, pp. 142-50.

Tian, M., Yin, Y., Yang, C., Zhao, B., Song, J., Liu, J., Li, X.-M. & He, T. 2015, 'CF4 plasma modified highly interconnective porous polysulfone membranes for direct contact membrane distillation (DCMD)', *Desalination*, vol. 369, pp. 105-14.

Tijing, L.D., Choi, J.-S., Lee, S., Kim, S.-H. & Shon, H.K. 2014, 'Recent progress of membrane distillation using electrospun nanofibrous membrane', *Journal of Membrane Science*, vol. 453, pp. 435-62.

Tijing, L.D., Choi, W.L., Jiang, Z., Amarjargal, A., Park, C.-H., Pant, H.R., Im, I.-T. & Kim, C.S. 2013, 'Two-nozzle electrospinning of (MWNT/PU)/PU nanofibrous composite mat with improved mechanical and thermal properties', *Current Applied Physics*, vol. 13, no. 7, pp. 1247-55.

Tijing, L.D., Ruelo, M.T.G., Amarjargal, A., Pant, H.R., Park, C.-H., Kim, D.W. & Kim, C.S. 2012, 'Antibacterial and superhydrophilic electrospun polyurethane nanocomposite fibers containing tourmaline nanoparticles', *Chemical Engineering Journal*, vol. 197, pp. 41-8.

Tijing, L.D., Woo, Y.C., Johir, M.A.H., Choi, J.-S. & Shon, H.K. 2014, 'A novel dual-layer bicomponent electrospun nanofibrous membrane for desalination by direct contact membrane distillation', *Chemical Engineering Journal*, vol. 256, pp. 155-9.

Tomaszewska, M., Gryta, M. & Morawski, A.W. 1998, 'The influence of salt in solutions on hydrochloric acid recovery by membrane distillation', *Separation and Purification Technology*, vol. 14, no. 1–3, pp. 183-8.

Tooma, M.A., Najim, T.S., Alsalhy, Q.F., Marino, T., Criscuoli, A., Giorno, L. & Figoli, A. 2015, 'Modification of polyvinyl chloride (PVC) membrane for vacuum membrane distillation (VMD) application', *Desalination*, vol. 373, pp. 58-70.

Tuinstra, F. & Koenig, J.L. 1970, 'Raman Spectrum of Graphite', *The Journal of Chemical Physics*, vol. 53, no. 3, p. 1126.

Valk, P.v.d., Pelt, A.W.J.v., Busscher, H.J., Jong, H.P.d., Wildevuur, C.R.H. & Arends, J. 1983, 'Interaction of fibroblasts and polymer surfaces: relationship between surface free energy and fibroblast spreading', *Journal of Biomedical Materials Research*, vol. 17, pp. 807-17.

van Oss, C.J. 2007, 'Development and applications of the interfacial tension between water and organic or biological surfaces', *Colloids Surf B Biointerfaces*, vol. 54, no. 1, pp. 2-9.

Verwey, E.J.W. & Overbeek, J.T.G. 1948, *Theory of the stability of lyphobic colloids*, Elsevier, Amsterdam.

Villadsen, J. & Michelsen, M.L. 1978, *Solution of Differential Equation Models by Polynomial Approximation*, Prentice-Hall, New Jersey.

Virgili, F. & Pankratz, T. 2017, *IDA Desalination Yearbook 2016-2017*, Media Analytics Limited.

Wang, E.N. & Karnik, R. 2012, 'Water desalination: Graphene cleans up water', *Nat Nanotechnol*, vol. 7, no. 9, pp. 552-4.

Wang, J., Qu, D., Tie, M., Ren, H., Peng, X. & Luan, Z. 2008, 'Effect of coagulation pretreatment on membrane distillation process for desalination of recirculating cooling water', *Separation and Purification Technology*, vol. 64, no. 1, pp. 108-15.

Wang, J., Zheng, L., Wu, Z., Zhang, Y. & Zhang, X. 2016, 'Fabrication of hydrophobic flat sheet and hollow fiber membranes from PVDF and PVDF-CTFE for membrane distillation', *Journal of Membrane Science*, vol. 497, pp. 183-93.

Wang, L., Li, B., Gao, X., Wang, Q., Lu, J., Wang, Y. & Wang, S. 2014, 'Study of membrane fouling in cross-flow vacuum membrane distillation', *Separation and Purification Technology*, vol. 122, no. 0, pp. 133-43.

Wang, P. & Chung, T.-S. 2012, 'Design and fabrication of lotus-root-like multi-bore hollow fiber membrane for direct contact membrane distillation', *Journal of Membrane Science*, vol. 421-422, pp. 361-74.

Wang, P. & Chung, T.-S. 2015, 'Recent advances in membrane distillation processes: Membrane development, configuration design and application exploring', *Journal of Membrane Science*, vol. 474, pp. 39-56.

Wang, P. & Chung, T.S. 2013, 'A new-generation asymmetric multi-bore hollow fiber membrane for sustainable water production via vacuum membrane distillation', *Environ Sci Technol*, vol. 47, no. 12, pp. 6272-8.

Wang, P., Teoh, M.M. & Chung, T.S. 2011, 'Morphological architecture of dual-layer hollow fiber for membrane distillation with higher desalination performance', *Water Res*, vol. 45, no. 17, pp. 5489-500.

Wang, X., Ding, B., Yu, J. & Wang, M. 2011, 'Engineering biomimetic superhydrophobic surfaces of electrospun nanomaterials', *Nano Today*, vol. 6, no. 5, pp. 510-30.

Wang, Z., Crandall, C., Sahadevan, R., Menkhaus, T.J. & Fong, H. 2017, 'Microfiltration performance of electrospun nanofiber membranes with varied fiber diameters and different membrane porosities and thicknesses', *Polymer*, vol. 114, pp. 64-72.

Wang, Z., Hou, D. & Lin, S. 2016, 'Composite Membrane with Underwater-Oleophobic Surface for Anti-Oil-Fouling Membrane Distillation', *Environ Sci Technol*, vol. 50, no. 7, pp. 3866-74.

Wang, Z., Sun, L., Wang, Q., Li, B. & Wang, S. 2014, 'A novel approach to fabricate interconnected sponge-like and highly permeable polyvinylidene fluoride hollow fiber membranes for direct contact membrane distillation', *European Polymer Journal*, vol. 60, pp. 262-72.

Wasim, M., Sabir, A., Shafiq, M., Islam, A., Azam, M. & Jamil, T. 2017, 'Mixed matrix membranes: Two step process modified with electrospun (carboxy methylcellulose sodium salt/sepiolite) fibers for nanofiltration', *Journal of Industrial and Engineering Chemistry*, vol. 50, pp. 172-82.

Wei, X., Zhao, B., Li, X.-M., Wang, Z., He, B.-Q., He, T. & Jiang, B. 2012, 'CF4 plasma surface modification of asymmetric hydrophilic polyethersulfone membranes for direct contact membrane distillation', *Journal of Membrane Science*, vol. 407-408, pp. 164-75.

Winter, D., Koschikowski, J. & Wieghaus, M. 2011, 'Desalination using membrane distillation: Experimental studies on full scale spiral wound modules', *Journal of Membrane Science*, vol. 375, no. 1-2, pp. 104-12.

Wolf, P.H., Siverns, S. & Monti, S. 2005, 'UF membranes for RO desalination pretreatment', *Desalination*, vol. 182, no. 1–3, pp. 293-300.

Woo, Y.C., Kim, Y., Shim, W.-G., Tijing, L.D., Yao, M., Nghiem, L.D., Choi, J.-S., Kim, S.-H. & Shon, H.K. 2016, 'Graphene/PVDF flat-sheet membrane for the treatment of RO brine from coal seam gas produced water by air gap membrane distillation', *Journal of Membrane Science*, vol. 513, pp. 74-84.

Woo, Y.C., Lee, J.J., Tijing, L.D., Shon, H.K., Yao, M. & Kim, H.-S. 2015, 'Characteristics of membrane fouling by consecutive chemical cleaning in pressurized ultrafiltration as pre-treatment of seawater desalination', *Desalination*, vol. 369, pp. 51-61.

Woodward, I., Schofield, W.C.E., Roucoules, V. & Badyal, J.P.S. 2003, 'Super-hydrophobic Surfaces Produced by Plasma Fluorination of Polybutadiene Films', *Langmuir*, vol. 19, pp. 3432-8.

Xiao, S., Shen, M., Guo, R., Huang, Q., Wang, S. & Shi, X. 2010, 'Fabrication of multiwalled carbon nanotube-reinforced electrospun polymer nanofibers containing zero-valent iron nanoparticles for environmental applications', *Journal of Materials Chemistry*, vol. 20, no. 27, pp. 5700-8.

Xiao, T., Wang, P., Yang, X., Cai, X. & Lu, J. 2015, 'Fabrication and characterization of novel asymmetric polyvinylidene fluoride (PVDF) membranes by the nonsolvent thermally induced phase separation (NTIPS) method for membrane distillation applications', *Journal of Membrane Science*, vol. 489, pp. 160-74.

Xie, M., Nghiem, L.D., Price, W.E. & Elimelech, M. 2013, 'A forward osmosis-membrane distillation hybrid process for direct sewer mining: system performance and limitations', *Environ Sci Technol*, vol. 47, no. 23, pp. 13486-93.

Xie, M., Nghiem, L.D., Price, W.E. & Elimelech, M. 2014, 'Impact of organic and colloidal fouling on trace organic contaminant rejection by forward osmosis: Role of initial permeate flux', *Desalination*, vol. 336, pp. 146-52.

Xu, J.B., Lange, S., Bartley, J.P. & Johnson, R.A. 2004, 'Alginate-coated microporous PTFE membranes for use in the osmotic distillation of oily feeds', *Journal of Membrane Science*, vol. 240, no. 1–2, pp. 81-9.

Xu, M., Zhang, T., Gu, B., Wu, J. & Chen, Q. 2006, 'Synthesis and properties of novel polyurethane−urea/multiwalled carbon nanotube composites', *Macromolecules*, vol. 39, no. 10, pp. 3540-5.

Xu, Y., Zhu, B.-K. & Xu, Y.-y. 2006, 'Pilot test of vacuum membrane distillation for seawater desalination on a ship', *Desalination*, vol. 189, no. 1, pp. 165-9.

Yan, H., Lu, X., Wu, C., Sun, X. & Tang, W. 2017, 'Fabrication of a super-hydrophobic polyvinylidene fluoride hollow fiber membrane using a particle coating process', *Journal of Membrane Science*, vol. 533, pp. 130-40.

Yan, Y.H., Chan-Park, M.B. & Yue, C.Y. 2005, 'CF_4 Plasma Treatment of Poly(dimethylsiloxane): Effect of Fillers and Its Application to High-Aspect-Ratio UV Embossing', *Langmuir*, vol. 21, pp. 8905-12.

Yang, C., Li, X.-M., Gilron, J., Kong, D.-f., Yin, Y., Oren, Y., Linder, C. & He, T. 2014a, 'CF4 plasma-modified superhydrophobic PVDF membranes for direct contact membrane distillation', *Journal of Membrane Science*, vol. 456, no. 0, pp. 155-61.

Yang, C., Li, X.-M., Gilron, J., Kong, D.-f., Yin, Y., Oren, Y., Linder, C. & He, T. 2014b, 'CF4 plasma-modified superhydrophobic PVDF membranes for direct contact membrane distillation', *Journal of Membrane Science*, vol. 456, pp. 155-61.

Yang, C., Tian, M., Xie, Y., Li, X.-M., Zhao, B., He, T. & Liu, J. 2015, 'Effective evaporation of CF4 plasma modified PVDF membranes in direct contact membrane distillation', *Journal of Membrane Science*, vol. 482, pp. 25-32.

Yang, X., Wang, R. & Fane, A.G. 2011, 'Novel designs for improving the performance of hollow fiber membrane distillation modules', *Journal of Membrane Science*, vol. 384, no. 1–2, pp. 52-62.

Yang, X., Wang, R., Shi, L., Fane, A.G. & Debowski, M. 2011, 'Performance improvement of PVDF hollow fiber-based membrane distillation process', *Journal of Membrane Science*, vol. 369, no. 1, pp. 437-47.

Yao, M., Woo, Y.C., Tijing, L., Cesarini, C. & Shon, H.K. 2017, 'Improving Nanofiber Membrane Characteristics and Membrane Distillation Performance of Heat-Pressed Membranes via Annealing Post-Treatment', *Applied Sciences*, vol. 7, no. 1, p. 78.

Yao, M., Woo, Y.C., Tijing, L.D., Shim, W.-G., Choi, J.-S., Kim, S.-H. & Shon, H.K. 2016, 'Effect of heat-press conditions on electrospun membranes for desalination by direct contact membrane distillation', *Desalination*, vol. 378, pp. 80-91.

Yeo, A.P.S., Law, A.W.K. & Fane, A.G. 2007, 'The relationship between performance of submerged hollow fibers and bubble-induced phenomena examined by particle image velocimetry', *Journal of Membrane Science*, vol. 304, no. 1–2, pp. 125-37.

Yip, N.Y. & Elimelech, M. 2014, 'Comparison of energy efficiency and power density in pressure retarded osmosis and reverse electrodialysis', *Environ Sci Technol*, vol. 48, no. 18, pp. 11002-12.

Yoon, K., Hsiao, B.S. & Chu, B. 2009, 'High flux ultrafiltration nanofibrous membranes based on polyacrylonitrile electrospun scaffolds and crosslinked polyvinyl alcohol coating', *Journal of Membrane Science*, vol. 338, no. 1-2, pp. 145-52.

Yoon, Y.I., Moon, H.S., Lyoo, W.S., Lee, T.S. & Park, W.H. 2008, 'Superhydrophobicity of PHBV fibrous surface with bead-on-string structure', *Journal of Colloid and Interface Science*, vol. 320, no. 1, pp. 91-5.

Yoon, Y.I., Moon, H.S., Lyoo, W.S., Lee, T.S. & Park, W.H. 2009, 'Superhydrophobicity of cellulose triacetate fibrous mats produced by

electrospinning and plasma treatment', *Carbohydrate Polymers*, vol. 75, no. 2, pp. 246-50.

You, H., Li, X., Yang, Y., Wang, B., Li, Z., Wang, X., Zhu, M. & Hsiao, B.S. 2013, 'High flux low pressure thin film nanocomposite ultrafiltration membranes based on nanofibrous substrates', *Separation and Purification Technology*, vol. 108, pp. 143-51.

Yun, Y., Ma, R., Zhang, W., Fane, A.G. & Li, J. 2006, 'Direct contact membrane distillation mechanism for high concentration NaCl solutions', *Desalination*, vol. 188, no. 1–3, pp. 251-62.

Zhan, N.Q., Li, Y.X., Zhang, C.Q., Song, Y., Wang, H.G., Sun, L., Yang, Q.B. & Hong, X. 2010, 'A novel multinozzle electrospinning process for preparing superhydrophobic PS films with controllable bead-on-string/microfiber morphology', *Journal of Colloid and Interface Science*, vol. 345, no. 2, pp. 491-5.

Zhang, H., Lamb, R. & Lewis, J. 2005, 'Engineering nanoscale roughness on hydrophobic surface—preliminary assessment of fouling behaviour', *Science and Technology of Advanced Materials*, vol. 6, no. 3–4, pp. 236-9.

Zhang, J., Song, Z., Li, B., Wang, Q. & Wang, S. 2013, 'Fabrication and characterization of superhydrophobic poly (vinylidene fluoride) membrane for direct contact membrane distillation', *Desalination*, vol. 324, pp. 1-9.

Zhao, D., Zuo, J., Lu, K.-J. & Chung, T.-S. 2017, 'Fluorographite modified PVDF membranes for seawater desalination via direct contact membrane distillation', *Desalination*, vol. 413, pp. 119-26.

Zhao, K., Heinzl, W., Wenzel, M., Büttner, S., Bollen, F., Lange, G., Heinzl, S. & Sarda, N. 2013, 'Experimental study of the memsys vacuum-multi-effect-membrane-distillation (V-MEMD) module', *Desalination*, vol. 323, pp. 150-60.

Zhao, L., Wu, C., Liu, Z., Zhang, Q. & Lu, X. 2016, 'Highly porous PVDF hollow fiber membranes for VMD application by applying a simultaneous co-extrusion spinning process', *Journal of Membrane Science*, vol. 505, pp. 82-91.

Zhao, X., Chen, W., Su, Y., Zhu, W., Peng, J., Jiang, Z., Kong, L., Li, Y. & Liu, J. 2013, 'Hierarchically engineered membrane surfaces with superior antifouling and self-cleaning properties', *Journal of Membrane Science*, vol. 441, pp. 93-101.

Zhiqing, Y., Xiaolong, L., Chunrui, W. & Xuan, W. 2013, 'Effect of pretreatment on membrane fouling and VMD performance in the treatment of RO-concentrated wastewater', *Desalination and Water Treatment*, vol. 51, no. 37-39, pp. 6994-7003.

Zhou, T., Yao, Y., Xiang, R. & Wu, Y. 2014, 'Formation and characterization of polytetrafluoroethylene nanofiber membranes for vacuum membrane distillation', *Journal of Membrane Science*, vol. 453, pp. 402-8.

Zhu, H. & Nyström, M. 1998, 'Cleaning results characterized by flux, streaming potential and FTIR measurements', *Colloids and Surfaces A: Physicochemical and Engineering Aspects*, vol. 138, no. 2–3, pp. 309-21.

Zhu, J., Jiang, L. & Matsuura, T. 2015, 'New insights into fabrication of hydrophobic/hydrophilic composite hollow fibers for direct contact membrane distillation', *Chemical Engineering Science*, vol. 137, pp. 79-90.

Zodrow, K.R., Bar-Zeev, E., Giannetto, M.J. & Elimelech, M. 2014, 'Biofouling and microbial communities in membrane distillation and reverse osmosis', *Environ Sci Technol*, vol. 48, no. 22, pp. 13155-64.

Zolotarev, P., Ugrozov, V., Volkina, I. & Nikulin, V. 1994, 'Treatment of waste water for removing heavy metals by membrane distillation', *Journal of Hazardous Materials*, vol. 37, no. 1, pp. 77-82.

Zuo, G. & Wang, R. 2013, 'Novel membrane surface modification to enhance anti-oil fouling property for membrane distillation application', *Journal of Membrane Science*, vol. 447, pp. 26-35.